Integrated geological and geophysical studies applied to understanding the evolution of the Offshore Amazon Basin

Alberto Machado Cruz

Sorbonne Université

Ecole doctorale Géosciences Ressources Naturelles et Environnement

Institut des Sciences de la Terre de Paris

Integrated geological and geophysical studies applied to understanding the evolution of the Offshore Amazon Basin

Par Alberto Machado Cruz

Thèse de doctorat en Géologie

Dirigée par :

Prof. Dr. Christian Gorini

Prof. Dr. Antonio Tadeu dos Reis

Prof. Dr. Cleverson Guizan Silva

Dr. Didier Grangeon

Dr. Marina Rabineau

Présentée et soutenue publiquement le 30 octobre 2018

Devant un jury composé de :

Prof.	Borgamano, Jean	CEREGE	(Rapporteur)
Dr.	Hamon, Youri	IFP Energies nouvelles	(Rapporteur)
Prof.	Santos, Roberto Ventura	Universidade de Brasília	(Examinateur)
Prof.	Droxler, André	Rice University	(Examinateur)
Dr.	Viana, Adriano Roessler	Petrobras	(Examinateur)
Prof.	Jolivet, Laurent	Sorbonne Universités	(Examinateur)
Prof.	Gorini, Christian	Sorbonne Universités	(Directeur de thèse)
Prof.	Reis, A. Tadeu dos	UERJ	(Co-Directeur thèse)

''*Apenas que... busquem conhecimento.*''

Acknowledgements

First of all I must express my gratitude to my PhD thesis advisors for their crucial contribution for this thesis work. I will always be grateful to Prof. Christian Gorini for his unconditional support along the years. Christian welcomed me with open arms when I arrived in France and this project would never have materialized without his personal dedication. I'm also very grateful to Prof. Tadeu dos Reis for his long-lasting guidance and inexhaustible willingness to work side by side during this PhD research project, despite being oceans away. Tadeu has been a true mentor for me since 2009 and it is thanks to his remarkable ability to provide kind (or not) encouragement always in the right time and form that I could persevere in my scientific education. I'm also very thankful to my co-advisors Cleverson Guizan Silva, Didier Grangeon and Marina Rabineau for their advices, motivation, kindness and immense knowledge. Moreover, I must thanks a lot my unofficial advisor Jean-Pierre Suc, Jean Letouzey and Daniel Praeg who came on board along the way but offered fundamental contributions to the development of this thesis.

I am extremely grateful to the members of the examining committee Prof. Jean Borgamano, Dr. Youri Hamon, Prof. Roberto Ventura Santos, Prof. André Droxler, Dr. Adriano Roessler Viana and Prof. Laurent Jolivet who accepted to taking part of my thesis jury in such a short schedule.

I gratefully acknowledge the financial support and scholarships granted during the completion of this study from CAPES (Coordination for the Improvement of Higher Level Education- Brazil) in the form of PhD grant. I also acknowledge the Brazilian Agência Nacional do Petróleo, Gás Natural e Biocombustíveis (ANP) for seismic and stratigraphic data made available to Universidade Federal Fluminense (UFF) and Universidade do Estado de Rio de Janeiro (UERJ). Special thanks are also due to CGG, GAIA and FUGRO for making additional seismic data available and for permission to publish our results, to the Brazilian Navy (DHN/LEPLAC- The Brazilian Continental Shelf Survey Programme) for permission to use the LEPLAC seismic lines, and to HIS Markit for the use of educational licenses of the software IHS Kingdom®.

Finally, I must be thank, remercier and agradecer all my friends and relatives who have always been on my side supporting me.

Abstract

The Offshore Amazon Basin (known in Portuguese as *Bacia da Foz do Amazon*) is located in the far north of the Brazilian Equatorial Margin. This basin has attracted the attention of the scientific community for several decades due to its large-scale sedimentary processes related to the colossal sediment influx provided by the Amazon River. However, most of the investigations carried on the Offshore Amazon Basin were restricted to the uppermost Quaternary succession of the Amazon Deep-sea Fan and some pioneer works aiming deeper strata lacked a reliable chronostratigraphic control. In order to better understand the temporal and spatial evolution of the post-rift stratigraphic succession of the Offshore Amazon Basin, multidisciplinary studies supported by interpretations of seismic, well log, chronostratigraphic data and geophysical potential field models were carried out during this PhD thesis.

The analysis of seismic, well log and chronostratigraphic data allowed better age estimates to a previously reported transition from predominantly carbonate to siliciclastic sedimentation across three different sectors (NW, Central and SE) of the Amazon shelf, as well as the sedimentary processes associated with such transition. Each of these three sectors of the Amazon shelf underwent different regimes of accommodation space creation during the Neogene, which resulted in different architectural styles of carbonate buildups across the NW, Central and SE shelves. On the Central and SE shelves, carbonate production gave way to terrigenous sedimentation around 8 Ma, whereas on the NW shelf carbonate production persisted until 5.5–3.7 Ma. Carbonate production was able to persist on the NW shelf thanks to the presence of a 150-km wide embayment in the Central shelf that captured and prevented the northwestward transport of sediments carried by the paleo-Amazon River until the embayment became completely filled at ca. 3.7 Ma.

The analysis of gravity and magnetic anomalies models coupled with seismic interpretations and lithological description from exploratory wells evidenced that the NW, Central and SE shelves are part of three distinct sub-basins underlain by crystalline basement domains with different origins and structural frameworks. These sub-basins were named as Cassiporé sub-basin (NW margin), Araguari sub-basin (Central margin) and Machadinho sub-basin (SE margin). The Cassiporé sub-basin is underlain by faulted segments of the Amazon craton composing a series of NW-SE oriented half-grabens. The Araguari sub-basin is underlain by the Araguaia-Rokelide suture zone where countless N-S orientated normal faults composing

grabens and half-graben were identified, pointing to intense crustal stretching in the region. The Machadinho sub-basin is underlain by a portion of the West African Craton that remained in South America after the Gondwanan breakup and seems to be the least affected by crustal stretching. More intense crustal stretching in the Araguari sub-basin probably made this region more prone to flexural subsidence, which favored the deposition of the major post-rift depocenters within its limits.

Seismic and chronostratigraphic analysis also allowed the identification of main phases of gravity-driven deformation (gravity tectonics) that effected the post-rift sedimentary succession of the Araguari and Machadinho sub-basin, resulting in the development of syn-sedimentary extensional and compressional faulting above *décollement* levels. During the Late Cretaceous (first phase) gravity-driven deformation was most likely caused by a seaward tilting of the basal *décollement* level in response to differential subsidence. A second phase of gravity-driven deformation between the Paleocene and the Middle Eocene took place only in the Machadinho sub-basin and was limited to the reactivation of normal and thrust faults. A third phase of gravity-driven deformation took place in both sub-basins probably caused by sedimentary loading over the upper slope during a period of intense shelfal progradation in the Late Oligocene. During the Early and Middle Miocene, a fourth phase of gravity-driven deformation took place in the Araguari sub-basin, probably as a result of differential subsidence. The fifth and most intense phase of gravity-driven deformation took place from the Late Miocene to Recent (notably during the Quaternary), driven by a major increase in sediment influx that resulted in the deposition of a voluminous aggrading-prograding shelf-slope wedge.

These results allowed the proposition of correlations between events within and outside the Offshore Amazon Basin. Such correlation are essentially based on the temporal coincidence and discussed in this thesis as hypotheses to be tackled and tested in future studies.

Résumé

Le Bassin de l'Embouchure de l'Amazone (en portugais *Bacia da Foz do Amazonas*) est situé dans l'extrême nord de la Marge Équatoriale Brésilienne. Ce bassin a attiré l'attention de la communauté scientifique pendant plusieurs décennies en raison de ses processus sédimentaires à grande échelle liés à l'afflux colossal de sédiments fourni par l'Amazone. Cependant, la plupart des investigations menées sur ce bassin étaient limités à sur la partie supérieure de la succession Quaternaire de le Cône d'Amazone et certains travaux pionniers visant des strates plus profondes ne disposaient pas d'un contrôle chronostratigraphique fiable. Afin de mieux comprendre l'évolution temporelle et spatiale de la succession stratigraphique post-rift du Bassin de l'Embouchure de l'Amazone, des études multidisciplinaires soutenues par des interprétations de données sismiques, diagraphiques, chronostratigraphiques et de modèles de anomalies gravitaires et magnétiques ont été réalisées au cours de cette thèse.

L'analyse des données sismiques, diagraphiques et chronostratigraphiques a permis d'obtenir une meilleure estimation de l'âge par rapport à une transition entre sédimentation carbonatée vers sédimentation terrigène dans trois secteurs différents (NW, Central et SE) de la plates-forme amazoniene, ainsi que les processus sédimentaires associés. Chacun des trois secteurs des plates-formes amazoniene a subi différents régimes de création d'espace d'accommodation pendant le Néogène, ce qui a favorisé à différents styles architecturaux d'accumulation de carbonates sur les plates-formes NW, Central et SE. Sur les plateaux Central et SE, la production de carbonates a fait place à une sédimentation terrigène autour de 8 Ma, alors que sur le plateau NW, la production de carbonates a persisté jusqu'à 5,5–3,7 Ma. La production de carbonates a pu persister sur le plateau NW grâce à une réentrance de 150 km dans le plateau Central qui a capturé et empêché le transport des sédiments transportés par le fleuve paléo-Amazone vers le NW jusqu'à ce réentrance soit complètement rempli autour de 3,7 Ma.

L'analyse des modèles d'anomalies gravimétriques et magnétiques couplée aux interprétations sismiques et à la description lithologique des puits d'exploration a montré que les plates-formes NW, Central et SE font partie de trois sous-bassins distincts composé par des domaines crustale d'origine et de structure différentes. Ces sous-bassins ont été nommés sous-bassin de Cassiporé (marge NW), sous-bassin Araguari (marge Centrale) et sous-bassin de Machadinho (marge SE). Le sous-bassin de Cassiporé repose sur des segments faillés du Craton

Amazonien qui constitue une série de demi-grabens orientés NW-SE. Le sous-bassin Araguari repose sur la zone de suture Araguaia-Rokelide où ont été identifiées d'innombrables failles normales orientées N-S composant des grabens et des demi-grabens, indiquant un étirement crustal intense dans la région. Le sous-bassin de Machadinho repose sur une partie du Craton Ouest-Africain qui est resté en Amérique du Sud après la séparation du Gondwana et semble être le moins affecté par l'étirement de la croûte. Un étirement plus intense de la croûte dans le sous-bassin d'Araguari a probablement rendu cette région plus sujette à la subsidence, ce qui a favorisé le dépôt des principaux dépocentres.

L'analyse sismique et chronostratigraphique a également permis d'identifier les principales phases de déformation gravitationnelle (*gravity tectonics*) qui ont affecté la succession sédimentaire post-rift des sous-bassins Araguari et Machadinho, entraînant le développement de failles d'extension et de compression syn-sédimentaires reliés par de niveaux basal de décollement. Au cours du Crétacé tardif (première phase), la déformation gravitationnelle était très probablement causé par une inclinaison vers la mer du décollement basal en réponse à une subsidence différentielle. Une seconde phase de déformation gravitationnelle entre le Paléocène et l'Eocène moyen n'a eu lieu que dans le sous-bassin de Machadinho et s'est limitée à la réactivation des failles normales et inverse. Une troisième phase déformation gravitationnelle a eu lieu dans les deux sous-bassins, probablement en raison de la charge sédimentaire sur la pente supérieure pendant une période de progradation intense au cours de l'Oligocène tardif. Pendant le Miocène inférieur et moyen, une quatrième phase de déformation gravitationnelle a eu lieu dans le sous-bassin d'Araguari, probablement en raison de la subsidence différentielle. La cinquième et la plus intense phase de déformation gravitationnelle a eu lieu depuis le Miocène supérieur (notamment au Quaternaire), entraînée par une augmentation importante de l'afflux de sédiments.

Ces résultats ont permis de proposer des corrélations entre des événements à l'intérieur et à l'extérieur du Bassin de l'Embouchure de l'Amazone. Ces corrélations reposent essentiellement sur la coïncidence temporelle et sont discutées dans cette thèse comme des hypothèses à aborder et à tester dans des études futures.

Table of Contents

INTRODUCTION

Introduction – Context and Objectives

The Offshore Amazon Basin (also known as Foz do Amazonas basin) is located on the Brazilian Equatorial margin (Figure 1), and was formed in a complex context of stretching and wrench tectonics that involved two main phases: a less intense Triassic-Jurassic phase related to the opening of the Central Atlantic Ocean; and a more intense Early Cretaceous phase related to the opening of the Equatorial South Atlantic Ocean (Matos, 2000; Zalan, 2004).

The post-rift stratigraphic record of the Offshore Amazon Basin comprises a Cretaceous megasequence of siliciclastic character (Limoeiro Formation), overlain by a Paleocene to Late Miocene mixed carbonate-siliciclastic platform (Marajó and Amapá Formations), in turn overlain by a thick siliciclastic succession deposited since the Late Miocene (Pará Group) (Schaller *et al.*, 1971; Brandão and Feijó, 1994; Figueiredo *et al.*, 2007). The thick Late Miocene to Recent siliciclastic succession distinguishes the Amazon shelf from other basins on the Brazilian Equatorial margin, in which shelfal carbonate production prevailed until the Recent (Figueiredo *et al.*, 2007; Soares *et al.*, 2007; Junior *et al.*, 2007; Condé *et al.*, 2007; Neto *et al.*, 2007).

Increasing siliciclastic influx into the Offshore Amazon Basin from the Late Miocene resulted in the accumulation of a ~9 km thick succession that constitutes the Amazon Deep-sea Fan (hereafter referred to as the Amazon Fan), deposition of which is thought to have been initiated about the same time of the cessation of carbonate sedimentation on the shelf (Figueiredo *et al.*, 2009; Silva *et al.*, 1999). These changes in the volume and nature of sedimentation on the continental margin have been associated with phases of Andean uplift leading to a transcontinental Amazon River flowing from the Andean range to the Atlantic Ocean (Hoorn *et al.*, 1995). However, the precise timing of events on the margin has been constantly revised, with ages varying from 11.8 Ma to 8.3 Ma proposed for the cessation of widespread carbonate sedimentation and for the base of the Amazon Fan (Figueiredo *et al.*, 2009; Gorini *et al.*, 2014). Such imprecise age estimates for the major environmental changes that have affected the Offshore Amazon Basin raise serious questions over correlations between events at a continental scale (e.g. between Andean orogeny and Amazon Fan growth).

The post-rift succession of the Offshore Amazon Basin includes a series of depocenters located along an axis suggested to coincide with deeply buried grabens, implying the tectonic framework has exerted some form of control on sediment distribution (Schaller *et al.*, 1971; Rezende and Ferradaes, 1971; Castro *et al.*, 1978). However, a variety of conflicting structural frameworks have been proposed for the Offshore Amazon Basin (Castro *et al.*, 1978; Costa *et al.*, 2002; Mohriak, 2003; Soares Júnior *et al.*, 2011), making correlations between sediment distribution and tectonic features problematic.

In the Amazon Fan, the major depocenter of the Offshore Amazon Basin, the post-rift succession has been deformed by gravity tectonics movements, resulting in paired belts of extensional faults and thrust-folds rooted on basal *décollement* levels (Silva *et al.*, 1999; Zalán, 1999; Perovano *et al.*, 2009). These gravity-driven structures on the outer shelf and upper slope have seafloor expression in places, and have been interpreted to affect sediment distribution, e.g. by controlling the location of the Amazon Canyon and by triggering recurrent mass failures from the upper slope (Reis *et al.*, 2010; Silva *et al.*, 1999; Perovano *et al.*, 2009). A possible correlation between the intensity of gravity-driven faulting and sedimentary influx into the Offshore Amazon Basin has been suggested (Silva *et al.*, 1999). However, limited constraints on the timing of gravity-driven deformation phases and on rates of sedimentation in the Offshore Amazon Basin have prevented a validation of a possible correlation between these two processes.

The overall objective of this PhD project is to improve our understanding of the post-rift evolution of the Offshore Amazon Basin, which took place in a dynamic setting of carbonate and siliciclastic deposition conditioned by the underlying tectonic framework of the margin and affected by syn-sedimentary gravity-driven deformation. The specific objectives are to obtain improved constraints on the age and character of stratigraphic units within the basin, to examine their relation to basement and syn-rift structures, to investigate the spatial and temporal evolution of carbonate vs siliciclastic sedimentation, and to examine the relationship between sediment influx to the margin and phases of gravity tectonics activity.

The PhD thesis is subdivided into six main chapters:

Chapter I presents an overview of the geodynamic and tectono-stratigraphic framework of the Offshore Amazon Basin and the regional context in which post-rift sedimentation took place.

Chapter II presents the dataset used in this study and describes the methodology used to achieve the goals of the study (e.g. seismic stratigraphy, biochronostratigraphy and well log correlation with seismic data).

Chapter III consists of an article already submitted for publication (Cruz *et al.* submitted), in which the Neogene stratigraphy of the Offshore Amazon Basin is investigated, with an emphasis on the Amapá Formation and its record of the spatial and temporal evolution of mixed siliciclastic and carbonate environments.

Chapter IV presents an investigation of the relation of the distribution of post-rift sedimentary units to the tectonic framework of the Offshore Amazon Basin, based on gravimetric, magnetic and seismic data. This chapter is written in the form of an article that will be submitted for publication as soon as the article comprising Chapter III is accepted.

Chapter V consists of a revised and expanded version of a study presented at the 2016 EGU General Assembly in Vienna (Cruz *et al.*, 2016), proposing a kinematic model for Cenozoic gravity-driven deformation phases in the Offshore Amazon Basin in relation to variable sediment influx to the margin, based on seismic observations and chronostratigraphic data.

Chapter VI is divided into two sections. First, the results of previous work conducted in the Offshore Amazon by our research group (in which I took part) are briefly discussed in light of the findings of this thesis. Second, a discussion addresses the post-rift evolution of the Offshore Amazon Basin in a regional context, integrating the results presented here with published information from neighboring regions.

Finally, some concluding remarks and perspectives for future studies are presented.

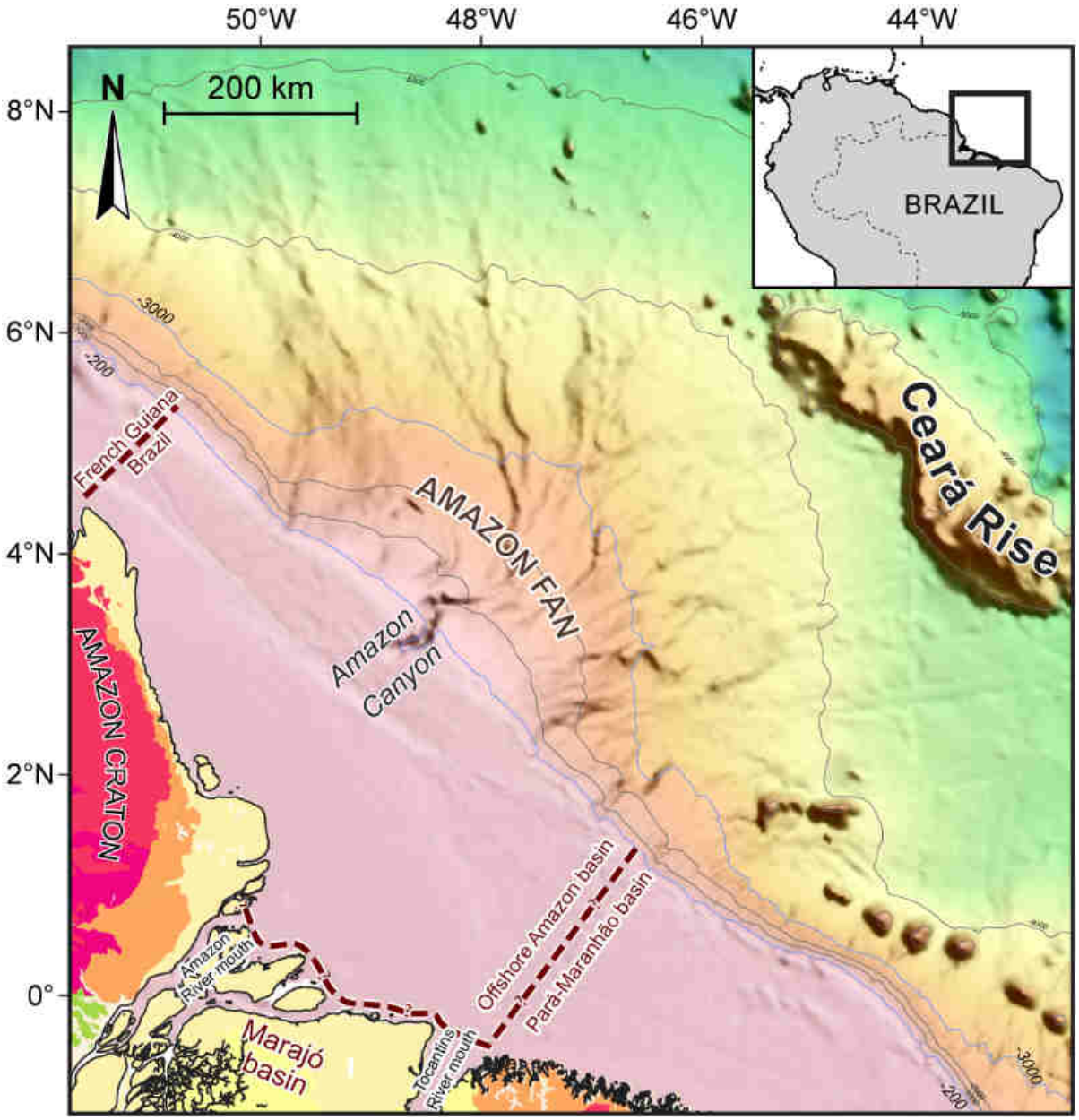

Figure I-1: Bathymetric map showing the location of the Offshore Amazon Basin and its limits according to Milani *et al.* (2007).

CHAPTER I
REGIONAL SETTING

Regional setting

The Offshore Amazon Basin is located in the northwesternmost portion of the Brazilian Equatorial Margin (Figure I-1). The basin is flanked by the Amazonian Craton to the west, whereas to the north, south and southeast its boundaries are not clearly defined (Figure I-1 andFigure I-2). The northern boundary of the Offshore Amazon Basin is commonly illustrated as equivalent to the political boundary between the Brazilian and French Guyana continental shelf (Figure I-1), an arbitrary limit with no geological meaning. To the south, the present-day shoreline has been used to separate the Offshore Amazon Basin from the intracratonic Marajó basin (Mohriak, 2003; Milani *et al.*, 2007; Figure I-1), but no structural feature separates the two basins. To the southeast, different boundaries lacking clear geological meaning have been proposed to separate the Offshore Amazon Basin from the Pará-Maranhão basin (Soares *et al.*, 2007). Thus whereas Milani *et al.* (2007) showed the limit as a projected line between the southern margin of the Tocantins River mouth (also known as Marajó Bay or south Amazon channel) and the shelf edge (Figure I-1), Mohriak (2003) positioned this boundary more than 500 km southward at Santana Island (Figure I-2). Mohriak (2003) also proposed that the distal boundary of the Offshore Amazon Basin could be assigned at the limit between continental and oceanic crust, but such limit has never been mapped in the region.

The investigations undertaken for this thesis encompass the stratigraphic record of the continental shelf, slope and adjacent abyssal plain. Altogether, the study area covers an area of approximately 600,000 km^2 of the Offshore Amazon Basin. The following sections outline the main geological aspects of the area of interest.

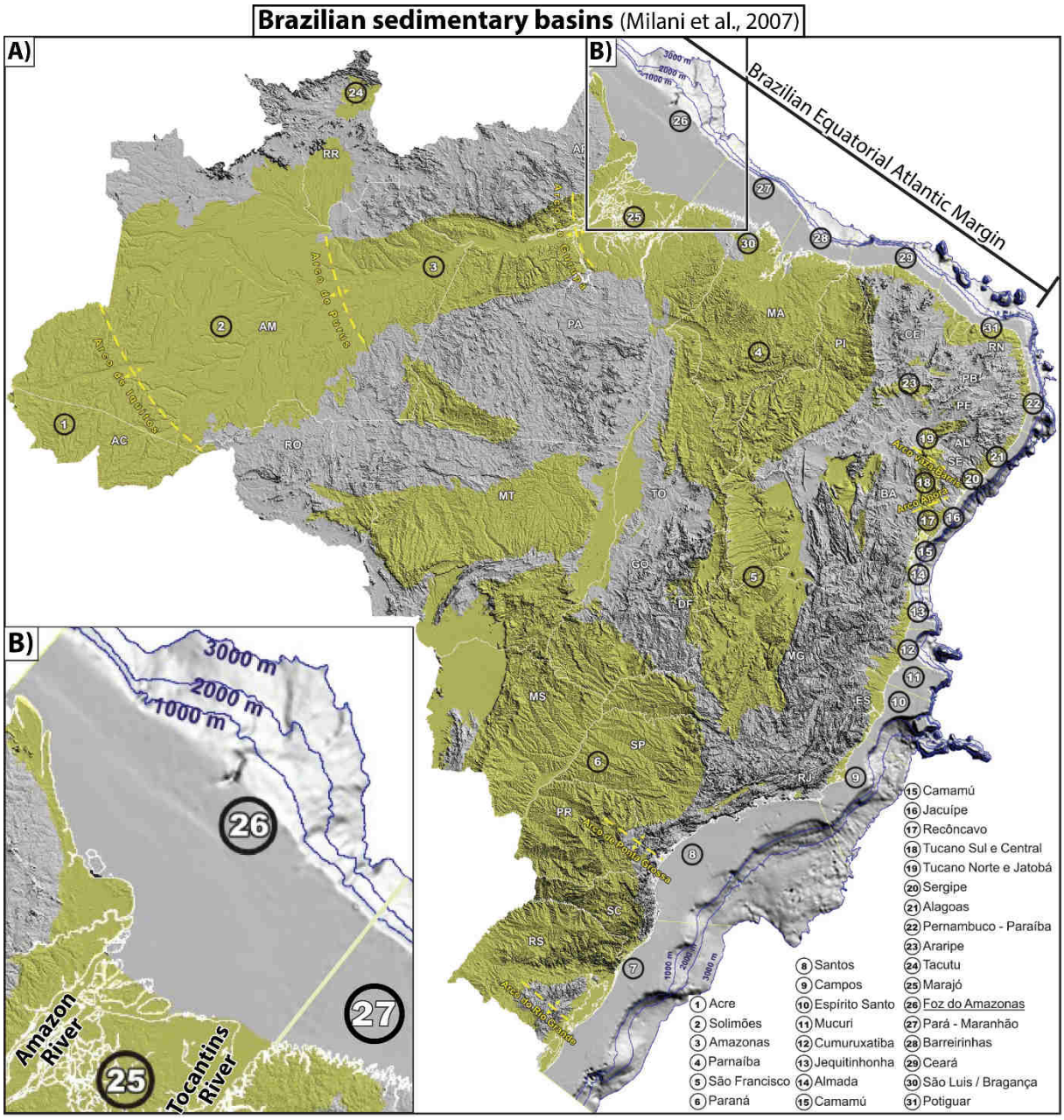

Figure I-1: Brazilian sedimentary basins and their boundaries according to Milani *et al.*, (2007). The Offshore Amazon Basin (number 26 above) is located on the far north of the Brazilian Equatorial Atlantic margin. Note that the boundary between the Offshore Amazon Basin and the Pará-Maranhão basin (number 27 above) is given as a straight line projected from the southern side of the Tocantins River mouth to the continental shelf edge. Modified after Milani *et al.*, (2007).

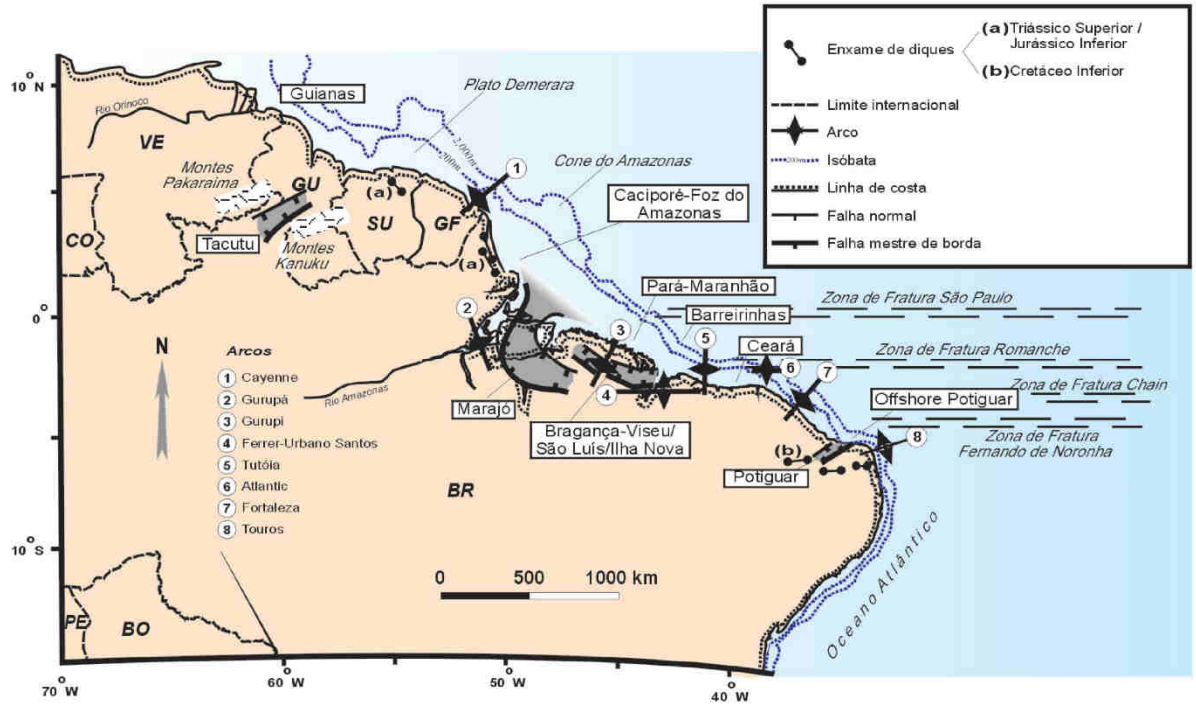

Figure I-2: I-3: Schematic geological map of the Brazilian Equatorial Atlantic margin according to Mohriak (2003). Note that the boundary between the Offshore Amazon Basin (Caciporé-Foz do Amazonas) and the Pará-Maranhão basin (indicated as number 3) is located farther south than the boundary on Milani *et al.* (2007).

I.1 TECTONIC FRAMEWORK

According to Figueiredo *et al.* (2007), the basement of the Offshore Amazon Basin is composed partly of cratonic domains (igneous and metamorphic rocks of the Amazon Craton) and partly by the African Neoproterozoic-Cambrian Rokelide suture zone (an orogenic belt composed of metamorphic rocks dated 570-500 Ma; Villeneuve, 2008; Figure I-4). However, the boundary between these two domains have never been defined, and the nature of the basement underlying the Offshore Amazon Basin may be more complex. Most reconstructions of the Gondwana supercontinent place the Rokelide suture zone in continuity with the Araguaia fold belt within South America, thus forming a single Araguaia-Rokelide suture zone that passes beneath the Offshore Amazon Basin (Brito Neves and Fuck, 2014). However, Villeneuve and Cornée (1994) considered that the Rokelide belt, together with the Brazilian Araguaia and Gurupi belts, form a triple junction separating the Amazon and São Luís–West African cratons in an area equivalent to the Marajó and Offshore Amazon Basins (Figure I-4B). If so, it may be that the Offshore Amazon Basin is also partially underlain by these two distinct Neoproterozoic Brazilian suture zones, as well as the Amazon Craton.

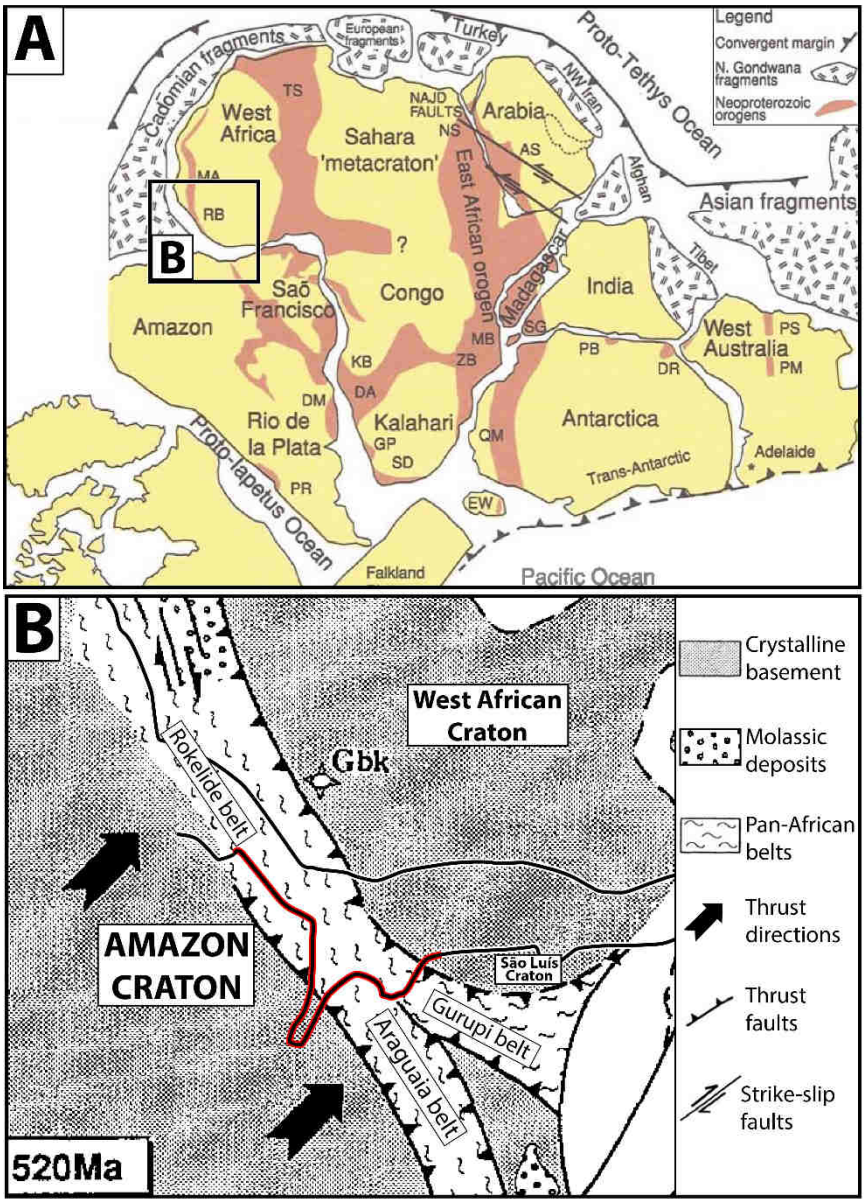

Figure I-4: Map of Gondwana showing the general arrangement of Neoproterozoic orogenic belts (Kusky *et al.*, 2003 modified by Kröner and Stern, 2005). B) Main structural features of the West African and Amazonian Cratons and surrounding orogenic belts around 520 Ma (modified after Villeneuve and Cornée, 1994). Present-day coasts of Brazil and Africa shown as black lines for geographical reference, with the coastline equivalent to the study area of this thesis highlighted in red.

Geodynamic context of basin formation

The area of the Offshore Amazon Basin began to accumulate sediments as early as the Late Triassic-Early Jurassic (235-194 Ma) when it was affected by deformation associated with the opening of the Central Atlantic (Figueiredo *et al.*, 2007). However, it is unclear exactly how the Offshore Amazon Basin was affected by this event. Whereas some authors suggest the setting of a rather quiescent sag basin to the region during the Late Triassic-Early Jurassic (Figueiredo *et al.*, 2007), others suggest that a branch of the Central Atlantic rift affected the region (Zalan, 2004; Soares Júnior *et al.*, 2008; Soares Júnior *et al.*, 2011; Figure I-5 and Figure

I-6A). According to the latter authors, the Central Atlantic rift branch was aborted near the Triassic-Jurassic transition and remained inactive until the Early Cretaceous (Zalan, 2004; Soares Júnior *et al.*, 2008; Soares Júnior *et al.*, 2011; Figure I-6). Soares Júnior *et al.* (2008) named this possible early aborted rift as "First event" in a model of three extensional phases for the opening of the Equatorial Atlantic.

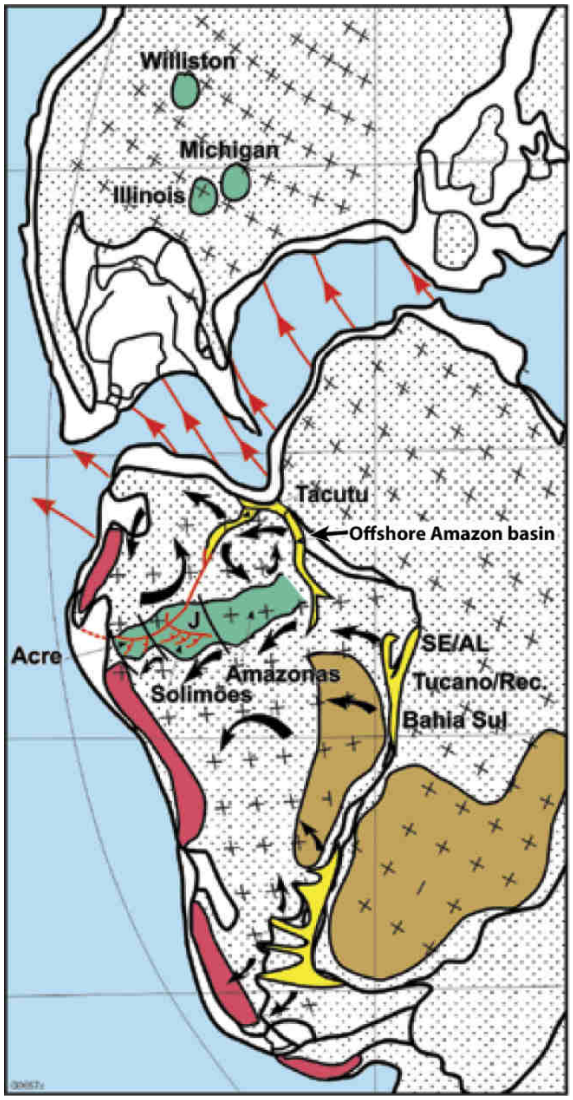

Figure I-5: Geotectonic scenario near the end of the Jurassic, showing an aborted branch of the Central Atlantic rift, shown in yellow, extending across the Offshore Amazon and Marajó basins (Zalan, 2004). According to Zalan (2004) and Soares Júnior *et al.* (2008), this aborted rift branch was formed in the Late Triassic, failed near the Triassic-Jurassic transition and remained inactive before being reactivated during the Early Cretaceous in the context of the opening of the Equatorial Atlantic.

The most intense rifting phase in the Offshore Amazon Basin took place during the Early Cretaceous in the context of the break-up of the South American and African continents and the opening of the Equatorial Atlantic Ocean (Matos, 2000; Figueiredo *et al.*, 2007; Soares Júnior *et al.*, 2008). The process of rifting involved movements of transform and extensional

nature that generated a series of complex marginal sedimentary basins along the Equatorial Atlantic Margin, characterized by multiple phases of subsidence and differing structural styles (Matos, 2000; Soares Júnior *et al.*, 2008). Júnior Soares *et al.* (2008; 2011) subdivided the Early Cretaceous rifting into two events (Second and Third events; Figure I-6B to G). According to Júnior Soares *et al.* (2008; 2011), between the Berriasian and the Aptian the initial opening of the Equatorial Atlantic marked a second rifting event when Late Triassic-Early Jurassic grabens of the First Event were reactivated, enlarged and prolonged to the south (Second event, Figure I-6B to E). This resulted in a connection between the rift system in the northern part of the Offshore Amazon Basin (Cassiporé Graben) and the newly formed Marajó Basin to the south. Thereafter, according to Júnior Soares *et al.* (2008; 2011), a Third Event (Albian) formed a rift system characterized by a series of normal faults that propagated from SE to NW along the Equatorial Margin, and evolved into continental break-up (Figure I-6F and G). According to these authors, it was after this third event, by the end of the Albian, that oceanic crust began to be created in the Offshore Amazon Basin.

The model of two Cretaceous rifting events proposed by Júnior Soares *et al.* (2008; 2011) is in overall agreement with a model for the geodynamic evolution of the Equatorial Atlantic proposed by Basile *et al.* (2005). According to the latter authors, the opening of the Equatorial Atlantic was dominated by divergent motions until the late Aptian. However, Basile *et al.* (2005) states that from late Aptian deformation began to take place along intra-continental transform faults leading to oceanic crust accretion during the latest Albian (Figure I-7), thus differing from the exclusively divergent rifting model proposed by Júnior Soares *et al.* (2008; 2011) for the Amazon margin. Nevertheless, Basile *et al.* (2005) also labeled most of the Offshore Amazon Basin and the conjugate African basin in Liberia as divergent margin segments (Figure I-8).

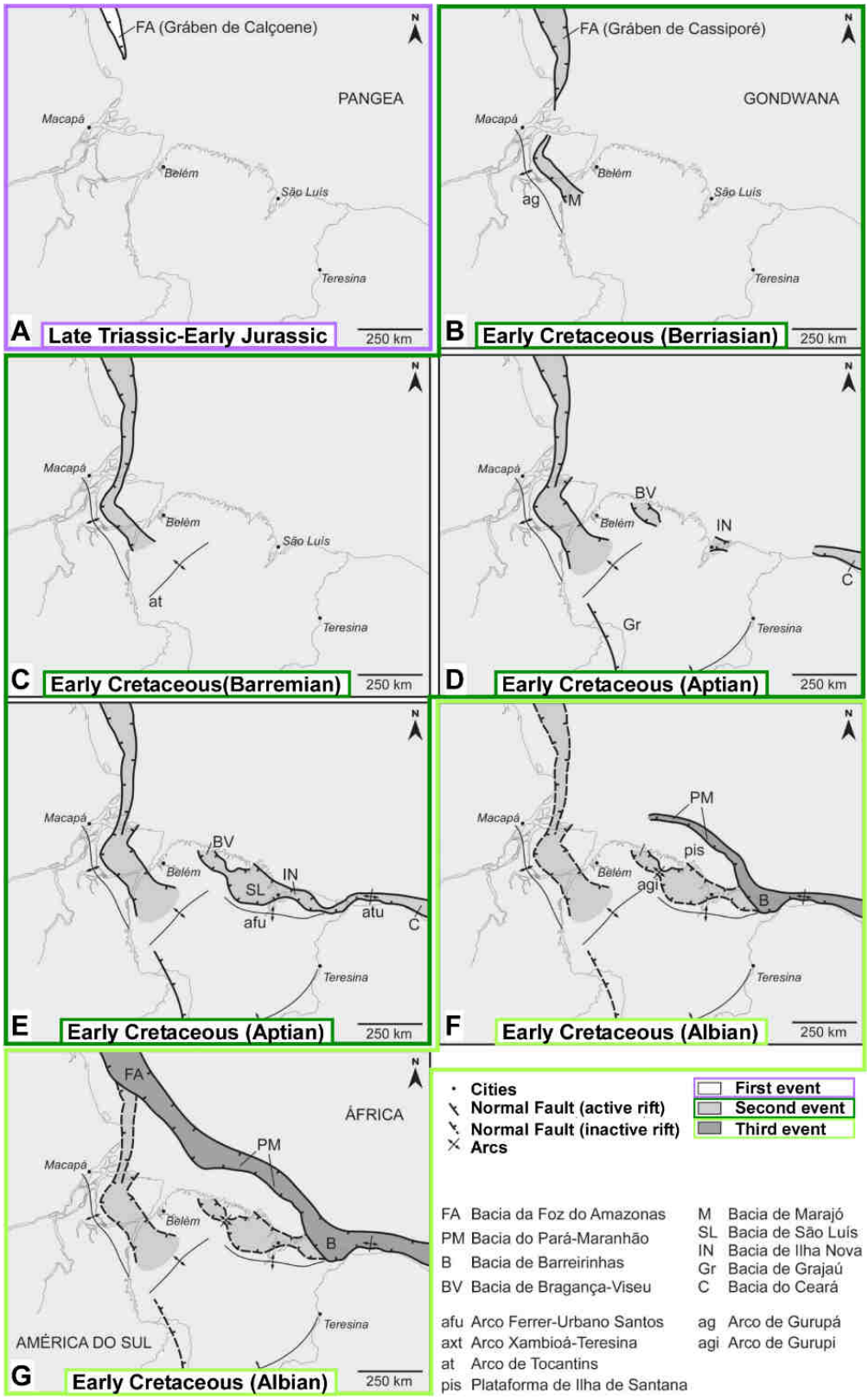

Figure I-6: Brazilian Equatorial Margin extensional events according to Soares Júnior *et al.* (2008): (A) First Event from Early Triassic to Late Triassic, highlighted in purple; (B-E) Second Event from Berriasian to Apitian, highlighted in dark green and (F-G) Third Event during the Albian, highlighted in light green. Note that the rifting the process in the northern part of the Equatorial margin is attributed to extensional motions associated with normal faults, with no strike-slip faulting.

In contrast, other authors have classified the Offshore Amazon Basin as a transform margin (Mohriak, 2003; Figueiredo *et al.*, 2007), in accordance with the geodynamic evolution of the Equatorial Atlantic proposed by Matos (2000). According to Matos (2000) rifting characterized by transtensional deformation started during the late Barremian, and climaxed during the Aptian in almost instantaneous opening of the Equatorial Atlantic (Matos, 2000). According to Matos (2000), during the Albian there was a diachronous transition from transtensional deformation to deformational processes related to the activation of transform faults and the emplacement of oceanic crust. From the Albian to the Cenomanian, rifting of the Equatorial Atlantic Margin would have been dominated by transtension and/or transpression in the context of wrench tectonics (Matos, 2000). It is worth noting that the large-scale model proposed by Matos (2000) encompasses the entire Equatorial Atlantic Margin, and no detailed rifting model has ever been provided by the studies focused on the Offshore Amazon Basin that supports a transform nature of the rifting process for this region.

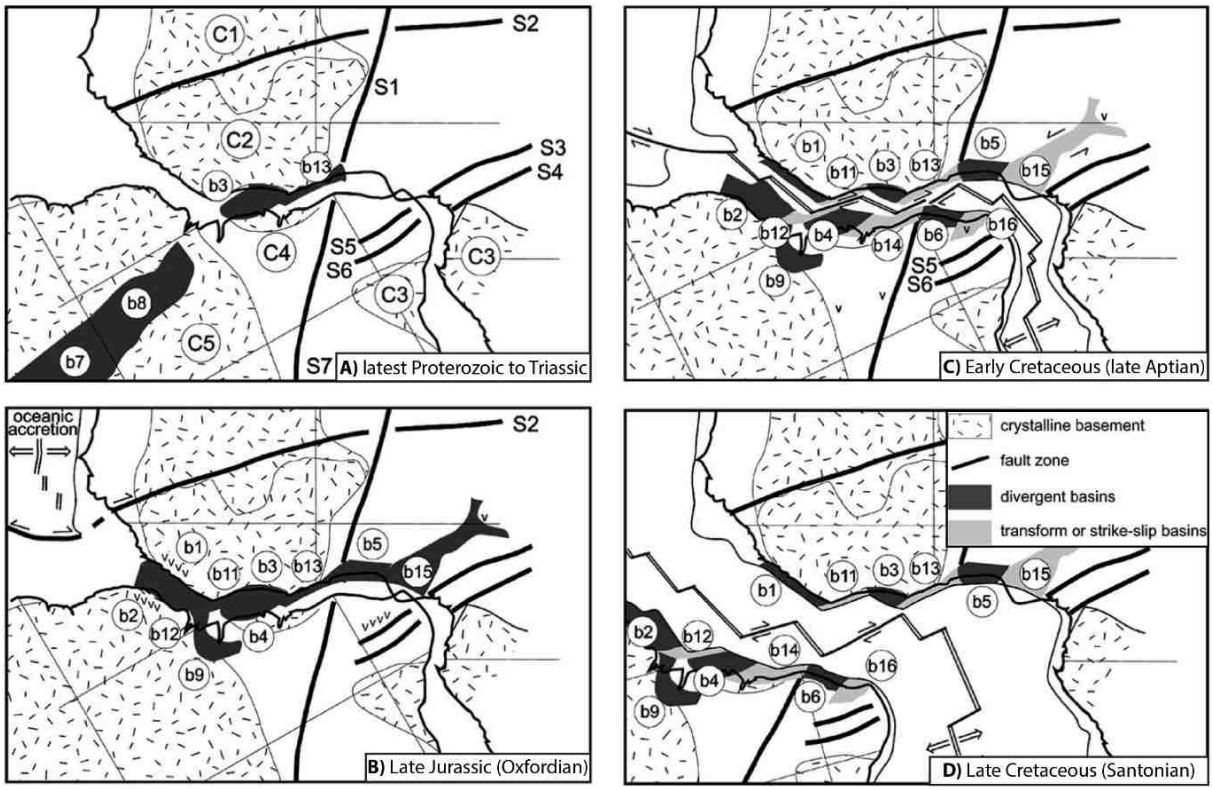

Figure I-7: Geodynamic evolution of the Equatorial Atlantic according to Basile *et al.* (2005). The equivalent position of the Offshore Amazon Basin is indicated by the "**b2**" and "**b12**" symbols. Note that, according to the authors, the Offshore Amazon Basin occupied a divergent margin segment until the Aptian, when a narrow transform segment formed in the southern part of the area.

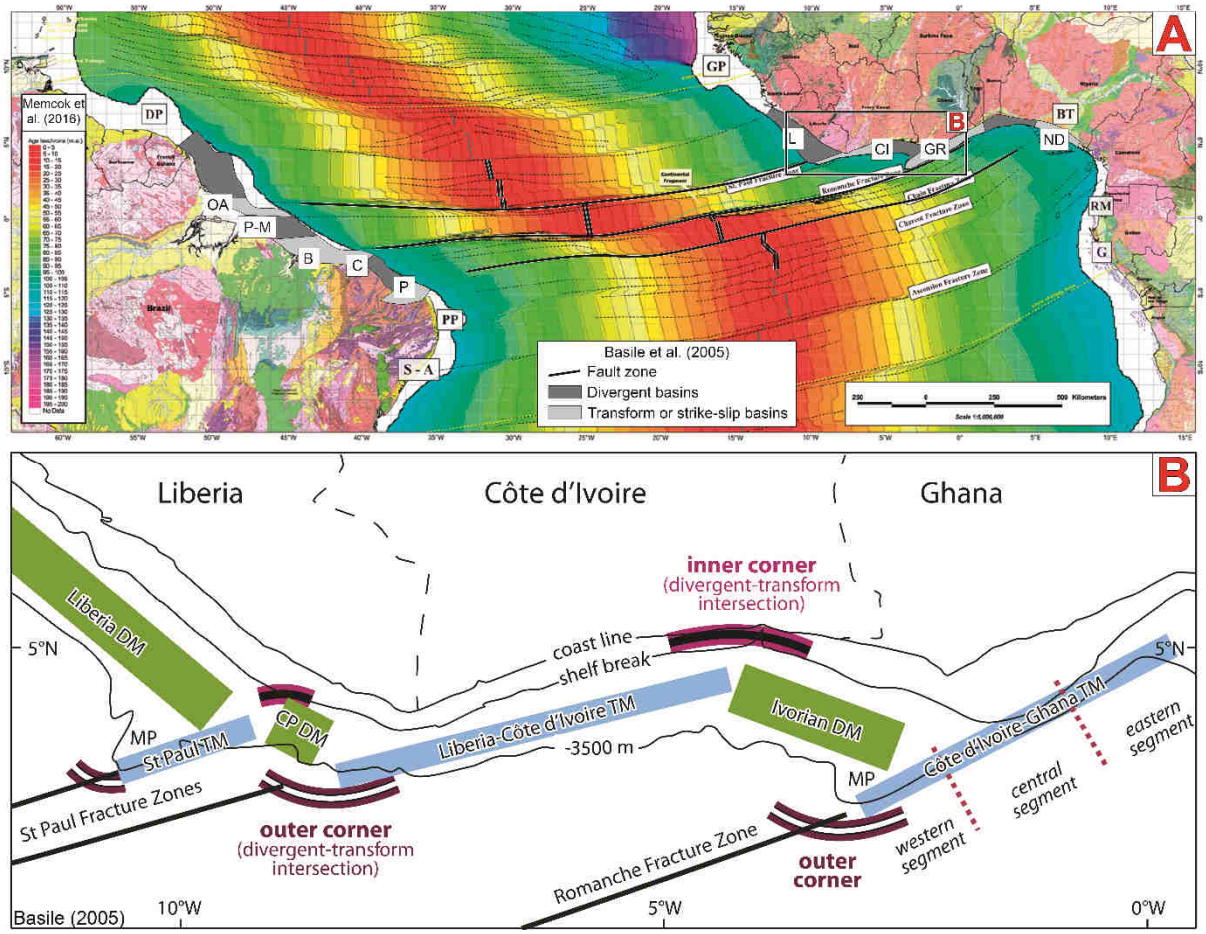

Figure I-8: **A)** Composite of figures from Basile *et al.* (2005) and Nemcok *et al.* (2012), respectively showing the basins of the Brazilian and African margins and the main structures of the Equatorial Atlantic Ocean. Divergent and transform basins classification according to Basile *et al.* (2005). **B)** Geodynamic map of the western African margin from Basile (2015). Note that the author classifies the Liberian margin, the conjugate margin of the Offshore Amazon Basin, as a divergent margin (DM).

Structural framework

Conflicting interpretations have been proposed for the regional crustal structures underlying the Offshore Amazon Basin (Castro *et al.*, 1978; Costa *et al.*, 2002; Mohriak, 2003; Soares Júnior *et al.*, 2011; Figure I-9), probably due to poor seismic imaging of the basement caused by the thickness (up to 12 km) of the overlying sedimentary succession (Braga, 1993).

According to Matos (2000), the classic structures of divergent margins, such as tilted half-grabens and the formation of depocenters controlled by listric faults, are not easily recognized within the basins of Brazilian Equatorial Margin. Instead, the sedimentary basins that comprise the margin are characterized by narrow continental shelves with sharp topographical breaks to the deep ocean floor, and separated from each other by a system of

transform faults (Matos, 2000). This morphological description supports the "transform margin" classification used to describe most of the Brazilian Equatorial Margin basins by Matos (2000), but may not be suitable for the Offshore Amazon Basin. In fact, most studies of the Offshore Amazon Basin indicate a prevalence of extensional features (such as grabens and half-grabens) over transform structures (like strike-slip faults), especially in the NW region (Castro *et al.*, 1978; Mohriak, 2003; Soares Júnior *et al.*, 2011; Figure I-9). Extensional features including grabens and half-grabens have also been recognized on seismic and geological cross-sections of the Offshore Amazon Basin, and the topographical transition from continental to oceanic basement has been depicted as gradual rather than sharp (Rezende and Ferradaes, 1971; Brouwer and Schwander, 1987; Silva *et al.*, 1999; Mohriak, 2003; Figueiredo *et al.*, 2007; Figure I-10).

It is worth noting that there is little consensus regarding the structural framework of the Central and SE regions of the Offshore Amazon Basin (Figure I-9). Whereas Castro *et al.* (1978) proposed that two branches of the a Marajó basin graben (Mexiana) extend northward into the Central-SE shelf, Costa *et al.* (2002) proposed that the Cassiporé graben extended all the way from the NW shelf to the Central shelf, where it intersects a fold belt parallel to a strike-slip fault zone (Figure I-9 A-B). Both Mohriak (2003) and Soares Júnior *et al.* (2011) depicted the Amazon shelf as dominated by normal faults intersected by strike-slip faults in the outer-middle shelf (Figure I-9 C-D). However, according to Soares Júnior *et al.* (2011), the strike-slip faults intersecting the Amazon Shelf were not in place until the Miocene, so these structures would be rather associated with intraplate post-rift tectonics.

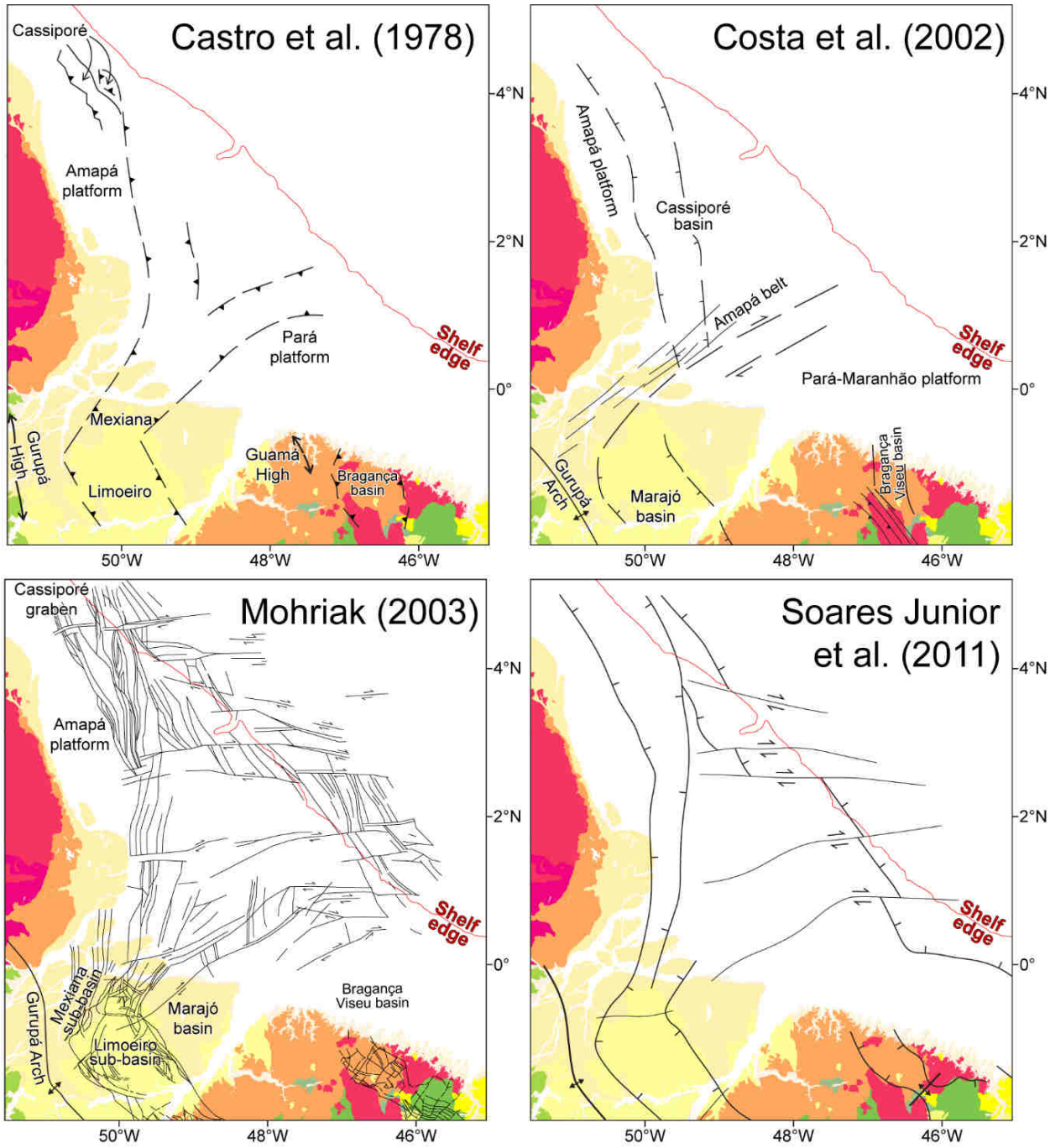

Figure I-9: Compilation of four different structural frameworks proposed for the Offshore Amazon Basin. All figures show onshore geology after the Geological Survey of Brazil database (CPRM, 2004). Note that only in the NW region is there some level of consensus, although Castro *et al.* (1978) and Mohriak (2003) depict the "Cassiporé graben" as a series of half-grabens bounded by seaward-dipping normal faults, while Costa *et al.* (2002) and Soares Júnior *et al.* (2011) depict it as a graben with normal faults extending along the NW shelf as far as the Amazon River mouth. Also note inconsistency regarding the names of some structural features.

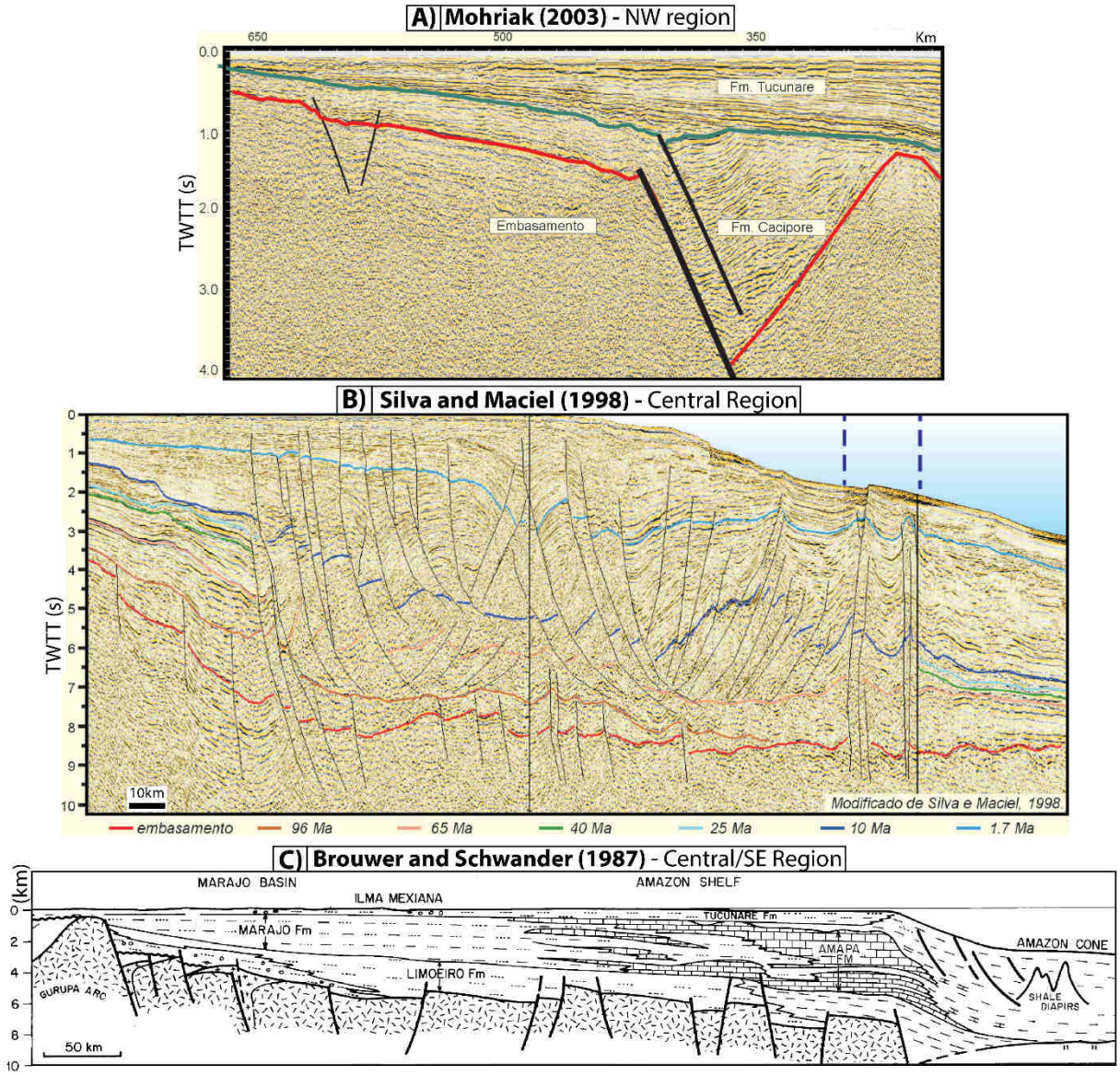

Figure I-10: Compilation of interpreted seismic and geological cross-sections of the Offshore Amazon Basin, showing extensional features affecting the basement. The authors offered no positioning for these cross-sections, their relative positions (NW, Central and SE regions) are deduced based on comparisons with the dataset of this thesis. **A)** Seismic section across the Amazon NW shelf showing the Cassiporé graben and stratigraphic thickening controlled by a normal fault (Mohriak, 2003). **B)** Seismic section across the Amazon Fan showing a series of normal faults offsetting the basement (in red) (Silva and Maciel, 1998 modified by Mohriak, 2003). **C)** Schematic geological cross-section of the Marajó basin and SE Amazon continental margin showing a series of normal faults affecting the basement (Brouwer and Schwander, 1987). Note in **B** and **C** that the interpreted topographical transition from continental to oceanic basement is gradual rather than sharp.

I.2 OFFSHORE AMAZON BASIN STRATIGRAPHY

The stratigraphic succession of the Offshore Amazon Basin was divided by Figueiredo *et al.* (2007) into three megasequences: pre-rift, syn-rift and post-rift (Figure I-11). The post-rift megasequence was subdivided into three phases (Schaller *et al.*, 1971; Brandão and Feijó, 1994; Figueiredo *et al.*, 2007) represented by (1) the Late Cretaceous-Early Paleocene Limoeiro Formation, (2) the Early Paleocene-Middle Miocene Marajó, Amapá and Travosas Formations, and (3) the Middle Miocene to Recent Pará Group (Figure I-11). Each of these mega-sequences is briefly described in the following sections, with greater detail for stratigraphic interval (post-rift megasequence) investigated in this thesis.

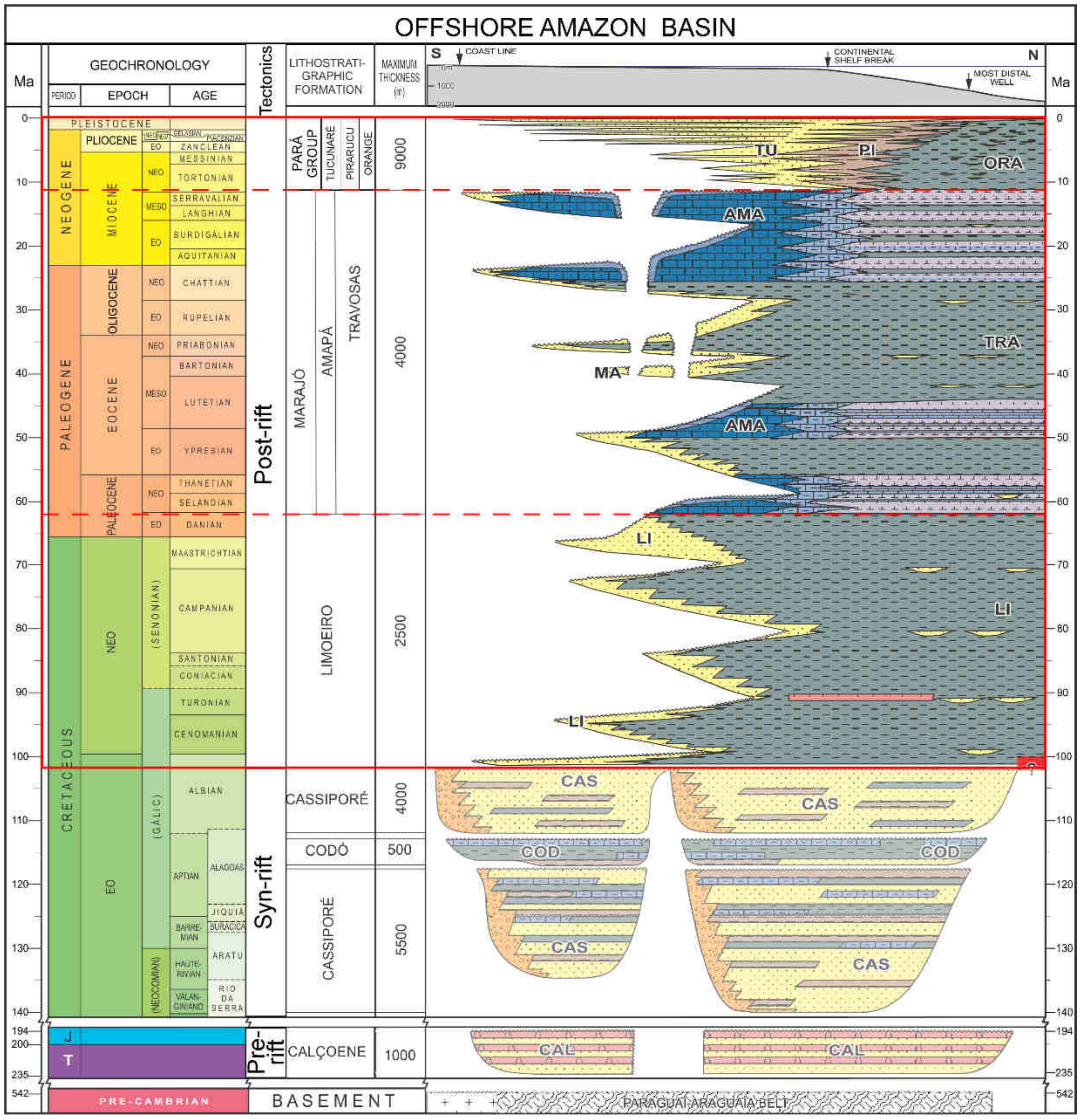

Figure I-11: Stratigraphic chart of the Offshore Amazon Basin; red box highlights the stratigraphic interval investigated in this study, dashed lines indicate the three post-rift megasequences (modified from Figueiredo *et al.*, 2007). Abbreviations stand for: Calçoene Formation (CAL), Cassiporé Formation (CAS), Codó Formation (COD), Limoeiro Formation (LI), Marajó Formation (MA), Amapá Formation (AMA), Travosas Formation (TRA), Tucunaré Formation (TU), Pirarucu Formation (PI) and Orange Formation (ORA).

I.2.1 Pre-rift and Rift megasequences

The pre-rift megasequence (deposited between ca. 222-186 Ma) is characterized by sandstones intercalated with basaltic flows of Triassic age (Calçoene Formation; Figure I-11), and extends across grabens and structural highs in uniform thickness (Brandão and Feijó, 1994; Figueiredo *et al.*, 2007). This megasequence was deposited in a desert environment, either in an intracratonic sag-type basin associated with a stable tectonic environment (Figueiredo *et al.*, 2007), or associated to a branch of the Central Atlantic rift that was later aborted, as described above (Soares Júnior *et al.*, 2011; Zalan, 2004). The maximum thickness of the Calçoene Formation is estimated at 1 km (Brandão and Feijó, 1994).

The deposition of the syn-rift megasequence took place during the Early Cretaceous during the opening of the Equatorial Atlantic Ocean. This megasequence is mainly composed of the regressive siliciclastic deposits of the Cassiporé Formation (fluvial-deltaic and lacustrine intercalated shales and fine sandstones) and the transgressive shales and calcilutites of the Codó Formation (Brandão and Feijó, 1994; Figueiredo *et al.*, 2007; Figure I-11 andFigure I-12). These formations were deposited within structural lows (grabens and half grabens) and attain a maximum thickness estimated at 7 km (Brandão and Feijó, 1994; Figueiredo *et al.*, 2007).

I.2.2 Post-Rift 1: Limoeiro Formation (Late Cretaceous to Paleocene)

According to Figueiredo *et al.* (2007), deposition of the post-rift megasequence deposition began near the end of the Albian with the deposition of the Limoeiro Formation, which records the onset of open marine sedimentation (Figure I-11). The Limoeiro Formation was first described by Schaller *et al.* (1971) as interbedded sandy and muddy sediments that extend beyond the structural lows of the basin, but are thickest within them. According to Brandão and Feijó (1994) these sediments were deposited in conditions varying from fluvial to bathyal, thus encompassing a range of depositional environments. According to Figueiredo *et al.* (2007) the Limoeiro Formation deposition took place from the latest Albian (ca. 102 Ma) to Early Paleocene (Danian) (Figure I-11).

According to Brandão and Feijó (1994), the Limoeiro Formation can be divided into a transgressive lower interval that is argillaceous and a prograding upper interval composed of fine to coarse arenites and silty shales. Figueiredo *et al.* (2007) later divided the upper interval of the Limoeiro Formation into two parts. Thus, according to these authors, the Limoeiro

Formation can be divided into three main intervals, which record: a latest Albian to Cenomanian transgressive phase; a Cenomanian to Campanian regressive phase; and a Campanian to Early Paleocene mainly transgressive phase. The maximum thickness of the Limoeiro Formation is estimated to be 2.5 km (Brandão and Feijó, 1994).

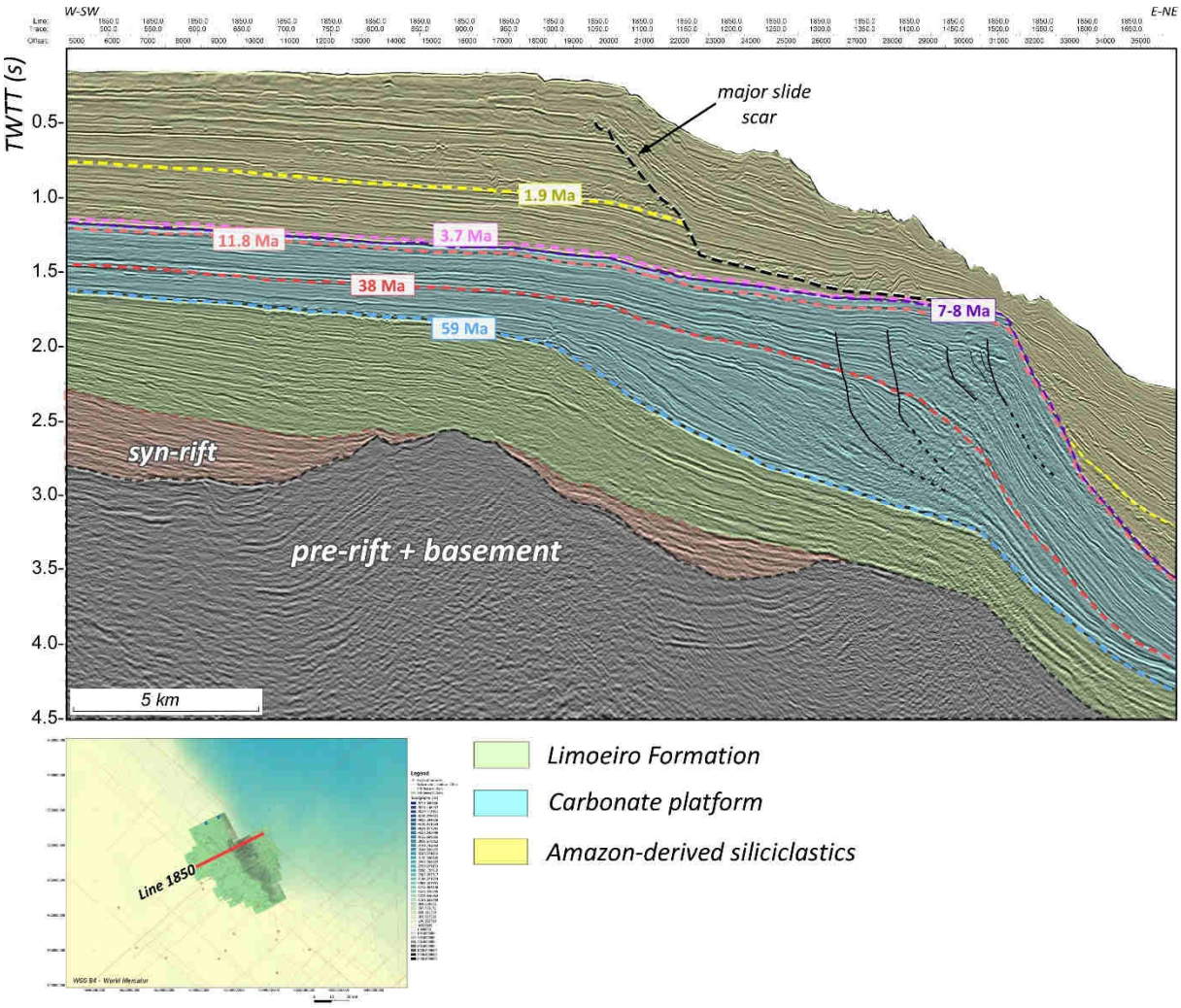

Figure I-12: Figure from Baker *et al.* (2015) of an interpreted seismic profile across the NW Amazon shelf, showing basement and pre-rift strata overlain by syn-rift deposits, in turn overlain by post-rift sandstones and shales of the Limoeiro Formation (in green); the latter is overlain by the Amapá Formation carbonate platform (in blue), in turn overlain by Amazon-derived siliciclastic sediments (in yellow).

I.2.3 **Post-rift 2:** Marajó and Amapá Formations (Paleocene to Late Miocene)

According to Figueiredo *et al.* (2007), the second post-rift megasequence was deposited from the Late Paleocene to Middle Miocene (Figure I-11). Brandão and Feijó (1994) proposed three coeval formations for the sediments deposited during this phase: (1) the proximal Marajó Formation, composed of siliciclastic sediments; (2) the laterally continuous Amapá Formation,

composed of shelfal carbonates and (3) the distal Travosas Formation, composed mainly of muddy sediments deposited across the slope and deep basin.

According to Carozzi (1981), the Amapá Formation is probably the largest coralgal-foraminiferal platform of the geological record and was built mainly through an intense bioaccumulation of red algae and large foraminifers. This author described five carbonate "belts" based on well data, each belt representing different depositional environment from proximal to distal: lagoon, finger coral bank, large foraminifer shoal, coralgal platform, apron and slope (Figure I-13). A proximal siliciclastic depositional environment consisting of fan deltas and lagoonal fine-grained clastics (Marajó Formation) was connected with the open ocean by transverse troughs partially filled with shales and carbonate olistoliths (Carozzi, 1981; Figure I-13).

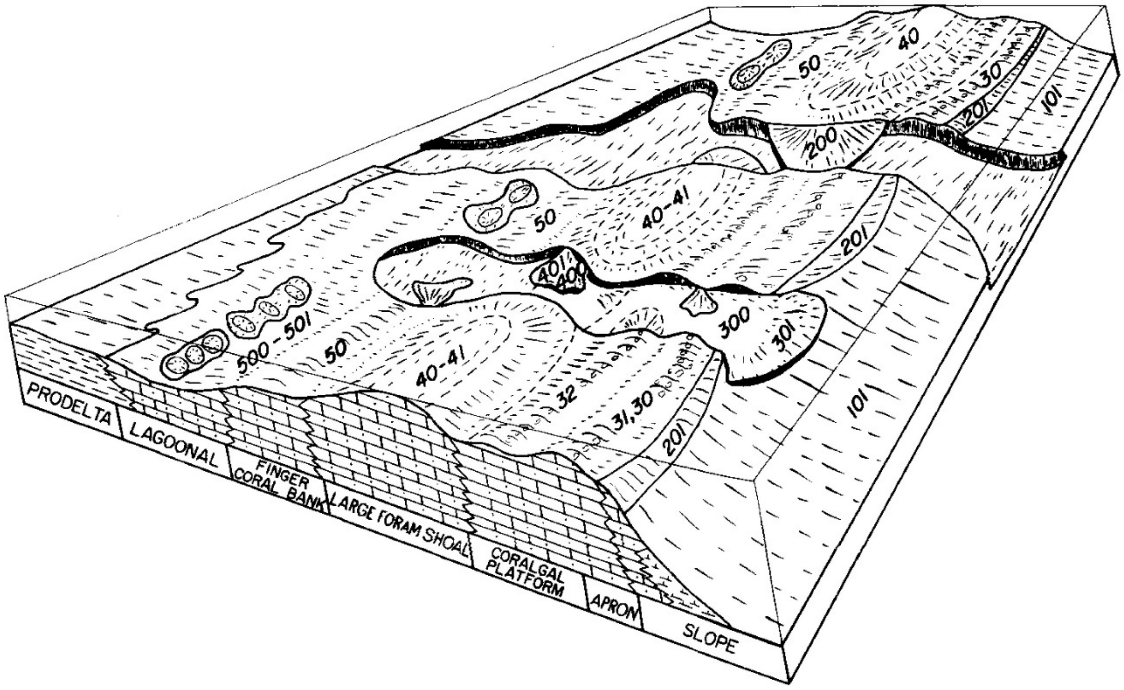

Figure I-13: Three-dimensional representation of the depositional model of the Amapá Formation (Carozzi, 1981).

Carozzi (1981) and Wolff and Carozzi (1984) also described the carbonate Amapá Formation in terms of the spatial evolution of depositional environments and divided it into four major depositional cycles (Figure I-14) interrupted by widespread subaerial exposure:

- Cycle I: Paleocene to Early Eocene, recording the establishment of a mixed carbonate-siliciclastic platform characterized by a broad lagoonal environment, with oolitic shoals and large, discontinuous foraminifer banks surrounded by mechanically reworked

calcarenites. Unlike subsequent phases, this first cycle includes no red algae deposits and the outer shelf record is mainly composed of nummulitid banks (Figure I-14A and B).

- Cycle II: Middle Eocene, recording expansion of carbonate-dominated sedimentary environments and the establishment of a broad belt of large foraminifer and/or red algae banks and their reworked calcarenites. Widening of this belt resulted in a narrower lagoon to landward, and to seaward promoted the progradation of outer shelf bank deposits over slope deposits of the previous cycle. During deposition, the proximal fan delta and the lagoonal shales remained under restricted hydrodynamic conditions behind the carbonate platform (Figure I-14C and D).

- Cycle III: Late Eocene to Late Oligocene, recording the stabilization and further landward and seaward expansion of carbonate-dominated environments. Nonetheless, during this cycle, in the central shelf the carbonate platform lost its contiguous foraminifer-red algae belt as a series of canyons/troughs partially filled with olistholiths and shales began to cut through banks/atolls (Figure I-14E and F).

- Cycle IV: Early to Middle Miocene, recording "destruction" of the carbonate shelf. The large foraminifer belt present in the former cycles was lost, and the outer shelf dominated by red algae banks. Increased breaching of the carbonate shelf was accompanied by canyons on the central part of the shelf. The extent of the proximal fan delta varied during this cycle and the former lagoonal environment gave way to open marine conditions (Figure I-14G and H).

It is worth noting that there are inconsistences in the ages attributed to the Amapá Formation depositional cycles by Carozzi (1981) and Wolff and Carozzi (1984). For instance, Carozzi (1981) attributed an approximately Paleocene age to the final deposition of Cycle I, while Wolff and Carozzi (1984) considered the same depositional cycle to have lasted until the end of Early Eocene (an ~8Ma discrepancy). Theses inaccuracies and revisions are likely due to the fact that these authors worked with pre-1980s well data and investigated calcareous sequences (which are commonly barren or poor in planktonic fossils). Therefore, although the environmental reconstruction of the Amapá Formation carbonates is of great value, caution is necessary in age comparisons between these early works and more recent models based on new geological data and timescales.

Several authors have suggests that shelfal carbonate sedimentation ceased in the Offshore Amazon Basin due to the arrival of large volumes of terrigenous sediments around the Middle to Late Miocene transition (Schaller *et al.*, 1971; Carozzi, 1981; Brandão and Feijó, 1994; Figueiredo *et al.*, 2007). Increasing terrigenous flux into the basin was argued to record the onset of a transcontinental Amazon River. However, both the cause of such a terrigenous influx into the basin and the age assigned for such an event have been a matter of debate. A review of this debate concerning the cessation of carbonate sedimentation in the Offshore Amazon Basin and the onset of the Amazon River is presented in subchapter I.4.

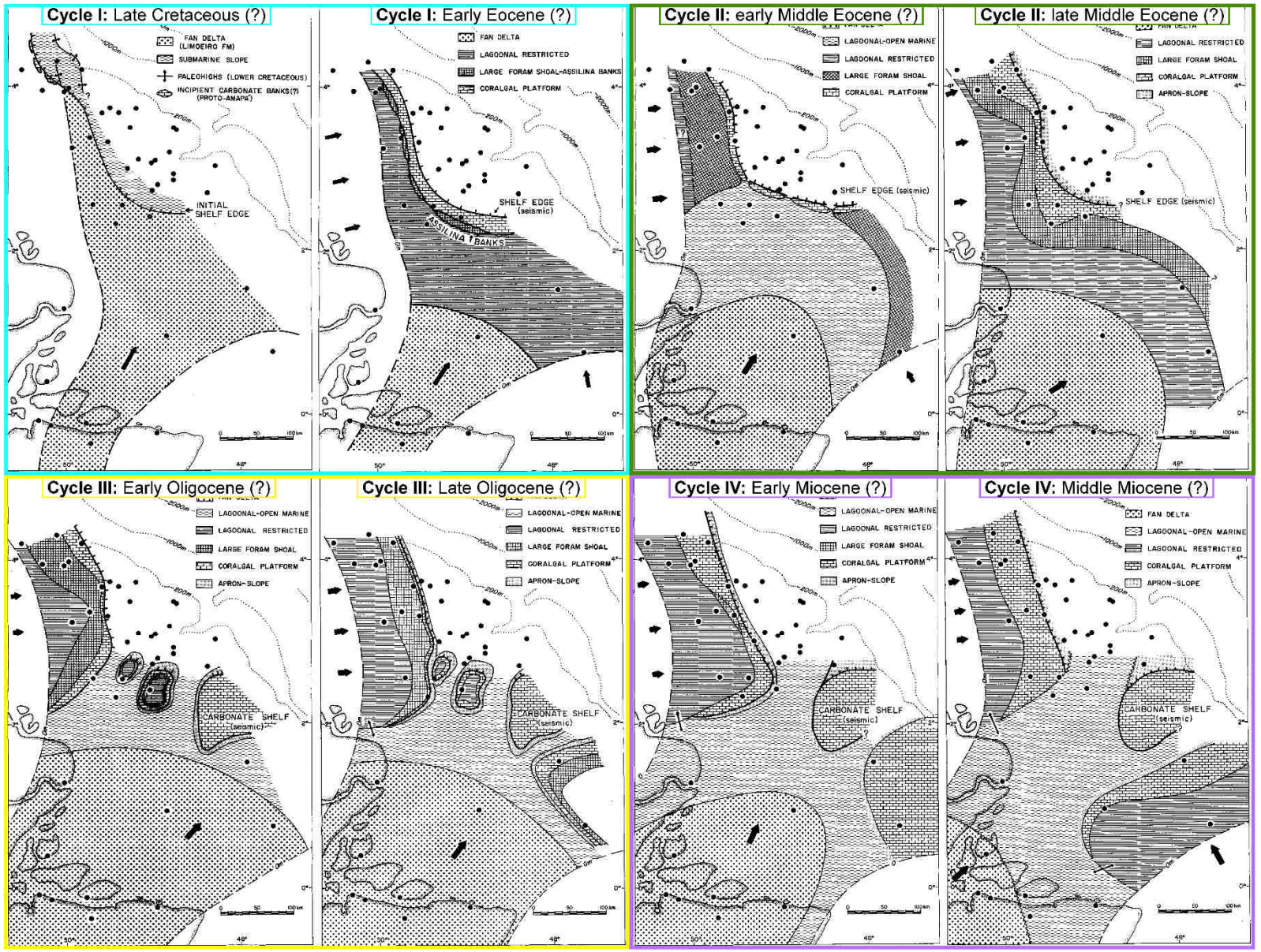

Figure I-14: Paleo-environmental maps of the four major depositional cycles of the Marajó and Amapá Formations: Cycle I (latest Cretaceous to Early Eocene) outlined in light blue; Cycle 2 (Middle Eocene) outlined in green; cycle 3 (Late Eocene to Late Oligocene) outlined in yellow and cycle 4 (Early to Middle Miocene) outlined in purple. Figure modified after Carozzi (1981), ages of cycles according to Wolff and Carozzi (1984).

I.2.4 **Post-Rift 3:** Pará Group (Late Miocene to Recent)

The third post-rift megasequence in the Offshore Amazon Basin differs considerably from coeval units in other basins of the Brazilian Equatorial Margin. Whereas in the Pará-Maranhão, Barreirinhas, Ceará and Potiguar basins tectonic stability and a low terrigenous sediment supply permitted the continued deposition of shelfal carbonates until the Recent, in the Offshore Amazon Basin carbonate production was interrupted in the Late Miocene by a massive influx of terrigenous sediments (Figueiredo *et al.*, 2007; Soares *et al.*, 2007; Junior *et al.*, 2007; Condé *et al.*, 2007; Neto *et al.*, 2007). This influx of sediments promoted burial of the former carbonate platform and the outbuilding of the Amazon Fan on the slope and abyssal plain. These terrigenous sediments compose the uppermost megasequence, which includes the formations of the so-called Pará Group: (1) The proximal Tucunaré Formation, composed of coarse to fine sands; (2) the laterally continuous Pirarucu Formation, composed of fine sands and muddy sediments; (3) the Orange Formation, composed of distal muddy sediments associated with layers of fine sands deposited by turbidity currents (Figueiredo *et al.*, 2007; Figure I-11).

Silva *et al.* (1999) described the third post-rift megasequence as a fluvial deltaic-continental slope progradational prism up to 9 km thick on the northwest part of the Amazon Fan and around 1.2 km thick elsewhere in the basin. These authors stated that the Offshore Amazon Basin was affected by intense flexural isostatic subsidence due to the sedimentary load of the Amazon Fan. This is in agreement with the flexural subsidence models of Driscoll and Karner (1994), who found the load of the Amazon Fan caused subsidence of up to 2.3 km beneath the major depocenter and a peripheral bulge associated with onshore uplift of up to 50 m (Figure I-15). Driscoll and Karner (1994) also suggested that flexural subsidence due to the load of the Amazon Fan could have generated ~200-300 m of accommodation space near the present-day coastline since the Middle Miocene.

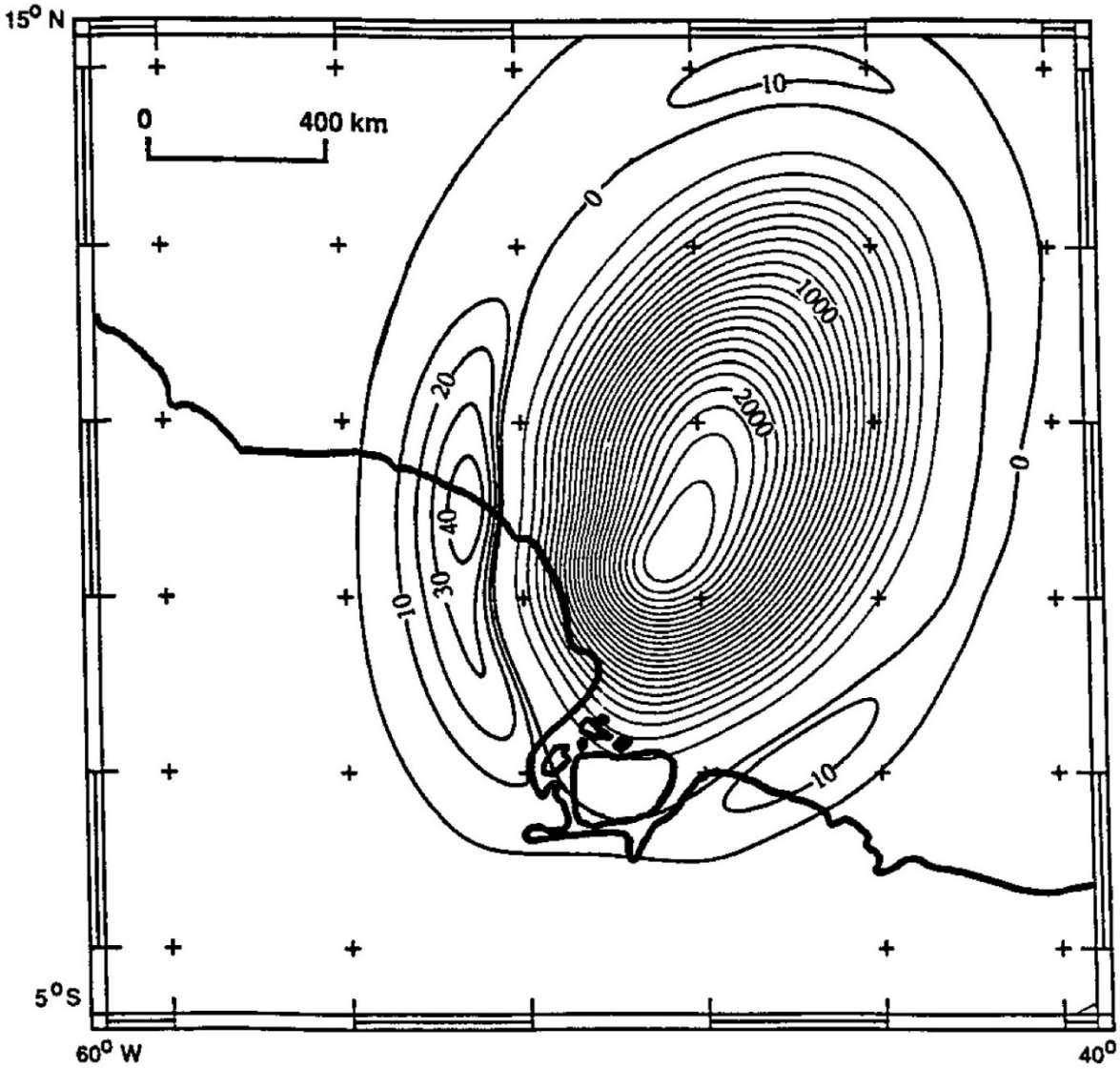

Figure I-15: Calculated flexural lithospheric deformation since due to the Amazon Fan loading according to digital models by Driscoll and Karner (1994) based on in-house data provided to the authors by the Brazilian Petroleum Corporation (PETROBRAS). Contour interval for flexural subsidence is 100m, versus 10m for peripheral bulge uplift.

I.3 THE AMAZON FAN AND GRAVITATIONAL PROCESSES

The Amazon Fan is a prominent physiographic feature of the Offshore Amazon Basin, covering an area of approximately 330,000 km^2 from the continental shelf to abyssal depths of over 4800m (Damuth *et al.*, 1988; Figure I-16). The Amazon Fan is the third largest deep-sea fan in the world (Rimington *et al.*, 2000), comparable in size to the Bengal, Indus and Mississippi fans. Its average gradient of 0.4˚contrasts with the steep continental slopes typical of the Brazilian Equatorial Margin (Damuth and Kumar, 1975; Silva *et al.*, 1999; Lopez, 2001). Damuth *et al.* (1988) divided the Amazon Fan into three major provinces (upper, middle and lower). The upper fan extends from the shelf break to about 3,000 m depth, the middle fan from 3,000 m to 4,000-4,200 m depth, and the lower fan extends to the 4,800 m isobath (Damuth *et al.*, 1988; Figure I-16). According to these authors, each of the three provinces is dominated by different morphological features:

- The upper fan is marked by several scarps up to hundreds meters high, and by the Amazon Submarine Canyon which is up to 600 m deep and extends from the outer shelf to about 1,400 m depth, where it abruptly widens to form a leveed distributary channel 20-50 km wide and up to 300 m deep. The average gradient of the upper fan is approximately 0.8°.

- The middle fan is characterized by numerous well-developed channel-levee systems, 0.8-1.0 km wide and up to 20-60m high, which often overlap and coalesce laterally. The average gradient of the middle fan is approximately 0.3°.

- The lower fan is characterized by smoother relief corresponding to numerous small distributary channels, less than 0.5 km wide and 5-30 m deep, generally without associated levees. The average gradient of the middle fan is approximately 0.1°.

The Amazon Fan has been affected by gravitational processes over different temporal and spatial scales (Reis *et al.*, 2010). These processes have resulted in the intercalation of both tectonic and sedimentary features that form an important part of the sedimentary architecture. The relevant features of syn-sedimentary tectonism and slope failure observed on the Amazon Fan are summarized in the following subtopics.

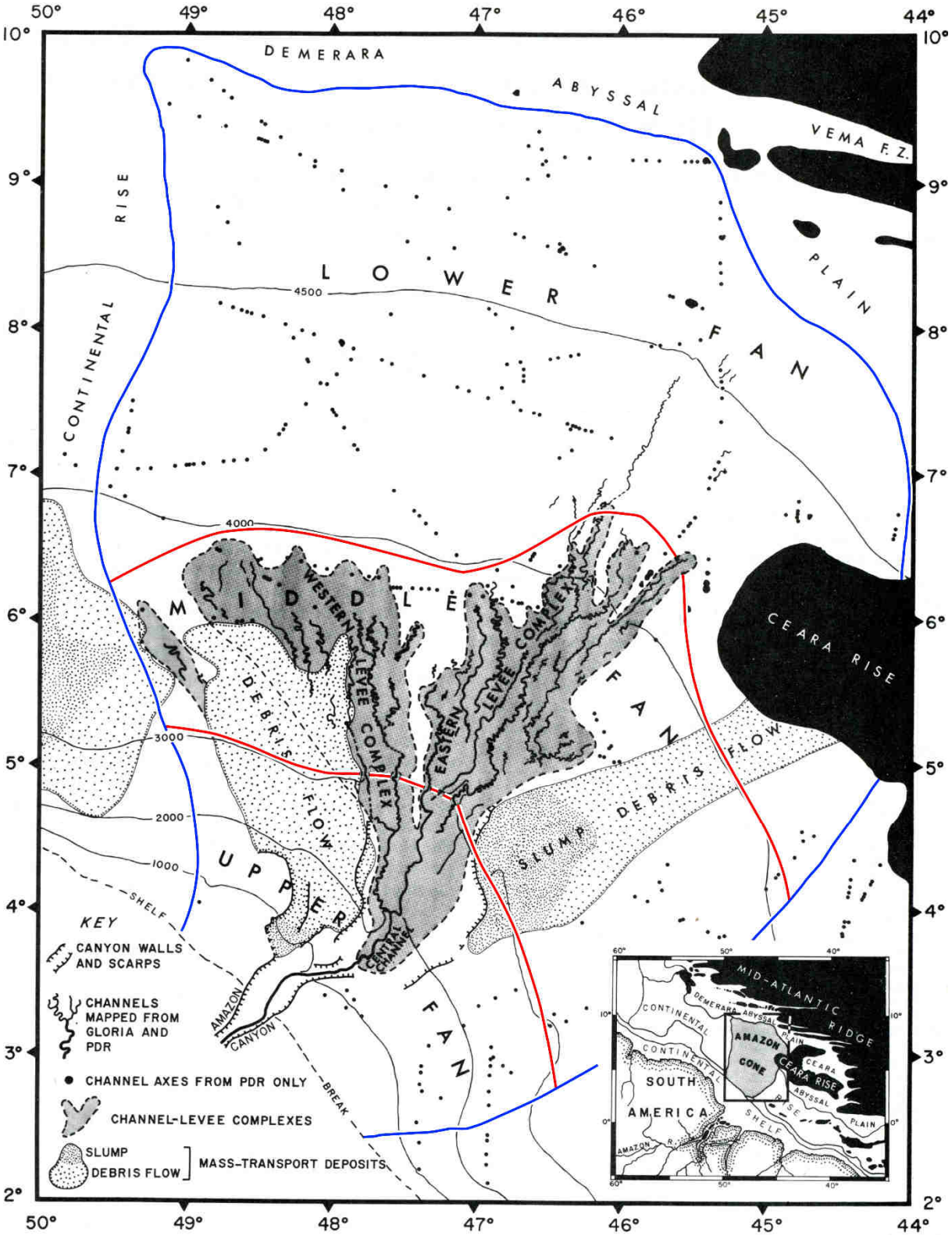

Figure I-16: Major morphological features and physiographic boundaries of the Amazon Fan mapped with side-scab sonar and bathymetric measurements. Limits of the Amazon Fan shown in blue lines and boundaries between the upper, middle and lower fan shown in red lines (modified after Damuth *et al.*, 1988).

I.3.1 Gravity tectonics in the Offshore Amazon Basin

In the Offshore Amazon Basin, gravity tectonics has promoted the downslope movement of thick Cretaceous to Recent sedimentary (Silva *et al.*, 1999; Cobbold *et al.*, 2004; Oliveira *et al.*, 2005; Perovano *et al.*, 2009; Reis *et al.*, 2010). This took the form of structural systems comprising a proximal extensional domain on the outer shelf/upper slope region, mechanically connected via basal *décollement* (or detachment) levels to a distal compressive domain (Figure I-17). This mechanism created a variety of tectono-sedimentary structures that allowed Oliveira *et al.* (2005) to define three tectonic domains in the Amazon Fan region: (1) a proximal extensional domain characterized by a belt of normal listric faults; (2) a less deformed intermediate domain; and (3) a distal compressional domain characterized by a belt of reverse faults expressed as thrust-and-fold belts, some with seafloor relief of up to 500 m.

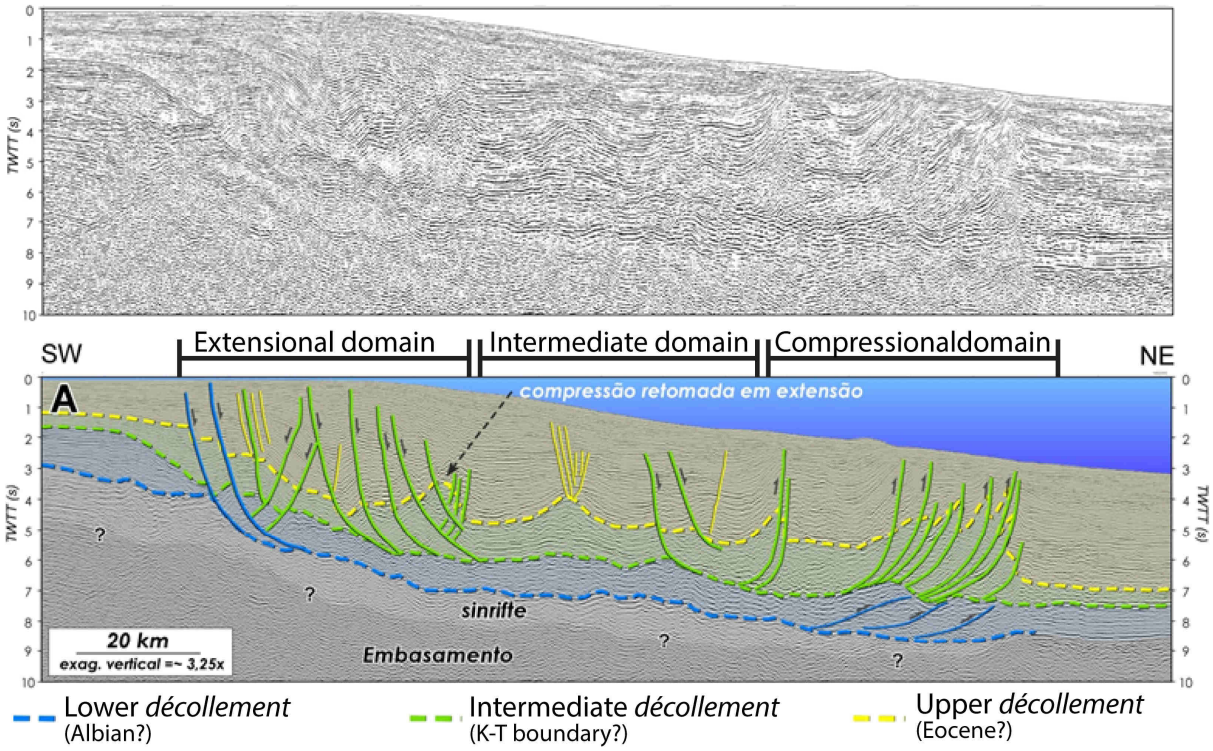

Figure I-17: Interpreted seismic profile illustrating the linked extensional–compressional fault system recording downslope movements above basal *décollement* levels (Perovano, 2012).

Silva *et al.* (1999) identified two stratigraphic levels that have functioned at some point as *décollement* levels. Perovano *et al.* (2009) later named these surfaces as the Lower detachment (Albian age?) and the Intermediate *décollement* (Cretaceous-Tertiary boundary, also identifying a third detachment level named the Upper *décollement* (Eocene age?) (Figure I-17). According to these authors, most structures related to the gravity tectonics are rooted on

the Intermediate *décollement* level (green in Figure I-16). The compressive thrust-fold belt associated with these level plays a key role in the development of the post-rift succession, both by deforming it and by affecting the seafloor morphology that influences patterns of sediment deposition (Perovano *et al.*, 2009). A preliminary study by Cruz (2013) presented evidence that syn-sedimentary gravity-driven deformation had its greatest activity during the Quaternary (the last ≈2.6 Ma), probably due to higher sedimentation rates and increased sedimentary loading, as suggested by Silva *et al.* (1999).

A structural asymmetry between the NW and SE portions of the gravity-driven extentional-compressive system was identified by Cobbold et al (2004) and Oliveira *et al.* (2005) as these authors pointed out that Amazon Fan's sedimentary succession was much more intensely deformed to the NW of the Amazon Canyon. This asymmetry led Oliveira *et al.* (2005) to propose a structural segmentation of two compartments separated by the Amazon Canyon: one smaller and less structurally complex in the SE; the other larger and more structurally complex in the NW (Figure I-18A). Oliveira *et al.* (2005) also pointed out that the thickest sediment depocenters lie between the normal faults of the extensional and the thrust faults of the compressional structural domains. These early studies suggested that gravity tectonics influenced sediment transfer between the shelf and the deep-basin, a finding subsequently reinforced by more detailed work by Perovano *et al.* (2009) and Reis *et al.* (2010) (Figure I-18B).

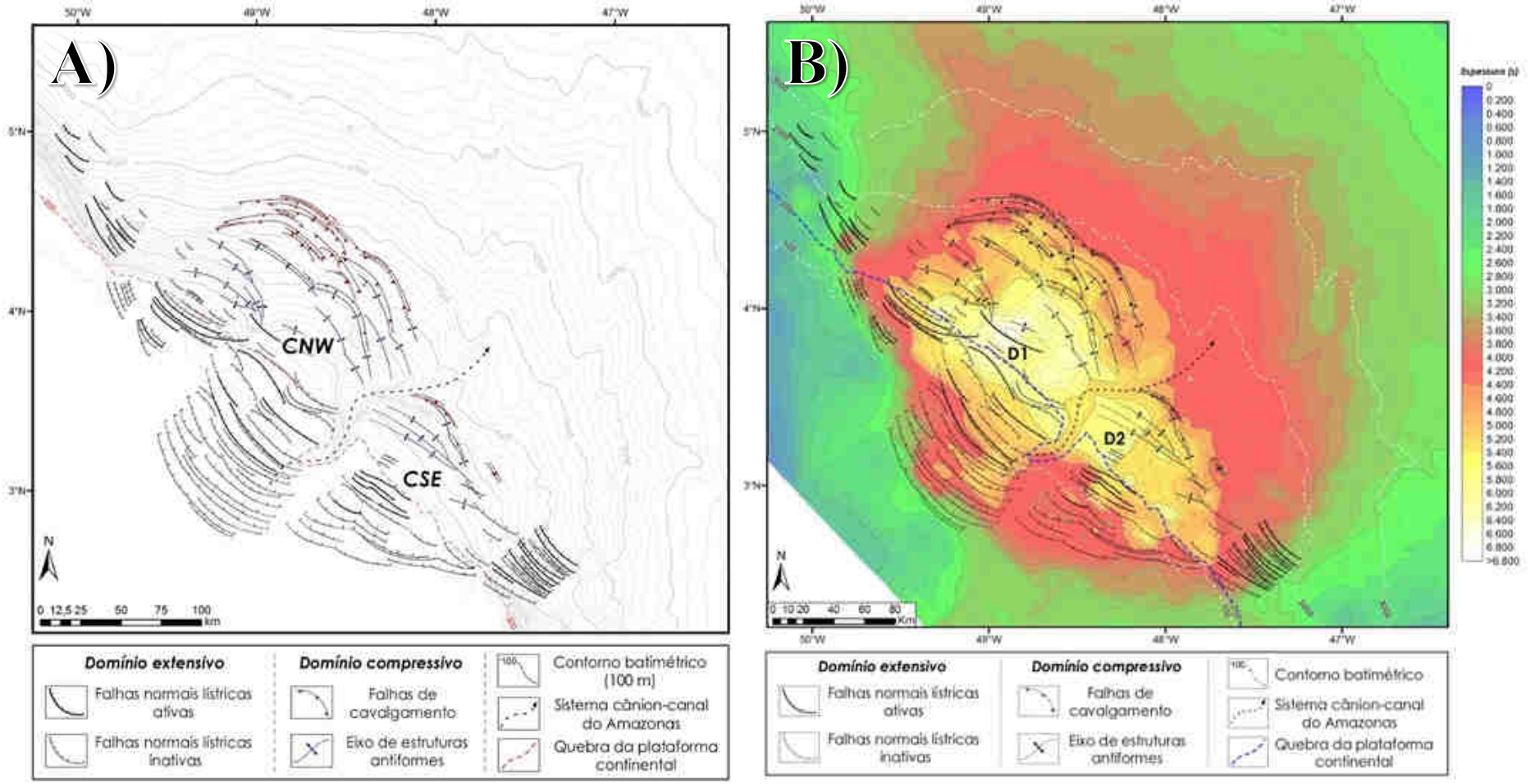

Figure I-18: **A**) Structural map of gravity tectonic structures in the Offshore Amazon Basin, showing a proximal compressional domain of normal faults on the shelf and upper slope, separated from an intermediate domain from a distal compressional domain of thrust-folds (CNW - NW Structural Compartment; CSE - SE Structural Compartment). **B**) Combined structural map and TWTT isopach map between the Intermediate detachment level and the seafloor. D1 and D2 indicate the main depocentres for the time interval considered. Note that the thickest successions are located between the extensional and compressional domains. Figures from Perovano *et al.* (2009).

I.3.2 Amazon Fan: mass-transport deposits and turbidites

The sedimentary succession of the Amazon Fan contains a complex system of turbiditic channel-levee systems interlayered with mass transport deposits, which have been investigated in a number of studies, including through scientific drilling (Damuth and Embley, 1981; Flood and Piper, 1997; Piper *et al.*, 1997; Maslin and Mikkelson, 1997; Maslin *et al.*, 2005). These studies used high-resolution seismic profiles of limited penetration (no more than 1 s or ~ 800 m), which restricted their investigation to the uppermost part of the Amazon Fan, corresponding to the late Quaternary succession. Only in the last decade have studies using deeper penetration seismic data to investigate the sedimentary architecture of the entire succession of the Amazon Fan (Late Miocene to Recent) become available in the scientific literature. Thus Araújo *et al.* (2009) identified large-scale mass-transport deposits in the Amazon Fan downslope of the gravity-tectonic compressive domain (Figure I-19). Reis *et al.* (2010) argued that these mass-transport deposits may have been triggered by tectonism and seafloor relief within the fold-and-thrust belts of the upper Amazon Fan, suggesting a long-lasting interplay between gravity tectonics and mass-wasting processes during the sedimentary evolution of the Amazon Fan.

Araújo *et al.* (2009) and Silva *et al.* (2010) also mapped large mass-transport deposits on the SE and NW flanks of the Amazon Fan (Figure I-20). These features lie in a different morpho-structural context than those located seaward of the gravity-driven fold-and-thrust belts on the Amazon Fan. Silva *et al.* (2010) referred to these peripheral mass-transport deposits as the Pará-Maranhão Megaslide in the SE and the Amapá Megaslide Complex in the NW (Figure I-20). The Pará-Maranhão Megaslide extends from approximately 700-5000 m depth to the adjacent abyssal plain (Figure I-20 and Figure I-21). The Amapá Megaslide Megaslide Complex (Figure I-20 and Figure I-22) is composed of a stacked series of megaslides within the stratigraphic succession, bounded by listric normal faults and tear zones on the upper slope and the NW flank of the Amazon Fan (Araújo *et al.*, 2009; Silva *et al.*, 2010).

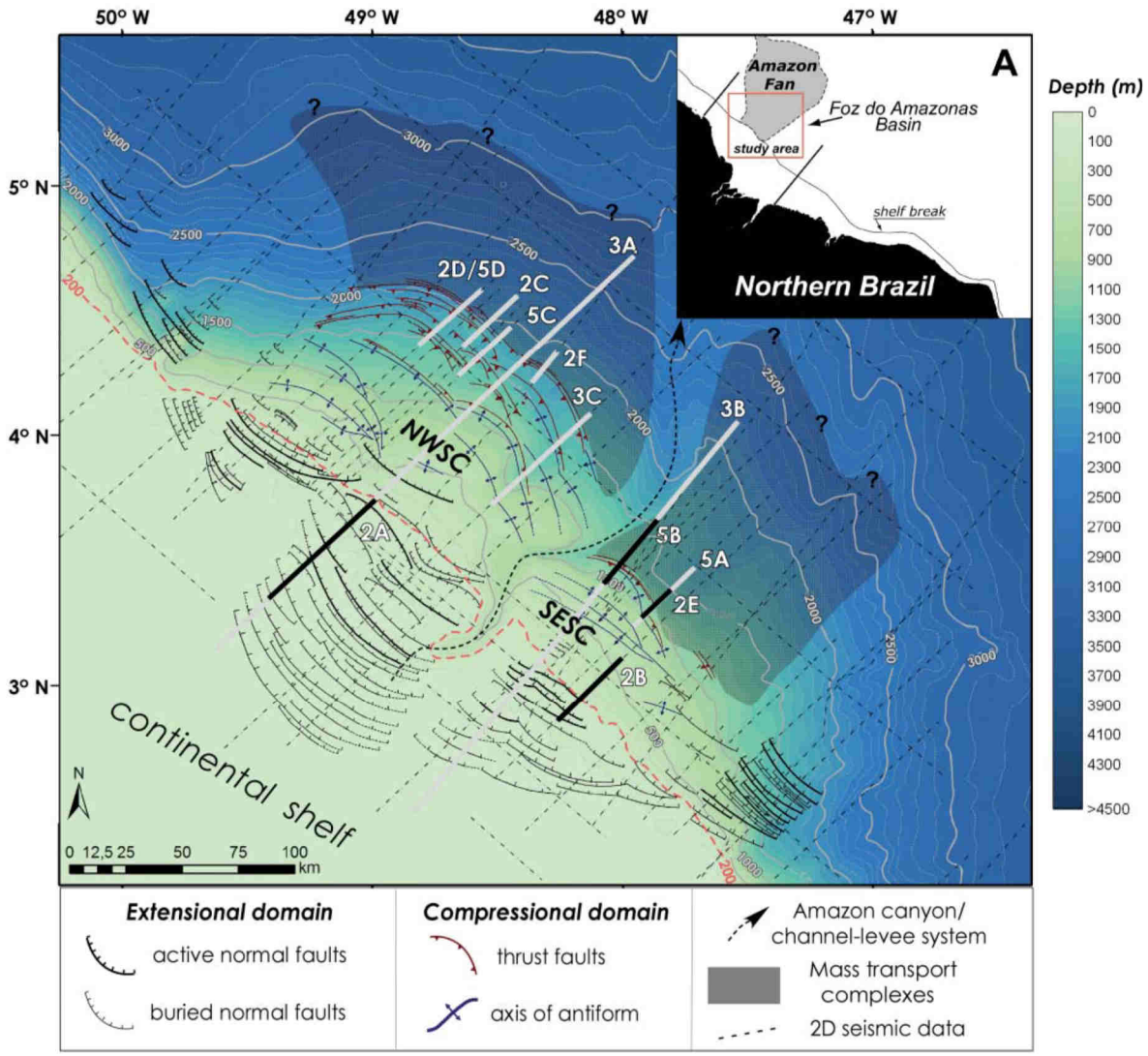

Figure I-19: Structural map of gravity tectonics structures in the Offshore Amazon Basin, showing large mass transport complexes mapped downslope of thrust-fold belts (Reis *et al.*, 2010).

Silva *et al.* (2010) pointed out that the main slide surfaces at the base of both the Pará-Maranhão Megaslide and the Amapá Megaslide Complex are laterally correlative to the Upper *décollement* level of the gravity tectonics system of the Amazon Fan identified by Perovano *et al.* (2009). This correlation suggests that the same surface acted as an impermeable layer, favoring fluid overpressure and facilitating multiscale gravitational collapse processes to act in the basin (Silva *et al.*, 2010).

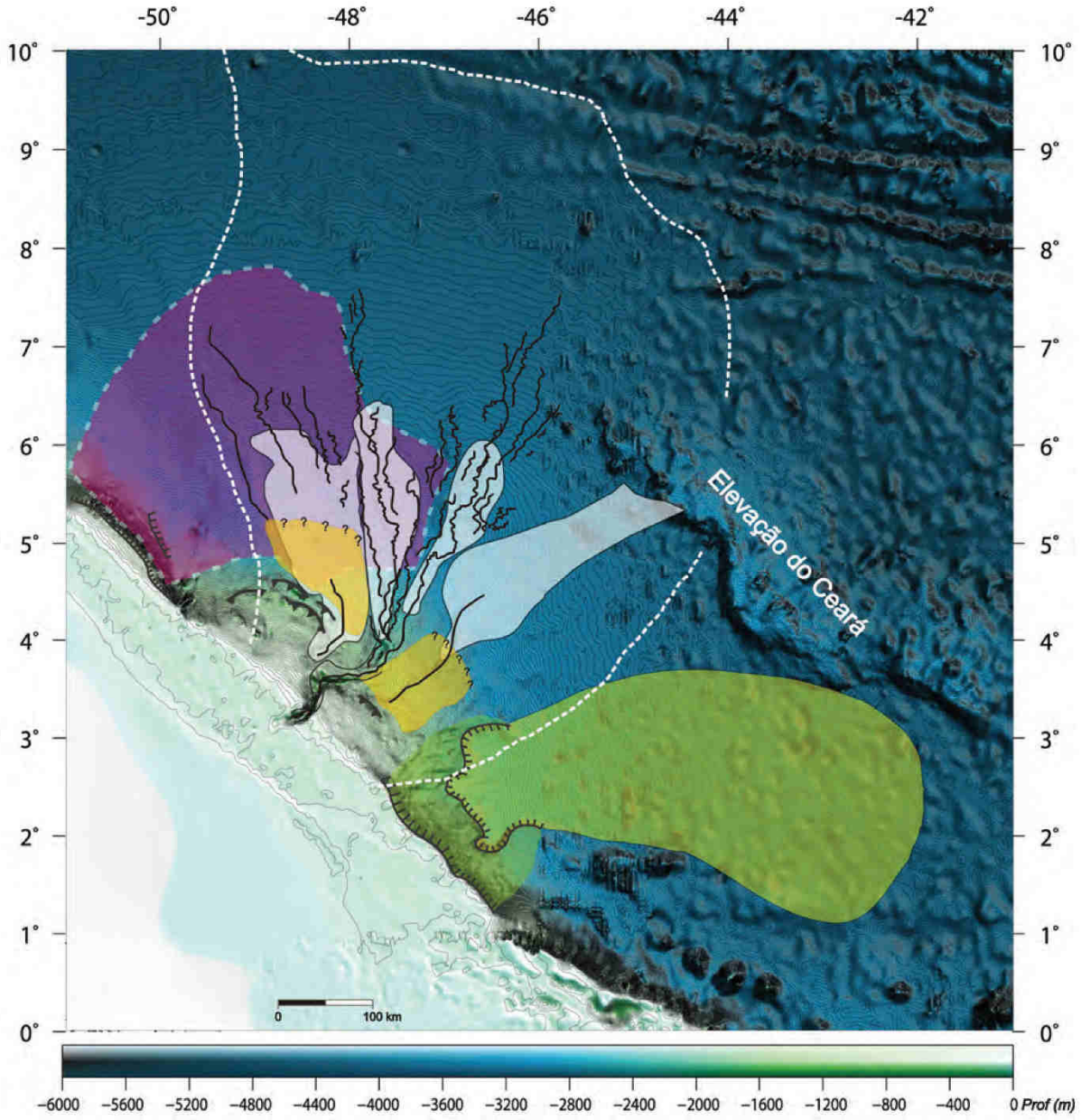

Figure I-20: Bathymetric map showing the distribution of large-scale mass-transport deposits and of megaslides in the Offshore Amazon Basin. MTDs located seaward of the gravity-driven fold-and-thrust belts mapped by Araújo *et al.*, (2009) shown in yellow and those mapped by Damuth (1983) shown in white. Area affected by peripheral megaslides shown in purple (Amapá Megaslide complex) and in green (Pará-Maranhão Megaslide). Modified after Araújo *et al.*, (2009).

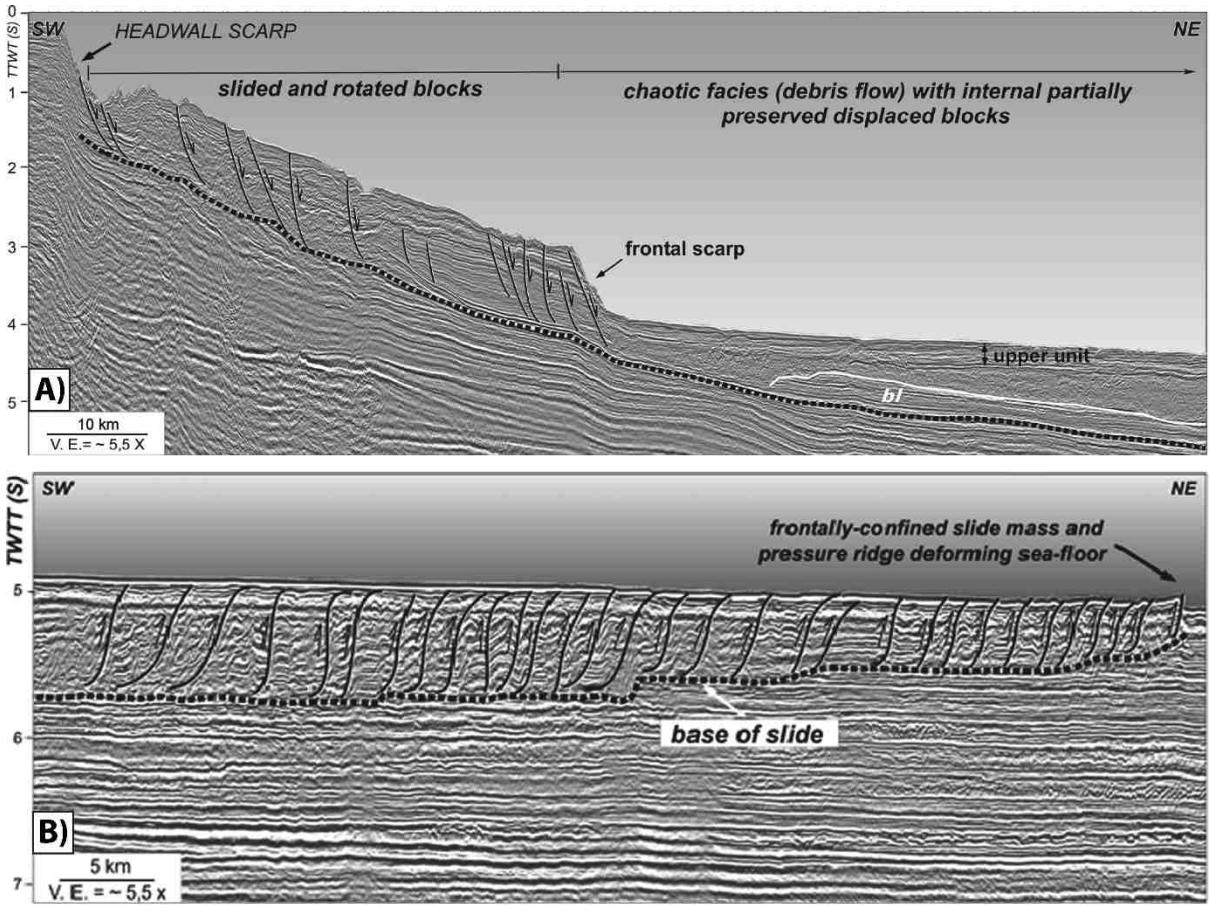

Figure I-21: Interpreted seismic profiles of the Pará-Maranhão Megaslide showing: **A)** Headwall scarp, displaced and rotated blocks, debris flow deposits and preserved block (*bl*) over a basal *décollement* level (dotted line) in the upslope portion of the megaslide (Silva *et al.*, 2010). B) Reverse faults and a pressure ridge associated with lateral confinement of the downslope portion of the megaslide.

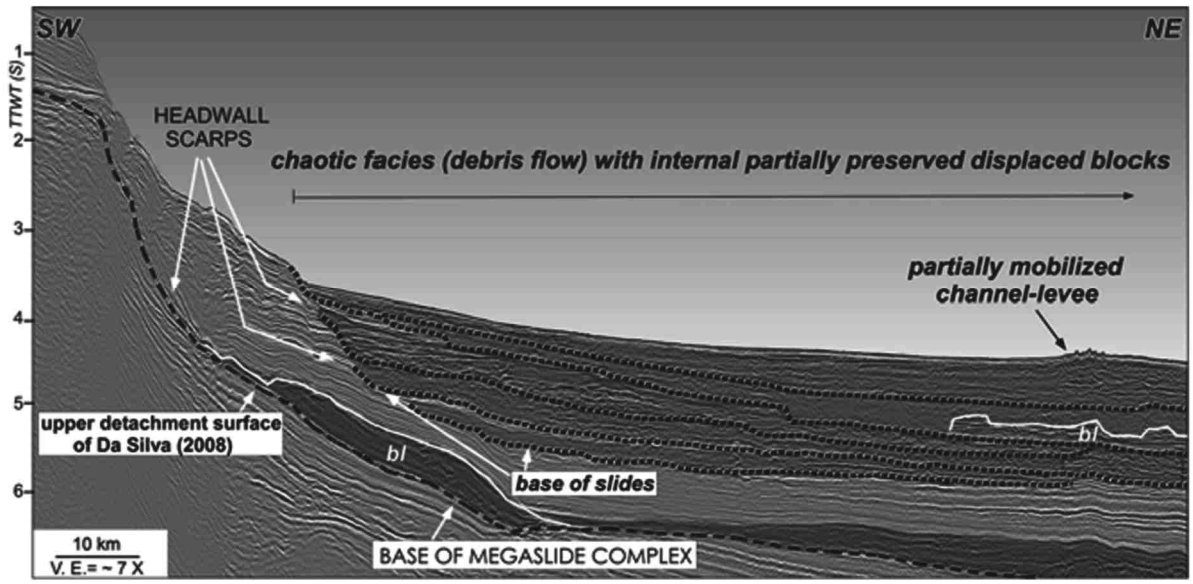

Figure I-22: Interpreted seismic profile across the Amapá Megaslide Complex showing a headwall scarp and upslope deposits of (*bl* = preserved block). Detachment surfaces (dashed lines) and megaslide deposits (dark gray). Silva *et al.* (2010).

Published studies of the entire stratigraphic succession of the Amazon Fan (e.g. Araújo *et al.*, 2009; Perovano *et al.*, 2009; Reis *et al.*, 2010; Silva *et al.*, 2010) make clear that mass-transport deposits represent one of its main architectural components. However, the temporal evolution and of these deposits and their interplay with other major stratigraphic elements (such as turbiditic deposits) is still poorly understood. Albuquerque (2009) conducted an early investigation of the sedimentary architecture of the Amazon Fan using deep penetration seismic profiles and was able to define three evolutionary phases:

1) A first phase corresponded to the onset of the turbiditic system, and is characterized by the first evidence of channelized sediment transport, notably small channels (without levees) interbedded with intervals of parallel flat reflections and chaotic facies (Figure I-23). This record of an incipient turbiditic system overlies a succession dominated by an intercalation of continuous parallel seismic reflections and chaotic packages;

2) A second phase is characterized by the presence of scattered channel-levee systems, mainly observed within the succession of the central part of the Amazon Fan (Figure I-23);

3) A third phase is marked by the deposition of well-developed turbidites, recorded by channel-levee systems up to 0.5s (TWTT) in relief distributed over the middle and lower fan. The channelized turbiditic deposits form complex groups exhibiting over- and onlapping relations, indicating vertical and lateral migration. Mass transport deposits occur at multiple levels interbedded with channel-levee complexes (Figure I-23).

The main architectural features used by Albuquerque (2009) to define the evolutionary phases of the Amazon Fan in terms of turbiditic activity are consistent with the model of Mutti (1985) based on outcrop studies (Figure I-24). Mutti (1985) defined three types of turbidite deposits according to their architecture and sandstone distribution pattern:

- **Type I turbidite** are depositional systems where sands occur in non-channelized bodies with strong lateral continuity and tabular geometries with extents of several tens of kilometers, grading downcurrent into thinner-bedded and finer-grained deposits. These deposits are preferentially found downslope from large-scale submarine erosive features formed during periods of particularly low sea level (Mutti 1985). Type I deposits are argued to originate from

large-scale slope failure of unconsolidated sediments, with most of the remobilized mass bypassing the slope region to be deposited deeper in the basin.

- **Type II turbidites** are depositional systems where sands are predominantly found in the lower parts of channel/canyon systems and in distal regions beyond them, forming channelized sand bodies of great extent that grade downcurrent into sand lobes. Unlike type I turbidites, type II may be associated with channelized deposits across the slope region. Like type I, type II turbidites involve resedimentation processes as they are fed by unconsolidated sediments of previously deposited shelfal successions that undergo mass failure. Type II turbidites are argued to preferentially form during periods of moderately low sea level, such as higher-order highstands within a major lowstand. Mutti (1985) also considered the possibility that some type II systems could be developed during highstands in a scenario of rapid progradation of fan-deltas across narrow continental shelves.

- **Type III turbidites** are typical channel-levee complexes, in outcrop composed of bodies with dimension of tens to a few hundred meters, although Mutti (1985) noted that modern examples are commonly much bigger. Type III systems are argued to involve relative small-scale resedimentation processes related to shelf-edge instability associated with the rapid progradation of deltaic systems during highstand periods.

In terms of stratigraphic architecture, there is a good correspondence between the model of turbidite systems proposed by Mutti (1985) and the evolutionary phases of the Amazon Fan defined by Albuquerque (2009). Albuquerque's first phase could be composed by Mutti's turbiditic systems types I and II as it is composed by an intercalation of continuous parallel seismic reflector and chaotic packages. The second and third phases of Albuquerque (2009) are clearly comparable to Type III turbidites of Mutti (1985) as it is characterized by well-developed channel-levee complexes.

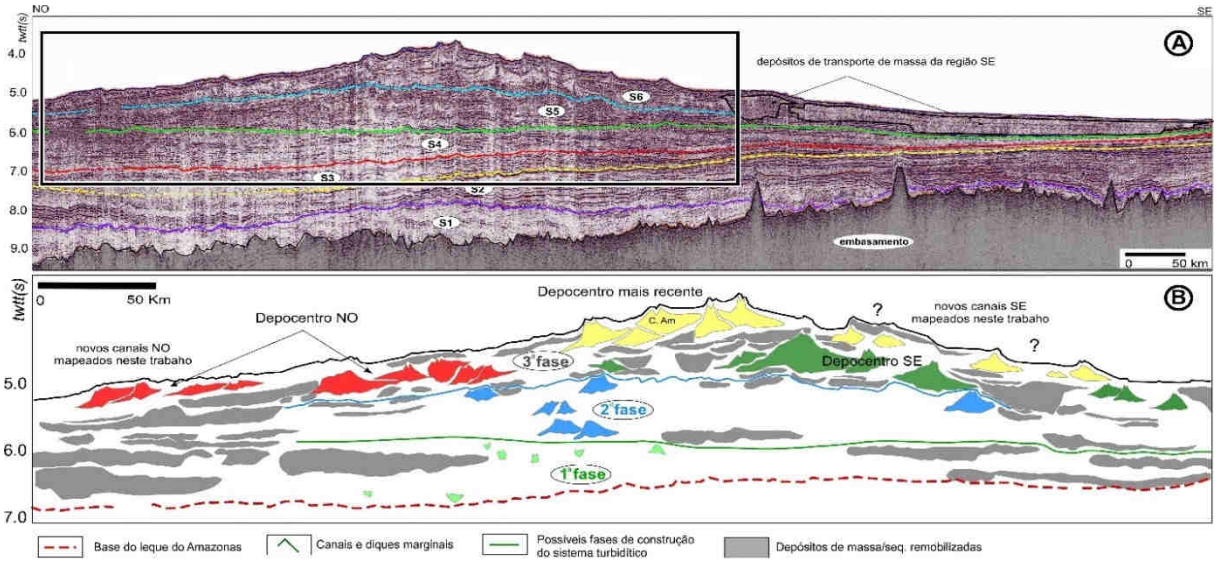

Figure I-23: A) Seismic profile showing the main seismic sequences mapped the Offshore Amazon Basin according to Albuquerque (2009). B) Interpreted geological section, illustrating the three defined phases of the turbiditic systems deposition in the Offshore Amazon Basin (Albuquerque, 2009). Interpreted mass transport deposits shown in gray, First phase turbidites shown in light green, Second phase turbidites show in blue and Third phase turbidites shown in dark green, red and yellow.

In contrast, at least one aspect of the Mutti (1985) model has been proven invalid in the case of the late Quaternary turbidite systems of the Amazon Fan, as the channel-levee complexes were deposited predominantly during periods of lowered sea level (Lopez, 2001), rather than highstands. Nevertheless, it would be interesting to test the impact of other processes argued by Mutti (1985) to act as controlling factors on turbiditic depositional patters (e.g.: slope bypass versus overbank deposition; remobilized volume involved in turbidite episodes; shelf exposure and deltaic progradation). This would require correlations between coeval sequences deposed on the shelf and slope region and in the deep-basin in the Offshore Amazon Basin, which to date has been prevented by limited chronostratigraphic control on its sedimentary succession.

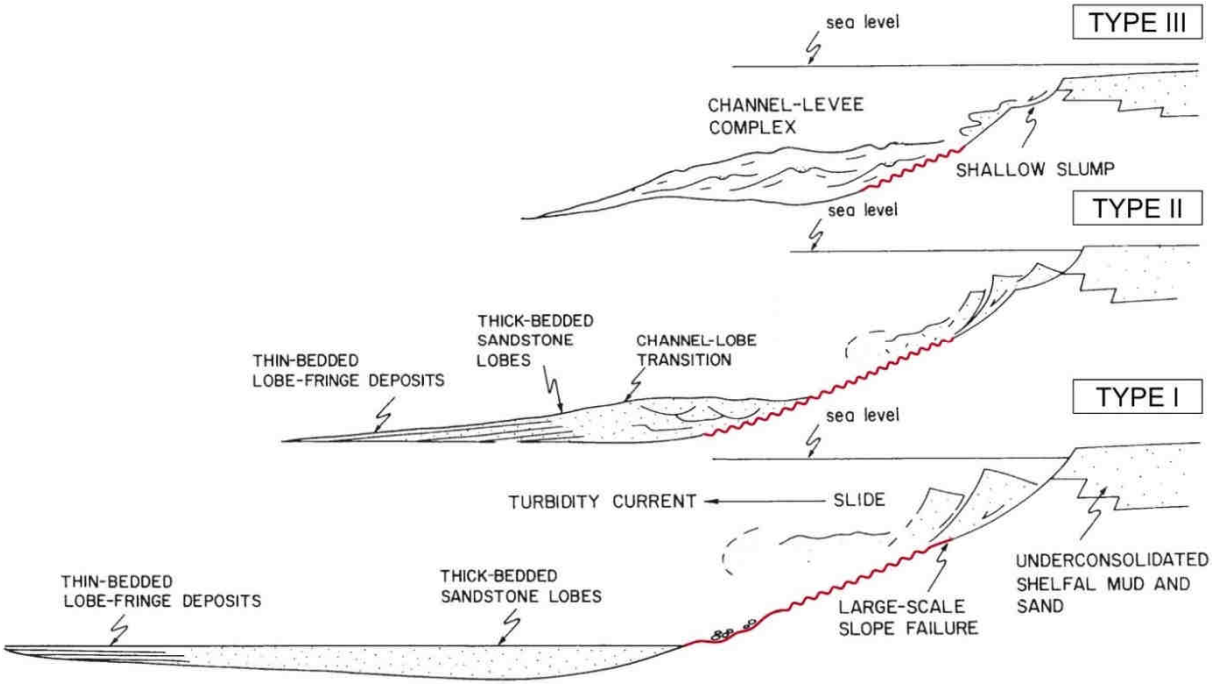

Figure I-24: Model of three types of turbidite depositional systems and their proposed relations with slope erosion, remobilized volume and sea level, according to Mutti (1985). Type I turbidites are associated with large-scale slope failures, widespread slope erosive features (in red) and very low sea level. Type II turbidites are associated with smaller slope failures, less extensive slope erosive features (in red) and moderately low sea level. Type III turbidites are said associated with small outer shelf-slope failures, narrow slope erosive features (in red) and high sea level.

I.4 THE ONSET OF THE TRANSCONTINENTAL AMAZON RIVER

The Amazon River drainage basin covers an area of 5.8 million km^2 of the northern part of South America (Roddaz *et al.*, 2005b). With an average water discharge of 6,642 km^3/year (~200,000 m^3/s), the Amazon is the largest river in the world and almost three times larger than the second (the Congo river, 1,308 km^3/year; Richey *et al.*, 1989; Dai and Trenberth, 2002). A suspended sediment load of up to ~1.2 x 10^9 tons/year is transported by the Amazon River to the Equatorial Atlantic Ocean, of which about 90% is composed of sediments originated from processes of erosion and dissolution in the Andean Mountain Range, with a smaller contribution from the Brazilian and Guiana Shields (Meade, 1994; Meade *et al.*, 1985).

Although the Amazon region has attracted the attention of the scientific community for several decades, the geological history of the Amazon River remains a fertile ground for disagreement and heated debates. The major disagreement concerns the timing and nature of the evolution of the Amazon River from a relatively short intracratonic drainage system to a transcontinental river. There is agreement that, at least until the Late Miocene, the Purus Arc (a

subsurface structural high in central Amazonia, Figure I-25) acted as a barrier between two drainage systems: a western system that ran from the Andean range to the Caribbean and an eastern Proto-Amazon River that drained the Guiana and Brazilian cratonic shields to the Atlantic Ocean (Campbell *et al.*, 2006; Figueiredo *et al.*, 2009; Latrubesse *et al.*, 2010). These two drainage systems eventually merged into a single transcontinental Amazon River extending from the Andean range to the Atlantic Ocean, as today, but there is little consensus about when or how this transcontinentalization took place. The main challenge lies in the limited accessibility of most of the modern Amazon drainage basin. To date, the dense rainforest has limited most outcrop investigation to few river banks and road cuts (Latrubesse *et al.*, 2010; Nogueira *et al.*, 2013), which researchers can reach with difficulty due to great distances and precarious infrastructures. The question of transcontinentalization has also been approached using a few wells and boreholes acquired for oil exploration in the western Amazonian basins (Hoorn, 1994; Latrubesse *et al.*, 2010; Soares *et al.*, 2017), but these data are sparsely distributed and their locations and sampling methods may not be ideal for academic purposes. Finally, different names and approaches applied to the same sedimentary formations across national borders in the western Amazon also raise difficulties for those attempting to get a better understanding of the region's geological history.

In part due to the difficulties associated with onshore investigations, some of the first age estimates for transcontinentalization were proposed by studies of the Offshore Amazon Basin. Evidence of the cessation of carbonate sedimentation on the Amazon shelf, and of the growth of the Amazon Fan, has been proposed to reflect the establishment during the Miocene of a transcontinental Amazon River and the arrival of the first Andean sediments into the basin (Schaller *et al.*, 1971; Carozzi, 1981; Brandão and Feijó, 1994; Figueiredo *et al.*, 2007; Hoorn *et al.*, 2010). However, the proposed Miocene onset of the Amazon River has been progressively revised due to improved age estimates for both the top of the carbonate platform and the base of the Amazon Fan. Thus while Carozzi (1981) inferred an onset of the transcontinental Amazon River in the early Middle Miocene, Hoorn *et al.* (2017) proposed a Late Miocene age between 9.4-9 Ma for the same event, a difference of at least 4.4 Ma between the two estimates.

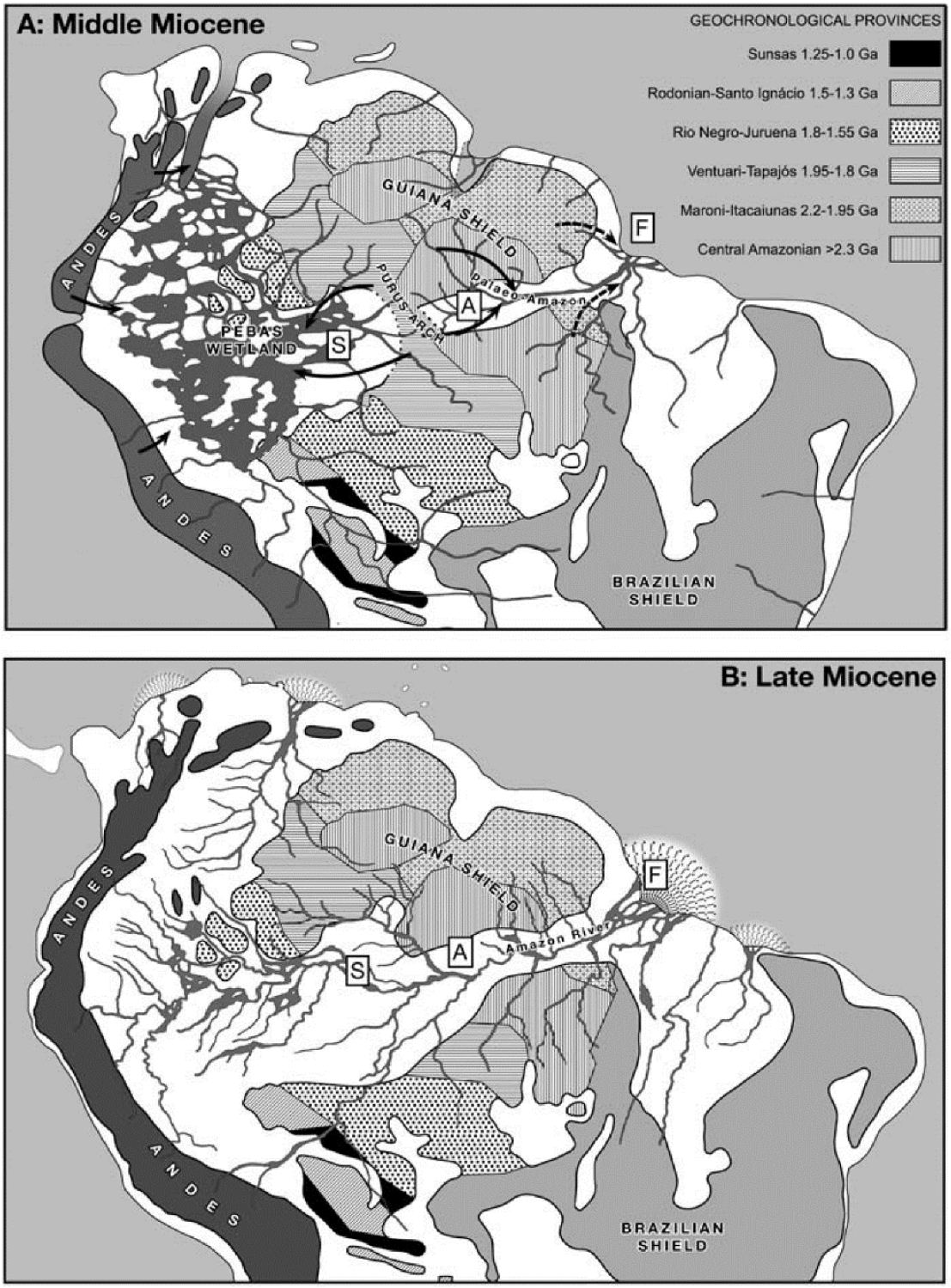

Figure I-25: Development of the trans-continental Amazon River. A) According to Figueiredo *et al.* (2009), until the Middle Miocene the Guiana and Brazilian cratonic shields were the primary source areas of the paleo–Amazon River, which did not extend beyond Purus arch. B) From the Late Miocene, a connection was established between a wetland in western Amazonia and the paleo–Amazon River in eastern Amazonia to form a transcontinental river. F – Offshore Amazon Basin, A - Amazonas basin, S - Solimões basin. Figure from Figueiredo *et al.* (2009).

Recently, the assumption that cessation of the carbonate sedimentation on the shelf in the Miocene was a consequence of the establishment of a transcontinental Amazon River has

been challenged by studies of onshore Amazonian sedimentary basins (Latrubesse *et al.*, 2010; Campbell *et al.*, 2006; Nogueira *et al.*, 2013; Ribas *et al.*, 2012; Rossetti *et al.*, 2015). These studies suggest that the transcontinental Amazon River must be younger than the Miocene, although there is no consensus on how much younger it could be. For instance, through the interpretation of onshore data (river banks, road cuts and wells) from western Amazonian basins, Latrubesse *et al.* (2010) argued that there was no connection between fluvial systems to the west and east of the Purus arch before ~5 Ma. According to these authors, "it was during the early Pliocene that the Amazon fluvial system integrated regionally and acquired its present appearance, and also when it started to drain water and sediments on a large scale to the Atlantic Ocean" (Figure I-26). An even younger age was proposed by Campbell *et al.* (2006), who argued that a lacustrine environment dominated most of the western Amazon region from the Late Miocene to the latest Pliocene. According to these authors, it was only during the earliest Quaternary (~2.5 Ma) that the drainage systems of the western Amazonian sedimentary basins began flowing eastward, either because the eastern rim of the Purus arch was breached, or because of headward erosion by the proto-Amazon River.

Regarding the Miocene cessation of carbonate sedimentation in the Offshore Amazon Basin, Campbell *et al.* (2006) proposed that this could be due to sea level oscillation without any change in the drainage systems supplying the Offshore Amazon Basin. These authors argued that during the Late Miocene, global sea level fell and remained much lower than the Middle Miocene average (according to Hardenbol *et al.*, 1998), which promoted the seaward migration of a proto-Amazon river mouth, carrying large volumes of siliciclastic sediments to the continental shelf. According to Campbell *et al.* (2006), this alone could be responsible for covering the carbonate platform with siliciclastic sediments. Other studies that propose Plio-Quaternary ages for the onset of the transcontinental Amazon River (eg. Latrubesse *et al.*, 2010; Nogueira *et al.*, 2013) do not offer any explanation for the arrival of large volumes of siliciclastic sediments into the Offshore Amazon Basin from the Late Miocene. So, it is interesting to note that the only alternative scenario to the arrival of the siliciclastic sediments to account for suppressed carbonate production is based on the assumption that the carbonate production ceased after the major sea level fall around the Middle/Late Miocene boundary (Campbell *et al.*, 2006). However, as discussed above in section I.2.3, there is also no agreement about the age and relative sea level scenario for the cessation of shelfal carbonate sedimentation. Whereas Carozzi (1981) stated that the top of the carbonate platform is marked by a transgression related to a sea-level rise, Figueiredo *et al.* (2009) stated that the same

stratigraphic level is marked by a "regional unconformity" formed during the Serravallian/Tortonian sea-level fall, known to be one of the most dramatic lowstands during the entire Cenozoic (Haq *et al.*, 1987).

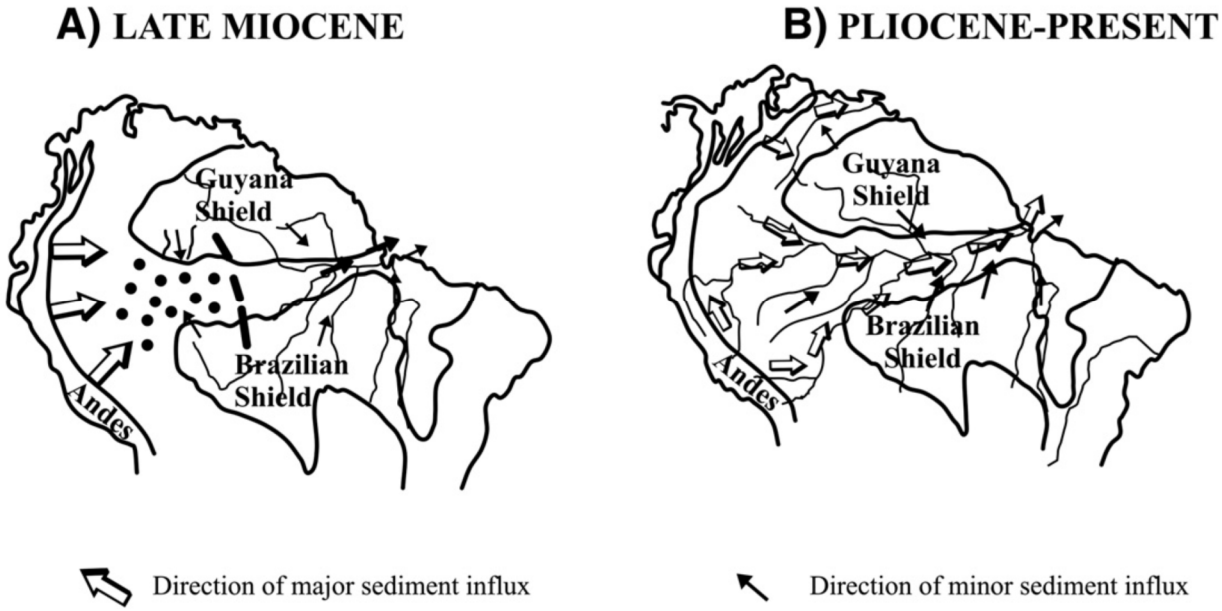

Figure I-26: Paleogeographical reconstructions of sediment influx in the Amazon basin during the Late Miocene (A) and from the Pliocene to present (B) according to Latrubesse *et al.* (2010). According to these authors, the reorganization of drainage systems in northern South America took place around the Miocene/Pliocene transition. The Amazon River is argued to have become totally integrated as a transcontinental drainage system only since the Pliocene.

Finally, it is interesting to note that several works attributed the cessation of carbonate production in the Amazon shelf and the initiation of Amazon Fan deposition to an intensification of the Andean orogeny during the Late Miocene (Hoorn *et al.*, 1995; Figueiredo *et al.*, 2009; Silva *et al.*, 1999; Damuth and Kumar, 1975; Hoorn *et al.*, 2017). However, such a direct correlation between Andean orogenic phases and the record of events in the Offshore Amazon basin must be treated with caution, given the above questions concerning the existence of a transcontinental Amazon River connecting these two domains. Furthermore, in addition to the continual revision of age estimates for the carbonate and siliciclastic successions in the Amazon Offshore Basin, estimated ages of Andean orogeny and uplift phases vary significantly depending on methodology and study area. For instance, while prolonged uplift phases were identified in the Bolivian Andes between 10-6 Ma by Garzione *et al.* (2008) using multiple

proxies, and between 10-4 Ma in the Venezuelan Andes by Bermudez *et al.* (2011) based on apatite fission-track data, in the Peruvian Andes Wise *et al.* (2008) used $^{40}Ar/^{39}Ar$ isotopic data to show that Late Miocene contractional deformation took place at around 8.7 Ma over a very short period of probably less than 150,000 years (Quechua II tectonic event). However, there seems to be an overall agreement that intense Andean orogeny started after 10 Ma and that, in the case of Peruvian-Ecuadorian Andes, orogenic deformation and uplift was mostly restricted to an early phase around 9-8 Ma (Quechua II) and a later phase around 6-5 Ma (Quechua III) (Steinmann *et al.*, 1999; Hungerbühler *et al.*, 2002; Garver *et al.*, 2014; Bermudez *et al.*, 2011; Garzione *et al.*, 2008; Rousse *et al.*, 2002; McKee and Noble, 1990).

CHAPTER II
DATA AND METHODS

Data and Methods

II.1 DATASET

The dataset available for this thesis is composed of a grid of reflection seismic data, information from wells and potential field models (gravity and magnetic). The seismic data include approximately 20,000 km of multi-channel seismic profiles, two blocks of multi-channel 3D seismic data covering an area of 3,800 km^2, and single-channel seismic profiles acquired during several research cruises (made available by the American Marine Geoscience Data System, www.marine-geo.org) (Figure II-1). The multi-channel seismic profiles were acquired during different surveys over many years, using different acquisition and processing techniques, and were made available by the Brazilian Navy, the Brazilian Petroleum and Gas Agency-ANP, Gaia, Fugro and the University of Texas Academic Seismic Portal. The multi-channel seismic profiles are distributed as: a) a regional grid of about 100 km spacing that extends from the outer shelf to the Ceará Rises (recording windows up to 13 s and ~20-100 m vertical resolution); b) a grid with 5-20 km spacing that extends from the inner shelf to about the 3000 m isobath (recording windows up to 10 s and ~10-100 m vertical resolution); c) a grid with ~15 km spacing in the Ceará Rise region (8 s recording window and ~10-50 m vertical resolution). The 3D seismic blocks were made available by *Compagnie Générale de Géophysique* (CGG) and are located on the NW outer shelf-slope region and in the Central middle shelf. The 3D surveys have a 25 m bin spacing of in-lines and crosslines (9 s recording window and ~10-100 m vertical resolution). The single-channel seismic profiles are mostly composed of "underway" profiles acquired during scientific surveys conducted in the Equatorial Atlantic Ocean. These profiles are variable in terms of resolution and penetration, and were useful only in the Ceará Rise region where the sediment units of interest to this study are thinner.

The well dataset includes data from 40 exploration wells made available by the Brazilian Petroleum and Gas Agency and from 7 scientific wells acquired by the Deep Sea Drilling Project (DSDP) and the Ocean Drilling Program (ODP) (Figure II-1). The exploration wells were drilled on the shelf and upper slope, whereas the scientific wells are more distally located on the Ceará Rise and nearby regions. All wells contain lithological descriptions and basic downhole log data (such as sonic, gamma ray, density caliper). Detailed chronostratigraphic data (based on micropaleontological data) are available from all 7 ODP-DSDP wells and from

4 exploratory wells. The locations of these wells in the most proximal and distal regions of the study area, covered by an extensive seismic dataset, afforded good lithological and chronostratigraphic constraints on the stratigraphic succession of the entire Offshore Amazon Basin.

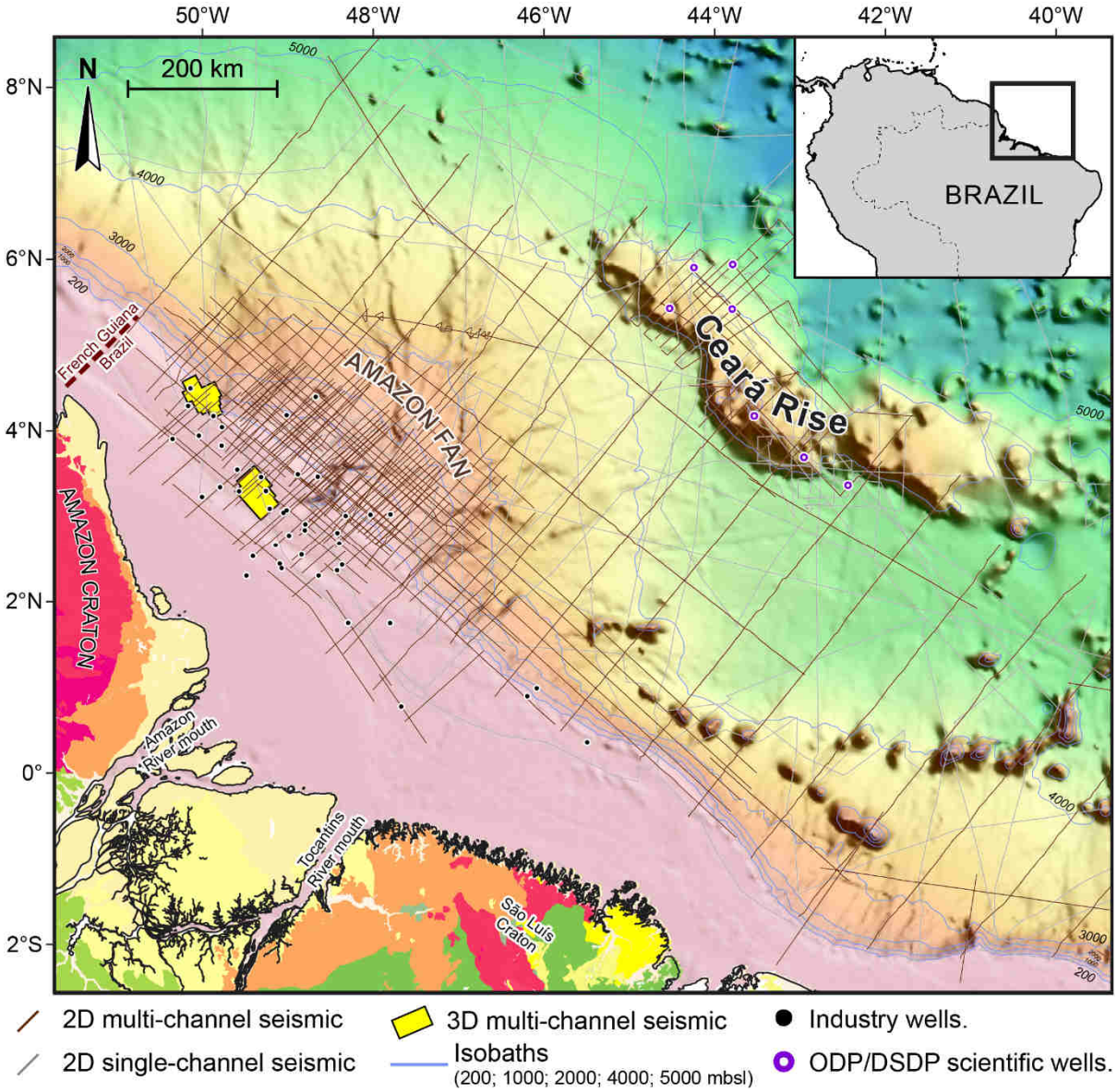

Figure II-1: Map showing seismic reflection data and wells available from the Offshore Amazon Basin. Note that seismic profiles cover the entire region between the continental shelf-slope, where industry wells are located, and the distal Ceará Rise region, where ODP/DSDP scientific wells are located.

Gravity data used in this thesis include the 2016 updated V24 version of the Sandwell *et al.* (2014) models of free-air anomaly and vertical gravity gradient (VGG). Magnetic data analysis is based on the Maus *et al.* (2009) EMAG2 model. Gravity models have resolution of 2-7 km and accuracy of about 2 mGal (Sandwell *et al.*, 2013; Sandwell *et al.*, 2014). The Maus

et al. (2009) EMAG2 magnetic model was based on a compilation of satellite, ship, and airborne magnetic measurements and has resolution of 2 arc min (~3.7 km).

The compilation of the dataset used in this thesis represents the accumulated effort of Professors Tadeu dos Reis, Cleverson Guizan Silva and Christian Gorini, as well as myself, to put to together an extensive collection of geophysical and geological data covering all the domains of the Offshore Amazon Basin. The assembly of all these different types of data into a single dataset consumed most of time and effort expended during the first year of this thesis, but was fundamental for the development of the research presented in the following chapters. This enhanced database was the first contribution of this thesis work to our research group and is already being used by other members to conduct a variety of academic studies.

II.2 METHODS

In order to investigate the post-rift stratigraphic architecture and geodynamic evolution of Offshore Amazon Basin, the following work steps were carried out: **(1)** Seismic stratigraphic investigation; **(2)** Well correlation with seismic data; **(3)** Chronostratigraphic analysis; and **(4)** Geophysical potential field analysis.

(1) Seismic stratigraphic investigation: Seismic reflection data were interpreted using the seismic interpretation software IHS Kingdom®. Standard practices in seismic interpretations were followed in order to identify the major architectural elements of the basin and evaluate their internal character and bounding surfaces in terms of environmental processes (Mitchum *et al.*, 1977; Mitchum and Vail, 1977; Vail *et al.*, 1977; Schlager, 1998; Pomar, 2001; Posamentier and Kolla, 2003; Schlager, 2005; Catuneanu, 2006; Catuneanu *et al.*, 2009; Burgess *et al.*, 2013; Figure II-2). Regional stratigraphic surfaces identified on seismic profiles are inferred to be associated with major changes in sedimentary environment, such as variations in sea level and sediment flux, which facilitates basin-wide stratigraphic correlations.

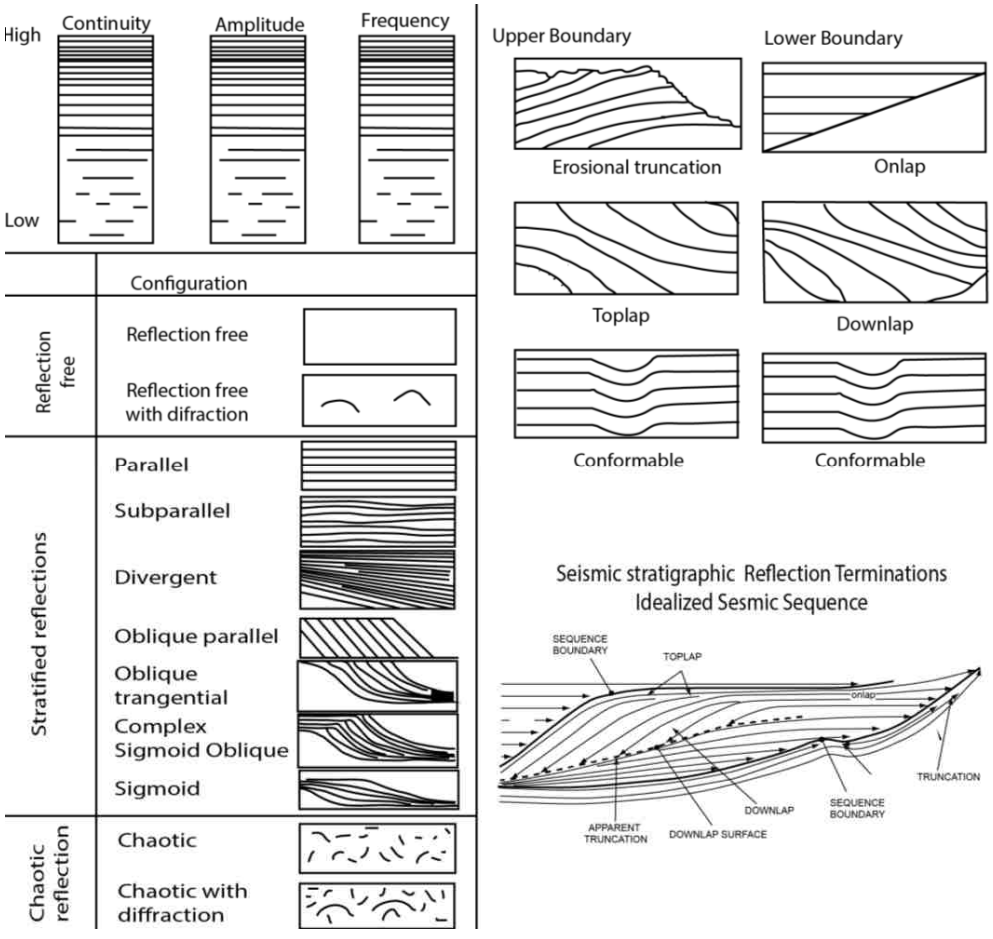

Figure II-2: Synthesis of seismic reflection horizons configurations and termination according to Mitchum *et al.* (1977) and Mitchum and Vail (1977). Figure modified by Papadimitriou (2017).

(2) Well correlation with seismic data: The stratigraphic investigation undertaken in this work was supported by 40 exploratory wells data over the shelf and upper Amazon Fan region, together with seven scientific wells in the distal Ceará Rise region (Figure II-1). All available wells contain lithological descriptions and geophysical log data (gamma ray, sonic, density and others). Well data was correlated with seismic data via synthetic seismograms (Figure II-3), created using rock density and sound wave time travel (logs RHOB and DT respectively) and, when available, checkshot data of travel-time from the surface to a measured depth. Comparisons between synthetic seismograms and the seismic data facilitated accurate correlations between seismic and well data (Figure II-3).

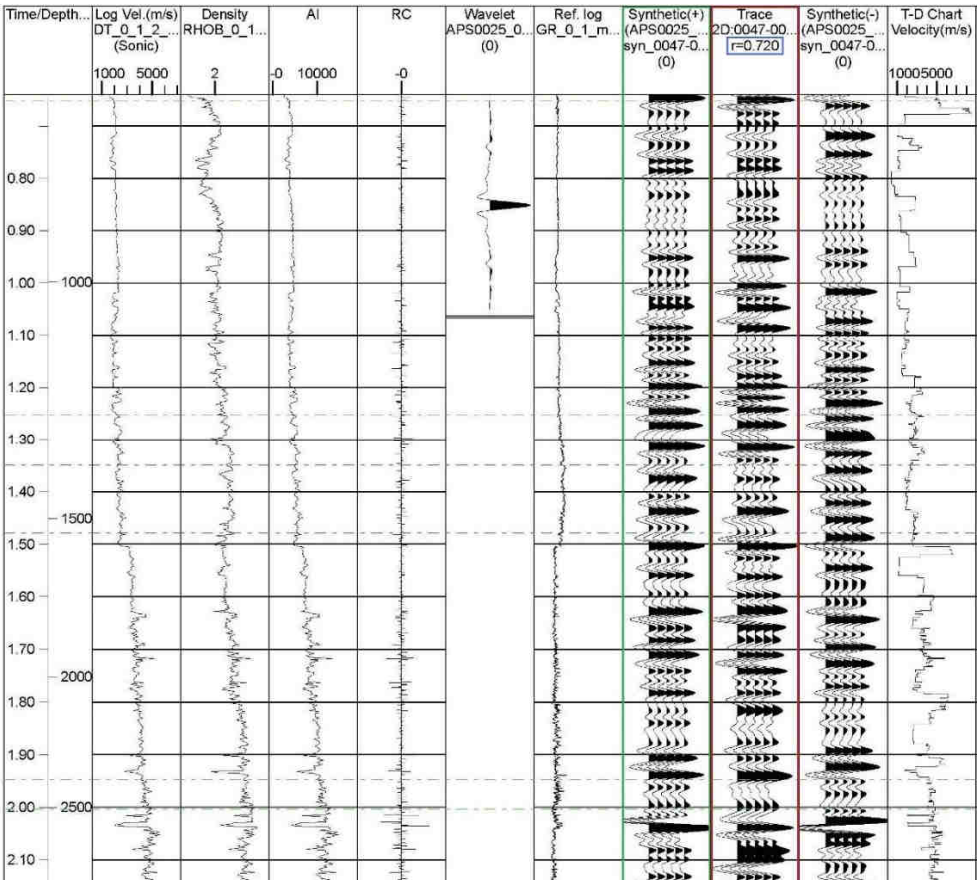

Figure II-3: IHS Kingdom® software interactive window showing a synthetic seismogram used to correlate seismic lines and well data. The synthetic seismogram created is presented in the column outlined in green. Seismic trace data (column outlined in red) extracted from the seismic line closest to the exploratory well are shown, together with the coefficient of correlation between the two (outlined in blue).

(3) Biostratigraphic analysis: Biostratigraphic data (mostly calcareous nannofossils) available from four industry wells and seven DSDP/ODP wells were used to build a chronostratigraphic model for the Offshore Amazon Basin. Ages were attributed by correlations between the biostratigraphic record and compilations of reliable constrained biohorizons defined by the first and/or last occurrence of key fossil species (Anthonissen and Ogg, 2012;

Raffi *et al.*, 2006; Zeeden *et al.*, 2013). Pre-assigned calcareous nannofossil zones (sensu Martini, 1971 or Okada and Bukry, 1980) available in well reports were not used to attribute ages for relevant stratigraphic surfaces due to uncertainties and imprecisions associated with this method. The major issues with pre- assigned calcareous nannofossils zones in exploratory wells rest in the fact that several species used to define these zones between the 1970s and the 1990s are now considered unreliable in terms of chronostratigraphy (see Raffi *et al.*, 2006), and different companies often used in-house zonations schemes that are not compatible with those in the public domain (see Campbell, 2010 and Figueiredo *et al.*, 2010 for an example of confusion caused by in-house zonation). Figure II-4 illustrates a few of the issues associated with the use of calcareous nannofossil zones. Nonetheless, in this work, when detailed planktonic biostratigraphic data was not available, ages were estimated for a few stratigraphic surfaces of lesser importance using calcareous nannofossil zones (sensu Martini, 1971 recalibrated to Anthonissen and Ogg, 2012) and benthic foraminifera data (according to Sousa *et al.*, 2003; BouDagher-Fadel, 2008; Hilgen *et al.*, 2012). In these cases, a low level of confidence was credited to the attributed ages and the surfaces were not used for correlation with regional and global events (such as Andean orogeny phases and glaciations).

(4) Geophysical potential fields analysis: As the post-rift succession of the Offshore Amazon Basin is thought to be influenced by deeply buried tectonic features (such as grabens and hosts), the crystalline basement structural framework was investigated using gravity and magnetic anomalies models in the public domain (Sandwell *et al.*, 2014; Maus *et al.*, 2009). Gravity and magnetic models were loaded in the seismic interpretation software IHS Kingdom® to allow correlations between potential field anomalies and seismic data interpretations. The gravity and magnetic anomalies signature of basement features identified in seismic profiles were then associated with similar potential field signatures (especially gravity; Figure II-5) where seismic profiles did not clearly image the basement. This approach is similar to those of recently published studies (e.g. Galvão and de Castro, 2017; Doo *et al.*, 2018; Tamay *et al.*, 2018) in the sense that observations of potential field anomalies were used to deduce the tectonic framework where it could not be observed by comparison with potential field anomalies caused by observed tectonic features nearby.

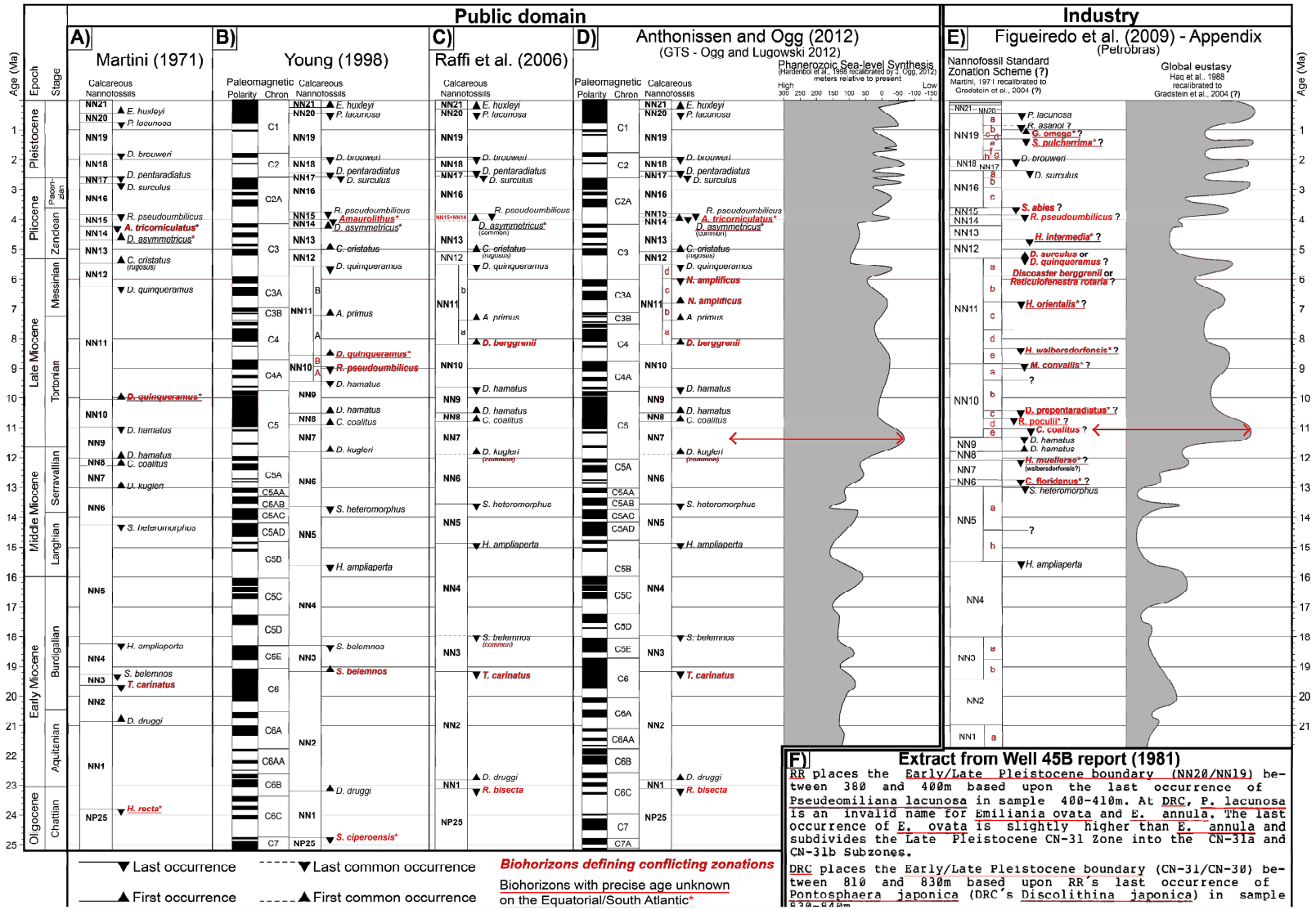

Figure II-4: **A** to **D)** NN zonations according to several authors. Note that several NN zones had its bounding biohorizons modified, which changes their nature and make zones defined in older reports uncorrelatable with modern time scales. Also note that ages of Paleomagnetic polarity inversions changed little since Young (1998), but the boundary ages of some zones (such as NN1 and NN10) changed significantly due to varying bounding biohorizons. **E)** Petrobras NN zonation published by Figueiredo *et al.* (2009) with bounding biohorizons deduced after their appendix tables. It is clear that Petrobras NN zonation is based on several biohorizons with precise ages unknown in public domain. Also note the mismatch in sea-level curves in relation to NN zones as the pronounced early Tortonian sea level fall is NN10 in age on Petrobras charts while in international charts it is NN7 in age. **F)** Extract of a well report written in 1981 exemplifying assumptions that have been shown to be false by more recent studies. For instance, in **F**, Denver Research Center (DRC) considers that *Emiliania ovata* is a synonym of *Pseudoemiliania lacunosa*, but Young (1998) consider these to be different species. DRC also places the Early/Late Pleistocene boundary at the "last occurrence" of *Pontosphaera japonica*, but Young *et al.* (2003) informs that *P. japonica* is still extant and can be found in nowadays oceans (which effectively invalidates DRC's Pleistocene zonation). Time scales are shown as presented originally.

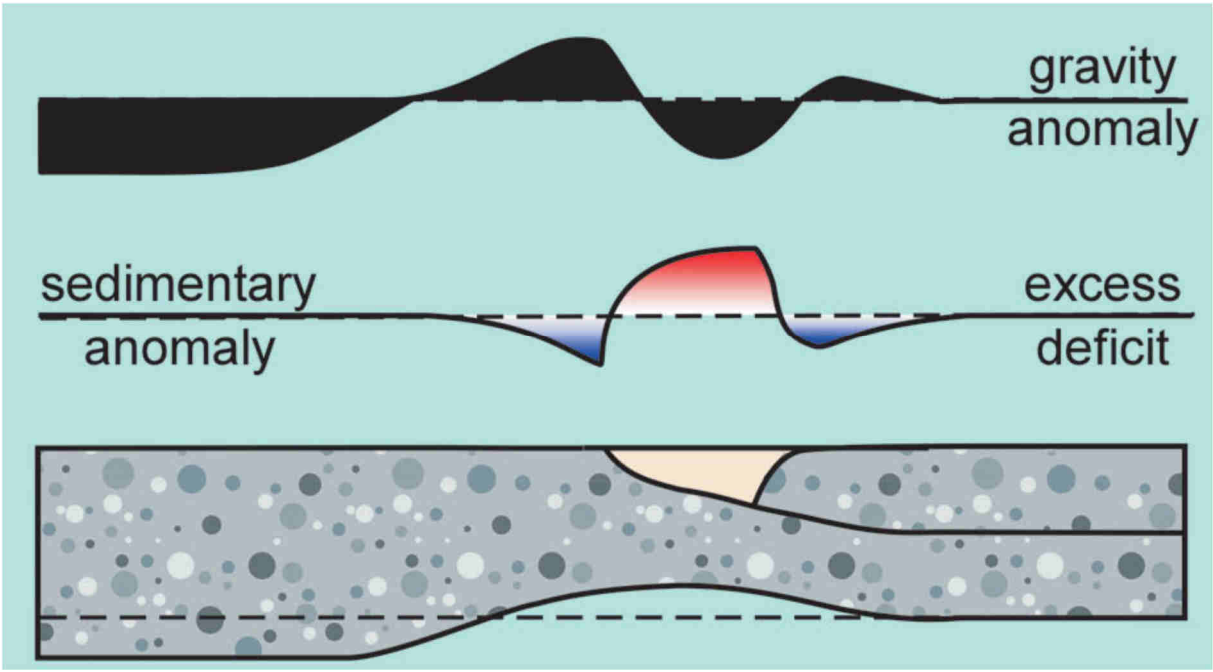

Figure II-5: Conceptual example of free-air gravity anomaly over a half graben (Welford and Hall, 2013). Note the gravity anomaly low values created by the "sedimentary excess" (i.e., deficit in gravity attraction in relation to surrounding areas due to lower density of sediments in comparison with higher density crystalline basement). This concept is used in this work to deduce the structural low of the tectonic framework in regions where it can't be visualized in the available seismic data.

CHAPTER III
NEOGENE EVOLUTION OF THE AMAZON SHELF

CHAPTER IV

This chapter consists of an article submitted to *Marine and Petroleum Geology*. The investigations here presented were based on analyses of seismic reflection profiles coupled with lithological and biostratigraphic data from exploratory wells. We defined a new age model for the basin and identified five main sedimentary units, each representing a distinct phase of carbonate production in the shelf. This allowed us to better understanding the last development stages of the Neogene Amazon mixed carbonate-siliciclastic platform and the processes involved in the suppression of carbonate sedimentation in tropical shelves. The study tackle some key subjects that appeals to marine geoscientists in both the scientific community and oil industry as our refined age models for architectural elements and death of shelfal carbonate sedimentation have potential implications both for exploration and the reconstruction of the South American paleogeographical history.

Neogene Stratigraphy and Depositional Environments of the Amazon shelf: the life and death of the Amapá Carbonate Platform

A.M. Cruz[a]; A. T. Reis[b]; J. Suc [a]; C. G. Silva[c]; D. Praeg[c,d,e]; D. Granjeon[f]; M. Rabineau[g]; S. Popescu[h]; C. Gorini[a]

[a] *Institut des Sciences de la Terre de Paris, Sorbonne Université. 4 Place Jussieu, 75005 Paris, France.*

[b] *Department of Geological Oceanography, School of Oceanography, Rio de Janeiro State University (UERJ). Rua São Francisco Xavier, 524, 4° Andar, Bl. E, Maracanã. Rio de Janeiro/RJ. CEP: 20.550-013, Brazil.*

[c] *Departamento de Geologia-Lagemar, Universidade Federal Fluminense (UFF). Av. Litorânea, s/n, Boa Viagem, Niterói, RJ, CEP: 24210-346, Brazil.*

[d] *Institute of Petroleum and Natural Resources, Pontifícia Universidade Católica do Rio Grande do Sul – PUCRS, Av. Ipiranga 6681, Porto Alegre, Brazil.*

[e] *Géoazur, UMR7329 CNRS, 250 Rue Albert Einstein, 06560 Valbonne, France.*

[f] *IFP Energies Nouvelles. 1-4 avenue de Bois-Préau, 92852 Rueil-Malmaison, France.*

[g] *Institut Français de Recherche pour l'Exploitation de la Mer (IFREMER), DRO/GM/LGG, BP 70, 29280 Plouzané, France.*

[h] *GeoBioStratData Consulting. 385 Route du Mas Rillier, 69140 Rillieux la Pape, France.*

Keywords: Mixed carbonate-siliciclastic platform; architecture of tropical carbonates; death of tropical carbonates; Neogene shelf paleogeography; Brazilian Equatorial Margin

Abstract

The continental shelf offshore the present-day Amazon River is known to have hosted a one of the world's largest mixed carbonate-siliciclastic platforms from the Late Paleocene to at least the Late Miocene. The character of this platform remains poorly understood and the causes and timing of the cessation of carbonate sedimentation controversial. Here we examine the Neogene succession of the Offshore Amazon Basin, based on the stratigraphic analysis of a grid of commercial 2D and 3D seismic reflection profiles correlated to revised micropaleontological data from exploration wells. Four main stages of distinct carbonate depositional patterns are defined and dated with reference to a new age model. The results provide improved constraints on the age of the transition from predominantly carbonate to siliciclastic sedimentation, which is shown to have varied through time across three different sectors of the shelf. On the Central and SE shelves, carbonate production gave way to terrigenous sedimentation between 9.1-7.78 Ma, whereas on the NW shelf carbonate production persisted until 5.5–3.7 Ma. Longer-lasting carbonate sedimentation on the NW shelf can be explained by a lesser influx of siliciclastic sediments, favored by the development of a 150-km wide embayment in the Central shelf. This embayment directed terrigenous sediments sourced from the paleo-Amazon River to the continental slope and deep ocean. As a result, carbonate production remained dominant across the NW shelf until 5.5 Ma, keeping up with base level oscillations. From 5.5–3.7 Ma (Early Pliocene), sediment supply from the paleo-Amazon River promoted the progressive burial of carbonates on the inner NW shelf beneath a prograding siliciclastic wedge up to 85 m thick, coeval with the progressive filling of the Central shelf embayment. Once the central embayment became completely filled, continuous sediment supply to the NW shelf resulted in the final transition from carbonate to siliciclastic-dominated environments on the Offshore Amazon Basin.

III.1 INTRODUCTION

Carbonate units were first reported in the Offshore Amazon Basin (hereafter Offshore Amazon Basin) by Schaller *et al.* (1971), who named them the Amapá Formation (hereafter Amapá carbonates). The Amapá carbonates comprise a succession of bioaccumulated units up to 4000 m thick (Brandão and Feijó, 1994), considered to be the largest known coralgal-foraminiferal platform in the geological record (Carozzi, 1981; Wolff and Carozzi, 1984). Deposition of the Amapá carbonates took place contemporaneously with siliciclastic sedimentation on the inner continental shelf (Marajó Formation), consisting of proximal fan deltas and lagoonal facies, connected to the open ocean by shelf-transverse troughs filled with shales interbedded with carbonate olistoliths (Schaller *et al.*, 1971; Carozzi, 1981).

Most studies concur that shelfal carbonate sedimentation started in the Offshore Amazon Basin during the Paleocene (Brandão and Feijó, 1994; Figueiredo *et al.*, 2007; Figueiredo *et al.*, 2009). However, estimates of the timing of cessation of carbonate deposition in the basin vary, from the Middle Miocene to the Early Pliocene (*e.g.* Schaller *et al.*, 1971; Carozzi, 1981; Figueiredo *et al.*, 2009, Gorini *et al.*, 2014). The origin of the terrigenous sediments that buried the carbonate platform is also a matter of dispute, one given greater importance due to the assumption that the end of carbonate deposition was coeval with the onset of rapid deposition of the Amazon deep-sea fan (Schaller *et al.*, 1971; Silva *et al.*, 1999; Figueiredo *et al.*, 2007; Figueiredo *et al.*, 2009). Based on stratigraphic analyses of offshore seismic and well data, the increase in supply of siliciclastic sediments to the offshore basin has been attributed to the onset of a transcontinental Amazon River, argued to have connected the Andean Range and the Atlantic Ocean around the Middle to Late Miocene transition (Castro *et al.*, 1978; Silva *et al.*, 1999; Dobson *et al.*, 2001; Figueiredo *et al.*, 2007; Figueiredo *et al.*, 2009; Hoorn *et al.*, 2017). This hypothesis has been questioned by paleogeographical reconstructions based on studies in onshore Amazonian basins, which consider a transcontinental Amazon River to have occurred during the Late Pliocene-Quaternary (e.g., Campbell *et al.*, 2006; Latrubesse *et al.*, 2010; Nogueira *et al.*, 2013). These models do not envisage an earlier westward enlargement of the paleo-Amazon River beyond the Brazilian and Guiana shields, and so require alternative paleogeographical reasons for the increase in offshore terrigenous influx since the Late Miocene.

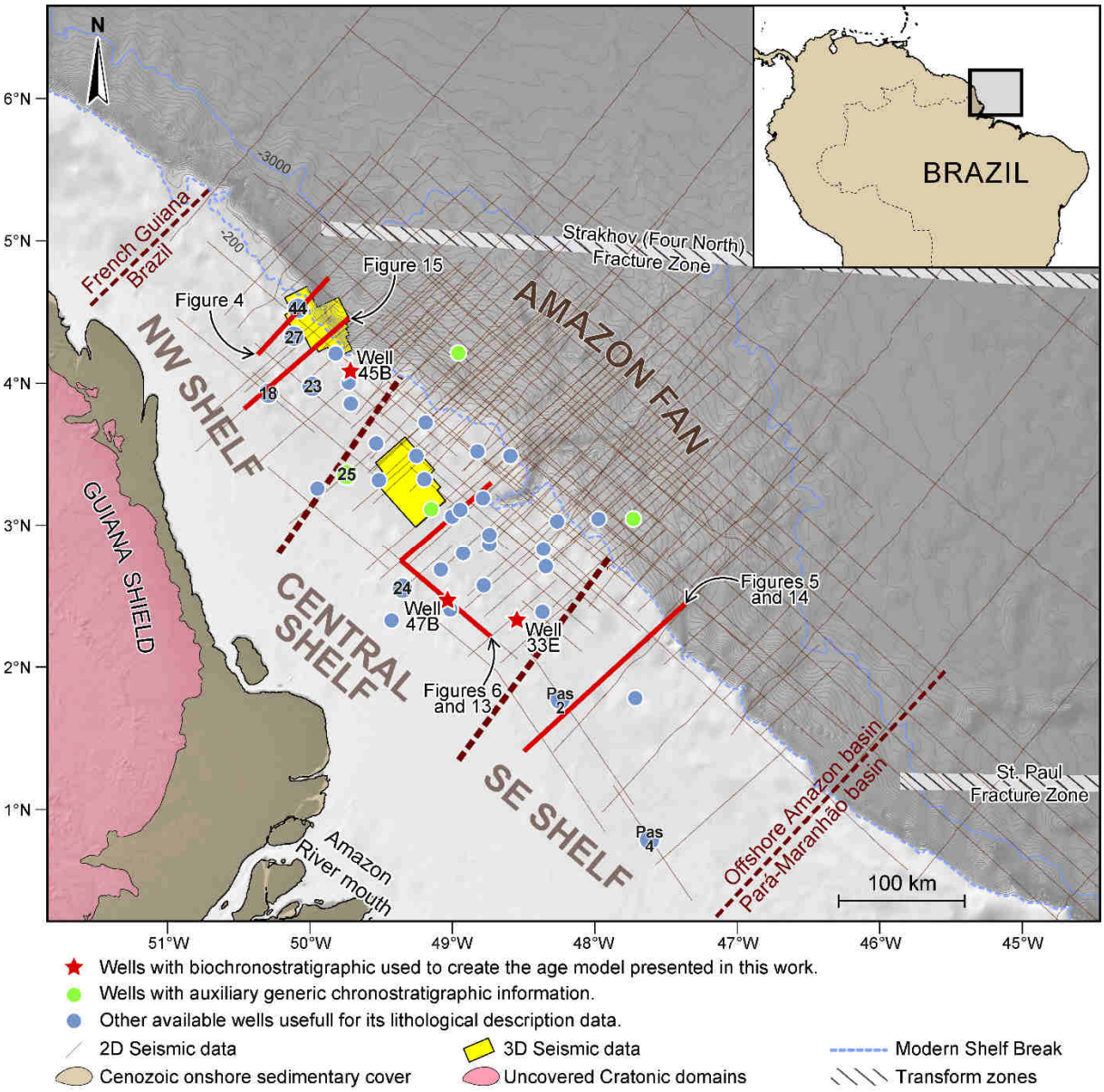

Figure III-1: Map of the study area showing the available seismic and well dataset. The Offshore Amazon Basin is subdivided into three regions, shown by thick dashed lines. Thin lines indicate seismic reflection profiles, yellow polygons indicate location of 3D seismic volumes. Exploration wells are shown by numbered red stars and green and blue dots. The locations of Figures III4–6 and III13–15 are shown by red lines. The dashed blue line demarks the modern shelf break.

Thus the timing and nature of the transition from a carbonate to a siliciclastic-dominated margin offshore the Amazon River remains controversial, and of great interest for the palaeogeography of this part of South America. The aim of this paper is to address these questions by examining the Neogene stratigraphic record of the Amazon shelf, the rich depositional record of which has received relatively little attention. We use a regional grid of commercial 2D and 3D seismic profiles correlated to well data across the Offshore Amazon Basin (Figure III-1) to define stratigraphic units in the context of a new age model for the Amapá carbonate platform. Biostratigraphic data from three key wells were revised and used

to assign ages to surfaces bounding the newly identified sedimentary units, and so to constrain the major changes in sedimentary environments across the Amazon shelf during the Neogene. The results allow us to reconstruct the interaction between carbonate and siliciclastic depositional environments in space and time during the major stages of development and progressive burial of the Amapá carbonate platform. Our findings also allow an assessment of the possible controls on this equatorial carbonate factory on a context of variable sediment supply from the paleo-Amazon River and sea level changes.

III.2 REGIONAL SETTING

The Offshore Amazon Basin is located in the northwestern portion of the Brazilian Equatorial Margin (Figure III-1), which was formed during the opening of the Equatorial Atlantic Ocean in a context of wrench tectonics that involved two phases: an early, less intense phase during the Triassic-Jurassic; and a later phase related to continental rifting during the Early Cretaceous (Matos, 2000).

Within the Offshore Amazon Basin, stratigraphic studies using seismic profiles tied to well data indicate that the rift succession is composed of Neocomian to Albian fluvio-deltaic, lacustrine and marine strata, infilling pull-apart half-grabens (Brandão and Feijó, 1994; Figueiredo *et al.*, 2007). Open marine clastic deposition began during the Eo-Albian (ca. 102 Ma) with the deposition of deep-water mudstones and siltstones and lasted until the Neo-Paleocene (Limoeiro Formation; Figure III-2). Most studies agree that from the Late Paleocene (ca. 59) to the Late Miocene, the basin was dominated by mixed carbonate-siliciclastic shelfal sediments (Marajo and Amapá Formations), laterally equivalent to deep-water calcilutites and mudstones (Travosas Formation; Figure III-2) (Wolff and Carozzi, 1984; Figueiredo *et al.*, 2007). The Amapá carbonate deposition can be subdivided into four major depositional cycles interrupted by periods of subaerial exposure (Carozzi, 1981; Wolff and Carozzi, 1984): Cycle I (Paleocene to Early Eocene); Cycle II (Middle Eocene); Cycle III (Late Eocene to Late Oligocene); Cycle IV (Early to Middle Miocene?). The latter cycle corresponds to the time interval investigated in this study, although its youngest age is uncertain as discussed below. From the Late Miocene, increasing siliciclastic input resulted in prograding shelf clinoforms that ultimately buried the Amapá carbonates (Gorini *et al.*, 2014).

The age of the cessation of the Amapá carbonates sedimentation has been repeatedly revised. Early studies placed carbonate sedimentation cessation at sometime in the Middle Miocene (Schaller *et al.*, 1971; Carozzi, 1981) or at the Middle to Late Miocene boundary

(Wolff and Carozzi, 1984; Brandão and Feijó, 1994). Silva *et al.* (1999) were the first authors to assign a precise age for the top of the carbonate platform, at 10 Ma. More recently, Figueiredo *et al.* (2007) proposed a revised age of ca. 10.7 Ma for this surface. Subsequently, based on calcareous nannofossil zonations, Figueiredo *et al.* (2009) assigned an age between 11.8-11.3 Ma for the top of the carbonate platform. This age model was questioned by Campbell (2010), and revised to 10.5 Ma by Figueiredo *et al.* (2010). More recently, based on calcareous nannofossil zonations, Gorini *et al.* (2014) argued that the top of the carbonate platform was not synchronous across the basin. These authors placed the end of carbonate sedimentation between 9.5-8.3 Ma on the Central shelf, and later in the NW shelf although no precise or inferred age was proposed.

Another disputed issue concerns the nature of the stratal relationships recording the transition from carbonate to terrigenous sedimentation in Offshore Amazon Basin. Based on well data, Carozzi (1981) proposed that the top of the carbonate platform was marked by a large transgression caused by a sea-level rise. In contrast, also based on well data, Figueiredo *et al.* (2009) proposed that the same stratigraphic level was marked by a "regional unconformity" associated with the Serravallian/Tortonian eustatic fall highlighted by Haq *et al.* (1987). However, based on seismic and well data, Gorini *et al.* (2014) showed that the carbonates are downlapped by shelf clinoforms, supporting an interpretation of the carbonate-siliciclastic boundary as a flooding surface.

Seaward of the shelf, the continental slope is dominated by the lobate form of the Amazon deep-sea fan (hereafter Amazon Fan; Figure III-1), a vast sedimentary depocenter that is interpreted to record an increase in siliciclastic influx since the Late Miocene (Silva *et al.*, 1999). The deposition of the Amazon Fan has been assumed to have begun around the same time that carbonate sedimentation on the shelf was suppressed (Schaller *et al.*, 1971; Silva *et al.*, 1999; Figueiredo *et al.*, 2007; Figueiredo *et al.*, 2009). Based on an extrapolation of latest Quaternary sedimentation rates in cores, Damuth and Kumar (1975) and Damuth *et al.* (1983) estimated a Middle to Late Miocene age for the initiation of the Amazon Fan, between 16.5-8 Ma. Silva *et al.* (1999), Figueiredo *et al.* (2007) and Figueiredo *et al.* (2009) proposed ages between 11.8-10.5 Ma for the base of the Amazon Fan. More recently, Hoorn *et al.* (2017) proposed an age of 9.4–9 Ma for the base of the fan, based on planktonic calcareous nannofossil zonations and a recent international time scale (Gradstein *et al.*, 2012). These authors also suggested for the first time that the Amazon Fan could post-date the cessation of shelfal carbonate sedimentation by 1-1.5 Myr.

Sedimentation rates in the Offshore Amazon Basin remained relatively low in the Late Miocene, with estimated values around 0.05 m/kyr, but dramatically increased during the Late Pliocene-Pleistocene to estimated values of 0.34 m/kyr and 1.22 m/kyr on the shelf and deep-sea fan regions, respectively (Figueiredo *et al.*, 2009; Gorini *et al.*, 2014). Corresponding sediment thicknesses (of up to 9 km) promoted isostatic subsidence and flexural deformation of the lithosphere, strongest beneath the fan and adjoining regions (Braga, 1993; Driscoll and Karner, 1994; Silva *et al.*, 1999; Rodger *et al.*, 2006).

The Amazon margin has also been affected by gravitational processes over differing temporal and spatial scales (Reis *et al.*, 2010; Reis *et al.*, 2016). During the Neogene, gravity tectonics resulted in the sliding of thick Cretaceous-Recent sedimentary sequences above multiple levels of basal décollements, to generate a structural system composed of a proximal extensional domain on the outer shelf and upper slope, giving way to a distal compressive domain (thrust-and-fold belts) on the slope above water depths of 2600 m (Cobbold *et al.*, 2004; Perovano *et al.*, 2009; Reis *et al.*, 2010). The uppermost seismically-detected décollement surface has been interpreted as a condensed section laterally correlative to the top of the Amapá carbonates (Reis *et al.*, 2016). This surface has also acted as a basal décollement during a series of large-scale slope failures recorded by a succession of giant mass transport deposits (MTDs) (Silva *et al.*, 2010; Reis *et al.*, 2016; Silva *et al.*, 2016).

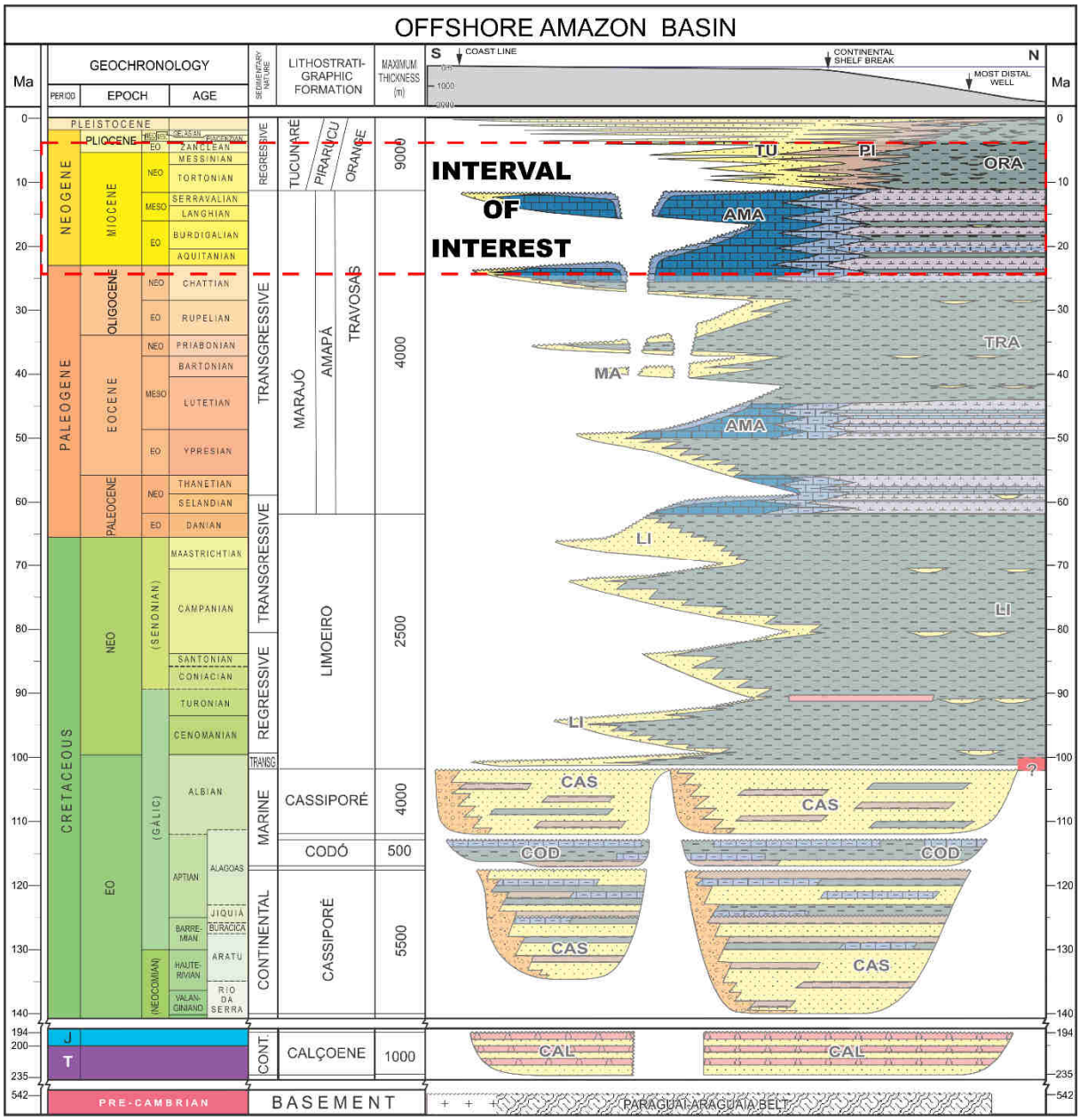

Figure III-2: Stratigraphic chart of the Amazon Offshore basin (simplified from Figueiredo *et al.*, 2007), with the stratigraphic interval investigated in this study indicated. Figueiredo *et al.* (2007) have placed the top of the Amapá carbonates at 10.5 Ma, while more recent studies have attributed ages between 11.8-8.3 Ma for the same surface (see text for details).

III.3 DATA AND METHODS

The study is based on a shelf-wide grid of multi-channel seismic reflection data, correlated to biostratigraphic and lithological data from exploration wells (Figure III-1). The seismic dataset includes 20,000 km of 2D seismic profiles and two 3D blocks covering a total area of 3,800 km^2 (Figure III-1). The 2D seismic profiles have record lengths of 10-13 seconds, with vertical resolution of 10–50 m (depending on depth and lithology). Seismic interpretation followed standard sequence stratigraphic methods, in which reflection relations (onlap,

downlap, truncation, conformity) are used to define units bound by unconformities and correlative unconformities (e.g. Mitchum and Vail, 1977; Vail *et al.*, 1977; Catuneanu, 2006). Seismic facies analysis of the internal character of the units was used together with lithological data from wells to interpret depositional environments and their variations across the shelf (Schlager, 1998; Pomar, 2001; Schlager, 2005; Burgess *et al.*, 2013).

Downhole information on unit lithology was obtained from 40 exploratory wells located across the shelf and upper slope (Figure III-1). Carbonate and siliciclastic units were identified from lithological descriptions on composite logs (cuttings and sidewall cores). An age model for these units was obtained by revision of biostratigraphic information from unpublished reports for wells 45B and 47B and published data from well 33E (Figueiredo *et al.*, 2009) (Figure III-1). The first and last occurrence of key calcareous nannoplankton key species were used to assign minimum and maximum possible ages to the main stratigraphic surfaces based on published biochronostratigraphic compilations (Martini, 1971; Young, 1998; Raffi *et al.*, 2006; Anthonissen and Ogg, 2012; Zeeden *et al.*, 2013), updated to astronomically-tuned geologic time scale (Gradstein *et al.*, 2012). Such time ranges of possible ages for unit boundaries were assigned based on their position relative to the markers in the wells. More precise ages for each surface were then proposed based on correlation to the global sea level variation curves of Miller *et al.* (2005) and Haq *et al.* (1987); recalibrated to the timescale of Gradstein *et al.* (2012).

In addition, data from 7 exploratory wells were used to estimate values of minimum non-eustatic accommodation space across the shelf during deposition of the upper succession of the Amapá Carbonates. Non-eustatic accommodation space was calculated by subtracting the value of maximum eustatic rise positions during the respective period of deposition, based on published curves (Haq *et al.*, 1987; Miller *et al.*, 2005), from the undecompacted thickness of sedimentary units at the well sites during the corresponding time span.

III.4 RESULTS

Results are organized into three main sections: (1) Depositional units and architecture of the upper Amapá Carbonates; (2) Age models for the Neogene units, based on revised biostratigraphic data further constrained by global curves of sea level oscillations; and (3) Calculations of non-eustatic accommodation space across the shelf.

III.4.1 Depositional units and architecture of the upper Amapá Carbonates

Based on correlation of seismic data to lithological information from wells, the upper sedimentary succession of the Amapá carbonates was divided into 5 main stratigraphic units, referred to as Units N1 to N5 (Figure III-3 to Figure III-6). For descriptive purposes, the shelf was divided into three regions: NW shelf, Central shelf and SE shelf (Figure III-1). The five units are less architecturally complex on the NW Shelf, where they are also more clearly imaged on seismic data, whereas on the Central shelf seismic imaging is poorer due to a greater thickness of the overlying Pliocene-Quaternary units and the occurrence of complex geometries, gravity tectonic deformations and mass wasting scars (Figure III-4 and Figure III-6). For clarity, in each of the following sections, units N1 to N5 will be described from the least to the more complex regions: the NW shelf, the SE shelf and finally the Central shelf.

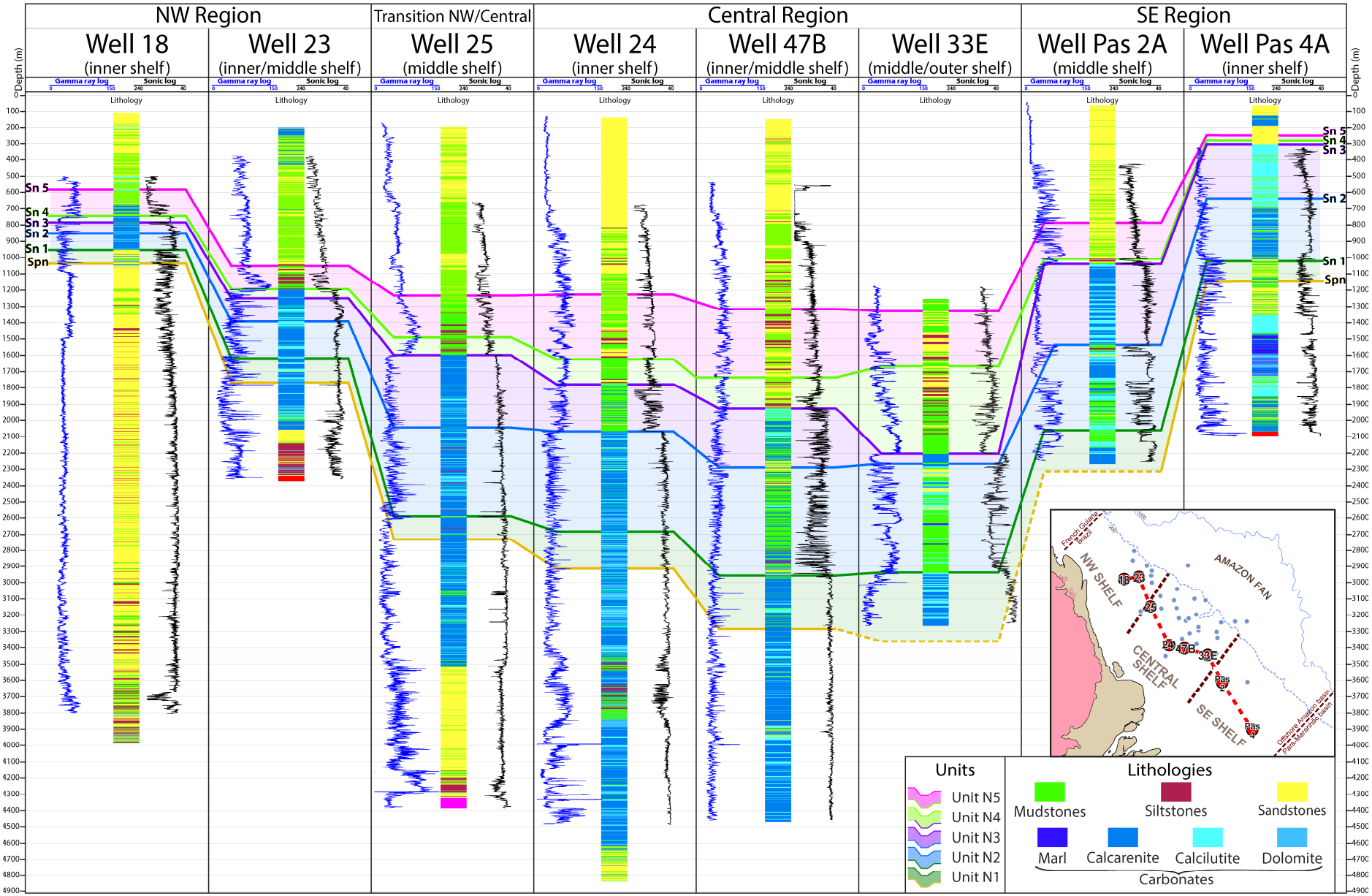

Figure III-3: Lithological data together with gamma ray and sonic logs of eight wells located in the Offshore Amazon Basin. Location of wells shown in Figure III-1. Colored lines represent the bounding surfaces of units N1 to N5 defined in this work. Well 33E after Figueiredo *et al.* (2009).

III.4.1.1 Unit N1

Unit N1 is the basal unit of the Neogene portion of the Amapá carbonates. Its lower limit, surface *Spn*, is an irregular surface, characterized by truncation of underlying reflectors and a few incisions, pointing to an erosive nature (Figure III-4 to Figure III-6). The top of the unit is marked by surface *Sn1*, varies in morphology from irregular to smooth, and its erosional or depositional nature is not clear from seismic data alone. Well data indicate that unit N1 is a mixed siliciclastic-carbonate unit, although the extent of carbonate-dominated strata varies across the shelf (Figure III-3).

In the NW shelf, unit N1 mainly comprises a relatively thin stratal package, 130 m thick on average, with a tabular aggrading geometry (Figure III-4). Near the shelf edge, unit N1 thickens to 540 m and comprises prograding clinoforms that downlap basal surface *Spn*, and completely cover the underlying units across the outer shelf-upper slope area. Top surface *Sn1* is regular and smooth across the NW shelf with no clear evidence of erosional features. Seismic resolution does not allow the recognition of features compatible with the occurrence of carbonate build-ups within unit N1 in the NW shelf. However, well data indicate that carbonate sedimentation was predominant during deposition of unit N1 across the mid-outer shelf, whereas dominantly siliciclastic sedimentation occurred across the inner shelf (e.g. wells 18 and 23, Figure III-3).

In the SE shelf, unit N1 mainly comprises strata with aggradational-retrogradational geometries, mostly limited to an area equivalent to the paleoshelf-upper slope of the underlying units, thinning considerably downslope (Figure III-5). The top surface *Sn1* is rather irregular. The internal seismic facies include internal aggrading mounded features across the mid-outer shelf, up to 400 m thick and 50 km wide, consistent with the presence of carbonate pinnacles and banks. As in the NW shelf, lithological data (e.g. wells Pas 2A and Pas 4A, Figure III-3) indicate that carbonate sedimentation was predominant across the mid-outer shelf, whereas siliciclastic sedimentation dominated the inner shelf.

In the Central shelf, unit N1 is similar in character to the SE shelf: beneath an irregular top surface *Sn1*, it is also an essentially aggradational-retrogradational unit, with an average thickness of 350 m and thinning considerably downslope (Figure III-6). Across this shelf portion, top surface *Sn1* is also an irregular surface. Near the outer shelf, internal reflectors locally onlap basal surface *Spn*. In contrast to the SE shelf, internal seismic facies do not include clear mounded features consistent with the occurrence of carbonate build-ups. Nonetheless, lithological data show that carbonate deposition took place across most of the Central shelf, and

that carbonate deposition was more extensive in the Central shelf than elsewhere in the basin during deposition of unit N1 (e.g. wells 24 and 47B, Figure III-3). Siliciclastic sedimentation could be locally present as infill of troughs (Figure III-6). We interpret the aggrading character of unit N1 to reflect widespread carbonate sedimentation that occupied most of the Central shelf, being only locally disrupted by crosscutting troughs connecting the innermost shelf to the slope region (Figure III-6) and that may have been tidally controlled (Wolff and Carozzi, 1984).

III.4.1.2 Unit N2

Unit N2 is bounded by basal surface *Sn1* and top surface *Sn2*, which is irregular with a variable morphology across the shelf, indicating an erosive nature. Well data indicate that the lithology of unit N2 varies across the different shelf regions, from predominantly carbonate to predominantly siliciclastic (Figure III-3).

In the NW shelf, unit N2 is essentially a tabular aggrading unit (~150 m thick) in the inner-middle shelf, thickening seaward to up 460 m on the outermost shelf where it forms aggrading-prograding clinoforms (Figure III-4). On seismic profiles, across the mid to outer shelf, top surface *Sn2* includes step-like features and truncates internal clinoform reflectors. Internal seismic facies do not include features consistent with the presence of carbonate build-ups (Figure III-4). However, lithological data show that N2 is composed of carbonates, from the inner to outer shelf (e.g. wells 18 and 23, Figure III-3).

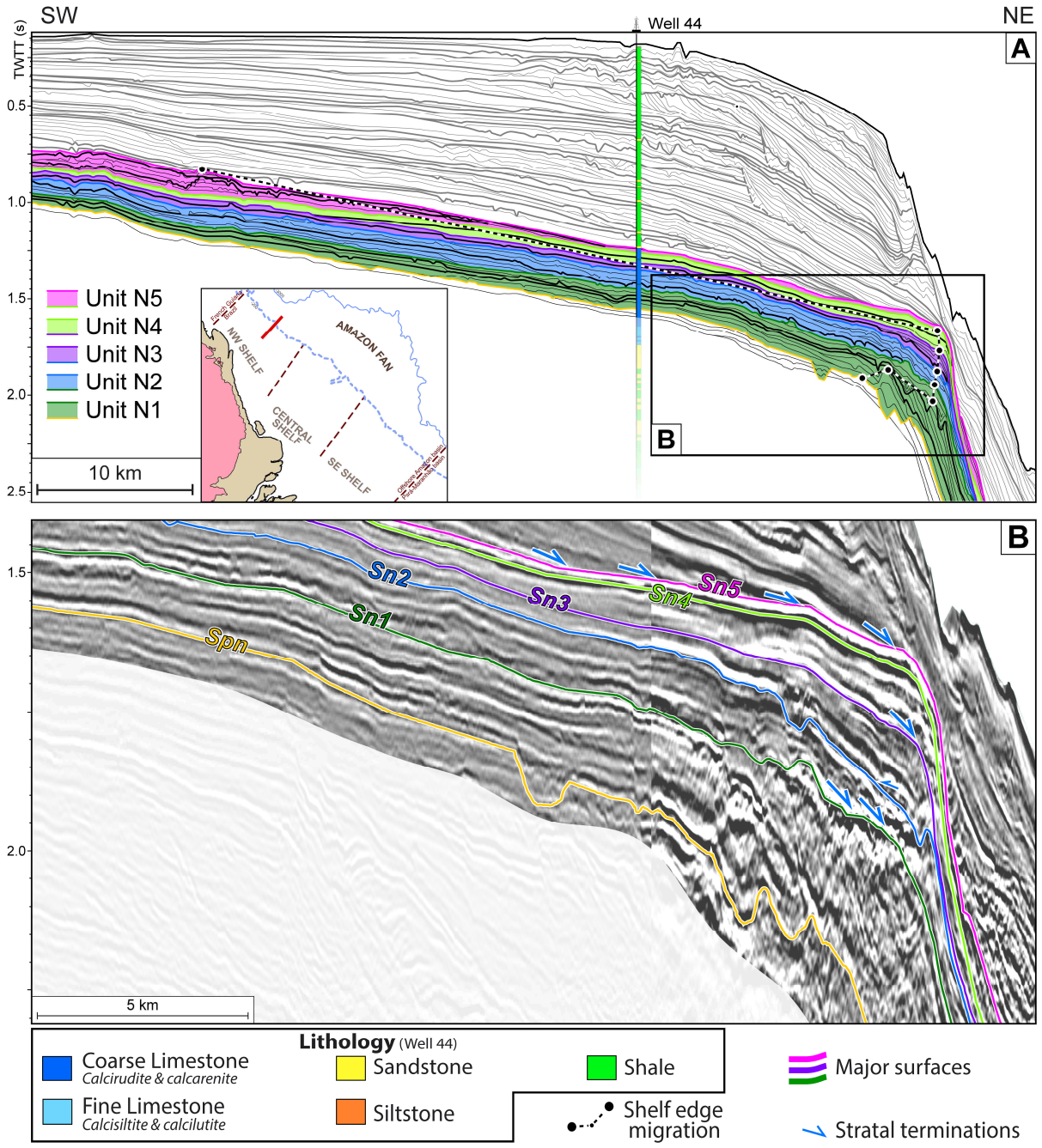

Figure III-4: Interpreted seismic profile across the NW sector of the Amazon shelf (location in Figure III-1) - (A) Line drawing of the stratigraphic interpretation, highlighting the main units defined in this work; dashed line with dots indicates shelf edge migration. (B) Zoom-in across the outer shelf-upper slope, showing units N1 to N5 and respective bounding surfaces.

Across the SE shelf, N2 is also a mainly aggrading unit that acquires a slight progradational character at the shelf edge (Figure III-5). In contrast to the NW shelf, unit N2 is thinner (~300 m) on the outer SE shelf, but thicker (up to 700 m) across the inner shelf (Figure III-5). Thinning of the unit on the outer shelf may reflect greater erosion beneath top surface *Sn2* (Figure III-5). Internal seismic facies include aggrading mounded features consistent with carbonate build-ups, which vary in form and dimension across the shelf: (1) carbonate banks

up to 10 km wide in the inner shelf (Figure III-5A); (2) pinnacles up to 3.5 km wide in the mid-shelf; and (3) flat-topped banks up to 40 km wide in the outermost shelf (Figure III-5B). Well data indicate that carbonate sedimentation dominates N2, except in the inner shelf where carbonates interfinger with siliciclastics (wells Pas 2A and Pas 4A, Figure III-3).

In the Central shelf, unit N2 is a predominantly aggrading unit, thinner in the outer shelf (300 m) than in the inner shelf (600 m) and more restricted in its seaward extent than underlying unit N1 (Figure III-6). Its top surface *Sn2* displays a series of steps and local canyon-like incisions reflecting intense erosion across the mid to outer shelf and upper slope (Figure III-6). In contrast to the NW and SE shelves, well data show that unit N2 is essentially composed of siliciclastics in the Central shelf, containing only thin carbonate layers (wells 47B and 33E; Figure III-3).

III.4.1.3 Unit N3

Unit N3 is bounded by erosive basal surface *Sn2*, and by a smooth top surface *Sn3* that presents no evidence of truncations on the shelf region (Figure III-4 to Figure III-6). Top surface *Sn3* corresponds to seismic surface A of Gorini *et al.* (2014), and Reis *et al.* (2016). Well data indicate that N3 varies in lithology across the shelf, from a carbonate-dominated to a mixed siliciclastic-carbonate composition (Figure III-3).

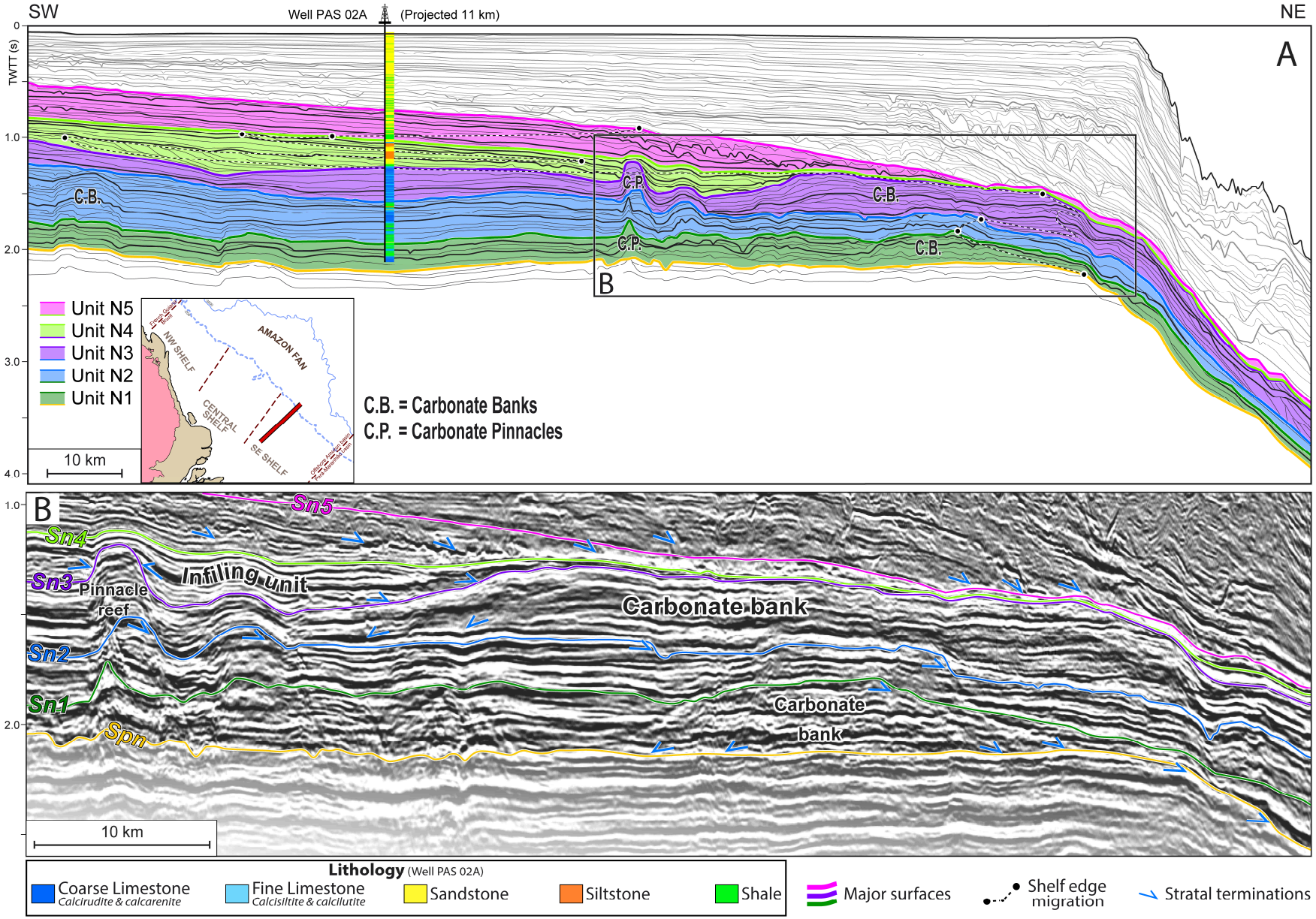

Figure III-5: Interpreted seismic profile across the SE sector of the Amazon shelf (location in Figure III-1) - (A) Line drawing of the stratigraphic interpretation, highlighting the main units defined in this work; dashed line with dots indicates shelf edge migration. (B) Zoom-in across the outer shelf-upper slope, showing units N1 to N5 and respective bounding surfaces.

In the NW shelf, unit N3 is a tabular aggrading unit that is relatively thin (<160 m) and almost absent on the upper slope (Figure III-4). Near the shelf edge, internal reflectors onlap basal surface *Sn2* (Figure III-4). Lithological data show that N3 is composed of carbonates, from the inner to outer shelf (e.g. wells 18 and 23; Figure III-3).

Across the SE shelf, unit N3 is an aggrading unit, thickening from ~320 m in the inner shelf to up to 550 m at the middle-outer shelf (Figure III-3). The shelf edge within N3 is shifted basinwards in comparison to unit N2 in the same area (Figure III-5). Across the outer shelf, top surface *Sn3* displays steps corresponding to reflector terminations (Figure III-5), although it is not clear if these are stratal truncations due to shelf edge erosion or apparent truncations generated by a series of retrogressive offlaps (due to backstepping of carbonate build-ups). Internal seismic facies include mounded features consistent with carbonate pinnacles up to 3.5 km thick on the mid-shelf and flat-topped banks up to 40 km wide on the outer shelf (Figure III-5). Lithological data indicate that carbonate sedimentation was predominant across the shelf (wells Pas 2A and Pas 4A, Figure III-3 and Figure III-5).

In the Central shelf, unit N3 is an aggrading-retrograding unit up to 360 m thick that thins basinward (Figure III-6). Top surface *Sn3* is irregular across the outer shelf and upper slope due to the occurrence of a series of morphological steps. By the end of unit N3 deposition, shelf edge retrogradation resulted in the most proximal position of the paleoshelf break during the Neogene (Figure III-6). Consequently, a 150 km wide embayment was formed in the Central shelf due to persisting retrogradation of the shelf edge since the deposition of unit N1 (Figure III-7C). Irregularities in top unit N3 are mainly related to internal aggrading reflectors interpreted as carbonate build-ups. Lithological data (wells 47B and 33E; Figure III-3) show that unit N3 is essentially composed of carbonates with siliciclastics being limited to inner shelf positions.

III.4.1.4 Unit N4

Unit N4 is bounded by basal surface *Sn3* and by top *Sn4*, which is smooth but interrupted in places by deep incisions related to erosive surfaces from the overlying unit (Figure III-6). Well data indicate that unit N4 is composed of carbonates in the NW shelf, but entirely of siliciclastics in the Central and SE shelf regions (Figure III-3).

Across the NW shelf, unit N4 is a tabular aggrading unit up 180 m thick, comparable to the underlying unit N3 (Figure III-4). Lithological data show that like N3, unit N4 is composed primarily of carbonates, from the inner to the outer shelf (e.g. wells 18 and 23; Figure III-3).

Across the Central and SE shelves, seismic data analysis shows that unit N4 is an essentially prograding-aggrading unit (Figure III-5 and Figure III-6). It is noteworthy that surface *Sn4* is the top surface of an infilling unit, which covers an unconformity within unit N4 at the top of prograding clinoforms (Figure III-5 and Figure III-6). As a whole, unit N4 tends to smooth the irregular morphology of carbonate build-ups at the top of underlying unit N3 (Figure III-5 and Figure III-6). On the SE shelf, unit N4 is restricted to and infills low areas on the inner to mid shelf (Figure III-5), whereas on the Central shelf it extends across the shelf (Figure III-6) and partially infills the large embayment previously formed in this region (Figure III-7D). Lithological data from both shelf regions show that unit N4 is purely siliciclastic in composition and overlies carbonates of unit N3 (wells 24, 47B, 33E, Pas 2A and Pas 4A, Figure III-3).

III.4.1.5 Unit N5

Unit N5 is bounded by basal surface *Sn4* and upper surface *Sn5*, which is smooth but interrupted in places by deep incisions caused by erosion within levels of the overlying sedimentary units (Figure III-6). Well data indicate that unit N5 is composed of carbonate or siliciclastic sediments (Figure III-3).

In the NW shelf, unit N5 is an aggrading package about 150 m thick across the inner to middle shelf, thinning to a tabular unit ~40 m thick on the outer shelf (Figure III-4). Lithological data indicate that the lower part of unit N5 is predominantly composed of carbonates, whereas its upper part is dominantly siliciclastic with thin (<10 m) carbonate layers (e.g. wells 18 and 23, Figure III-3). However, internal seismic facies include isolated mound-like features up to 4 km wide, most common on the inner shelf in the upper part of the unit, suggesting isolated carbonate dominated environments occurred sparsely distributed in the NW shelf during the final deposition of unit N5. The deposition carbonates within upper unit N5 across the NW shelf records the last expression of the Amapá carbonates in the Offshore Amazon Basin.

On the Central and SE shelves, unit N5 consists of prograding units (Figure III-5 and Figure III-6). On the inner-middle Central shelf, the unit is about 400 m thick and thickens up to 800 m near the shelf edge (Figure III-6). In contrast, on the SE shelf, the unit is only up to 230 m thick on the inner-middle shelf and thins significantly on the outermost shelf (Figure III-5). Lithological data indicate that unit N5 is basically composed of siliciclastics in both areas (e.g. wells 47B; 33E; Pas 2A and Pas 4A; Figure III-3).

Finally, seismic data also show that across the inner to outer shelf, the thick siliciclastic units that cover unit N5 are essentially composed of seaward prograding clinoforms that downlap surface *Sn5* (Figure III-4 to Figure III-6), so as to completely infill the Central shelf

embayment (Figure III-7E). We thus envisage *Sn5* as a maximum flooding surface, based both on its smooth seismic character and on downlap by the overlying siliciclastic unit (Figure III-4 and Figure III-5).

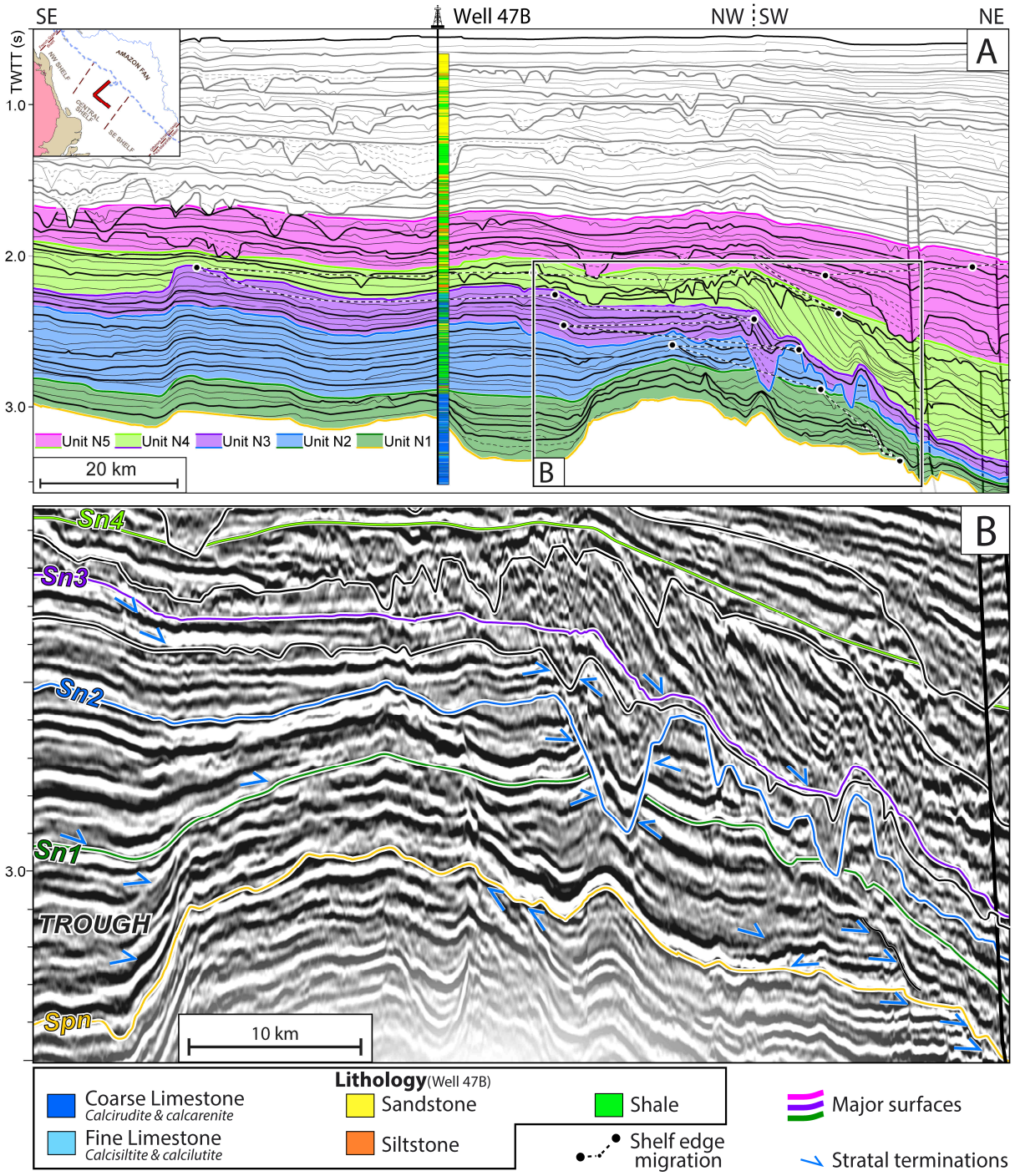

Figure III-6: Interpreted seismic profile across the Central sector of the Amazon shelf (location in Figure III-1) - (A) Line drawing of the stratigraphic interpretation, highlighting the main units defined in this work; dashed line with dots indicates shelf edge migration. (B) Zoom-in across the outer shelf-upper slope, showing units N1 to N5 and respective bounding surfaces.

.

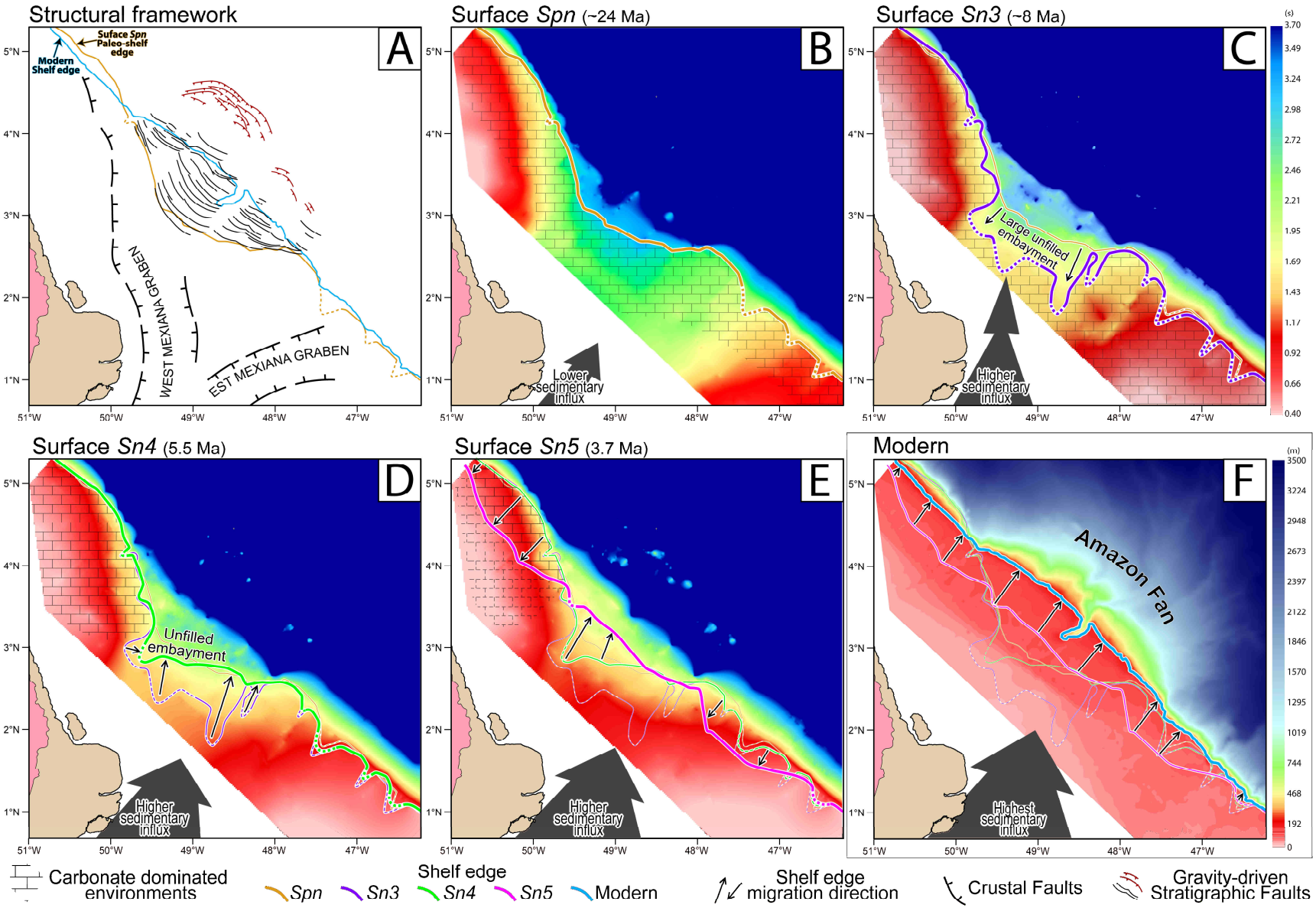

Figure III-7: A - Structural framework compiled from Schaller *et al.* (1971) and Perovano *et al.* (2009). Faults associated to gravity tectonics are compiled from Perovano *et al.* (2009) and Reis *et al.* (2010). B to E - Two-way travel time (s) maps of stratigraphic surfaces mapped in this work, coupled with bathymetric maps (m) of the present-day Amazon shelf. Paleo-shelf edge positions defined from interpreted seismic data are shown as thick colored lines. In B, note that the shelf edge position in the central region at ca. 24 Ma was nearly coincident with the most proximal gravity tectonic-related faults. Also note that the large embayment formed due to shelf-edge retrogradation in the Central shelf was filled between ca. 8-3.7 Ma and only then was carbonate sedimentation completely suppressed on the NW shelf.

III.4.2 Age models of the Neogene horizons: constraining biostratigraphy by global curves of sea level oscillations

Age constraints for the stratigraphic surfaces bounding the five units recognized within the Neogene Amapá carbonates, (*Spn* and *Sp1-5*; Figure III-3) are obtained from biostratigraphic data from three exploratory wells (wells 33E; 45B and 47B; Figure III-8 toFigure III-10). Ages were estimated based on the positions of each surface in the three wells relative to the first and last occurrences of key calcareous nannofossils species dated with reference to published chronostratigraphic compilations (Martini, 1971; Young, 1998; Raffi *et al.*, 2006; Anthonissen and Ogg, 2012; Zeeden *et al.*, 2013) updated to astronomically-tuned ages (Gradstein *et al.*, 2012). Our approach of using first and last occurrences of fossil species with well-constrained ages results in a more reliable and detailed chronostratigraphic model for the Neogene succession of the Offshore Amazon Basin than that proposed in previous studies (Figueiredo *et al.*, 2009; Cruz *et al.*, 2014; Gorini *et al.*, 2014). In particular, we do not rely on the predefined calcareous nannoplankton zonations applied to wells from the 1980s, which include fossiliferous markers that were used to define calcareous nannoplankton zonations based on pioneering works of Martini (1971) and Bukry (1973) that are now considered to be poorly constrained (Raffi *et al.*, 2006). Such unreliable calcareous nannoplankton species were commonly used for biochronological zonation at the time most wells in the Offshore Amazon Basin were drilled and a simple recalibration of pre-defined fossiliferous zones to modern time scales could led to substantial imprecision. In addition, we use other calcareous nannoplankton fossils that have been found to be useful in terms of chronostratigraphy in recently published works (see Raffi *et al.*, 2006 and Zeeden *et al.*, 2013).

Biostratigraphic data revised as above were subsequently correlated to global curves of sea level oscillations (Figure III-11), to allow us better constrain ages of the Neogene stratigraphic surfaces, and thus of the deposition of units N1 to N5.

III.4.2.1 ***Surface Spn*** *(unit N1 basal boundary)*

In well 45B (Figure III-10), surface *Spn* corresponds to the last recorded occurrence of *Reticulofenestra bisecta* and *Cyclicargolithus abisectus* (23.13–24.67 Ma; Anthonissen and Ogg, 2012). In well 47B (Figure III-8), the same surface lies 150 m below the first recorded occurrence of *Helicosphaera carteri* (22.03 Ma; Anthonissen and Ogg, 2012). These

fossiliferous markers constrain the age of surface *Spn* to an age between 24.67 Ma (in well 45B) and 22.03 Ma (in well 47B).

Comparison of this biostratigraphic age range for surface *Spn* (22.03-24.67 Ma) with global sea-level curves (Figure III-11) shows that it coincides with a pronounced sea-level fall at ca. 24 Ma in the curves of both Haq *et al.* (1987) and Miller *et al.* (2005). We thus can attribute an age of latest Oligocene to earliest Miocene age (ca. 24 Ma) to this erosive surface (Figure III-6), marking it the approximate base of the Neogene sedimentary succession in the Offshore Amazon Basin.

III.4.2.2 ***Surface Sn1*** *(top of unit N1, base of unit N2)*

In well 47B (Figure III-8), surface *Sn1* corresponds to the last recorded occurrence of *Sphenolithus belemnos* (17.95–19.03 Ma; Anthonissen and Ogg, 2012) and is stratigraphically placed only 15 m below the first recorded occurrence of *Sphenolithus heteromorphus* (17.71 Ma; Anthonissen and Ogg, 2012). These fossiliferous markers in well 47B constrain the age of Surface *Sn1* to 17.71-19.03 Ma.

Comparison of this biostratigraphic age range with global sea-level curves (Figure III-11) shows that *Sn1* can be correlated to the inflexion point of a major Burdigalian global sea level rise. Thus, surface *Sn1* can be interpreted as a maximum flooding surface at ca. 18 Ma (Figure III-11). This suggests that the mid-outer shelf aggrading mounded features of seismic unit N1 are essentially carbonate build-ups formed in the context of transgressive and highstand depositional systems.

III.4.2.3 ***Surface Sn2*** *(top of unit N2, base of unit N3)*

In well 47B, the occurrence range of *Discoaster kugleri* (10.8–11.93 Ma; Zeeden *et al.*, 2013) begins 40 m below and ends 55 m above surface Sn2 (Figure III-8). Thus, the age of surface *Sn2* lies between 10.8–11.93 Ma.

Comparison to global sea level curves allows us to confidently correlate *Sn2* with the major Tortonian sea-level fall, whose final erosion is dated at ca. 11 Ma (Haq *et al.*, 1987; Miller *et al.*, 2005). Thus, surface *Sn2* is interpreted as a major unconformity, consistent with seismic evidence of deeply-incised erosive features (Figure III-6).

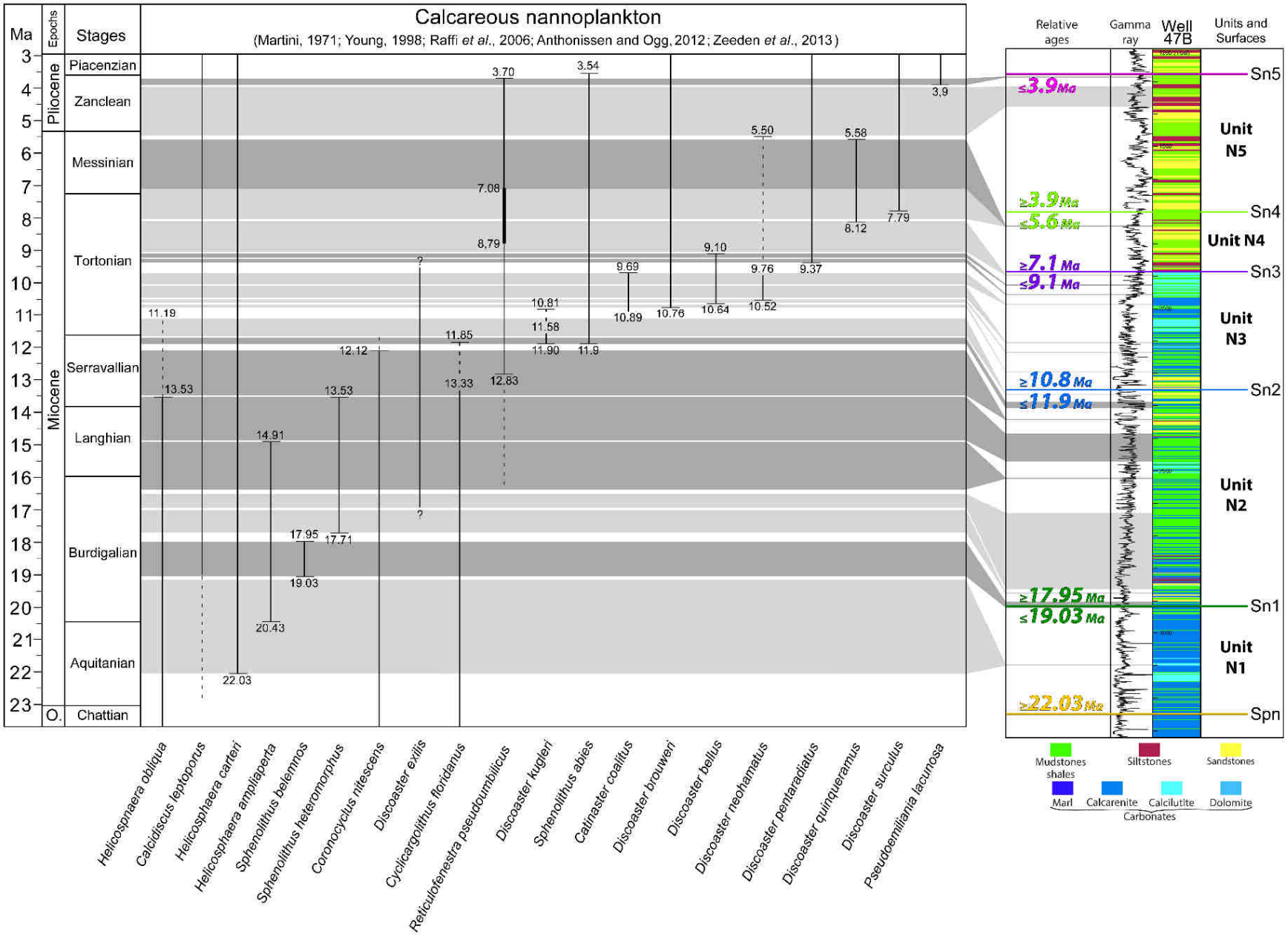

Figure III-8: Chronostratigraphic model for well 47B (location in Figure III-1). Ages are based on the first and last appearance of indicated calcareous nannofossil species.

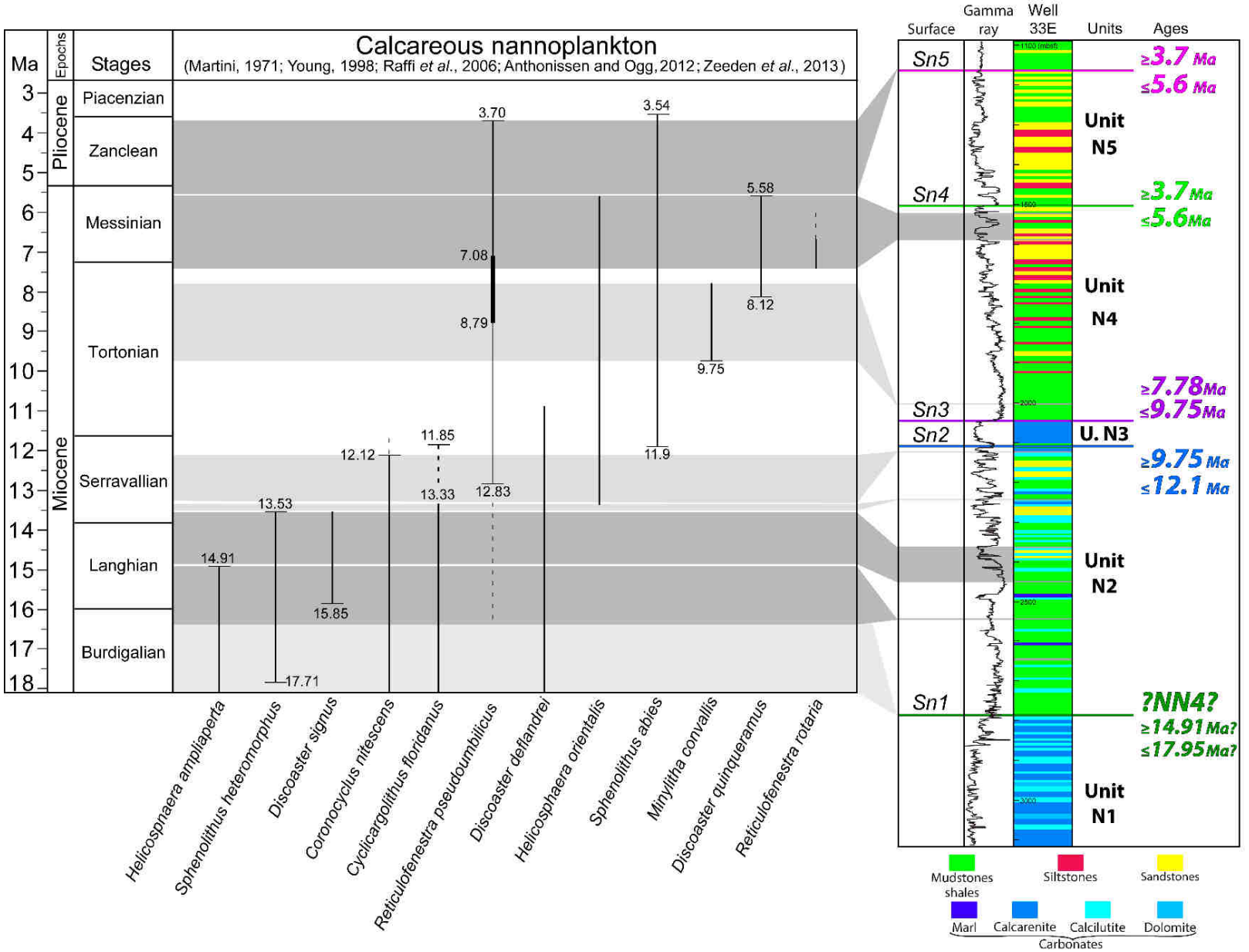

Figure III-9: Chronostratigraphic model for well APS 33E (location in Figure III-1). Ages are based on the first and last appearances of the indicated calcareous nannofossil species.

III.4.2.4 ***Surface Sn3*** *(top of unit N3, base of unit N4)*

In well 47B, surface *Sn3* (the top of the Amapá Carbonates in the Central shelf) lies 30 m above the first coherent occurrence of *Discoaster quinqueramus* (dated at 8.12 Ma in the North Pacific, Anthonissen and Ogg, 2012) and 40 m above the highest recorded occurrence of *Discoaster bellus* (dated at 9.1 Ma in the Equatorial Atlantic; Zeeden *et al.*, 2013). Also in well 47B, surface *Sn3* is equivalent to the highest sampled level within the *Reticulofenestra pseudoumbilicus* paracme (8.794 to 7.087 Ma; Zeeden *et al.*, 2013). In well 33E, surface *Sn3* is overlain by sediments containing *Minylitha convallis* (Figure III-9), whose last consistent occurrence in the Equatorial Pacific took place between 8.3-7.78 Ma (Raffi *et al.* 2006). Assuming similar ages in the Atlantic Ocean for the last occurrence of *Minylitha convallis* and the first occurrence of *Discoaster quinqueramus*, the age of surface *Sn3* probably lies between 7.78-8.12 Ma. More conservatively, considering that the precise ages for the last occurrence of *Minylitha convallis* and the first occurrence of *Discoaster quinqueramus* in the Equatorial Atlantic remain to be verified, the age of surface *Sn3* must lie between 7.087-9.1 Ma.

Within the time span of 7.087-9.1 Ma, an inflexion point of a sea-level transgressive trend can be placed at ca. 8 Ma, considering sea-level curves from Haq *et al.* (1987) and Miller *et al.* (2005) (Figure III-11). Taking into consideration the smooth non-erosive seismic character of surface *Sn3* and the occurrence of overlying strata downlap on the inner shelf (Figure III-5 andFigure III-6), we can interpret *Sn3* as a maximum flooding surface consistent with the ca. 8 Ma global sea level rise. In a such a context, the flat-topped carbonate banks and narrow pinnacles identified across the SE and Central shelves of the Offshore Amazon Basin during deposition of unit N3 can be interpreted as carbonate build-ups formed as a response to the relative sea level rise and shoreline transgression at ca. 8 Ma.

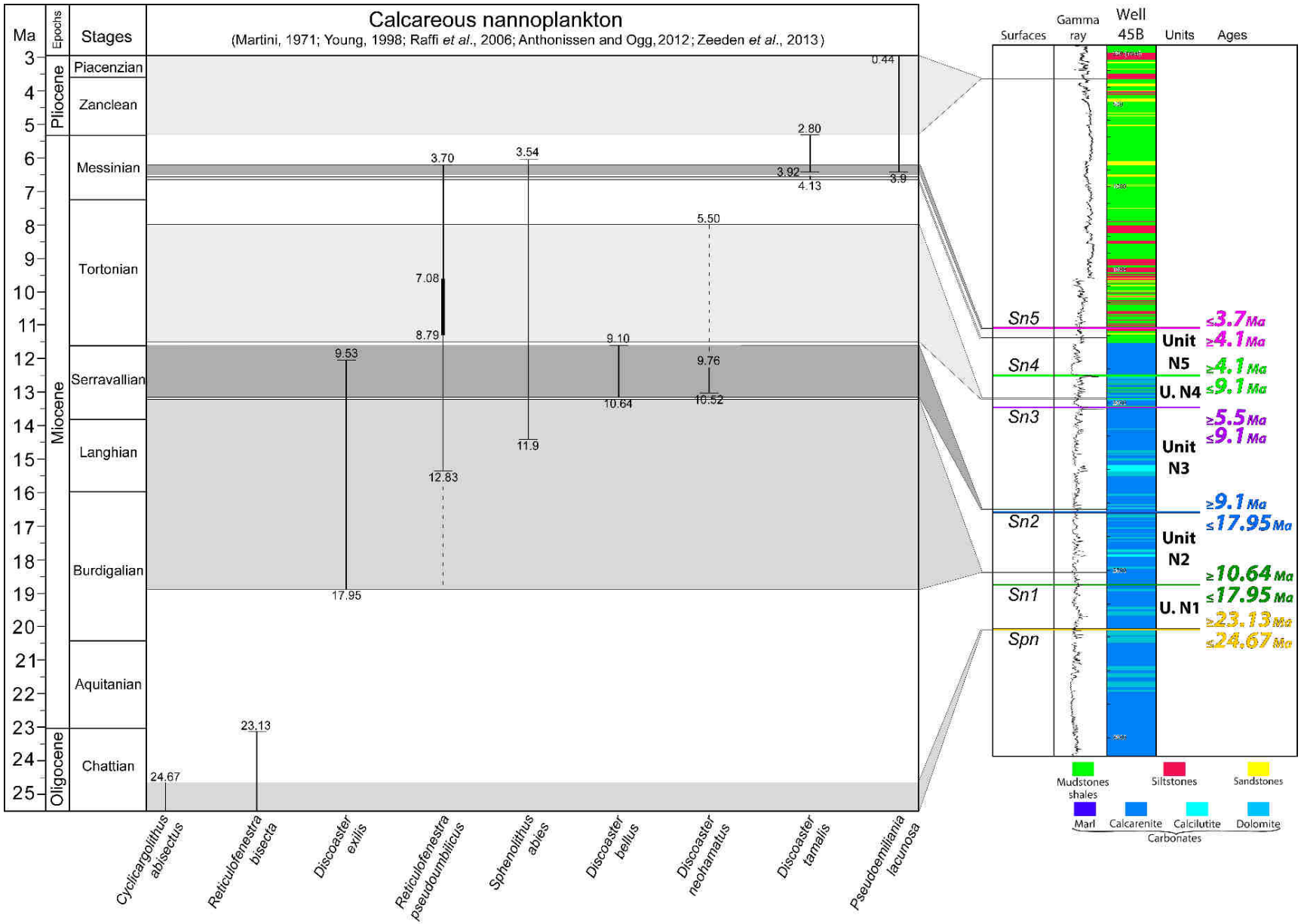

Figure III-10: Chronostratigraphic model for well 45B (location in Figure III-1). Ages are based on the first and last appearances of the indicated calcareous nannofossil species.

III.4.2.5 ***Surface Sn4*** *(top of unit N4, base of unit N5)*

In well 47B (Figure III-8), surface Sn4 lies about 50 m above the last recorded occurrence of *Discoaster quinqueramus* (precisely dated at 5.58 Ma; Anthonissen and Ogg, 2012), while in well 45B (Figure III-10) it lies about 100 m below the first recorded occurrence of *Discoaster tamalis* (4.1 Ma; recalibrated after Young, 1998). These fossiliferous markers indicate the age of surface *Sn 3* to lie between 5.58- 4.1 Ma.

Within this time span of 5.58-4.1 Ma, *Sn4* can be correlated to an inflexion point of a sea-level rise trend at ca. 5.5 Ma, considering the curves from both Haq *et al.* (1987) and Miller *et al.* (2005) (Figure III-11). Thus we interpret *Sn4* as a maximum flooding surface, consistent with seismic evidence of a smooth character, and downlap by the overlying unit (Figure III-4 and Figure III-5).

III.4.2.6 ***Surface Sn5*** *(top of unit N5)*

In well 45 B, surface *Sn4* lies about 40 m above the top of the Amapá Carbonates, at the stratigraphic level of the last recorded occurrence of *Reticulofenestra pseudoumbilicus* (Figure III-10), which indicates an age no younger than 3.7 Ma for this surface (Anthonissen and Ogg, 2012). In well 47B (Figure III-8), *Sn4* only lies 10 m above the highest sampled level containing *Reticulofenestra pseudoumbilicus* and *Pseudoemiliania lacunosa* (at least as old as 3.9 Ma; recalibrated after Young 1998). These fossiliferous markers constrain surface *Sn5* to an age between 3.9-3.7 Ma.

Comparison to global sea level curves shows that this surface can be correlated to a sea-level rise close to the Zanclean/Piacenzian boundary, dated at circa 3.7 Ma considering the curves from both Haq *et al.* (1987) and Miller *et al.* (2005) (Figure III-11). Thus we interpret *Sn5* as a maximum flooding surface, consistent with seismic evidence of a smooth character, and downlap by the overlying unit (Figure III-4 to Figure III-6).

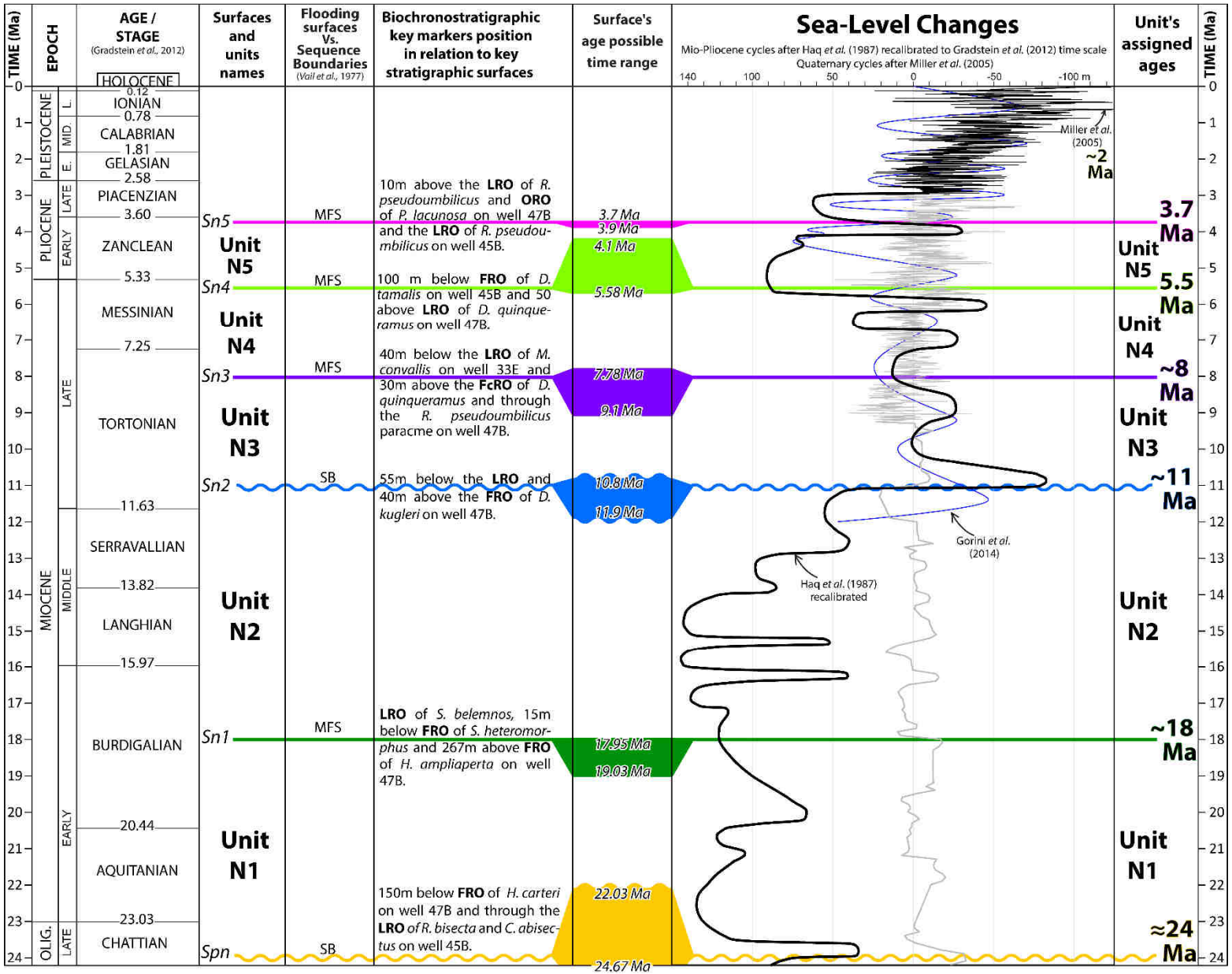

Figure III-11: Chart summarizing the age model for sequences N1 to N5 proposed in this study and their correlation to geological ages/stages of Gradstein *et al.* (2012). Unit ages are based on biostratigraphic data from the wells in Figure III-8 to Figure III-10, refined by correlation between each surface's oldest and youngest possible age with global sea level curves of Haq *et al.* (1987) and Miller *et al.* (2005).

III.4.3 Calculation of non-eustatic accommodation space

Calculations of non-eustatic accommodation space across the Offshore Amazon Basin were performed using the proposed ages and observed thicknesses of units N1 to N5, applied to seven wells on the inner-middle shelf, in positions where seismic interpretation supports near-continuous deposition between the bounding surfaces *Spn* to *Sn5*.

Calculated rates of creation of minimum non-eustatic accommodation space in the seven wells are presented in Figure III-12. Considering the entire shelf of the Offshore Amazon Basin:

i. Rates of non-eustatic accommodation space increased from ca. 18-8 Ma, decreased during a more quiescent phase between 8-5.5 Ma, and subsequently increased again to reach a maximum during the Quaternary (Figure III-12);
ii. Comparing the different shelf regions, rates were consistently higher in the Central shelf since 24 Ma, resulting in a greater depth of paleo-surfaces there (Figure III-7);
iii. The rates of creation of non-eustatic accommodation space varied between the NW and SE shelves prior to and after 8 Ma: prior to 8 Ma, creation of accommodation space was more intense in the SE shelf than in the NW shelf, after 8 Ma more accommodation space was created in the NW shelf than in the SE shelf. This change can be seen by comparing wells at similar positions on the SE and NW shelves, e.g. inner shelf wells 23 and Pas 4A, or mid-shelf wells 18 and Pas 2A (Figure III-12).

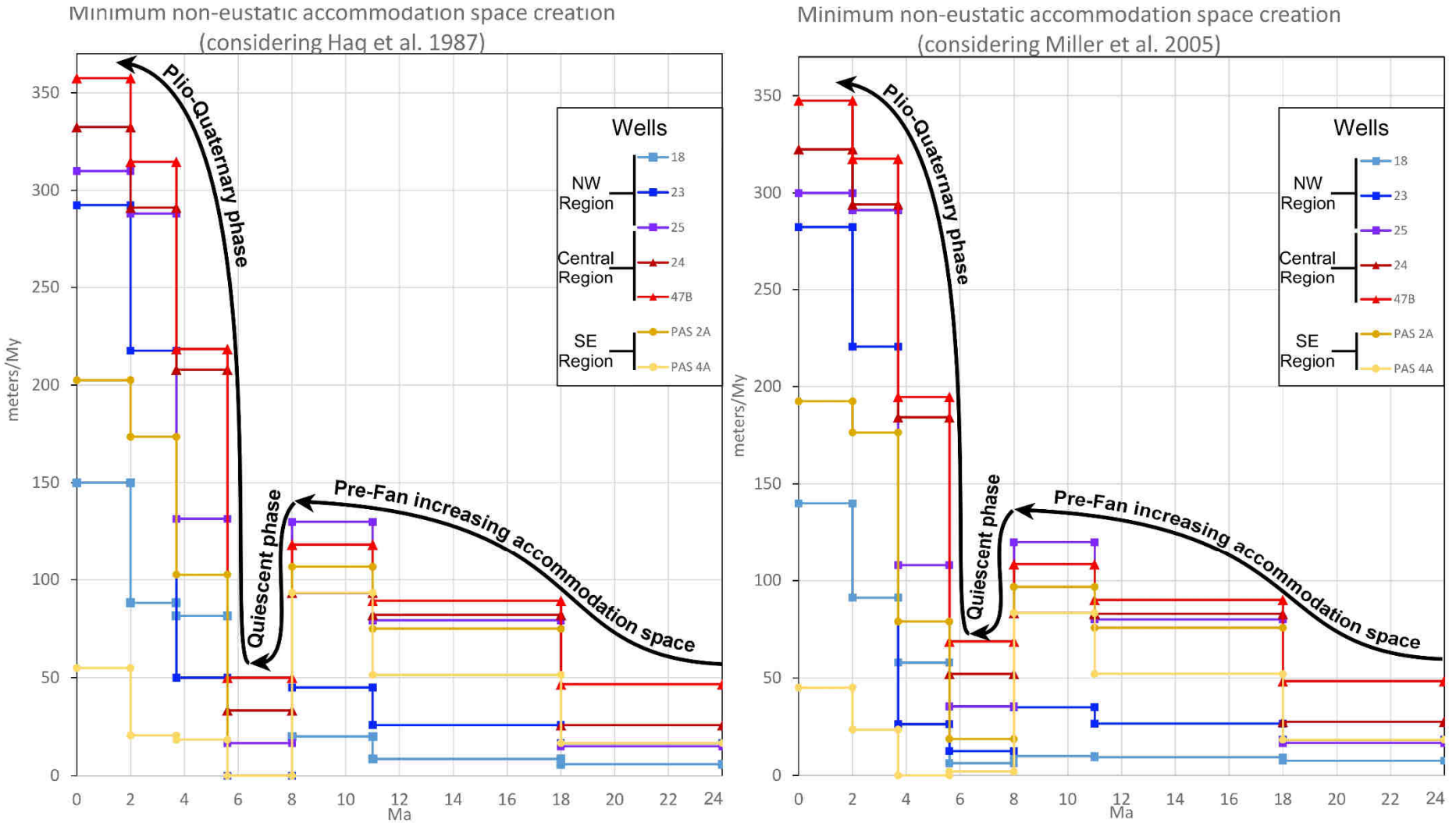

Figure III-12: Graphs summarizing calculations of the non-eustatic accommodation space required for the deposition of each Neogene sedimentary unit on the Amazon shelf, based on the observed thicknesses and proposed ages of units N1 to N5.

III.5 DISCUSSION

The results above provide a new picture of the Neogene evolution of the Offshore Amazon Basins, allowing a more detailed characterization of spatial and temporal changes in carbonate and siliciclastic deposition across the continental shelf. In this section, we first examine the deposition of the Neogene units in relation to the variable rates of creation of non-eustatic accommodation space along the shelf, the patterns of which we argue to indicate responses to tectonism and/or loading. We then discuss the stratigraphic and paleogeographical evolution of carbonate vs siliciclastic environments through time across the Amazon shelf.

III.5.1 Meaning of non-eustatic accommodation space creation

Accommodation space creation in marine environments is argued to be mainly controlled by the interaction of eustatic variations with subsidence (Catuneanu, 2002). Subsidence includes the effects of isostatic compensation for loading and the underlying tectonic subsidence (which may be due to rifting, cooling and flexure). By subtracting the eustatic component from the undecompacted thickness of stratigraphic units (subsection III.4.3), we obtain a minimum estimate of the accommodation space created by all forms of subsidence.

This approach may overestimate the eustatic component as it assumes that all accommodation space created by eustasy would be immediately filled-up. Nevertheless, we consider that, on the inner-middle shelf, such imprecisions should not account for more than a few tens of meters for sediment intervals hundreds of meters thick. In this context, the trends of the non-eustatic accommodation signal illustrated in Figure III-12 indicate that since at least 24 Ma, the Offshore Amazon Basin was affected by creation rates of non-eustatic accommodation space that varied across the three shelf sectors (NW, Central and SE), resulting in greater thicknesses of the units N1-N5 in the Central shelf (Figure III-4 toFigure III-6). This indicates that the margin was affected by greater subsidence in the Central shelf, due to either localized extension and/or to cooling, or along-shelf flexure of the lithosphere. Higher subsidence rates in the Central shelf could also be related to lithospheric thinning inherited from the Atlantic Rift related to the occurrence of a series of deep-buried extensional structures (Figure III-7A; Schaller *et al.*, 1971).

Intense flexural subsidence on the Offshore Amazon Basin has been classically attributed to a loading effect of rapid deposition of the Amazon Fan (e.g. Driscoll and Karner, 1994). However, our calculations of non-eustatic accommodation space show that the differential subsidence of the Amazon shelf since 24 Ma long pre-dates the initiation of the Amazon Fan, recently dated by Hoorn *et al.*, (2017) to 9.4–9 Ma. We suggest that greater subsidence in the Central shelf could instead be responsible for capturing the basin's sediment input, and thus acting as a major controlling factor on the distribution of thicker depocenters, which are located more than 200 km northward of the Amazon River mouth. In that sense, flexural subsidence caused by loading of the Amazon Fan would be a positive feedback on a margin that was already prone to differential subsidence before the onset of a higher influx of sediment. Differential subsidence along the shelf may also explain why, during the deposition of units N2 to N3 (18-8 Ma), carbonate environments could be persistent and distributed across the more quiescent NW shelf, whereas in the Central and SE shelves the carbonate factory was only intermittently active due higher rates of accommodation space creation that favored the fast drowning of bioconstructor organisms.

The calculated rates of creation of non-eustatic accommodation space may also provide a missing piece to an alternative model for the cessation of the carbonate production on the Amazon shelf without the onset of a transcontinental Amazon River during the Late Miocene. The sudden reduction of regional subsidence verified around 8 Ma (Figure III-12) may have slowed down the creation of accommodation space on the coastal-inner shelf region. The sedimentary load transported by the paleo-Amazon River would no longer be "withheld" by intense accommodation space creation on the coastal-innermost shelf region so that the proximal siliciclastic systems may have been finally able to advance over the Amazon shelf, suppressing carbonate production everywhere near the mouth of the paleo-Amazon River. This hypothesis and that of a Late Miocene transcontinental Amazon River are not mutually exclusive, but it is clear to us that it is possible to envisage a scenario of carbonate suppression on the Amazon margin without the assumption of significant enlargement of the paleo-Amazon River catchment area.

III.5.2 Neogene evolution of the Amazon shelf: interaction of carbonate vs siliciclastic environments through time

Our results on the depositional architecture of the Amazon mixed carbonate-siliciclastic shelf (section III.4.1), refined age models (section III.4.2) and calculations of non-eustatic accommodation space (section 4.3) allow us to divide the Neogene history of the Amazon shelf into four main depositional stages: From ca. 24–8 Ma **(Stage 1)** the Amazon shelf was characterized by a predominantly aggrading mixed carbonate-siliciclastic shelf; from ca. 8–5.5 Ma **(Stage 2)** the Amazon shelf was subjected to increasing volumes of siliciclastic input, with different implications for carbonate deposition in the NW, Central and SE shelf sectors; from 5.5–3.7 Ma **(Stage 3)**, the Central shelf embayment became gradually filled by sediments from the paleo-Amazon River, resulting in the progressive burial of carbonates in the NW shelf; and from 3.7 Ma **(Stage 4)**, the entire Amazon shelf became essentially siliciclastic.

Stage 1 (ca. 24-8 Ma)

We argue that the predominantly aggrading trend of a mixed carbonate-siliciclastic shelf that prevailed in the basin during the deposition of N1-N3 was caused by a combination of global sea-level rise during the deposition of unit N1 (between ca. 24 and 18 Ma; Haq *et al.*, 1987; Figure III-11) and the subsequent increase in rates of creation of non-eustatic accommodation space (subsidence) during deposition of units N2 to N3.

During deposition of unit N1, the Amazon shelf experienced laterally variable trends of shelf edge migration: the SE and Central Amazon shelves underwent a general landward migration of the shelf edge (together with carbonate backstepping and upper slope sedimentary collapse), while progradation was observed on the NW shelf (Figure III-4 to Figure III-7). These contrasting trends of sedimentary architecture in different shelf sectors were most likely a result of differential subsidence along the Amazon shelf. As shown by results (section III.4.3), between ca. 24-18 Ma, rates of creation of non-eustatic accommodation space were comparatively low in the Amazon shelf, but higher in the SE and Central shelves than in the NW shelf. An additional factor controlling shelf edge migration may have been better conditions of carbonate production in the NW shelf, which is located farther from the proto-Amazon River - the main source of terrigenous sediment input. The NW shelf seems to have evolved in an architectural trend similar to that of a pure carbonate shelf, which exports higher volumes of sediments (reworked carbonates) toward the slope region during highstands and is less prone to drowning during eustatic rises (e.g., Handford and Loucks, 1993; Schlager *et al.*,

1994; Betzler *et al.*, 2013). In such a context, with comparatively higher terrigenous influx, the Central and SE regions behaved in a manner similar to that of a typical siliciclastic platform which tends to retrograde during substantial rises in sea level (Catuneanu, 2002).

Differential subsidence appears to have affected carbonate production on the Amazon shelf from around 18 Ma. At that time, the coralgal platform on the Central shelf was drowned most likely due to intense subsidence (Figure III-12) combined with global sea-level rise (Haq *et al.*, 1987; Miller *et al.*, 2005; Figure III-11) and carbonate sedimentation was replaced by predominantly siliciclastic sedimentation (Figure III-13). An additional restraining factor for carbonate production on the Central shelf during Stage 1 may have been a comparatively higher influx of terrigenous sediments (mostly muddy), capable of reducing the availability of hard substrate and of increasing the turbidity of the water column, which are both critical elements for bioconstructor organisms (Woolfe and Larcombe, 1998). In any case, terrigenous sedimentation never prevailed over carbonate production in the Central shelf prior to ca. 18 Ma, being restricted to troughs that conducted siliciclastic sediments directly to the slope (Figure III-13). Meanwhile, on the SE and NW shelves, where subsidence rates were less intense (Figure III-12), carbonate production was able to persist throughout the middle-outer shelf domains, while siliciclastic proximal systems retreated progressively landward (Marajó Formation) to prevail only on the inner shelf (Figure III-14 and Figure III-15).

Considering the deposition of N2, calculations of non-eustatic accommodation space (section 4.3) between ca. 18-11 Ma (Figure III-12) also suggest that differential subsidence was a major controlling factor for sedimentary architecture along the Amazon shelf. During this period, the creation of non-eustatic accommodation space increased notably in the SE and Central shelves (Figure III-12), but different stratal architectures and carbonate distribution indicates that subsidence acted differently over these two shelf sectors. A contrasting trend of shelf edge migration throughout different sector of the Amazon shelf persisted as the edge of the Central shelf continued to retrograde while the NW shelf prograded, but by this time the SE shelf edge also experienced a slightly prograding trend. It is likely that a prolonged Langhian-Serravalian sea-level fall (Haq *et al.*, 1987; Figure III-11) favored the prograding trend seen in the SE shelf during the deposition of unit N2 as intense creation rate of non-eustatic accommodation space was verified during this period (Figure III-12). Meanwhile, in the Central shelf, intense subsidence probably compensated a trend of falling sea-level until the end of the deposition of unit N2, when the dramatic early Tortonian sea-level drop (Haq *et al.*, 1987; Figure III-11) led to exposure of the entire shelf. Deep and large incisions observed in seismic profiles (Figure III-6B) are evidence of incision by rivers and large-scale slope instabilities.

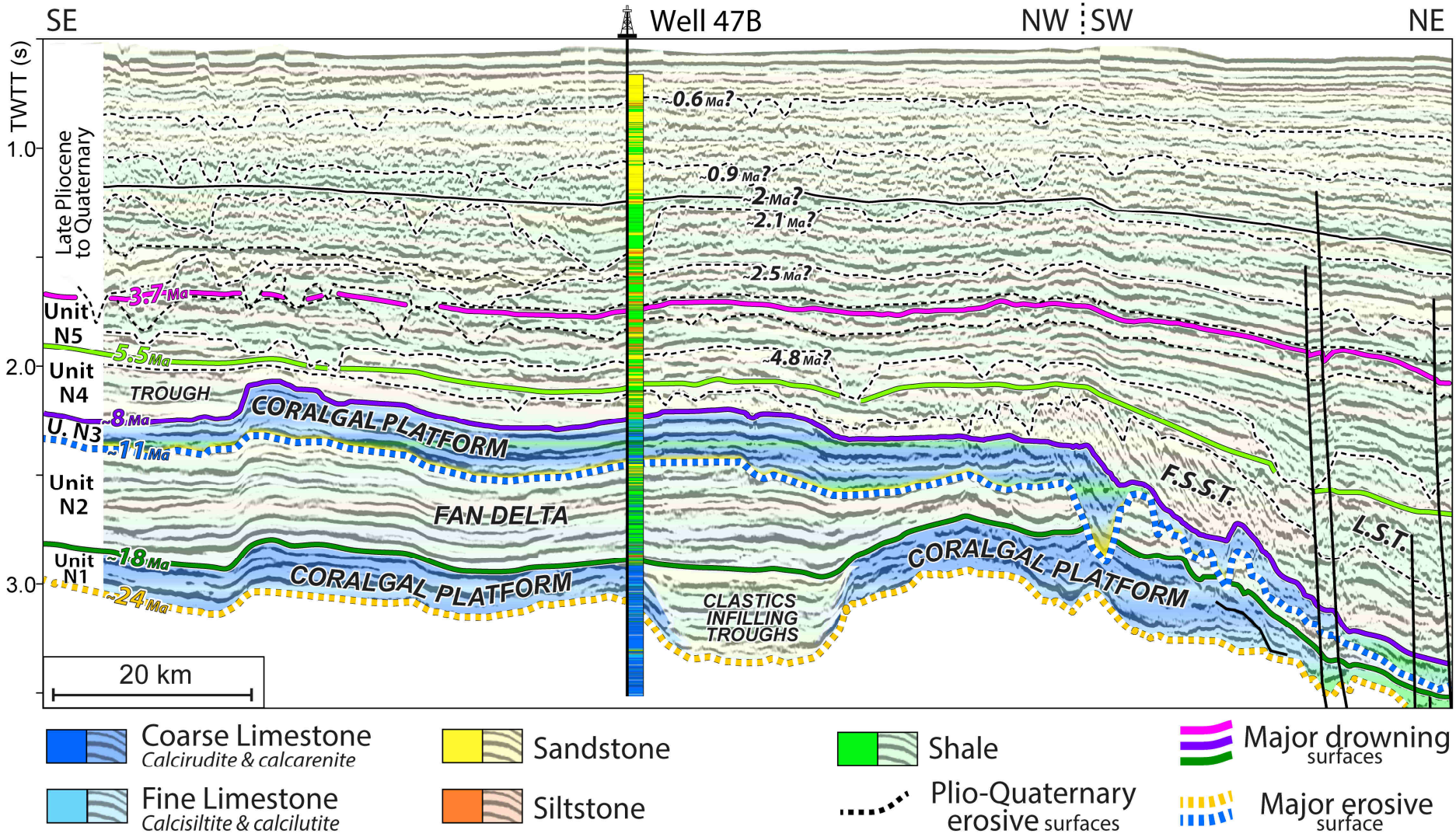

Figure III-13: Interpreted seismic profile (location in Figure III-1) highlighting each age-constrained surface across the Amazon shelf, together with lithological interpretations based on correlation to well 47B (and neighboring wells). Note that carbonate sedimentation resumed above the Tortonian erosive surface (ca. 11 Ma) and persisted until ca. 8 Ma when a prograding wedge covered the shelf. Pliocene-Quaternary sequence boundaries after Gorini *et al.* (2014).

A dramatic eustatic drop that occurred at the beginning of the Late Miocene (ca. 11 Ma; Haq *et al.*, 1987; Figure III-11) resulted in deep incisions and extensive surface truncations across the Central shelf (Figure III-6 and Figure III-13). According to Haq *et al.* (1987), after this major sea-level drop, global sea level rose during the Late Miocene, but remained lower than in the Early-Middle Miocene (Figure III-11). We therefore suggest that the reestablishment of carbonate production on the Central shelf during the deposition of unit N3 (ca. 11-8 Ma) was most likely a consequence of the extended eustatic lowering in the Late Miocene, which may have partially compensated the intense creation of non-eustatic accommodation space in the region. During the deposition of unit N3, the same eustatic lowering enabled carbonate bioconstructor organisms to colonize more distal portions of the SE shelf (Figure III-14).

For both the Central and SE shelves, lithological data also reveal that the carbonates of unit N3 represent the ultimate expression of carbonate environments of the Amapá Platform over these regions (Figure III-3, Figure III-5 and Figure III-6). At around 8 Ma, the Amazon shelf experienced its most important environmental change during the Neogene, as terrigenous sediments began to be supplied in volumes large enough to bury the carbonate units of the Central and SE shelves. Correlation of seismic analyses and our age model to global sea level curves indicates that the cessation of carbonate production on the Central and SE shelves was coeval with a sea-level highstand (Figure III-11), as previously proposed by Carozzi (1981), during the latest Tortonian. In such a context, it is interesting to note that the death of the carbonate platform in the Central and SE shelves probably post-dates the onset of deposition of the Amazon Fan, rather than pre-dating it as reported by Hoorn *et al.* (2017). According to these authors, high sedimentary fluxes marked the beginning of fan deposition between 9.4-9 Ma, whereas our biostratigraphic data point to a cessation of carbonate production on the Central and SE shelves at some point between 7.78-9.1 Ma (most likely around 8 Ma; Figure III-13 and Figure III-14). However, as our age model shows that the oldest possible age for the top of the Amapá carbonates in the Central and SE shelves (9.1 Ma) is comparable to the earliest possible age for the Amazon Fan initiation (9 Ma), the two events may have been coeval. Nonetheless, long-lasting carbonate production most likely persisted on the shelf after the onset of deposition of the Amazon deep-sea fan.

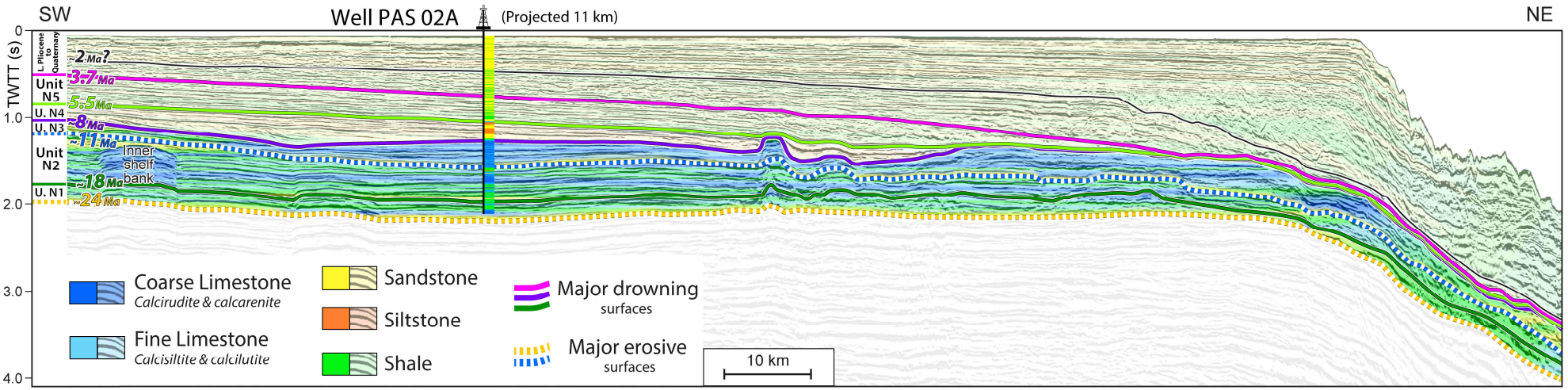

Figure III-14: Interpreted seismic profile (location in Figure III-1) highlighting each age-constrained surface across the Amazon shelf, together with lithological interpretations based on correlation to well Pas 02A (and neighboring wells). Note that carbonate sedimentation resumed above the Tortonian erosive surface (ca. 11 Ma) in the form of pinnacle reefs and wide carbonate banks.

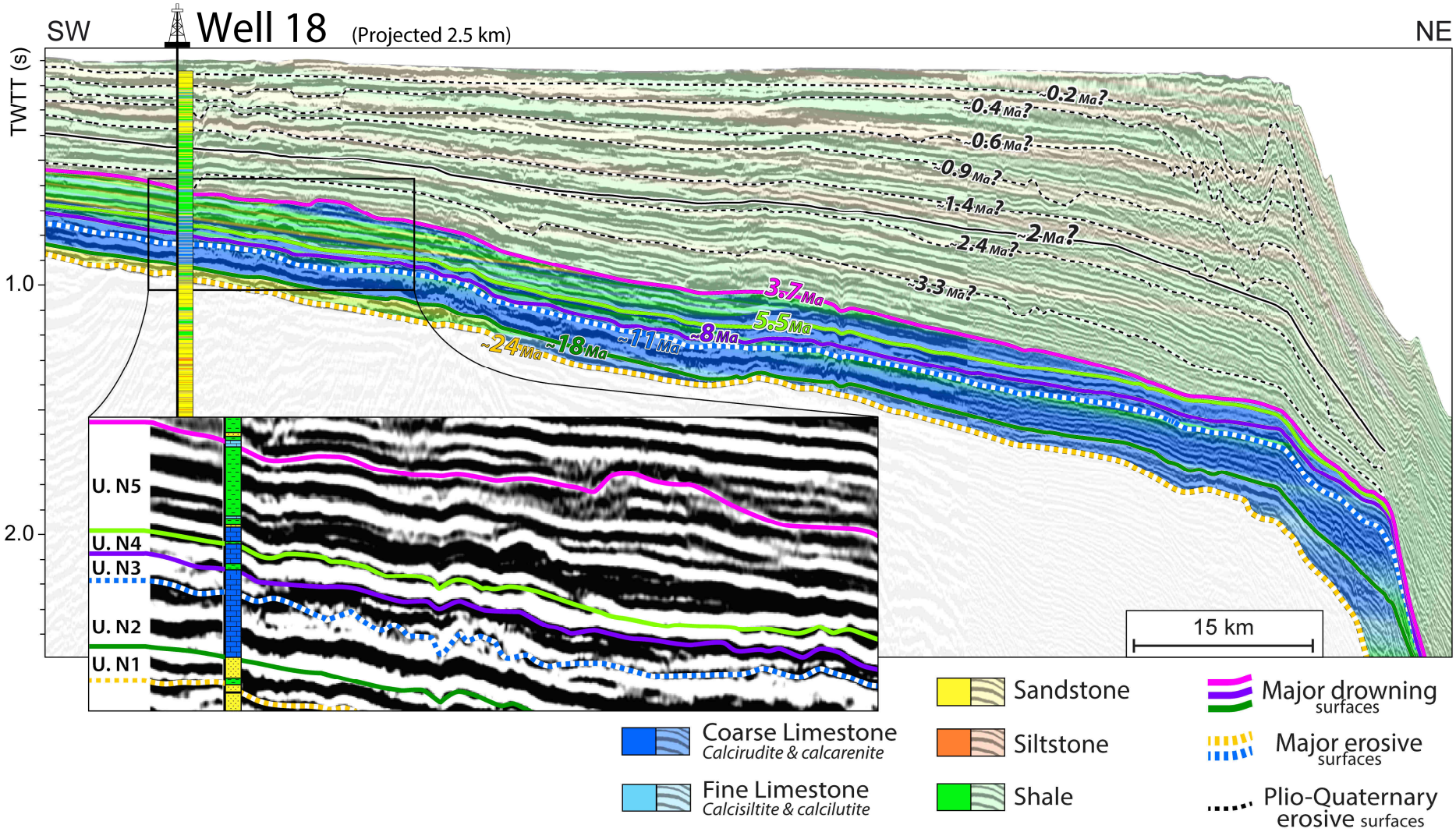

Figure III-15: Interpreted seismic profile (location in Figure III-1) highlighting each age-constrained surface across the Amazon shelf, together with lithological interpretations based on correlation to well 47B (and neighboring wells). Note that carbonate sedimentation resumed above the ca. 8 Ma Tortonian flooding surface and persisted until the Early Pliocene (unit N5), when a prograding wedge covered the former inner paleo-shelf. Pliocene-Quaternary sequence boundaries after Gorini *et al.* (2014).

Stage 2 (ca.8 Ma-5.5 Ma)

During the development of Unit N4 (ca. 8–5.5 Ma), deposition of terrigenous sediments on the Amazon shelf was clearly controlled by the morphology of the former carbonate platform, being mostly confined to inherited topographic lows in the Central and SE shelves (Figure III-13 and Figure III-14). The confinement of terrigenous sediments to topographic lows at the top of the carbonate platform was probably caused by a decrease in accommodation space creation in the area during the Late Miocene-Early Pliocene (quiescent phase in Figure III-12). Meanwhile, seismic and well data indicate that carbonate production persisted across the NW shelf during the deposition of unit N4 (Figure III-4), confirming that carbonate production persisted for much longer in this area than nearer to the Amazon River mouth as proposed by Gorini *et al.* (2014). We further argue that carbonate production on the NW shelf was only able to persist during deposition of Unit N4 due to the presence of the large embayment on the Central shelf that captured the Amazon-derived siliciclastic input, virtually isolating the NW shelf from the sediments carried by the Paleo-Amazon River (Figure III-7).

Stage 3 (ca. 5.5–3.7 Ma)

During the development of Unit N5 (Early Pliocene; 5.5–3.7 Ma), a thick prograding wedge (~85 m) advanced across the inner shelf in the NW region (Figure III-15), showing that the increasing supply of terrigenous sediments was able to circumvent the partially filled embayment on the Central region. Carbonate sedimentation on the NW shelf was able to persist in the form of continuous layers only on the outer shelf. These observations suggest that during the Early Pliocene, the entire Amazon shelf was already subject to conditions comparable to those of the present, with carbonate production greatly reduced due to environmental stresses on bioconstructor organisms, such as increasing turbidity and higher nutrient availability. Such a finding is further supported by the microfacies analysis of wells 18 and 27 (see Figure III-1 for locations) conducted by Wolff and Carozzi (1984), who pointed out that the uppermost units of the carbonate platform represent the first time that bryozoan fragments were the dominant sedimentary components. Although bryozoan fragments are rarely dominant in post-Paleozoic tropical carbonate shelf deposits (Taylor and Allison, 1998), they have been reported to thrive in conditions of limited luminosity and increased nutrient supply (Pomar, 2001). As such, deposition of unit N5 on the NW shelf marks a transition between an environmental context established during the Early Miocene (ca. 18 Ma), when carbonate production prevailed across the inner to outer shelf, and the modern depositional pattern in which restricted carbonate

sedimentation results only in local thin occurrences interbedded with terrigenous Late Pliocene-Quaternary successions (Figure III-15).

Stage 4 (3.7 Ma onwards)

From 3.7 Ma onwards the Amazon shelf was dominated by siliciclastic sediment supply to form prograding clinoforms (Figure III-13 to Figure III-15). During this stage, carbonate sedimentation resumed episodically on the outer Amazon shelf, presumably during periods of reduced terrigenous influx as reported for the last marine transgression (Moura *et al.*, 2016). Nevertheless, such sparse and short-lived carbonate production episodes after 3.7 Ma are not comparable to the widespread carbonate-dominated deposition that resulted in platform environments, which ceased to exist around 8 Ma in the margin's Central and SE shelf and around 5.5 Ma on the NW shelf.

III.6 SUMMARY AND CONCLUSIONS

This study provides new insights into the nature and evolution of mixed carbonate-siliciclastic sedimentary environments on the equatorial continental margin offshore the Amazon River, through the correlation of seismically-defined stratigraphic units to lithological and biostratigraphic data in wells, comparison of the resulting age-constrained depositional units to global sea level curves, and calculation of non-eustatic accommodation space.

One major outcome of this study is to show that the dynamics of mixed carbonate and siliciclastic shelf environments may be strongly influenced by accommodation space creation along a margin. In the case of the Amazon shelf, the differential creation of non-eustatic accommodation space resulted in the development of a 150 km wide embayment on the Central shelf. Such differential creation of accommodation space, suggested to reflect underlying forms of tectonic subsidence, was the most important factor controlling the distribution and functioning of the carbonate factory during the Neogene.

Another outcome is an alternative model to explain the increased influx of terrigenous sediments into the Offshore Amazon Basin during the Late Miocene. We argue that a reduction in the rates of accommodation space creation around 8 Ma may have allowed the progradation of terrigenous depositional systems that were previously being held in proximal positions within the basin. Our results do not exclude the possible establishment of a transcontinental Amazon

River during the Late Miocene, but suggest that this may not be necessary to explain the depositional history of the Amazon margin.

Our results also testify to the endurance of carbonate bioconstructor organisms during the Neogene in equatorial environments, where only large sea level rises and high terrigenous influxes were able to put an end to regional carbonate production. In this regard, we divided the Amapá Carbonates (the Amazon carbonate platform) into three different shelf regions (SE, Central and NW) according to the internal architecture of the carbonate platform. The inferred effects of differential non-eustatic accommodation space creation on the three shelf regions include:

(1) During a period of increasing creation of accommodation space between ca. 18-8 Ma, carbonate production grew to dominate the inner parts of the SE and NW shelves as terrigenous sedimentation retreated landward. In contrast, in the Central shelf where the highest rates of accommodation space creation are recorded, bioconstructor organisms were unable to keep up with rising sea levels, such that carbonate sedimentation was suppressed until ca. 11 Ma when a global sea level fall allowed recolonization of the shelf;

(2) A dramatic reduction in accommodation space creation at ca. 8 allowed the progradation of proximal siliciclastic depositional systems, burying carbonates that had previously developed on the SE and Central shelves. Widespread carbonate production was able to persist only in the NW shelf as this area was isolated from the paleo-Amazon River, the sedimentary load of which was captured by the broad embayment on the Central shelf and forced to directly to the continental slope;

(3) From 5.5 Ma onward, the Amazon shelf witnessed another phase of increasing creation of accommodation space, probably related to flexural subsidence related to the sedimentary load caused by an ever increasing sediment influx to the margin. Between ca. 5.5-3.7 Ma, sedimentation on the NW shelf underwent a transition from predominantly carbonate to predominantly siliciclastic, as the large embayment on the Central shelf was gradually filled, allowing terrigenous sediment to finally reach the NW shelf. It was only after complete infilling of the central embayment around 3.7 Ma that terrigenous sediments were able to prograde cross the entire NW shelf, leading to cessation of carbonate production on the Amazon continental shelf.

CHAPTER IV
THE AMAZON MARGIN TECTONIC FRAMEWORK

CHAPTER IV

This chapter consists of an article that is due to be submitted once the article composing Chapter III is accepted for publication. In light of results revealing that three regions of the Offshore Amazon Basin have a distinct geodynamic and depositional history (CHAPTER III), an investigation was undertaken based on gravity and magnetic anomalies models in order to determine if underlying tectonic structures may have controlled post-rift sedimentation. As such, the main goal of the investigation presented here was to verify if the differential accommodation space creation on the NW, Central and SE shelves could be related to distinct tectonic domains along the margin. Models of gravity and magnetic anomalies in the public domain were used to interpret the underlying tectonic framework in regions where seismic data were unavailable or the crystalline basement was too deeply buried to be properly imaged. This study tackles a key subject to achieve a better understanding of the post-rift evolution of the Offshore Amazon Basin, the major depocenters of which are reported to be conditioned by underlying tectonic features inherited from the rift phase (Castro *et al.*, 1978; Silva *et al.*, 1999).

IV.1 INTRODUCTION

The Offshore Amazon Basin (known in Portuguese as *Bacia da Foz do Amazonas*) is an Atlantic-type passive basin located on the far north of the Brazilian Equatorial Margin (Figure IV-1). Early studies conducted in this area indicate that the Offshore Amazon Basin's major post-rift depocenters are located approximately along the axis of deeply buried grabens inherited from the rift phase (Rezende and Ferradaes, 1971; Schaller *et al.*, 1971; Castro *et al.*, 1978; Figure IV-4).This spatial coincidence suggests some influence of underlying tectonic structure on post-rift sediment distribution. However, the correlation between the major post-rift depocenters and deep-buried tectonic features is uncertain, as the basement configuration is not well described, with several tectonic frameworks proposed since the 1970s (e.g. Castro *et al.*, 1978; Costa *et al.*, 2002; Mohriak, 2003; Soares Júnior *et al.*, 2011). These conflicting interpretations are most likely a consequence of the great thickness of the sedimentary succession, which is commonly >8 km thick beneath the SE-Central shelves and up to 12 km thick on the Amazon deep-sea fan region (Braga, 1993), which hinders proper seismic observation of the underlying rift-phase tectonic features.

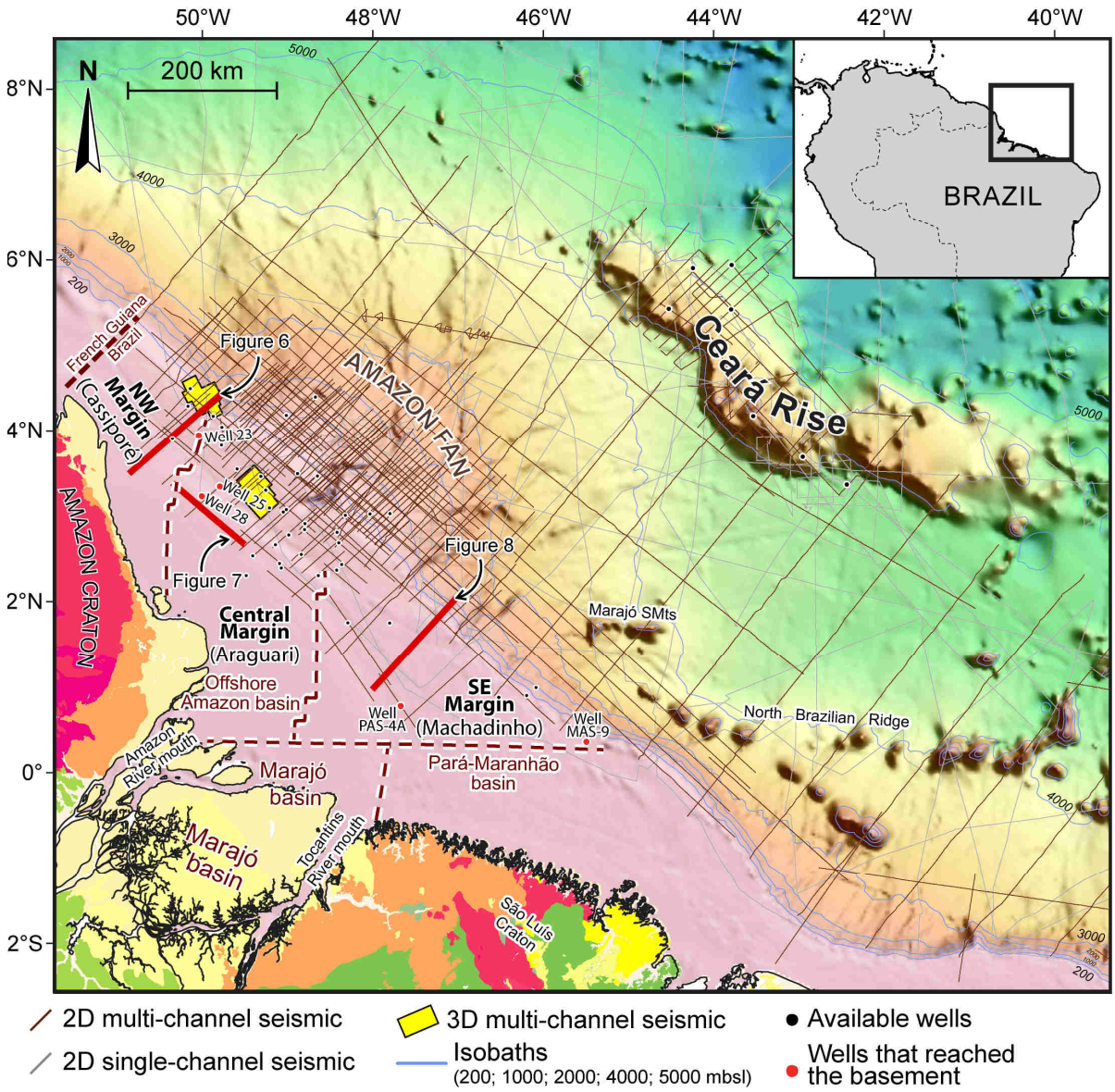

Figure IV-1: Map of the study area showing the available seismic and well dataset. The locations of Figure IV-6 to Figure IV-8 are shown as thick red lines

A lack of knowledge concerning the post-rift stratigraphic succession of the Offshore Amazon Basin also hindered attempts to appraise the possible influence of tectonic heritage. Although the stratigraphy of the basin has been the object of investigations by both the academic community and the oil industry since the early 1970s (*e.g.* Damuth and Fairbridge, 1970; Schaller *et al.*, 1971), until recently most studies (in the public domain) focused their investigations on the upper Quaternary succession. It was only during the last decade that studies conducted by my research group (GEOMARGEM group) began to systematically investigate and describe the stratigraphic architecture and features of the entire post-rift succession(Araújo *et al.*, 2009; Silva *et al.*, 2010; Reis *et al.*, 2016; Silva *et al.*, 2016; Gorini *et*

al., 2014). On the Amazon deep-sea fan, these studies have provided evidence of different forms of slope features: extensional and compressive faulting within the upper fan that records its ongoing gravity-driven collapse above overpressured detachments, as well as a Neogene history of large scale slope instability and sediment failure that has resulted in giant mass transport deposits (Reis *et al.*, 2010, 2016; Silva *et al.*, 2016). In addition, they have detailed the sedimentary processes related to a transition from predominantly carbonate to siliciclastic shelfal sedimentation (Gorini *et al.*, 2014). The most recent work (Cruz *et al.*, CHAPTER III) demonstrates that the Amazon shelf can be divided into three sectors (NW, Central and SE) based on distinct Neogene stratigraphic architectural and lithological elements. The distinct sedimentary records within the NW, Central and SE shelf sectors are interpreted to have been mainly caused by variations in carbonate production in response to different rates of non-eustatic accommodation space creation, probably due to differential subsidence (Cruz *et al.*, CHAPTER III). In this study, it was speculated that such variable geodynamic behavior along the Amazon shelf was likely to have been caused by a tectonic heritage related to uneven lithospheric stretching and thinning.

In order to verify if the variable geodynamic settings of the NW, Central and SE shelf sectors as inferred by Cruz *et al.* (CHAPTER III) coincide with domains of distinct structural framework, we conducted an investigation based on publicly-available models of gravity and magnetic anomalies, correlated with evidence from multi-channel reflection seismic data and from a few exploration wells.

The gravity models used in this study are the updated 2016 version V24 of the Sandwell *et al.*(2014) free-air gravity anomaly and vertical gravity gradient (VGG). Magnetic anomaly analysis is based on the Maus *et al.* (2009) EMAG2 model. These models were loaded in to Kingdom seismic interpretation software to allow correlations between potential fields and seismically interpreted structures. Due to the relatively low resolution of the gravity and magnetic models, 7 km and ~3.7 km respectively (Maus *et al.*, 2009; Sandwell *et al.*, 2014), our investigation is limited to first-order regional structures. Lithological descriptions of the basement available from a five wells (Figure IV-1) were also used in association with interpreted seismic profiles and potential field anomaly maps in order to examine the nature of the basement underlying different sectors of the Amazon margin.

IV.2 GEOLOGICAL SETTING

There is little consensus regarding the basement rocks and tectonic structures underlying the Offshore Amazon Basin. The crystalline basement has been reported to include igneous and metamorphic rocks of the Amazon Craton, together with metamorphic rocks of the Rokelide suture zone (Figueiredo *et al.*, 2007). The Rokelide suture zone is a Neoproterozoic-Cambrian (570-500 Ma) orogenic belt that outcrops in West Africa (Villeneuve, 2008; Figure IV-2). Most reconstructions of the Gondwanan supercontinent place the continuation of the Rokelide suture zone within South America along the Araguaia Neoproterozoic metamorphic belt, thus forming a single North-South trending Araguaia-Rokelide suture zone (Brito Neves, 2002; Brito Neves and Fuck, 2014; Figure IV-2). However, a third Neoproterozoic metamorphic orogenic belt may also underlie the Offshore Amazon Basin, as Villeneuve and Cornée (1994) proposed that the NW-SE trending Gurupi suture zone (750–550 Ma; Klein and Moura, 2008) forms a triple junction with the Araguaia and Rokelide belts in the region that roughly correspond to the boundary of the Marajó and Offshore Amazon Basins (Figure IV-2B). This hypothesis must be taken with caution as Klein and Moura, (2008) considered the western limit of the Gurupi belt to be uncertain and placed a possible triple junction between this suture and the Rokelide and Araguaia belts more to the south in their maps (beyond the Offshore Amazon Basin region).

The tectonic opening of the Offshore Amazon Basin is controversial and several schemes have been proposed for its age and evolution. According to Brandão and Feijó (1994) and Figueiredo *et al.* (2007), the basin dates back to the Late Triassic-Early Jurassic (235-194 Ma) when sandstones intercalated with tholeiitic basalts (Calçoene Formation) started to accumulate in a pre-rift sag basin. Other authors have proposed that a branch of the Central Atlantic rift extended over the Offshore Amazon Basin during this time (Zalan, 2004; Soares Júnior *et al.*, 2011). There is a general consensus that the basin's major rift phase took place during the Early Cretaceous in the context of the breakup of the South American and African continents and the opening of the Equatorial Atlantic Ocean (Matos, 2000; Figueiredo *et al.*, 2007; Soares Júnior *et al.*, 2008). However, the nature of the rifting process is also contentious, as some authors have invoked prevalent transform motions (Matos, 2000; Figueiredo *et al.*, 2007; Mohriak, 2003), while others consider the Offshore Amazon a divergent basin created due to prevailing extensional stresses (Basile, 2015; Basile *et al.*, 2005; Soares Júnior *et al.*, 2011).

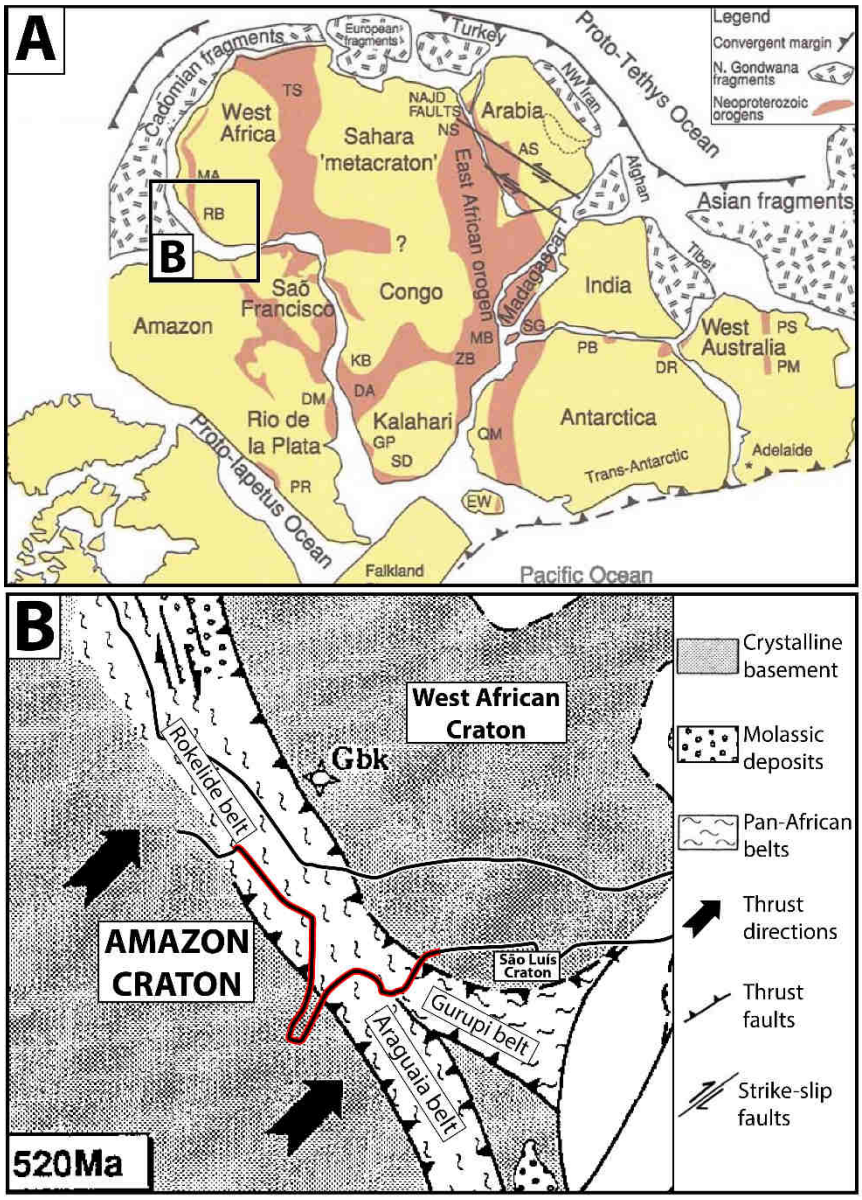

Figure IV-2: **A)**Map of Gondwana showing the general arrangement of Neoproterozoic orogenic belts according to Kusky *et al.* (2003) (modified by Kröner and Stern, 2005).**B)** Main structural features of the West African and Amazonian Cratons and surroundings belts around 520 Ma (modified after Villeneuve and Cornée, 1994). Modern day Brazilian and African coastlines shown as black lines for reference, with the coastline equivalent to this thesis' study area highlighted in red.

As a result of uncertainty as to the basement structure and rifting process, several conflicting tectonic frameworks have been proposed for the region. Figure IV-3 exemplifies some of the tectonic frameworks that have been proposed for the Offshore Amazon and Marajó basins. Only in the NW region there is some agreement among authors, as several studies report the presence of roughly NW-SE trending normal faults there, although Castro *et al.* (1978) and Mohriak (2003) arranged these as a series of half-grabens (the "Cassiporé graben") while Costa *et al.* (2002) and Soares Júnior *et al.* (2011) depicted a single elongate graben extending along

the NW shelf to the area of the Amazon River mouth. In the Central and SE shelves, there is no consensus as to the tectonic framework; while Castro *et al.* (1978) stated that that two branches of the Marajó basin graben extend northward into the Central-SE shelf, Costa *et al.* (2002), Mohriak (2003) and Soares Júnior *et al.* (2011) proposed that these regions were intersected by a series of normal and strike-slip faults of differing configurations (Figure IV-3). It is worth noting that among these works, Costa *et al.* (2002) and Soares Júnior *et al.* (2011) are the only peer-reviewed studies, while Mohriak (2003)supports some of the interpreted tectonic features with data (interpreted seismic profiles).

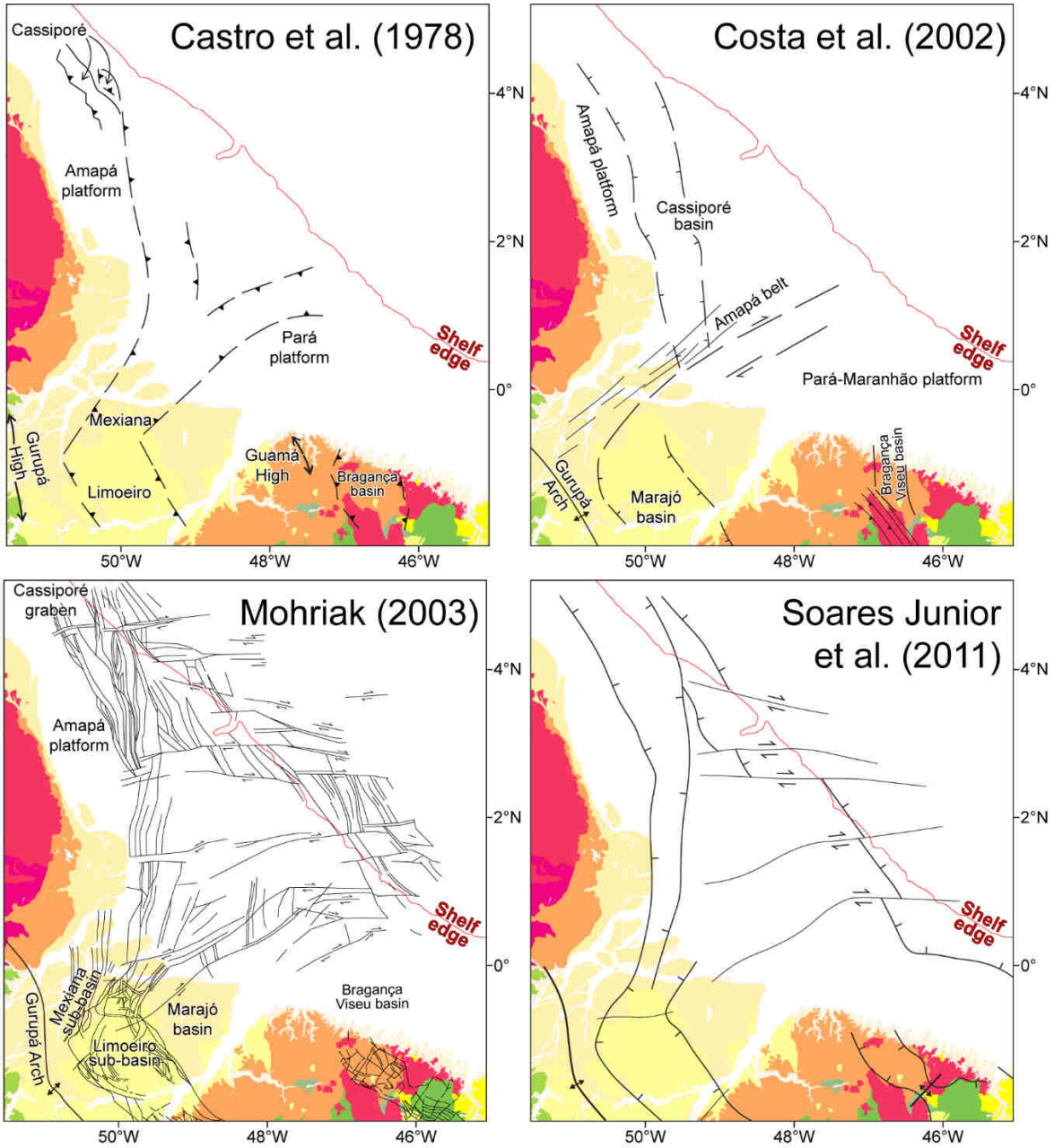

Figure IV-3: Compilation of different structural frameworks proposed for the Offshore Amazon Basin. Geologic map after the Geological Survey of Brazil database (CPRM, 2004).

According to Castro *et al.* (1978), post-rift deposition within the Offshore Amazon Basin was strongly controlled by earlier tectonic structures. These authors located the thickest post-rift successions along a NE-SW axis defined by underlying grabens inherited from Lower Cretaceous rifting (Figure IV-4). Although structural schemes conflicting with that proposed by Castro *et al.* (1978) have been proposed for the Offshore Amazon Basin, their statement that the post-rift succession was tectonically controlled seems to be supported by more recent studies that also recognize remarkable variations in Cenozoic sedimentary thickness along the Amazon margin (Silva *et al.*, 1999; Perovano *et al.*, 2009; Cruz *et al.*, CHAPTER III). Late Miocene to Recent sedimentary thickeness variation along the Amazon margin could be explained by isostatic flexural subsidence due to loading by the up to 9 km thick Amazon Fan as suggested by Braga (1993) and Driscoll and Karner (1994). However, Cruz *et al.* (CHAPTER III) argued that the thickness variation in shelfal sedimentary units predating the initiation of the Amazon Fan could not be the result of isostatic flexural subsidence in response to sedimentary loading because sediment influx into the basin was very low before the Late Miocene (see Figueiredo *et al.*, 2009 and Dobson *et al.*, 2001), implying that some kind of tectonic control must have favored thicker sedimentary accumulation in the central part of the margin.

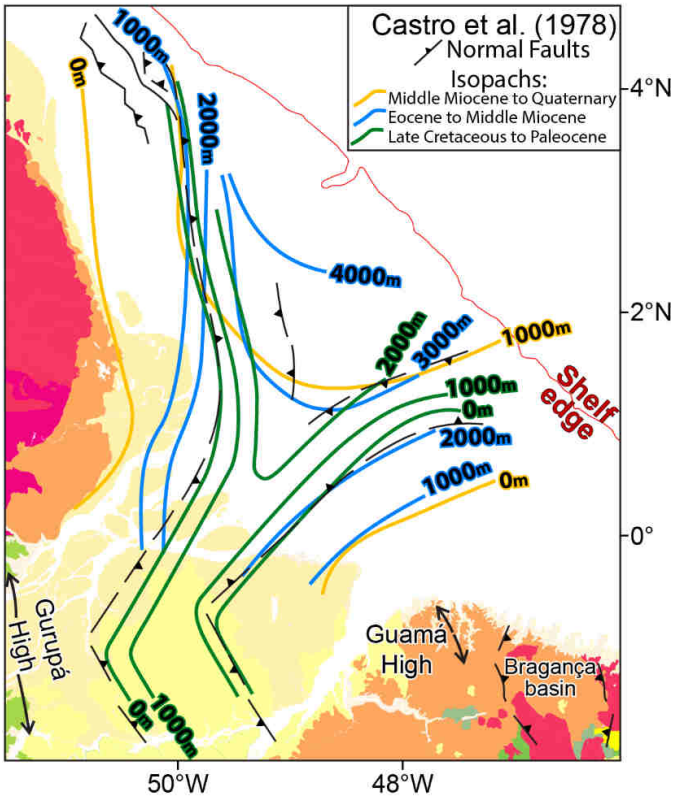

Figure IV-4: Superposition of structural framework and isopach maps of Offshore Amazon Basin post-rift megasequences according to Castro *et al.* (1978). Note that the authors located the basin's thickest post-rift successions along a NE-SW axis defined by underlying grabens. Geologic map after the Geological Survey of Brazil database (CPRM, 2004).

IV.3 TECTONIC DOMAINS OF THE AMAZON MARGIN

I recognize three domains of the Amazon margin with distinct structural styles: the NW margin, Central margin and SE margin (Figure IV-5). Here I describe the character of each of these domains in terms of potential field anomalies correlated with interpreted seismic profiles, in order to interpret the underlying structural framework.

NW margin

The NW margin is characterized by clear NW-SE trending free-air gravity anomalies on the shelf and a large lobe of negative values toward the slope and abyssal plain, and some N-S aligned anomalies with positive values near the limit with the Central shelf (Figure IV-5A). The VGG gravity gradient map (Figure IV-5B) also reveals NW-SE trending anomalies on the Central shelf, which gradually attenuate northward near the border between Brazil and French Guiana, but end abruptly to the south along a clear N-S boundary with the Central margin. An E-W oriented anomaly can be identified In the VGG map, and I interpret it as the continuation of a major strike-slip fault that crosses the adjacent abyssal plain all the way from the Ceará Rise to at least the NW continental slope, possibly extending landward into the shelf near the Brazil and French Guyana border (Figure IV-5B and D). The very clear NW-SE trending gravity anomalies observed on the shelf gradually dissipate against the possible landward extension of this major strike-slip fault and northward of this alignment gravity anomalies follow a different trend (WNW-ESE; Figure IV-5D).

Magnetic anomalies have different orientations than gravity anomalies across the region, with, wide WNW-ESE trending anomalies dominate the shelf and upper slope areas on the NW margin (Figure IV-5C). The character of magnetic anomalies in the NW lower slope-abyssal plain area are not clear, but a NE trend is apparent (Figure IV-5C). Unlike the gravity anomalies, the magnetic anomalies maintain the same general trend across the area of the Brazilian-French Guyana border.

The comparison of interpreted seismic lines and potential fields indicates a good correlation between low gravity values and structural lows generated by tilted blocks (Figure IV-6). The northwest-southeast trending gravity anomalies are therefore interpreted as half-grabens (hereafter referred to as Cassiporé half grabens following the nomenclature used by Castro *et al.*, 1978). The comparison also suggests that in places the highest magnetic anomalies

are coincident with the deepest parts of some of the Cassiporé half-grabens, but this is not seen everywhere and the overall trend of magnetic anomalies does not follow the structural framework inferred from gravity and seismic data (Figure IV-6). Seismic data also indicate that the post-rift succession thickens significantly seaward, with the Cenozoic units notably increasing from 0.2 seconds (twtt) beneath the inner shelf to over 2.0 seconds (twtt) beneath the outer shelf (Figure IV-6). The single available well that reached the basement on the NW margin (well 23, Figure IV-1) penetrate 31 meters of undifferentiated igneous rocks.

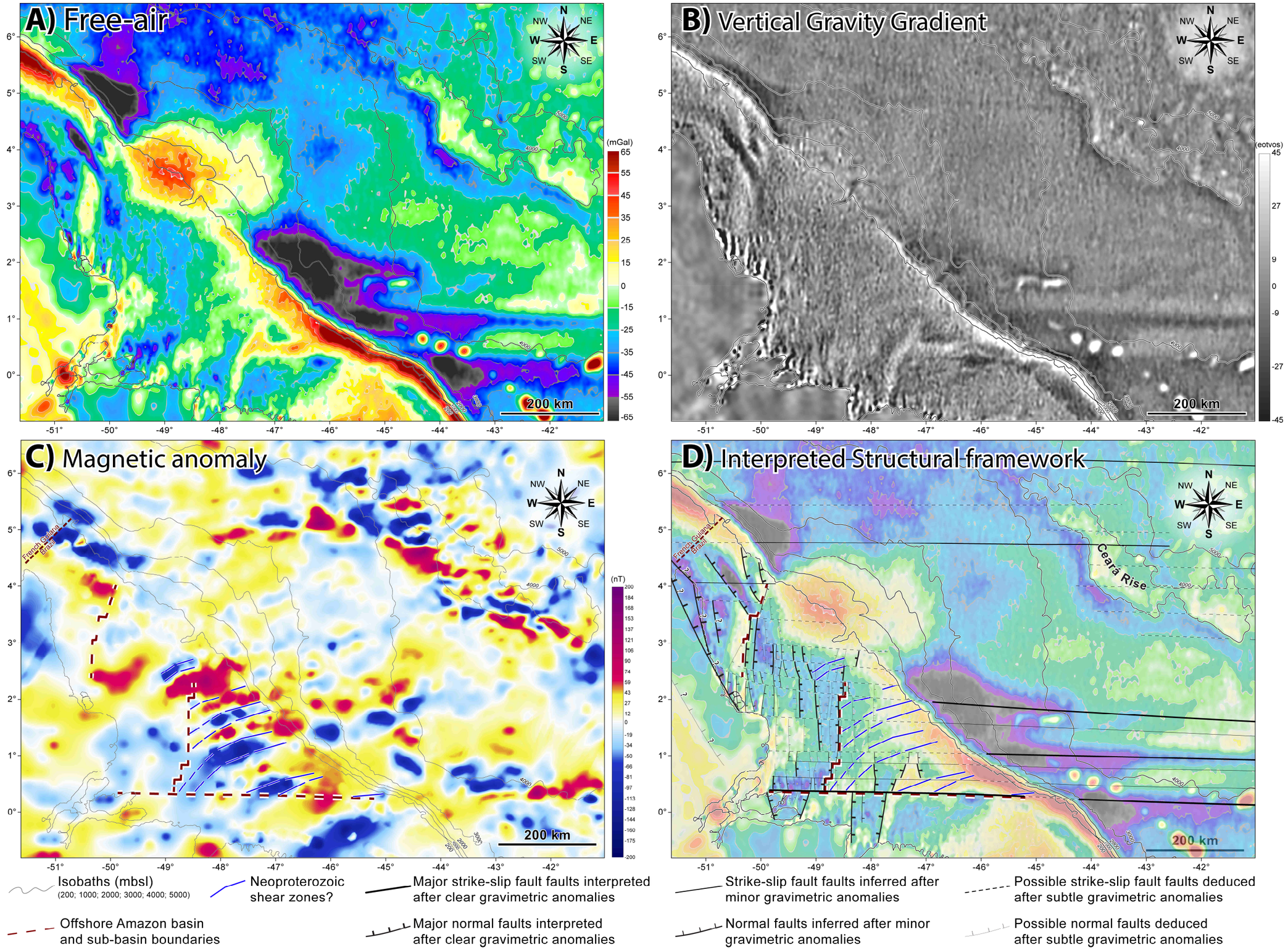

Figure IV-5: Geophysical potential field anomalies on the Amazon continental margin. Coastline and isobaths are shown for geographical reference, and the limits of the NW, Central and SE margins are shown in C and D. **A)** Free-air gravity anomalies according to Sandwell *et al.* (2014). **B)** Vertical Gravity Gradient (VGG) anomalies also according to Sandwell *et al.* (2014). **C)** Magnetic anomalies according to Maus *et al.* (2009). **D)** Interpreted structural framework superimposed on free-air gravity anomalies map.

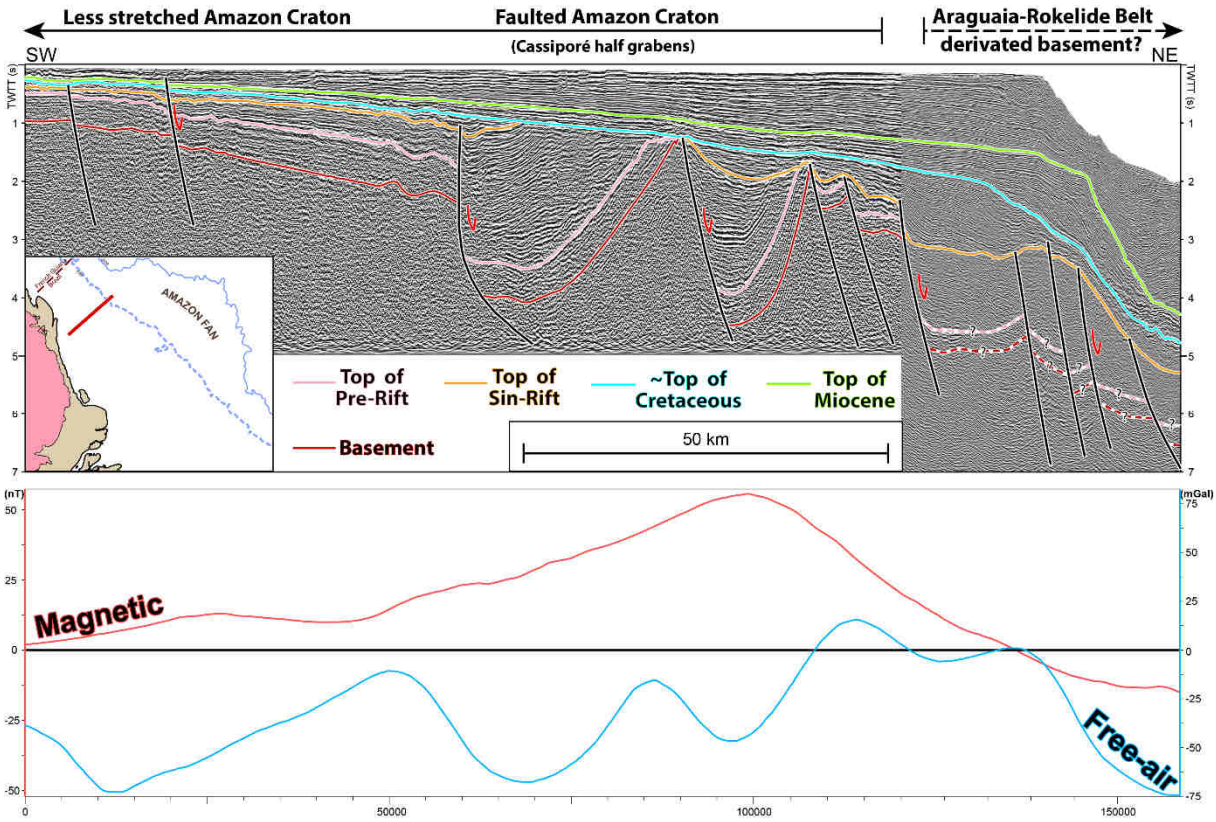

Figure IV-6: Top: interpreted seismic profile across the NW margin. Bottom: free-air and magnetic anomalies along the same profile, extracted from models by Sandwell *et al.* (2014) and Maus *et al.* (2009), respectively. Note that structural lows bounded by seaward dipping normal faults are associated with low free-air gravity anomalies.

Central margin

The Central margin is characterized by high free-air gravity anomalies on the inner shelf near the Araguari river mouth (Amapá estate), low anomalies with a general N-S trend in the inner-middle shelf, and very high anomalies in the Amazon Fan region (Figure IV-5A). The VGG gravity gradient map of the Central margin (Figure IV-5B) has an overall smooth character with no clear anomaly trends. The magnetic anomaly map (Figure IV-5C) shows clear NE-SW to ENE-WSW trends on the inner shelf that become more subtle in the Amazon Fan region, showing that gravity and magnetic anomalies have different orientations also in this part of the margin.

The basement and syn-rift sedimentary units lie at depths beyond seismic penetration across most of the Central margin. Although the thick post-rift succession makes it difficult to confidently interpret the structural framework, some first order observations can be made based on seismic lines close to the SE margin, where the basement is shallower. Where observed, the

basement and basal sedimentary units of the Central margin are complexly structured, affected by a series of normal faults that form graben-like structural lows (Figure IV-6). The basal sedimentary units contain evidence of at least three phases of tectonic deformation: a lowermost unit (pre-rift?) is highly deformed at the transition between the NW and Central margins; it is overlain by a unit that is less deformed in this area, but highly deformed to the SE (syn-rift?); this unit is in turn overlain by a unit that is more deformed to the SE (Figure IV-6). Comparison with potential fields (Figure IV-6) indicates that the grabens-like structures identified from seismic lines are correlated with low free air gravity anomalies on the inner-middle shelf. This correlation allows a confident interpretation of the N-S trending free air gravity anomalies as a series of structural lows (graben-horsts and/or half-grabens) across the Central margin (Figure IV-5D). Seismic interpretation also shows that post-rift sedimentary units in the Central margin thicken significantly toward the center of the basin (as reported by previous works; Castro *et al.*, 1978; Silva *et al.*, 1999; Perovano *et al.*, 2009), with the Cenozoic units notably increasing from 0.9 seconds (twtt) near the boundary with the SE margin to over 5.0 seconds (twtt) in the central portion of the inner shelf and over 9.0 seconds in the Amazon Fan region.

The base of wells 25 and 28 (location on Figure IV-1) reached basement to penetrate thick basalt layers (60 m 370 m, respectively), indicating the occurrence of large basaltic flows in the Central margin. In well 25, thin basalt layers (<5 m thick) are also intercalated with overlying syn-rift sedimentary units (as reported by Brandão and Feijó, 1994), thus attesting to the persistence of volcanic activity during the rift phase.

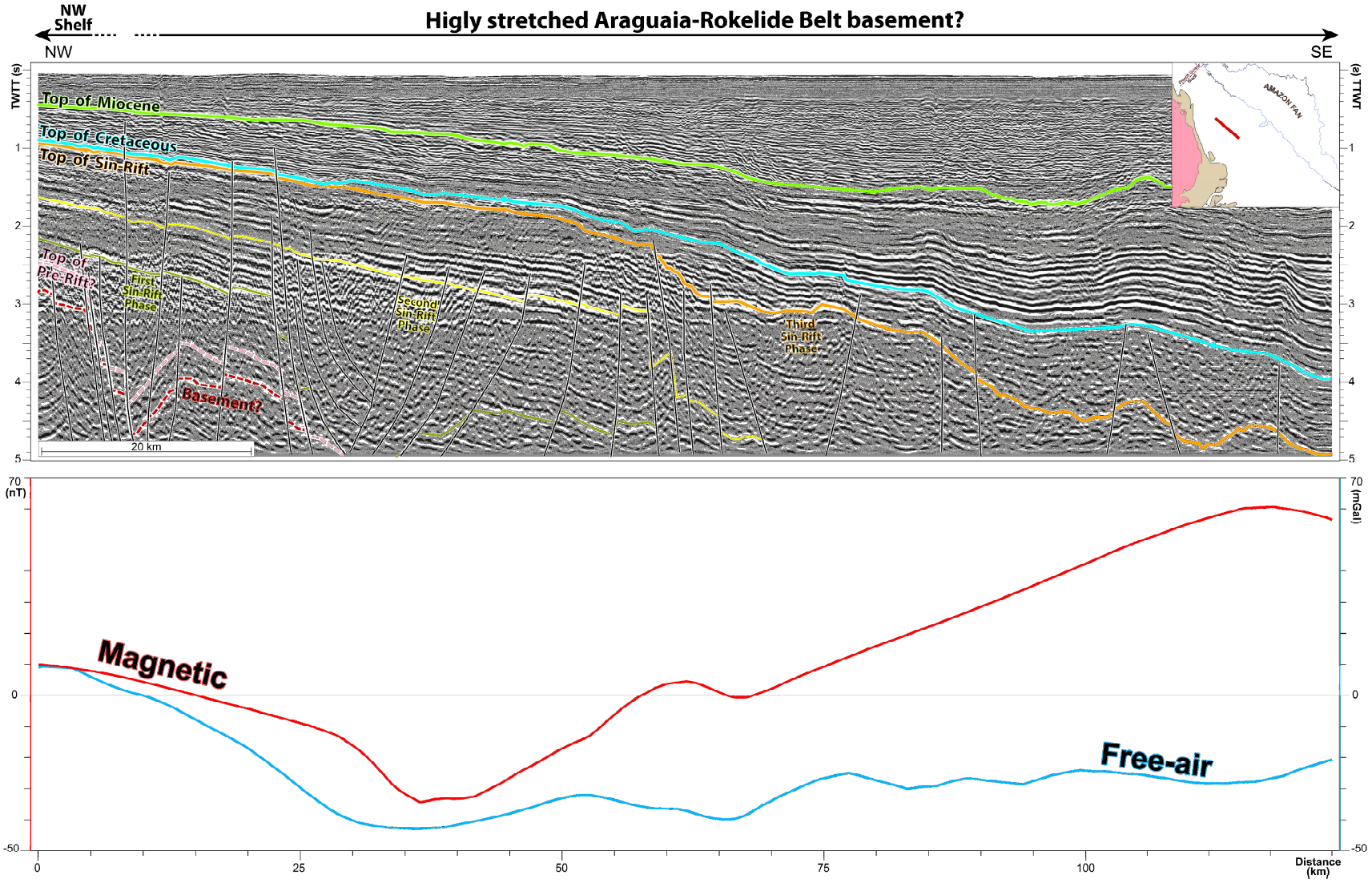

Figure IV-7: Top: interpreted seismic profile across the Central margin. Bottom: free-air gravity and magnetic anomalies along the same profile extracted from models by Sandwell *et al.* (2014) and Maus *et al.* (2009), respectively. Note that some fault-bounded structural lows at basement level beneath the inner shelf are associated with low free-air anomalies

SE margin

The SE margin is characterized by a seaward increase of free-air gravity values toward the shelf edge, associated with subtle ENE-WSW trending anomalies across the shelf and a large area of negative values on the continental slope and rise (Figure IV-5A). In the south, some free-air anomalies are displaced along a series of east-west alignments, here interpreted as strike-slip faults aligned with low anomalies observed to seaward in the abyssal plain and related to the Saint Paul Fracture Zone. The VGG map (Figure IV-5B) has a smooth character with no clear anomalies on most of the shelf, but to the south a clear positive anomaly marks the limit between the Offshore Amazon basin and the Pará-Maranhão platform (São Luís Craton). Magnetic anomalies on the SE shelf show clear ENE-WSW trends that are well correlated with free-air gravity anomalies (Figure IV-5A and B). Magnetic anomalies in the SE slope-abyssal plain region have a less clear pattern, with some NNE trending highs and lows associated with volcanic highs of the North Brazilian Ridge. It is worth mentioning that the magnetic anomalies of the SE margin are remarkably similar to those in Liberia, on the African conjugate margin, where a reverse correlation between free-air and magnetic anomalies can also be observed (Figure IV-9).

The limit between the Central and SE margins is assigned along a N-S line that separates regions with free-air anomalies that mainly trend N-S (Central shelf) versus ENE-WNW (SE shelf) (Figure IV-5D). Toward the continental slope and rise, this distinction is less clear, but an E-W alignment that separates a domain of higher free-air anomalies and more subtle magnetic anomalies on the Central margin from a domain of lower free-air anomalies and more intense magnetic anomalies associated with volcanic highs to the SE (Figure IV-5D). I interpret this E-W alignment as a strike-slip fault, separating the Central margin slope and the SE margin slope.

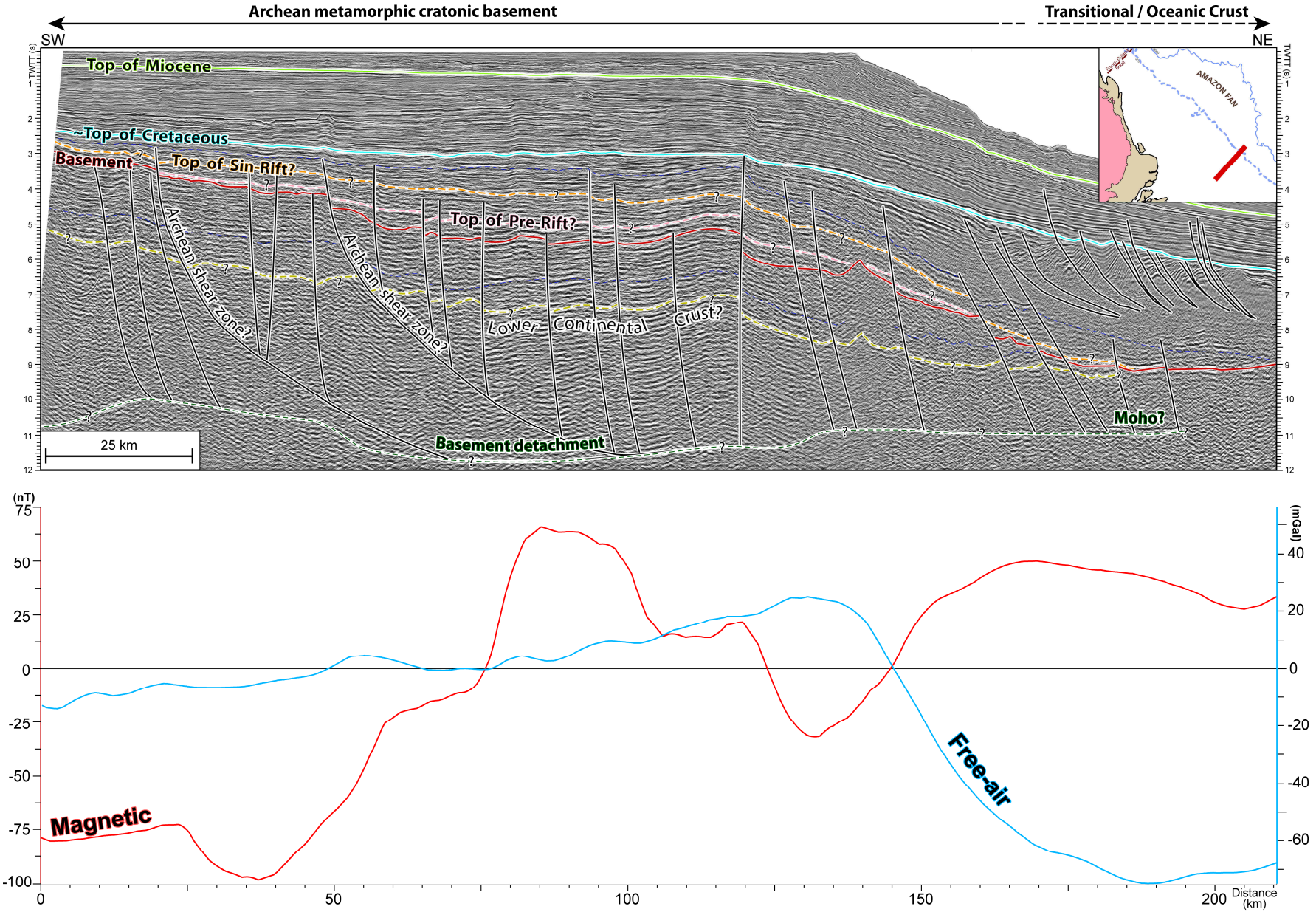

Figure IV-8: Top: interpreted seismic profile across the SE margin. Bottom : free-air gravity and magnetic anomalies along the same profile, extracted from models by Sandwell *et al.* (2014) and Maus *et al.* (2009), respectively. Note that the seaward dipping normal faults have no clear expression in free-air anomalies.

Seismic profiles across the SE margin afford poor imagery of deeply buried basement and basal sedimentary units (Figure IV-8). Nonetheless, it is clear that the overlying sedimentary succession in the SE margin is less structurally influenced than in the NW and Central shelf, affected by only a few normal faults with low offsets (Figure IV-8). Structural lows in the SE margin seem to be wide, of low amplitude and not (Figure IV-8), different than structural lows observed elsewhere on the margin (Figure IV-6 and Figure IV-7). Seismic interpretations also indicates that, unlikely other parts of the Amazon margin, the post-rift sedimentary succession of the SE shelf does not thicken significantly seaward, with Cenozoic units increasing from 2.9 seconds (twtt) beneath the inner shelf to 3.8 seconds (twtt) beneath the outer shelf (Figure IV-8).

Comparison of an interpreted seismic profile across the SE margin with potential field anomalies indicates that some structural lows are associated with comparatively low free-air values and high magnetic values (Figure IV-8). However, such a correlation is not apparent in other seismic profiles, suggesting that major potential field anomalies may not be related to structural lows in the SE margin. The magnetic and gravimetric anomalies observed in the SE margin are instead here assumed to have the same origin as similar anomalies observed in Liberia (Figure IV-9), where they have been attributed to Neoarchean-Paleoproterozoic shear zones (Behrendt *et al.*, 1974; Behrendt and Wotorson, 1974). This interpretation is supported by the composition of basement rocks at the base of wells PAS-4A and MAS-9 on the SE margin (location on Figure IV-1), the former penetrating 25 m of biotite-gneiss while the latter 55 m of non-specified metamorphic rocks, which is similar to the prevailing lithology (biotite-rich paragneiss and migmatite) in southern Liberia (Behrendt and Wotorson, 1974; Tysdal and Thorman, 1983).

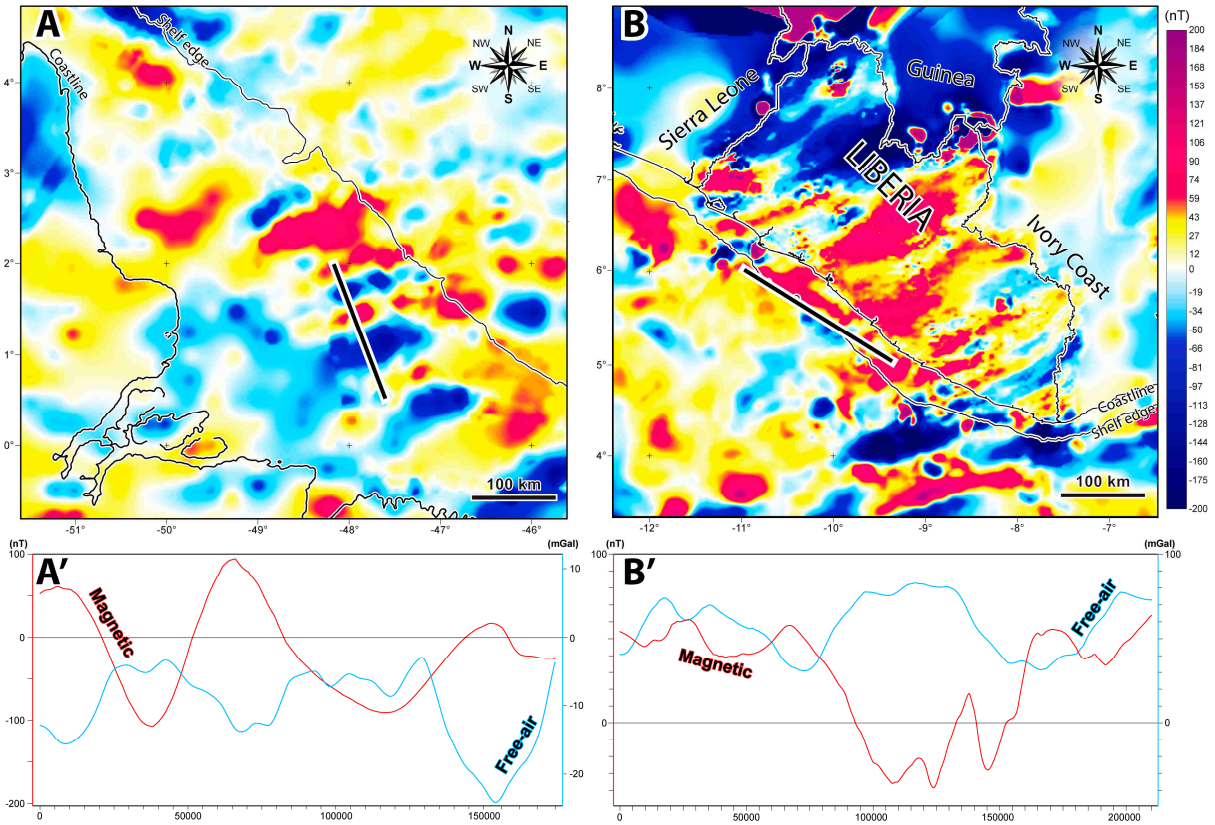

Figure IV-9: Comparison between magnetic anomalies on the SE Amazon margin (**A**) and in Liberia (**B**). Note that magnetic and free-air gravity anomalies are inverse correlated in both the SE Amazon margin (**A'**) and in the conjugate Liberian margin (**B'**). The nature of the crystalline basement in the SE Amazon margin is here inferred to be the same as of that of the West African Craton.

IV.4 DISCUSSION

The integration of gravity and magnetic anomalies with seismically-imaged basement and syn-rift structures presented above demonstrates that the Amazon margin can be divided into three regions of distinct structural framework (Figure IV 10). These three regions are approximately coincident with areas of differing post-rift stratigraphic architectures linked to varying Neogene geodynamics by Cruz *et al.* (CHAPTER III). These three regions are assumed to represent distinct sub-basins (Figure IV-10), here named from NW to SE as: the Cassiporé sub-basin (after the Cassiporé half-grabens); the Araguari sub-basin (after the Araguari River) and the Machadinho sub-basin (after nearby Machadinho Island). The particularities of these sub-basins are inferred to reflect the complex rifting processes of the Amazon margin, which generated a heterogeneous structural framework that strongly controlled syn- to post-rift sediment deposition.

IV.4.1 The Offshore Amazon sub-basins

The inner limit of the Offshore Amazon Basin is recognized as a series of E-W trending strike-slip faults (aligned with the Saint Paul Fracture Zone), which separate the central Araguari sub-basin from the Marajó basin, and the Machadinho sub-basin in the SE from the Pará-Maranhão basin (Figure IV-5D and Figure IV-10).

In contrast, in the east the Offshore Amazon Basin has no clear distal limits, being open toward the oceanic domain (i.e. a typical marginal basin). A distal boundary could be arbitrarily defined in the Machadinho sub-basin around the 2000-3000 isobaths where E-W trending free-air anomalies related to the Saint Paul Fracture Zone point to the presence of oceanic crust (Figure IV-5A and Figure IV-10). In the Cassiporé and Araguari sub-basins the seaward extension of continental crust cannot be identified neither in the available seismic data or potential field models.

Cassiporé sub-basin

Based on the gravity anomalies in Figure IV-5, a northern limit of the Cassiporé sub-basin can be placed near the Brazil-French Guiana border, at the landward extension of the strike-slip fault crossing the contiguous abyssal plain. However, as seismic data is not available to verify the presence of distinct structural styles in this region, it is also possible that the Cassiporé sub-basin extends NW into the French Guiana margin. In the southeast, the boundary of the Cassiporé sub-basin corresponds to a sharp transition from an area of prevailing NW-SE free-air and VGG anomalies and a more structurally complex domain (Figure IV-7) with N-S free-air anomalies and smooth VGG character (Figure IV-5A and B). To the west, the inner limit of the Cassiporé sub-basin corresponds to a transition from fault-bounded rotated blocks to less deformed basement of the Amazonian Craton, which outcrops onshore in the Brazilian state of Amapá.

The basement underlying the Cassiporé sub-basin basement is inferred to be composed of portions of the Amazon Craton that were stretched and thinned during rifting. This is supported by the pronounced seaward thickening of post-rift sedimentary units across the shelf (Figure IV-6), which could reflect the eastward increase of crustal stretching. Such seaward shelfal strata thickening in the Cassiporé sub-basin is noticeable throughout the entire post-rift

record and indicates that the Cassiporé sub-basin was always prone to more intense subsidence over on the outer shelf-slope regions, a trend the was intensified since the Pliocene in response to the Amazon Fan loading (Figure IV-6). The proximity with the outcropping Amazon Craton in the Brazilian Amapá state also favors the assumption that the basement of the Cassiporé sub-basin is mostly composed by this craton (Figure IV-10). Onshore in the state of Amapá, the Amazon Craton is mostly composed of Paleoproterozoic granite-greenstone mobile belts (Maroni-Itacaiunas or Transamazonic province), in places associated with inliers of Archean terranes and mafic sills-dikes as well as granitoid intrusions (Cordani and Teixeira, 2007; Cordani *et al.*, 2009; da Rosa-Costa *et al.*, 2006; Santos *et al.*, 2000). A similar composition is likely for the basement underlying the Cassiporé sub-basin, with the possible addition of younger sills-dikes originated during rifting. However, as several authors consider that the Araguaia-Rokelide suture zone crosses the Offshore Amazon Basin (Brito Neves and Fuck, 2014; Klein and Moura, 2008; Villeneuve and Cornée, 1994), it is also possible that basement in the distal portions of the Cassiporé sub-basin is derived from this Neoproterozoic orogenic belt.

The NW-SE orientation of the Cassiporé half-grabens has been argued either to be controlled by the Rokelide-Araguaia belt (Basile *et al.*, 2005), or to be related to an aborted branch of the North Atlantic rift (Zalan, 2004; Soares Júnior *et al.* 2011). The fact that some of the highest magnetic anomalies coincide with the axes of half-grabens in the Cassiporé sub-basin (Figure IV-6) could suggest the presence of igneous rocks (dikes and sills?), favoring the interpretation of an aborted rift. Alternatively, the long-wavelength magnetic anomalies on the NW shelf may predate the Atlantic rifting and reflect zones of crustal weakness related to the Paleoproterozoic mobile belts of the easternmost Amazon Craton (Cordani and Teixeira, 2007), which gave way to extensional faults during the opening of the Equatorial Atlantic. In this scenario, the NW-SE orientated Cassiporé half-grabens would be the result of E-W extensional forces related to the Equatorial Atlantic rifting obliquely affecting WNW-ESE zones of weakness. I favor such an interpretation as the basement of the Cassiporé sub-basin is more likely to be composed of the Amazon Craton than the Rokelide-Araguaia belt, and there is no evidence that the Cassiporé half-grabens extend further than the Brazilian-French Guiana border. If a branch of the Central Atlantic rift system was indeed active in the region during the Late Triassic-Early Jurassic, structures associated with it may underlie the modern slope-continental rise. Such hypothetical Late Triassic-Early Jurassic extensional structures would have been affected by the rifting of the Equatorial Atlantic in the Early Cretaceous and may be

unrecognizable in the available dataset due to extreme crustal stretching and/or superposition of two distinct structural styles.

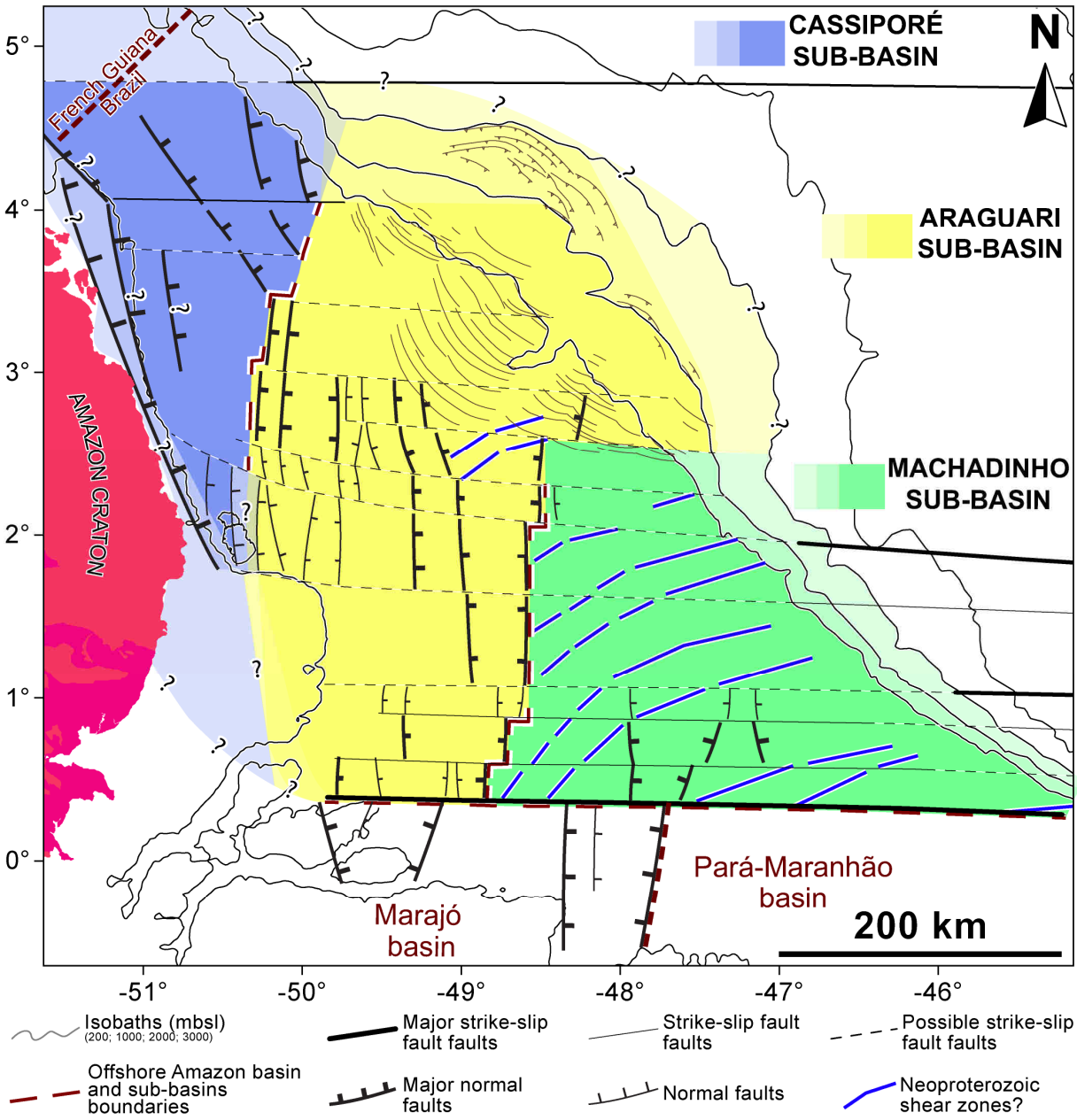

Figure IV-10: Simplified structural framework of the Offshore Amazon Basin based on an integrated analysis of seismic reflection and potential field data. Thin lines on the Araguari sub-basin outer shelf-slope region represent faults recording gravity-driven deformation of the post-rift sedimentary succession, simplified from Perovano *et al.* (2009).

Araguari sub-basin

The boundary between the Araguari and Machadinho sub-basins is not clear but tentatively placed along an axis marking a transition between clear N-S trending and subtle ENE-WSW trending free-air anomalies (Figure IV-5B). The distinction of these two areas is supported by the fact that in the Araguari sub-basin there is no clear correlation between free-air and magnetic anomalies, while in the Machadinho sub basin these anomalies have the same general trend (Figure IV-5A and C). In the south, the inner limit of the Araguari sub-basin proximal limit corresponds to a series of E-W trending strike-slip faults (aligned with the Saint Paul Fracture Zone), which separate the Offshore Amazon Basin from the Marajó basin (Figure IV-5D).

The N-S trend of gravity anomalies in the Araguari sub-basin, interpreted to be caused by grabens and/or half-grabens, is aligned with N-S gravity anomalies in the Marajó basin (Figure IV-5D), that are also most likely caused by in this onshore basin the N-S grabens. Grabens in the Marajó Basin have been reported to follow the direction of suture zones (Araguaia belt) formed during the Neoproterozoic amalgamation of the Gondwana supercontinent, which constitute linear zones of strong lateral anisotropy more likely to be affected by faulting during rifting processes (Zalán and Matsuda, 2007). As gravity and magnetic anomalies do not change in orientation between the Marajó basin and the Araguari sub-basin (Figure IV-5), it is likely that the Araguaia belt extends northward in the Offshore Amazon Basin along the general N-S trend of an Araguaia-Rokelide suture zone as suggested by other authors (Paixão *et al.*, 2008; Villeneuve and Cornée, 1994; Brito Neves and Fuck, 2014; Klein and Moura, 2008), but mostly restricted to the Araguari sub-basin. This is supported by VGG maps (Figure IV-5B) that show no clear limit between the Marajó basin and the Araguari sub-basin, but a sharp limit between the Cassiporé and Araguari sub-basins compatible with a boundary between a cratonic domain and highly extended metamorphic basement. Hence, I suggest that the N-S Araguaia-Rokelide suture zone conditioned the emplacement of the N-S grabens identified in the Araguari sub-basin (Figure IV-5D andFigure IV-7), as proposed in the nearby Marajó basin (Zalán and Matsuda, 2007). It is also possible that the extensional structures were associated with an aborted branch of the Central Atlantic rift (as proposed by Zalan, 2004 and Soares Júnior *et al.*, 2008), but this hypothesis is opposed

by the lack of an identifiable connection between the Araguari sub-basin and the Central Atlantic passing through the Cassiporé sub-basin and the French Guiana margin.

The interpretation that the basement of the Araguari sub-basin is composed of highly stretched crust is in agreement with Lara (1994), who stated that the southern region of the Marajó basin is underlain by continental crust, whereas its central and northern portions are underlain by "transitional" crust recording higher amounts of extension. The northward intensification of crustal extension may have affected the Offshore Amazon Basin, resulting in thinner crust underlying the Araguari sub-basin. In turn, crustal thinning may have created a region more prone to flexural subsidence (due to sedimentary load and/or mantle-convection-driven), thus influencing sediment distribution and the location of post-rift depocenters along the axis of the Araguari sub-basin. This could account for the intense creation of accommodation space in the Araguari sub-basin during the Miocene (Cruz *et al.* CHAPTER III). A N-S trend of crustal weakening reflected by the Araguari sub-basin could have also promoted the offset of the Amazon canyon 200 km northwest of the Amazon River mouth (Figure IV-10), in contrast to most of the canyons of large rivers that are located directly ahead of their respective rives mouth (e.g. Congo, Nile, Mississippi, Indus, Bramaputra). As such, I speculate that greater subsidence along the Araguari sub-basin could have "captured" river courses during sea-level lowstands and diverted sediment transport to favor a northward shift of the Amazon canyon and deep-sea fan.

Machadinho sub-basin

The southern limit of the Machadinho sub-basin is defined by the same set of E-W trending strike-slip faults (aligned with the Saint Paul Fracture Zone) that separate the Araguari sub-basin from the Marajó basin (Figure IV-5D). The strike-slip faults are represented by gravity anomalies that are discrete along the boundary with the Marajó basin, but well-defined along the Pará-Maranhão basin (Figure IV-5A and B). Unlike other parts of the Offshore Amazon Basin, the presence of oceanic crust in the eastern Machadinho sub-basin is assumed from a series of E-W trending free-air anomalies where the Saint Paul Fracture Zone intersects the continental slope around the 2000-3000 isobaths (Figure IV-5A). The Machadinho and Araguari sub-basins are clearly distinguished by the fact that gravity and magnetic anomalies have the same alignment in the former, whereas no clear correlation is observed in the latter.

Based on similarities between potential field anomalies in the Machadinho sub-basin and in Liberia (Figure IV-9), it can be assumed that the crust in both regions has the same origin and has been affected by the same tectonic events. The southern portion of the outcropping West African craton in Liberia (Eburnean province) is mainly composed of Archean rocks subsequently metamorphosed during the so-called Paleoproterozoic Eburnean Orogeny at ca. 2,100-2,000My (Behrendt and Wotorson, 1974; Tysdal and Thorman, 1983). These rocks form extensive areas of folded biotite-rich paragneiss and migmatite, but also include granitic gneiss and more restricted bodies of amphibolite and intrusive granite and pegmatite (Behrendt and Wotorson, 1974; Tysdal and Thorman, 1983). This composition compares to that of basement rocks in wells PAS-4A (biotite-gneiss) and MAS-9 (non-specified metamorphic rocks), thus reinforcing the correlation between the two regions.

This correlation suggests that the boundary between the Machadinho and Araguari sub-basins corresponds to that between basement rocks of the West African Craton and, as inferred above, a Neoproterozoic mobile belt. It may seem puzzling that the boundary between the sub-basins (cratonic vs. mobile belt) is marked by discrete gravity anomalies, whereas the boundary between the cratonic provinces underlying the Machadinho sub-basin and the São Luís Craton is well-defined (Figure IV-5A and B). This could be due to the greater depths to basement in the central region, which make gravity anomalies less pronounced. However, the age and composition of the basement underlying the Machadinho sub-basin versus neighboring domains may also play a role in contrasting gravity anomalies. The São Luís Craton is also considered to be a fragment of the West African Craton that remained part of South America after the breakup of Gondwana and is mainly composed of Paleoproterozoic granitoids associated with a metavolcano-sedimentary sequence formed between ca. 2,240-2,090 Ma, as well as rare remobilized Archean crust (Klein *et al.*, 2005; Brito Neves *et al.*, 2002). Assuming that the long-wavelength potential field anomalies in the Machadinho sub-basin have an Archean origin as in Liberia (ca. 2,700 Ma; Behrendt and Wotorson, 1974), it is likely that the basement is considerably older than the adjacent São Luís Craton. The São Luís Craton would thus represent a later accretion to the West African Craton created during the Eburnean orogenic cycle (as stated by Klein *et al.*, 2005), which was reported to have features of an "archaic weak orogeny type" (Vidal *et al.*, 2009; Feng *et al.*, 2018). This type of archaic orogeny could have amalgamated the cratonic provinces underlying the Machadinho sub-basin and the São Luís Craton to produce a sharp contact between the two domains. In contrast, the intense modern-type Neoproterozoic-Cambrian orogeny (Brasiliano-Pan African cycle, 550-500 My) that

created the Araguaia-Rokelide suture zone (Kröner and Stern, 2005; Villeneuve and Cornée, 1994; Herz *et al.*, 1989), would have thrust and amalgamated this orogenic belt in the Araguari sub-basin with the cratonic basement of the Machadinho sub-basin in such a way that variations in crustal thickness and lithology between the two domains may be gradual. This is consistent with Brito Neves (2002) who studied outcrops of Neoproterozoic mobile belts onshore in Brazil and stated that the "Brasiliano tectonogenesis was strong and widespread (affecting the fold belts and their basement) and these processes affected many areas so intensely that it is locally difficult to discriminate between Brasiliano and pre-Brasiliano terranes".

Finally, the Precambrian magnetic and gravity anomalies observed in potential field data (Figure IV-5) do not correspond to distinct structures on seismic profiles across the margin, which reveal only Cretaceous faults with only subtle offsets (Figure IV-8). This suggests that the Machadinho sub-basin was weakly affected by syn-rift deformation during the opening of the Equatorial Atlantic. Accordingly, the minor seaward thickening of the post-rift sedimentary succession in the Machadinho sub-basin may be a consequence of a low degree of E-W crustal stretching that resulted in little cross-shelf differential subsidence.

IV.4.2 General considerations

The strike-slip faults interpreted to mark the northern and southern boundaries of the Offshore Amazon Basin are aligned with transform faults in the adjacent abyssal plain (Figure IV-5A and B), suggesting a continuity between structures in the continental and oceanic domains. Such continuity could be interpreted as the influence of inherited Gondwanan geological features on continental breakup. Inheritance is a theme of an ongoing debate in the scientific community, and the possible role of pre-rift crustal features in the architecture and tectonic evolution of rifted margins may vary with location. For instance, while some studies have reported a strong control by pre-rift geological features, such as mobile belts, in the segmentation of rifted margins (Tommasi and Vauchez, 2001; Tsikalas *et al.*, 2008; Brito Neves, 2002; de Castro *et al.*, 2012; Behn and Lin, 2000), others have suggested that inherited structures in the continental crust did not significantly influence the location of breakup or of structures in the oceanic crust (Gerya, 2013; Taylor *et al.*, 2009; Manatschal *et al.*, 2015). In the case of the Offshore Amazon Basin, the sharp contact between a metamorphosed Archean domain beneath the Machadinho sub-basin and the Paleoproterozoic domain of the São Luís

Craton (as expressed in the VGG map on Figure IV-5B) is inferred to have facilitated a major transcurrent fault in response to E-W stresses during the Equatorial Atlantic opening. In the Cassiporé sub-basin, the approximate northward limit of the half-grabens marks a change in the orientation of gravity anomalies that is clearly in alignment with an E-W VGG anomaly across the abyssal plain (Figure IV-5B). These findings support a relationship between crustal segmentation in continental and oceanic domains. This is consistent with de Castro *et al.* (2012), who argued that breakup along the southernmost portion of the Brazilian Equatorial Margin (the Potiguar Basin) was strongly controlled by Precambrian terrain boundaries and reactivated shear zones. The findings presented here suggest that the segmentation of the entire Brazilian Equatorial Margin may have been inherited from pre-rift Gondwanan geological features.

Furthermore, the apparent structural continuity between the Araguari sub-basin and the onshore Marajó basin - both underlain by the Araguaia-Rokelide belt and affected by N-S aligned grabens - may indicate that the formation of the Offshore Amazon basin predates the opening of the Equatorial Atlantic. The Marajó Basin initiated as a Paleozoic sag basin (Ordovician-Silurian) that was later affected by extensional stresses that probably stated as early as the Late Triassic-Jurassic (along an aborted branch of the Central Atlantic rift as speculated by Zalan, 2004) or during the Early Cretaceous opening of the Equatorial Atlantic (Zalán and Matsuda, 2007). In either case, it is possible that Paleozoic sedimentary rocks are preserved within the deep-buried grabens of the Araguari sub-basin, as is the case in the of the contiguous Marajó Basin (Costa *et al.*, 2002; Zalán and Matsuda, 2007). A Paleozoic age is also reported for sandstones in the coastal area of Liberia near Monrovia on the African conjugate margin (Behrendt and Wotorson, 1974). The Araguari sub-basin, that stood between Liberia and the Marajó basin prior to continental break-up, is likely to have also received Paleozoic sediments. Thus I speculate that the Araguari sub-basin probably contains a Paleozoic sedimentary succession and may have been affected by the Late Triassic to Jurassic Central Atlantic rifting, just as it is assumed for the Marajó basin. If proven correct, this inference has implications for hydrocarbon systems as the major source rocks in South American basins lie in Paleozoic formations. For example, Devonian formations are reported to contain some of the most important intracratonic source rocks in the world (Milani and Zalan, 1999), and Silurian muds have been pointed out as possible source rocks in the nearby Amazonas and Parnaíba basins (Ferreira *et al.*, 2015; Araújo, 2017). Additionally, organic-rich sediment deposited in the Tethys during the Jurassic are also reported to be important source rocks worldwide (Milani *et al.*, 2000) and could be present in the Araguari sub-basin if the aborted rift hypothesis of

Zalán (2004) is correct. Although available data does not allow a detailed investigation of the sedimentary successions within the deeply buried grabens of the Araguari sub-basin, future exploratory investigations based on deep-penetrating data should consider the possibility that hydrocarbon systems with reservoir and source rocks with ages varying from Paleozoic to Cenozoic are present in the region. This hypothesis is similar to that of Zalán (2016) who used recently acquired PSDM 3D reflection seismic data to propose the existence of a 5 km thick pre-rift Paleozoic intracratonic sedimentary succession "captured and preserved" below sediments related to the South Atlantic opening in the Santos basin (East Brazilian Margin).

IV.5 CONCLUSIONS

An integration of geophysical potential field anomalies with buried basement and syn-rift structures interpreted from seismic profiles indicate that the Offshore Amazon Basin is composed of three segments here considered to be structurally distinct sub-basins: the Cassiporé sub-basin (NW margin), the Araguari sub-basin (Central margin) and the Machadinho sub-basin (SE margin).

Correlation with lithological data from offshore wells and published geological information from onshore outcrops suggests that the crystalline basement underlying the Offshore Amazon basin has distinct origins in each of the sub-basins. The Cassiporé sub-basin is underlain by faulted segments of the Paleoproterozoic Amazon Craton, composing a series of NW-SE oriented half-grabens. The Araguari sub-basin is underlain by the Neoproterozoic Araguaia-Rokelide suture zone, with N-S oriented normal faults composing a series of grabens and half-grabens. The Machadinho sub-basin is underlain by a portion of the Archean West African Craton that remained in South America after the Gondwanan breakup, together with the Paleoproterozoic São Luís Craton that outcrops south of the study area.

The variable composition and structural framework of the Offshore Amazon sub-basins is argued to be responsible for the distinct geodynamic behavior recognized across the study area (Cruz *et al.*, CHAPTER III). In particular, the Cassiporé and Machadinho sub-basins are underlain by cratonic basement, whereas the central Araguari sub-basin is underlain by a Neoproterozoic mobile belt stretched during Atlantic rifting that could have contributed to the central Amazon margin being more prone to subsidence. As such, it is possible that both regional scale processes (such as mantle dynamics) and local processes (such as isostatic flexure due to sedimentary loading) promoted higher subsidence rates in the Araguari sub-basin compared to the Cassiporé and Machadinho sub-basins.

CHAPTER V
SYN-SEDIMENTARY GRAVITY-DRIVEN DEFORMATION ON THE AMAZON MARGIN

CHAPTER V

In this chapter I present a revised and expanded version of a study first outlined at the 2016 EGU General Assembly in Vienna (Cruz *et al.*, 2016), addressing Cenozoic gravity tectonics activity in the Offshore Amazon Basin. The temporal and spatial evolution of syn-sedimentary gravity-driven deformation within the Cenozoic succession of the basin is addressed and developed in the light of the findings presented in the previous chapters.

Temporal and spatial evolution of gravity-driven systems on the Amazon margin: Interplay between tectonism and sediment influx

Abstract: The post-rift sedimentary succession of the Offshore Amazon Basin is known to have experienced large-scale gravity-driven deformation (gravity tectonics), resulting in the development of syn-sedimentary extensional and compressional faulting above *décollement* level, but the number and ages of the main deformational phases have been poorly constrained. In this work, I use a regional grid of reflection seismic profiles tied to chronostratigraphic data from six exploration and scientific wells to identify five major phases of gravity-driven deformation within two sub-basins of the Offshore Amazon Basin and explore their relation to sediment influx to the margin. Gravity tectonics most intensely affected the central Araguari sub-basin, which contains the thickest depocenters, and also affected the Machadinho sub-basin to the SE. The lower post-rift mega-sequence was reached by only a few wells and is poorly imaged on seismic profiles, but is interpreted to have experienced a first phase of gravity-driven deformation (gravity gliding?) in the Late Cretaceous that affected both sub-basins. A second phase of gravity-driven faulting resulted in the reactivation of normal and thrust faults in the Machadinho sub-basin between the Paleocene and the Middle Eocene, but was less intense than in the Late Cretaceous and apparently did not affect the Araguari sub-basin. A third phase of gravity-driven deformation (gravity spreading?) took place in both sub-basins in the Late Oligocene, a period marked by intense shelfal progradation in all parts of the Offshore Amazon Basin. After this phase, syn-sedimentary gravity-driven faulting took place only in the Araguari sub-basin. During the Early and Middle Miocene, a fourth phase of gravity-driven deformation (gravity gliding?) took place in the Araguari sub-basin. The fifth and most intense phase of gravity-driven deformation (gravity spreading) took place from the Late Miocene to Recent (notably during the Quaternary), driven by a major increase in sediment influx that resulted in the deposition of a voluminous aggrading-prograding shelf-slope wedge. All five phases of syn-sedimentary gravity-driven faulting were associated with periods of across shelf differential subsidence that promoted the basinward tilting of basal *décollement* levels and/or periods of high sediment influx to the Offshore Amazon Basin resulting in progradation of the shelf edge and increased deposition on the slope, suggesting an interplay between differential subsidence and sedimentary load in the outer shelf-upper slope region and gravity tectonics.

V.1 INTRODUCTION

In the Offshore Amazon Basin (known in Portuguese as the Foz do Amazonas Basin), gravity tectonics is recognized to have affected large areas of the outer continental shelf and upper slope (Figure V-1), resulting in deformation of most of the post-rift stratigraphic succession by belts of extensional and compressional faults developed above deep *décollement* surfaces (Silva *et al.*, 1999; Cobbold *et al.*, 2004; Oliveira *et al.*, 2005; Perovano *et al.*, 2009; Reis *et al.*, 2010). The post-rift sedimentary units of the Offshore Amazon Basin include three megasequences defined by Brandão and Feijó (1994) and Figueiredo *et al.* (2007): 1) Upper Cretaceous, composed of open-marine siliciclastic sediments (Limoeiro Formation); 2) Upper Paleocene to Upper Miocene, comprising a mixed siliciclastic-carbonate platform and adjacent slope sediments (Marajó, Amapá and Travosas Formations); and 3) Late Miocene to Recent, characterized by intense siliciclastic influx that created a thick prism of prograding sediments dominated by the Amazon Deep-Sea Fan (referred to hereafter as the Amazon Fan).

In the Amazon Fan (central part of the Offshore Amazon Basin), gravity-driven syn-sedimentary deformation was first described by Silva *et al.*, (1999), who noted the existence of a proximal series of normal growth faults on the outer shelf and upper slope, associated with a distal series of thrust faults to seaward on the upper slope. The area described by Silva *et al.*, (1999) is within the Araguari sub-basin as defined by Cruz *et al.* (CHAPTER IV). Gravity-driven deformation in that area was shown to affect the entire post-rift succession, with some faults extending from seabed to depths over 10 km below seabed (Silva *et al.*, 1999; Cobbold *et al.*, 2004). The faults are distributed over a large area between ~100-2100 meters below sea level and were grouped by Oliveira *et al.* (2005) into three tectonic domains: (1) a proximal extensional domain characterized by a belt of listric normal faults; (2) an intermediate domain of limited deformation; (3) and a distal compressive domain characterized by a belt of reverse faults grouped in thrust-and-fold belts (Figure V-1). These three domains are mechanically connected via three *décollement* levels (Lower, Intermediate and Upper) that allow the sliding of most of the overlying post-rift sequences toward the deep basin (Perovano *et al.*, 2009; Silva *et al.*, 1999). The Lower *décollement* is interpreted to be relate to inactive fold-and-thrust belts; most of the seafloor faults are rooted on the Intermediate *décollement*, while those associated with the Upper *décollement* have only local expression (Perovano *et al.*, 2009; Reis *et al.*, 2010). Perovano *et al.* (2009) and Reis *et al.* (2016) further showed that although the Upper *décollement* had little effect on gravity tectonics, it played a major role in mass wasting processes that generated a series of megaslides on the NW and SE flanks of the Amazon Fan.

Cobbold et al (2004) and Oliveira *et al.* (2005) pointed out that gravity tectonics deformation has not affected the entire upper Amazon Fan area with the same intensity, and identified an asymmetry in tectonic features distributions as much more extensional-compressional faults where identified to NW of the Amazon submarine canyon than to the SE. This asymmetry led Oliveira *et al.* (2005) to propose a segmentation of the upper Amazon Fan into two compartments: the SE Compartment is smaller (~115 km wide) and less structurally complex, with fewer extensional-compressional faults; the NW Compartment is larger (~152 km wide) and more structurally complex, with more extensional-compressional faults. Oliveira *et al.* (2005) also considered that position of the present-day Amazon submarine canyon, located on the axis between the two compartments, points to an influence of gravity tectonics in the transfer of sediment from the shelf to the deep-basin on the Amazon Fan. Oliveira *et al.* (2005) and Perovano *et al.* (2009) further evidenced the interplay between sedimentation and gravity-driven deformation by showing that the major depocenters of the Offshore Amazon Basin are fault-bounded and located within the NW and SE Compartments of the Amazon Fan, between the normal faults of the extensional domain and thrust faults of the compressive domain.

Silva *et al.* (2011) used seismic data and physical experimental models to conclude that the Amazon Fan region was affect by gravity tectonics during two main stages with different deformational mechanisms. According to these authors, there was a first gravity-driven deformational stage before the initiation of the Amazon Fan growth that was dominated by gravity gliding (in which thick sedimentary strata slides rigidly downslope). Still according to Silva *et al.* (2011), a later stage of gravity-driven deformation was dominated by gravity spreading (in which thick sedimentary strata distorts under its own weight by vertical collapse) triggered by the sedimentary load of the Amazon Fan. However, these authors were unable to assign ages to their main stages of gravity tectonics or further detail and individualize phases of more intense deformation during the Offshore Amazon Basin post-rift succession. As such, better understanding of the interplay between gravity tectonics and sediment supply in the Offshore Amazon basin has been precluded by limited chronostratigraphic constraints on the deposition of sedimentary units and major phases of deformation. A preliminary study conducted by Cruz *et al.* (2013) based on reflection seismic and calcareous nannofossil data concluded that most of the observed deformation in the Amazon Fan took place during the Quaternary, when sedimentation rates increased dramatically. However, the temporal and spatial evolution of pre-Quaternary gravity tectonics in the basin remains poorly understood. Furthermore, studies of gravity tectonics systems in the Offshore Amazon Basin have almost

exclusively focused on the Amazon Fan itself, so that gravity tectonics in other sub-basins have not been described.

In this chapter, I address the timing of syn-sedimentary deformation in the Offshore Amazon Basin in order to investigate the post-rift evolution of its gravity tectonics systems. To do so, I used a regional dataset composed of more than 20,000 km of 2D multi-channel seismic profiles, as well as 40 exploratory wells in the shelf-slope region and 7 ODP/DSDP wells in the distal Ceará Rise region (Figure V-1). This dataset provides more robust constraints on the age and character of the post-rift stratigraphic succession than was available for the previous studies of Perovano *et al.* (2009) and Reis *et al.* (2010). The study focuses on the two parts of the Offshore Amazon Basin: the SE Compartment of the Amazon Fan (central region) and the almost unexplored slope area of the Machadinho sub-basin (southeastern region). We avoided the more intensely deformed sedimentary succession of the NW Compartment of the Amazon Fan, as it its structural complexity makes it difficult to identify deformation phases. In order to define the major depositional and deformational phases in the other two areas, an age model was established for the Paleogene succession using calcareous nannofossil data from wells, and associated with the age model proposed by Cruz *et al.* (CHAPTER III) for the Neogene succession of the Offshore Amazon Basin. The resulting chronostratigraphic framework allows insights into the gravity tectonics processes that have controlled the sedimentary architecture of the Offshore Amazon Basin through the Cenozoic, and has implications for petroleum systems, notably in regards to the timing of fluid migration and trapping. The Late Cretaceous succession was examined only superficially as it is poorly imaged by seismic data and sampled by only a few wells.

V.2 GRAVITY-DRIVEN DEFORMATION PHASES IN THE OFFSHORE AMAZON BASIN

Seven main deformation phases of distinct style and/or intensity are identified within the Cenozoic succession of the Offshore Amazon Basin. Each phase corresponds to Cenozoic stratigraphic units newly defined here based on seismic profiles, or previously defined by Cruz *et al.* (CHAPTER III). The Paleogene succession is divided into four seismically identified stratigraphic units here named P1 to P4. The Neogene shelfal units N1 to N6 identified by Cruz *et al.* (CHAPTER III) were divided into two groups, called Units N1-3 and Units N4-6 based on deformation style and intensity. In addition, above the Neogene units, an uppermost unit here named Q is identified that encompasses most of the Quaternary sedimentary succession of the Offshore Amazon Basin.

For clarity, in the following sections, seismic units P1 to Q are described in terms of the chronostratigraphic constraints on their ages (section V.2.1), the varying styles and affected area of gravity-driven deformation observed on seismic profiles (section V.2.2) and the estimated sedimentation rates during the deposition of each unit across the shelf, slope and deep-basin regions (section V.2.3).

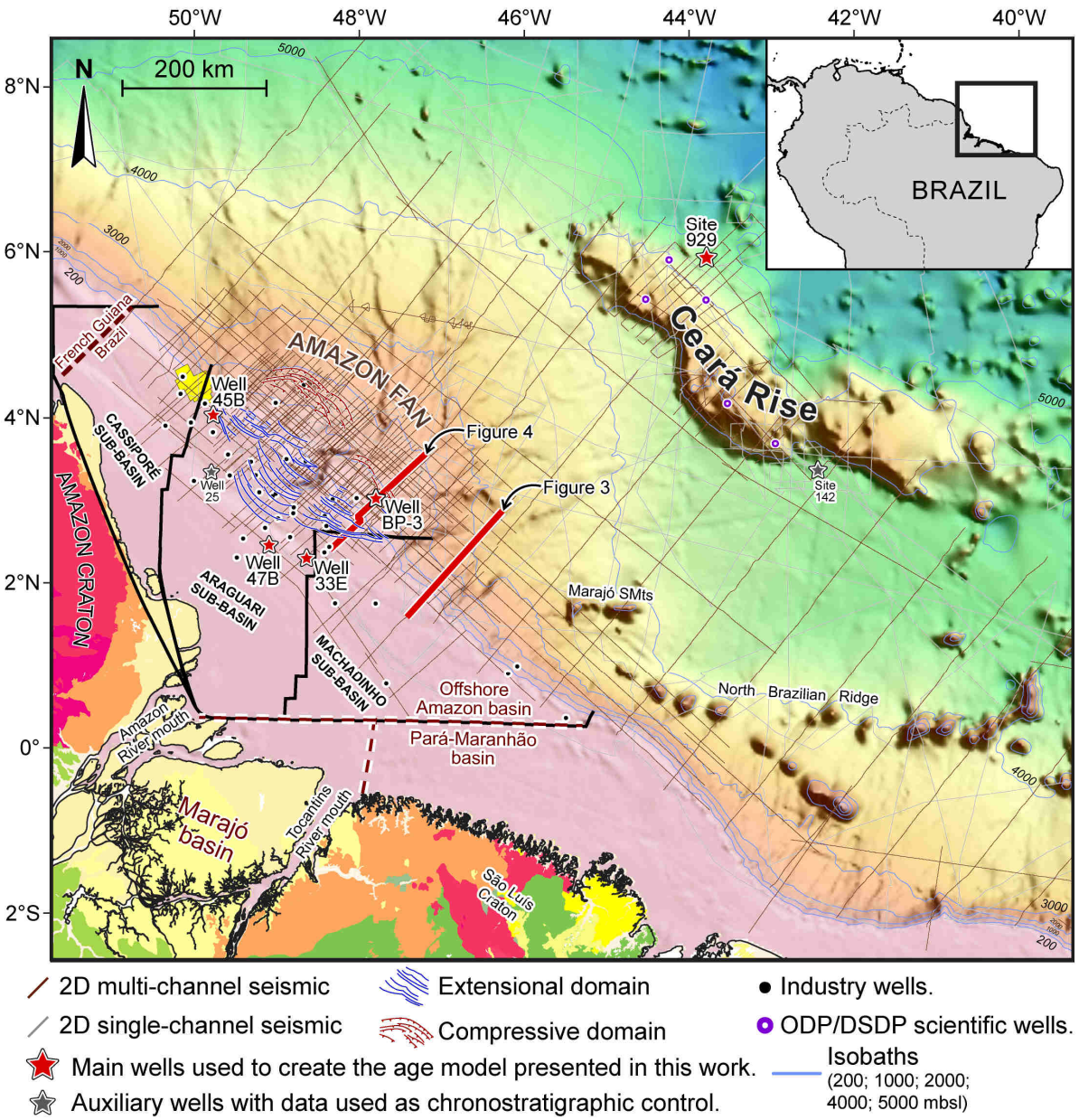

Figure V-1: Map of the study area showing the available seismic and well dataset. Offshore Amazon Basin limits and divisions defined in CHAPTER IV (Cassiporé, Araguari and Machadinho Sub-basins) also shown. The locations of Figure V-3 andFigure V-4 are shown as thick red lines. Structural map of gravity tectonic structures on the Amazon Fan region (extensional and compressive domains) simplified from Perovano *et al.* (2009)

V.2.1 Age model

In order to extend the Neogene chronostratigraphic model proposed by Cruz *et al.* (CHAPTER III) to the Paleogene units of the Offshore Amazon Basin, we used several wells: three industry wells located on the shelf, another on the Amazon Fan (between the extensional and compressive domains) and one ODP well on the distal Ceará Rise (Figure V-1). Following the methodology used by Cruz *et al.* (CHAPTER III), the ages of key stratigraphic surfaces

were estimated based on the first and last occurrences of key calcareous nannoplankton species according to well reports, which allowed us to assign age ranges for the surfaces based on published biochronostratigraphic compilations (Anthonissen and Ogg, 2012; Zeeden *et al.*, 2013; Young, 1998; Raffi *et al.*, 2006; Martini, 1971) updated to astronomically-tuned ages (Gradstein *et al.*, 2012).

This approach allows an age model to be proposed for the surfaces bounding units P1 to Q, which correspond to the entire Cenozoic stratigraphic succession of the Offshore Amazon Basin. Below the biochronostratigraphic constraints on the estimated age of each key stratigraphic surface are presented.

Surface *Sp1* (Base of Unit P1)

This surface is equivalent to the base of the Amapá Carbonates in the shelf region. The only available well with biochronostratigraphic data to reach surface *Sp1* is 45B. The composite log assigns the base of the Amapá Carbonates to the first occurrence of *Micula murus* (69 Ma; Anthonissen and Ogg, 2012). This disagrees with Figueiredo *et al.* (2007), who assigned an age of ~58 Ma to the transition from predominantly siliciclastic to mixed carbonate-siliciclastic sedimentation on the Offshore Amazon Basin. The base of the Amapá Carbonates could be placed at a level marking the first deposition of calcareous sediments in well 45B, which is equivalent to the last recorded occurrence of *Micula Murus* (66 Ma; Anthonissen and Ogg, 2012). Alternatively, the base could be placed at a slightly higher level, marking the onset of consistent carbonate deposition (Figure V-2). This level contains the last recorded occurrence of *Heliolithus kleinpelli*, indicating an age of 59.5 Ma (Anthonissen and Ogg, 2012), close to that assigned by Figueiredo *et al.* (2007). These two stratigraphic levels are only 85 m apart in well 45B and cannot be differentiated on seismic profiles as they lie within the same horizon. Therefore, I assign a most likely age of 66 Ma for surface *Sp1*, although an age as recent as 59.5 Ma could also be possible for this surface.

Surface *Sp2* (Top of Unit P1 and base of Unit P2)

An age between 38 Ma and 35.4 Ma is assigned to this surface, as in well 45B and ODP site 929 (Figure V-2) it is equivalent to a stratigraphic level between the last occurrences of *Chiasmolithus grandis* and *Reticulofenestra reticulata* (Anthonissen and Ogg, 2012). Surface *Sp2* could be associated with the beginning of small-scale Antarctic glaciation around 38 Ma (Kennett and Shackleton, 1976; Zachos *et al.*, 2001a; Katz *et al.*, 2011), which is depicted as a

sharp eustatic drop at 37.6 Ma in the sea-level curve of Haq *et al.* (1987) or at 36.2 Ma in the sea-level curve of Miller *et al.* (2005).

Surface *Sp3* (Top of Unit P2 and base of Unit P3)

In well 45B (Figure V-2), this surface is equivalent to a level between the last occurrence of *Discoaster barbadiensis* (34.76 Ma; Anthonissen and Ogg, 2012) and the last occurrence of *Coccolithus formosus* (32.92 Ma; Anthonissen and Ogg, 2012). In ODP site 929 on the Ceará Rise, the surface is equivalent to a level between the last occurrence of *Discoaster saipanensis* (34.44 Ma; Anthonissen and Ogg, 2012) and the last occurrence of *Coccolithus formosus* (32.92 Ma). This indicates an age between 34.4 Ma and 32.9 Ma for surface *Sp3*. This prominent surface may be related to the largest eustatic event during this time span, a sea-level fall near the Eocene-Oligocene transition at ca. 33.5 Ma that reflects major global cooling (Haq *et al.*, 1987; Miller *et al.*, 2005; Miller *et al.*, 2009) associated with the development of large ice sheets on Antarctica (Miller *et al.*, 2009; Miller *et al.*, 2011; Katz *et al.*, 2011).

Surface *Sp4* (Top of Unit P3 and base of Unit P4)

In well 45B (Figure V-2), this surface corresponds to a level above the last occurrence of *Coccolithus formosus* (32.9 Ma; Anthonissen and Ogg, 2012) and below the last recorded occurrences of *Reticulofenestra bisecta* (23.13 Ma; Anthonissen and Ogg, 2012) and *Cyclicargolithus abisectus* (~24.5 Ma; Young, 1998 recalibrated to Gradstein *et al.*, 2012 timescale). In well BP-2, the surface corresponds to the top of an interval reported as "*early Oligocene*" with no other chronostratigraphic detail. On the Ceará Rise, surface *Sp4* may correlate to a high amplitude and semi-continuous seismic horizon that in ODP site 929 (Figure V-2) is dated as 28.09 Ma by the last common occurrence of *Chiloguembelina cubensis* (Anthonissen and Ogg, 2012). Surface *Sp4* may correspond to the major Paleogene sea level fall close to the Early/Late Oligocene boundary which is around 28 Ma (Haq *et al.*, 1987; Miller *et al.*, 2005; Kominz *et al.*, 2008). These data suggest an age between 32.9-24.5 Ma for surface *Sp4*, most likely ca. 28 Ma.

Surface *Spn* (Top of Unit P4 and base of Units N1-3)

This surface was identified and dated by Cruz *et al.* (CHAPTER III) and represents the approximate base of the Neogene succession. Surface *Spn* crosses wells 45B and 47B between the last occurrence of *Cyclicargolithus abisectus* and the first recorded occurrence of *Helicosphaera carteri*, respectively, indicating an age between 24.67-22.03 Ma (Anthonissen

and Ogg, 2012). Surface *Spn* may be related to a major sea-level fall reported at 24 Ma (Haq *et al.*, 1987; Miller *et al.*, 2005). In well BP-3, the surface lies at a level generically reported as "close to the top of the Oligocene" (Figure V-2). On the Ceará Rise, surface *Spn* corresponds to a high amplitude continuous seismic horizon that crosses ODP Sites 928 and 929 just above the last occurrence of *Sphenolithus ciperoensis* (24.43 Ma; Anthonissen and Ogg, 2012), supporting an age of ca. 24 Ma.

Surface *Sn3* (Top of Units N1-3 and base of Units N4-6)

This surface was identified and dated by Cruz *et al.* (CHAPTER III) and marks the cessation of widespread carbonate sedimentation on the Central and SE shelves of the Offshore Amazon basin. Surface *Sn3* crosses well 47B above the last recorded occurrence of *Discoaster bellus* (Zeeden *et al.*, 2013) and bellow the last occurrence of *Minylitha convallis* (Raffi *et al.* 2006) in well 33E between (Figure V-2), indicating an age between 9.1-7.78 Ma (Anthonissen and Ogg, 2012). Surface *Sn3* is interpreted as a maximum flooding surface related to a sea-level rise that took place at ca. 8 Ma (Haq *et al.*, 1987; Miller *et al.*, 2005).

Surface *Sq* (Top of Units N4-6 and base of Unit Q)

In well BP3 (Figure V-2), this surface lies at a level marked by the last occurrence of *Discoaster brouweri* (1.93 Ma ; Anthonissen and Ogg, 2012). In wells 45B and 25, the surface corresponds to a level identified as the base of calcareous nannofossil zone "NN19", also dated to 1.93 Ma (Anthonissen and Ogg, 2012), thus supporting an age of ca. 2 Ma for Surface *Sq*.

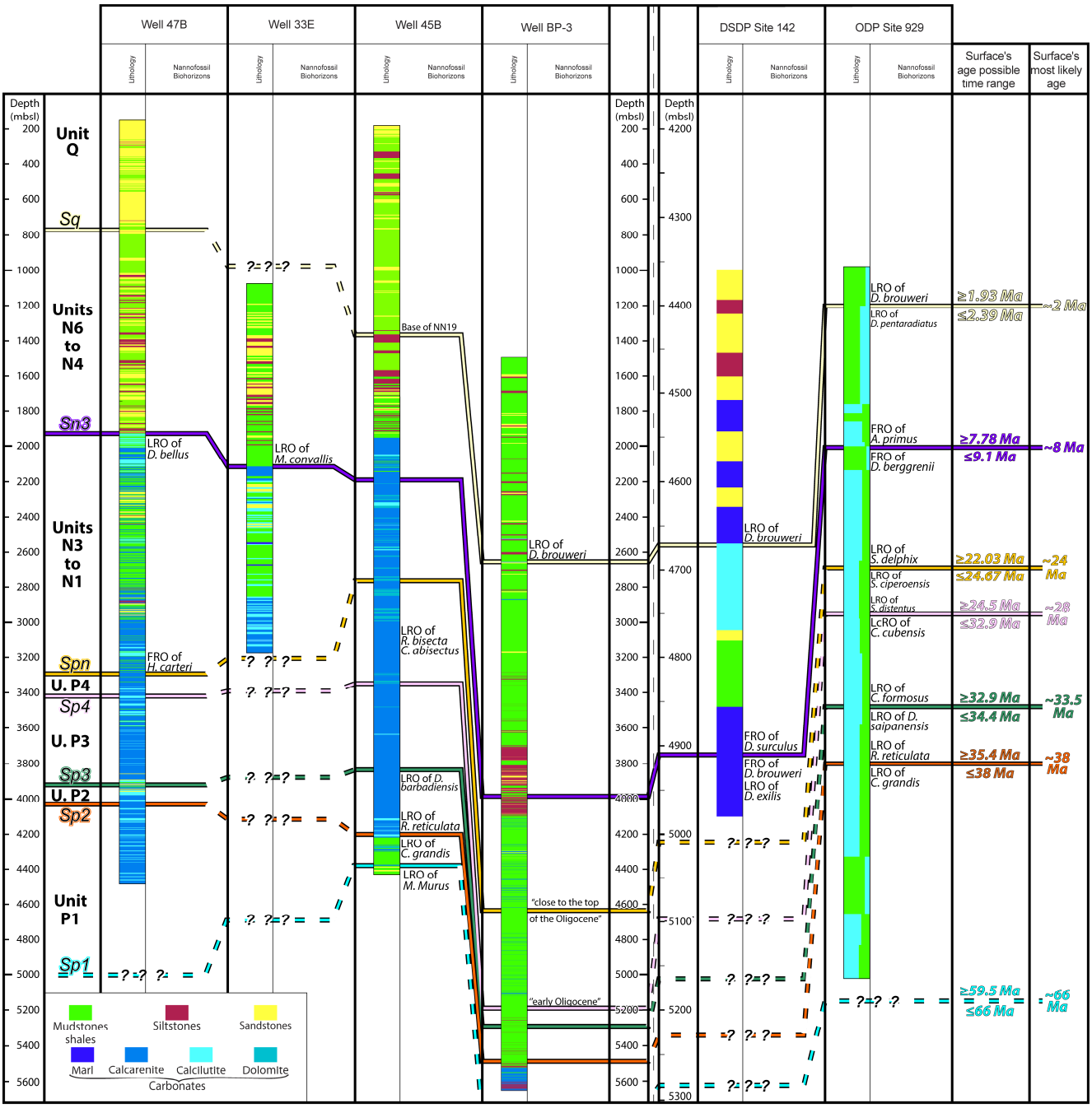

Figure V-2: Lithological and biohorizon data of wells used to construct the Cenozoic chronostratigraphic model of the Offshore Amazon Basin. Colored lines represent the surfaces *Sp1* to *Sq* defined in this work and in Cruz *et al.* (CHAPTER III). Well 33E after Figueiredo *et al.* (2009).

V.2.2 Gravity-driven deformation in the Offshore Amazon Basin

Application of the above age model to seismically-interpreted stratigraphy and structures allows a characterization of the main phases of gravity tectonics in the Offshore Amazon Basin during the Cenozoic, as well as of intervening quiescent phases. Deformation phases were defined from syn-tectonic sedimentary features observed on seismic profiles (Figure V-3 and Figure V-4), such as updip-expanded wedges against normal faults and onlaps and/or pinching out against compressive structures (folds and thrust faults). For this purpose, I followed the methodology and terminology of Diegel *et al.* (1995), Rowan *et al.* (2004) and Reis *et al.* (2005). I also present isopach maps for each of the units defined here, in order to describe the overall sedimentary distribution during the successive phases of gravity-driven deformation (Figure V-5).

In the following subsections, I describe the main architectural elements that allowed the definition of main phases of gravity-driven deformation in the Offshore Amazon Basin during the Cenozoic. First I present evidence of deformation phases in the structurally simpler Machadinho sub-basin in the SE portion of the basin (subsection V.2.2.1); than the more structurally complex region within the Araguari sub-basin in the central portion of the basin, corresponding to the SE Compartment of the Amazon Fan (subsection V.2.2.2).

V.2.2.1 ***Machadinho sub-basin*** *(SE region)*

In the Machadinho sub-basin, most deformation pre-dates deposition of the Cenozoic units (P1 to Q), as the sedimentary units below surface *Sp1* show the effects of both extensional and compressive faulting that respectively resulted in expanded wedges on the paleo-upper slope and a series of thrust-fold belts on the paleo-lower slope (Figure V-3). The presence of observable updip-expanded wedges against normal faults in pre-Cenozoic strata on the Machadinho sub-basin attest the syn-sedimentary nature of gravity-driven deformation in the region (Figure V-3).

Gravity-driven faulting in the Machadinho sub-basin is associated with a single *décollement* surface located within the Late Cretaceous succession (below surface *Sp1*). It is difficult to determine the position of the *décollement* in seismic profiles due to poor imaging of deep-buried units, but the surface is assumed to be equivalent to the Lower *décollement* identified by Silva *et al.* (1999) and Perovano *et al.* (2009) in the upper Amazon Fan.

Unit P1 (~66-38 Ma)

Gravity-driven faulting reduced in intensity during this first Cenozoic phase, but continued to affect the Machadinho sub-basin upper slope as indicated by slight thickening of unit P1 between the proximal normal faults and the distal thrust faults. Unit P1 is about 0.5 s (twtt) thick in the intermediate domain between the extensional and compressive belts, versus only about 0.25 s (twtt) thick in the surrounding slope areas (Figure V-3). Seismic profiles show that shelfal strata of unit P1 is organized as an essentially aggrading succession (Figure V-3) in the Machadinho sub-basin. The isopach map in Figure V-5B shows that unit P1 is thicker on the shelf (over 1 s twtt) than across the paleo-slope (commonly less than 0.6 s twtt), suggesting a regime of low shelf-to-slope sediment transfer during this phase.

Unit P2 (~38-33.5 Ma)

Unit P2 is about 0.3 s (twtt) thick in the upper slope extensional domain and gradually thins downslope to reach about 0.18 s (twtt) on the lowermost slope, with no thickness variations or structures indicative of gravity-driven faulting (Figure V-3). As such, unit P2 records a quiescent phase in terms of gravity tectonics. Seismic profiles show a major seaward shift of shelfal sedimentation during the deposition of unit P2, with only thin strata deposited in the area equivalent to the previous paleo-shelf unit (Figure V-3). The seaward shift in shelfal sedimentation in the Machadinho sub-basin can be seen in the isopach map (Figure V-5C), as unit P2 is thinner on the inner-middle shelf (commonly < 0.2 s twtt) than across the outermost shelf-upper slope region (typically 0.4-0.6 s twtt), suggesting high shelf-to-slope sediment transfer during this phase.

Unit P3 (~33.5-28 Ma)

Unit P3 also shows no significant thickness variations or structures indicative of gravity-driven faulting, being about 0.4 s (twtt) thick across the upper slope extensional domain and thinning downslope to about 0.15 s (twtt) on the lowermost slope (Figure V-3). As such, unit P3 records a quiescent phase in terms of gravity tectonics in the Machadinho sub-basin. Seismic profiles show that shelfal strata of unit P3 are organized as an aggrading succession (Figure V-3). The isopach map in Figure V-5D shows that unit P3 in the Machadinho sub-basin maintains consistent thicknesses on the shelf and slope regions of 0.2-0.4 s (twtt), suggesting a regime of moderate shelf-to-slope sediment transfer during this phase.

Unit P4 (~28-24 Ma)

Unit P4 in the Machadinho sub-basin shows subtle but clear thickness variations associated with gravity-driven faulting (Figure V-3). This is most evident in the compressive domain, where reactivation of deeply buried thrust faults promoted folding of overlaying units and the thickening of strata of unit P4 on seaward of the thrust-folds (Figure V-3C). Unit P4 is about 0.35 s (twtt) thick across the upper slope extensional domain, thins downslope to reach about 0.18 s (twtt) on the lower slope compressive domain and thicks significantly ahead of seaward of the thrust-folds to reach up to 0.6 s (twtt). Seismic profiles show progradation of shelfal sedimentation, with only thin strata deposited in the area equivalent to the paleo-shelf of the underlying unit (Figure V-3). A seaward shift in shelfal sedimentation can be seen in the isopach map (Figure V-5E), as unit P4 is thinner on the inner-middle shelf (commonly <0.2 s twtt) than over the outermost shelf-upper slope region (typically 0.4-0.6 s twtt), suggesting high shelf-to-slope sediment transfer during this phase.

The deposition of unit P4 marks the last phase of significant gravity-driven deformation in the Machadinho sub-basin.

Units N1-3 (~24-8 Ma)

The deposition of this group of units was marked by intense shelfal aggradation to reach thicknesses of over 1 s (twtt) on the outer shelf and commonly no more than 0.4 s (twtt) over the slope (Figure V-3 and Figure V-5F). Small-scale mass failures may have occurred during this phase in the upper slope region, as the top of the units (surface *Sn3*) depicts a series of step-like features and truncates a series of seismic horizons interpreted as slide scars. However, the absence of any distinguishable downslope mass-transport deposits within the units suggests either that larger mass failure events post-date deposition of this group, and/or that mass transport deposits were dispersed over large areas to form sedimentary bodies too thin to be identified in available seismic profiles.

Units N4-6 (~8-2 Ma)

The deposition of this group of units was marked by aggradation and progradation of shelfal units, which reach about 0.5 s (twtt) thickness on the shelf, thin considerably on the upper slope to about 0.2 s (twtt), thicken downslope to about 1 s (twtt), and gradually thin toward the deep basin to about 0.2 s (twtt) (Figure V-3 and Figure V-5G). The area of greatest thickness on the slope overlies a buried extensional domain (previously active during the Late Cretaceous and the deposition of units P1 and P4), and it is interesting to note that this fault

system was not reactivated by such sediment loading. Instead, a series of glided and/or rotated blocks can be seen within the upper slope deposits, which represent the most proximal portion of two large-scale mass transport deposits previously identified by Reis *et al.* (2016).

Unit Q (~2-0 Ma)

This unit is marked by intense aggradation and progradation of the shelfal succession associated with large-scale upper slope mass failures and mass-transport deposits in the deep basin. The unit reaches about 1.5 s (twtt) on the shelf, thins on the upper slope to less than 0.1 s (twtt), and thickens downslope to about 1.5 s (twtt) (Figure V-3 and Figure V-5G). The upper slope thinning is inferred to be due to mass wasting, recorded downslope by a series of mass-transport deposits interbedded with stratified deposits on SE flank of the Amazon Fan. These deposits were previously identified and described by Reis *et al.* (2016).

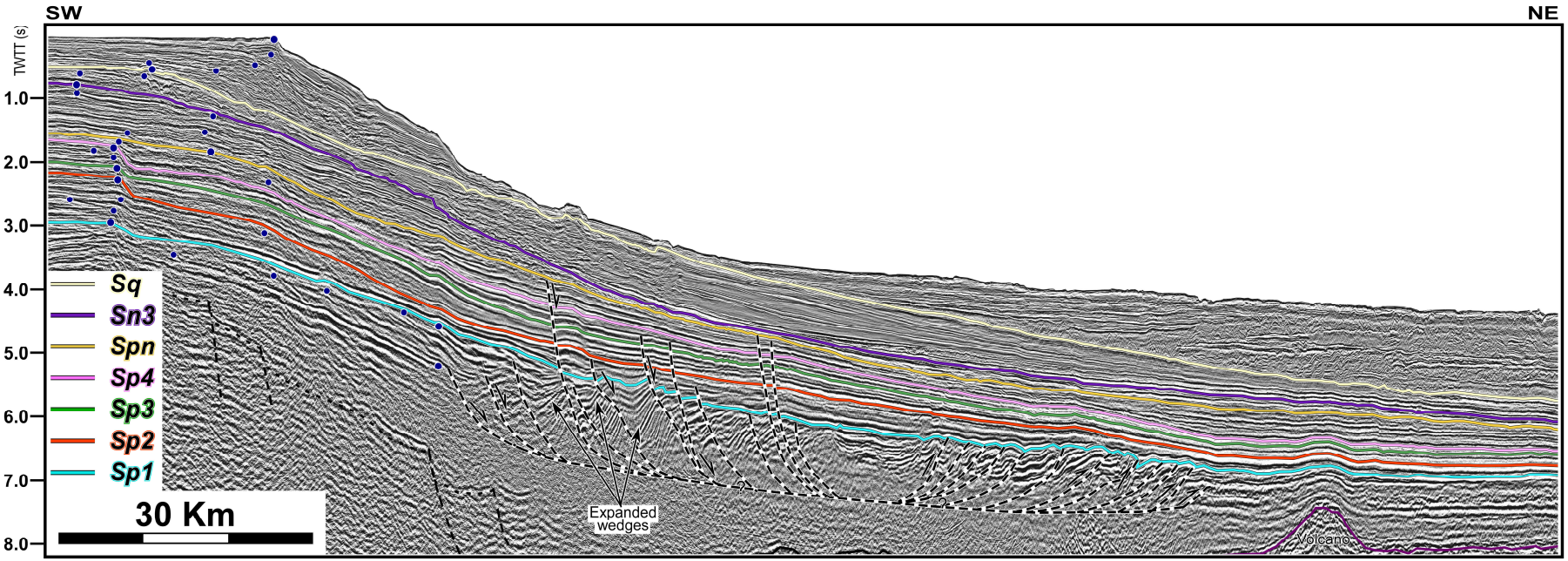

Figure V-3: Interpreted seismic profile illustrating the linked extensional–compressional system gliding over a basal *décollement* level across the slope region on the Machadinho sub-basin. Blue dotes show the shelf-edge trajectory. Note that seismic horizons bellow surface *Sp1* (ca. 66 Ma) are strongly rotted and bended, indicating that gravity-driven deformation was intense in the Machadinho sub-basin during the Late Cretaceous. Also note that gravity tectonics ceased on the Machadinho sub-basin after surface *Spn* (ca. 24 Ma). See Figure V-1 for seismic profile position.

*V.2.2.2 **Araguari sub-basin** (SE Compartment of the Amazon Fan)*

It is unclear whether gravity tectonics structures present in the Araguari sub-basin pre-Cenozoic succession are syn-sedimentary or post-sedimentary, as the stratigraphic succession underlying unit P1 is poorly imaged (Figure V-4). The lowest *décollement* level in this area is within pre-Cenozoic strata (Limoeiro Formation?), as stated by previous authors (Silva *et al.*, 1999; Perovano *et al.*, 2009). I am unable to assign a reliable age to this surface as no well has reached it and its shelfward extension is unclear. Thus it is possible that gravity-driven deformation in the Araguari sub-basin postdates the Cenozoic.

Most of the observed gravity-driven faulting in the Araguari sub-basin is associated with a second *décollement* level, as reported by previous authors (Silva *et al.*, 1999; Perovano *et al.*, 2009). This Intermediate *décollement* (Perovano *et al.*, 2009) lies not far below *Sp1* (~66Ma) and thus must be latest Cretaceous in age, although a more precise age can not be assigned.

We did not identified any significant faulting associated to the Upper *décollement* level defined by Perovano *et al.* (2009) in the portion of the Araguari sub-basin described in this paper (SE compartment of the Amazon Fan). This does not contradict the findings of this early work, however, as the authors stated that the Upper *décollement* level acted as a fault-rooting surface only in the more structurally complex NW compartment while it only capped paleo-fold and thrust belts (drape folds) in the SE compartment.

Unit P1 (~66-38 Ma)

No thickness variations indicative of gravity-driven faulting could be identified in the Araguari sub-basin during the deposition of unit P1, which is commonly about 0.7-0.5 s (twtt) thick across the upper slope extensional domain and gradually thins downslope to about 0.25 s (twtt) on the lowermost slope (Figure V-4). As such, unit P1 records a quiescent phase in terms of gravity tectonics in the Araguari sub-basin. Seismic profiles show that shelfal strata of unit P1 is organized as a basal condensed section formed during a major flooding event, overlain by a mainly prograding succession (Figure V-4).

The isopach map in Figure V-5B shows that unit P1 is thicker on the shelf of the Araguari sub-basin (>1 s twtt) than over its paleo-slope (commonly <0.6 s twtt), suggesting low shelf-to-slope sediment transfer during this phase. Some areas with high thickness values (>1s twtt) in the isopach map in Figure V-5B are caused by post-depositional shortening of unit P1

Unit P2 (~38-33.5 Ma)

Unit P2 is up to 0.75 s (twtt) thick in the upper slope extensional domain and gradually thins downslope to about 0.25 s (twtt) on the lowermost slope (Figure V-4). This unit shows no significant thickness variations indicative of gravity-driven faulting in the Araguari sub-basin and represents a quiescent phase syn-sedimentary tectonism. Seismic profiles show unit P2 shelfal strata is organized as an aggrading-prograding succession (Figure V-4).

The isopach map in Figure V-5C shows that unit P2 is thinner on the inner-middle shelf (commonly <0.2 s twtt) than over the outer shelf-upper slope region (typically 0.4-0.6 s twtt), suggesting high shelf-to-slope sediment transfer during this phase. As in the case of unit P1, some areas with high thickness values (over 1s twtt) in the isopach map in Figure V-5C are caused by post-depositional shortening of unit P2.

Unit P3 (~33.5-28 Ma)

Unit P3 also shows no significant thickness variations indicative of gravity-driven faulting, being about 0.2 s (twtt) thick in the upper slope extensional domain and gradually thinning to about 0.1 s (twtt) on the lowermost slope (Figure V-4). Unit P3 records a quiescent phase in terms of gravity tectonics in the Araguari sub-basin. Seismic profiles show that shelfal strata of unit P2 are organized as an essentially aggrading succession in the Araguari sub-basin, restricted to a more proximal position than shelfal strata of the underlying unit (Figure V-4). The isopach map in Figure V-5D shows that unit P3 is thicker on the inner-middle shelf (about 0.4 s twtt) than across the outer shelf-slope region (about 0.2-0.1 s twtt), suggesting low shelf-to-slope sediment transfer during this phase.

Unit P4 (~28-24 Ma)

Unit P4 is about 0.5 s (twtt) thick in the extensional domain (outer shelf-upper slope) and only about 0.2 s (twtt) thick in the compressive domain (mid-lower slope), showing significant thickness variations related to gravity tectonics (Figure V-4). The influence of gravity-driven deformation is evident at the transition from the extensional to the compressive domains, where major thrust faults root on the second *décollement* level (Intermediate *décollement* of Perovano *et al.*, 2009). Unit P4 is the lowest to be clearly affected by faults rooted on this *décollement*, indicating that it was not mechanically active prior to deposition of P4. Seismic profiles show progradation of shelfal sedimentation in the Araguari sub-basin during the deposition of unit P4, with only thin strata deposited in the area corresponding to the paleo-shelf of the underlying

unit (Figure V-4). Seismic profiles also show that unit P4 includes thin strata (less than 0.3 s twtt) located between thrust-folds that are associated with updip truncations (Figure V-4B).

The isopach map in Figure V-5E shows that Unit P4 is considerably thicker in the outer shelf-slope regions (from 0.2 s to >1 s twtt) than in the inner-middle shelf (typically <0.2 s twtt), indicating efficient sediment transfer to the slope and deep basin. The isopach map in Figure V-5E also shows that the main depocentres are fault-bounded and in the extensional domain.

Units N1-3 (~24-8 Ma)

This group of units is up to 1.2 s (twtt) thick in the extensional domain and thin over the compressive domain to no more than 0.3 s (twtt) (Figure V-4), reflecting a phase of gravity-driven deformation. On the shelf, the units show an overall aggradational-retrogradational trend in most of the Araguari sub-basin (see Cruz *et al.*, CHAPTER III), but eastward near the boundary with the Machadinho sub-basin the retrogradational component is reduced, and only near the top surface *Sn3* is a subtle backstep observed (Figure V-4). These units include unusually thin strata (less than 0.5 s twtt) located between fold-and-thrust belts and associated with updip truncations (Figure V-4B).

The isopach map in Figure V-5F shows that the group of units is commonly thicker on the shelf of the Araguari sub-basin (>1 s twtt) than over the paleo-slope (mostly <0.4 s twtt), despite some depocenters within the upper slope extensional domain reach more than 1 s (twtt) thickness. The overall distribution suggests low shelf-to-slope sediment transfer during this phase.

Units N4-6 (~8-2 Ma)

This group of units is up to 1.3 s (twtt) thick in the extensional domain thick and about 0.8 s (twtt) thick in the compressive domain (Figure V-4), a rather homogenous distribution across the SE compartment of the Amazon Fan. However, an influence of gravity tectonics can be clearly seen on the edges of the SE compartment, where the units pass from only 0.4 s (twtt) thick landward of the first listric fault of the extensional domain to about to 1.2 s (twtt) thick immediately seaward of this fault; whereas the opposite is seen in the compressive domain, where the units are only 0.8 s (twtt) thick on thrust-folds but thicken seaward of such features to up to 1.5 s (twtt). Seismic profiles also show that shelfal strata of the units are organized as a prograding prism over a basal condensed section, interpreted to have formed during a major flooding event (Figure V-4).

The isopach map in Figure V-5G shows that the units have a rather uniform thickness of 0.8-1.2 s (twtt) over most of the SE portion of the Araguari sub-basin, including the SE compartment of the Amazon Fan, thickening slightly (to up to 1.8 s) seaward of thrust-folds of the compressive domain. It is interesting to note that the major depocenters are located outside the study area, within the adjacent NW compartment of the Amazon Fan (Figure V-5G). This overall sedimentary distribution indicates that during this phase large sediment volumes were being deposited outside the study area and bypassing the SE compartment to be deposited seaward of the tectonically structured domains.

Unit Q (~2-0 Ma)

Deposition of this unit took place during the most intense phase of gravity-induced deformation in the Araguari sub-basin, as indicated by the substantial variation of sedimentary thickness from the extensional domain (up to 4.5 s twtt) to the compressive domain (no more than 1.5 s twtt in the major thrust-fold belt) (Figure V-4). Seismic profiles show that the unit experienced marked aggradation and progradation of shelfal successions (Figure V-4). This is inferred to have promoted a seaward migration of faulting within the extensional domain, with proximal listric faults "sealed" as the shelf-edge migrated seaward. In the compressive domain, the third and most distal thrust belt was created during the deposition of unit Q.

The isopach map of unit Q in Figure V-5H shows that the major depocenters (>3 s twtt) are located between the normal faults of the extensional domain and the thrust faults of the compressive domain, highlighting the importance of gravity-driven deformation on sediment distribution during this phase. Outside the gravity-tectonic domains, unit Q is only up to 0.8 s (twtt) thick on the shelf of the Araguari sub-basin and up to 2.4 s (twtt) thick seaward of the compressive domains, suggesting strong shelf-to-slope sediment transfer during this phase.

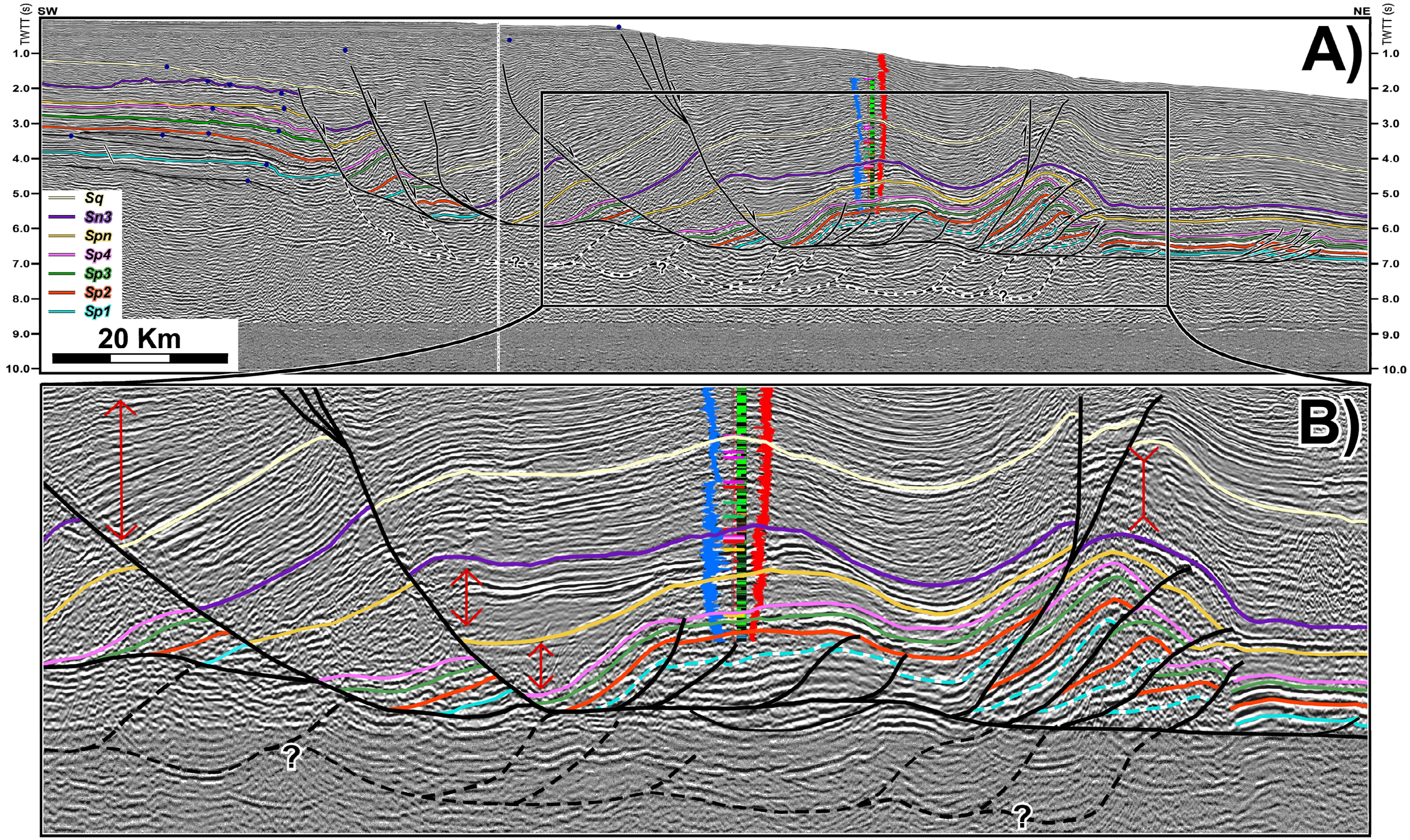

Figure V-4: Interpreted seismic profile illustrating the linked extensional–compressional system gliding over two *décollement* levels across the outer shelf-slope region on the Araguari sub-basin. Blue dotes show the shelf-edge trajectory. Red arrows indicate sedimentary thickening or thinning related to normal and thrust faults, respectively. Note that seismic horizons bellow surface *Sp1* (ca. 66 Ma) are thrusted and folded, indicating that gravity-driven deformation probably affected the Araguari sub-basin during the Late Cretaceous. Also note that gravity-driven deformation on the Araguari sub-basin persisted until the Recent as some of the faults in the extensional affect the present day seabed. See Figure V-1 for seismic profile position.

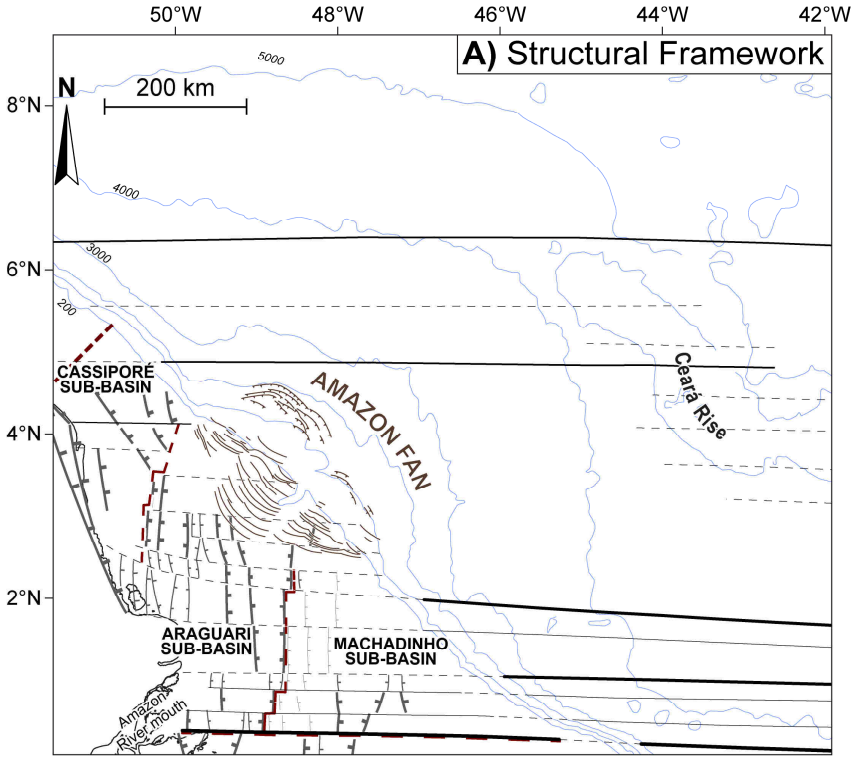
A) Structural Framework
50°W
48°W
46°W
44°W
42°W
8°N
6°N
4°N
2°N
N
200 km
5000
4000
3000
200
CASSIPORÉ SUB-BASIN
AMAZON FAN
Ceará Rise
ARAGUARI SUB-BASIN
MACHADINHO SUB-BASIN
Amazon River mouth

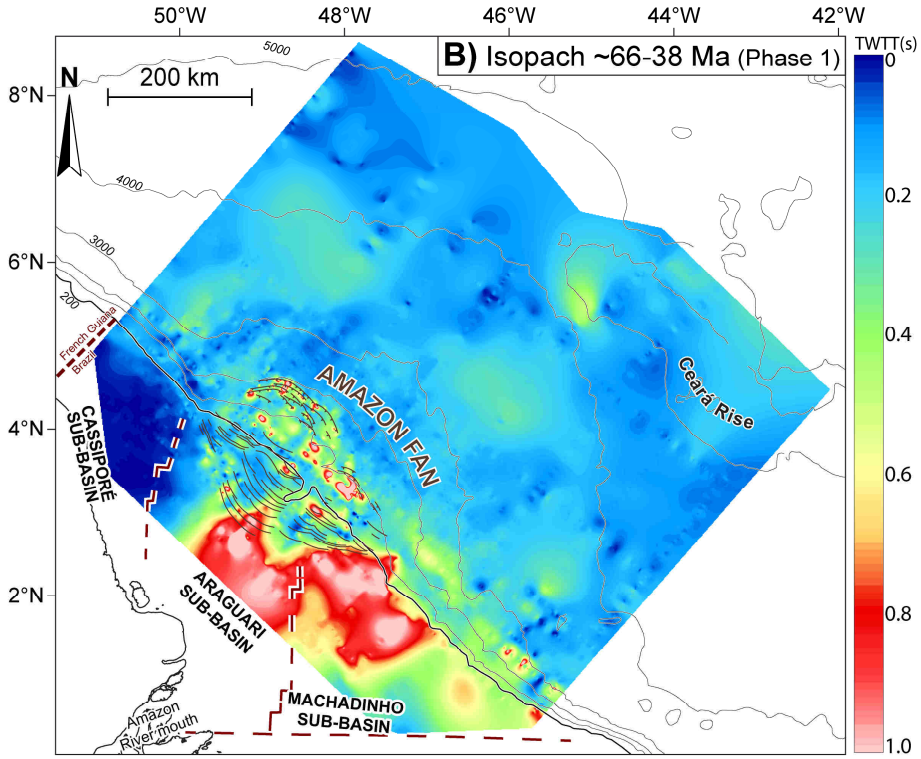
B) Isopach ~66-38 Ma (Phase 1)
TWTT(s)
0
0.2
0.4
0.6
0.8
1.0
50°W
48°W
46°W
44°W
42°W
8°N
6°N
4°N
2°N
N
200 km
5000
4000
3000
200
French Guiana
Brazil
CASSIPORÉ SUB-BASIN
AMAZON FAN
Ceará Rise
ARAGUARI SUB-BASIN
MACHADINHO SUB-BASIN
Amazon River mouth

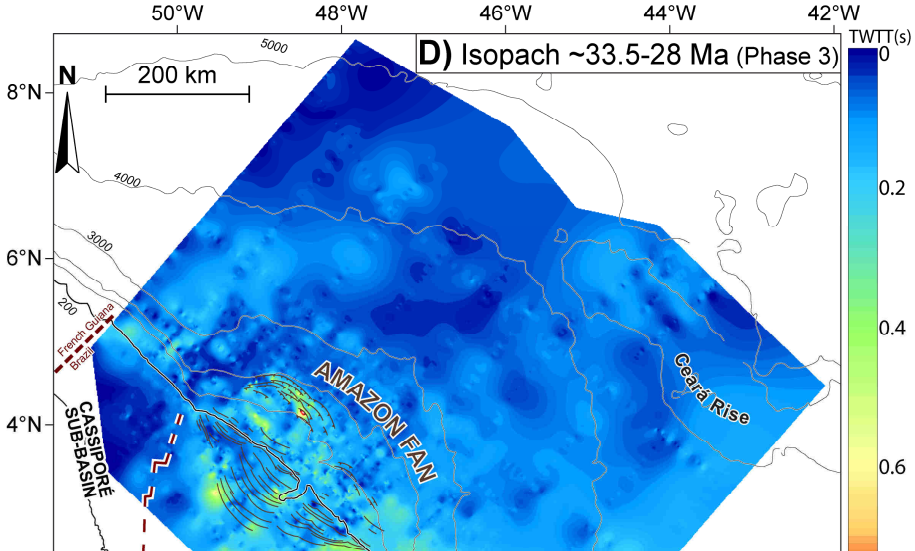
D) Isopach ~33.5-28 Ma (Phase 3)
TWTT(s)
0
0.2
0.4
0.6
50°W
48°W
46°W
44°W
42°W
8°N
6°N
4°N
N
200 km
5000
4000
3000
200
French Guiana
Brazil
CASSIPORÉ SUB-BASIN
AMAZON FAN
Ceará Rise

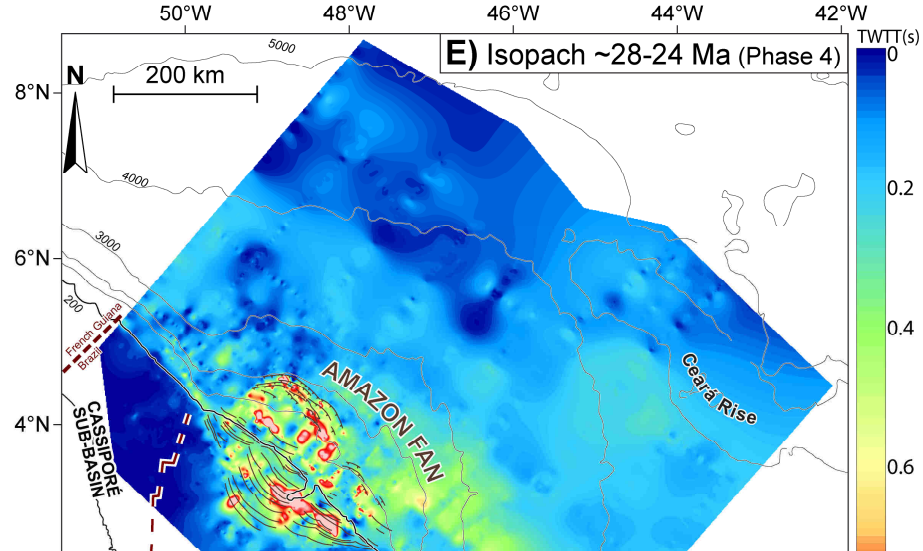
E) Isopach ~28-24 Ma (Phase 4)
TWTT(s)
0
0.2
0.4
0.6
50°W
48°W
46°W
44°W
42°W
8°N
6°N
4°N
N
200 km
5000
4000
3000
200
French Guiana
Brazil
CASSIPORÉ SUB-BASIN
AMAZON FAN
Ceará Rise

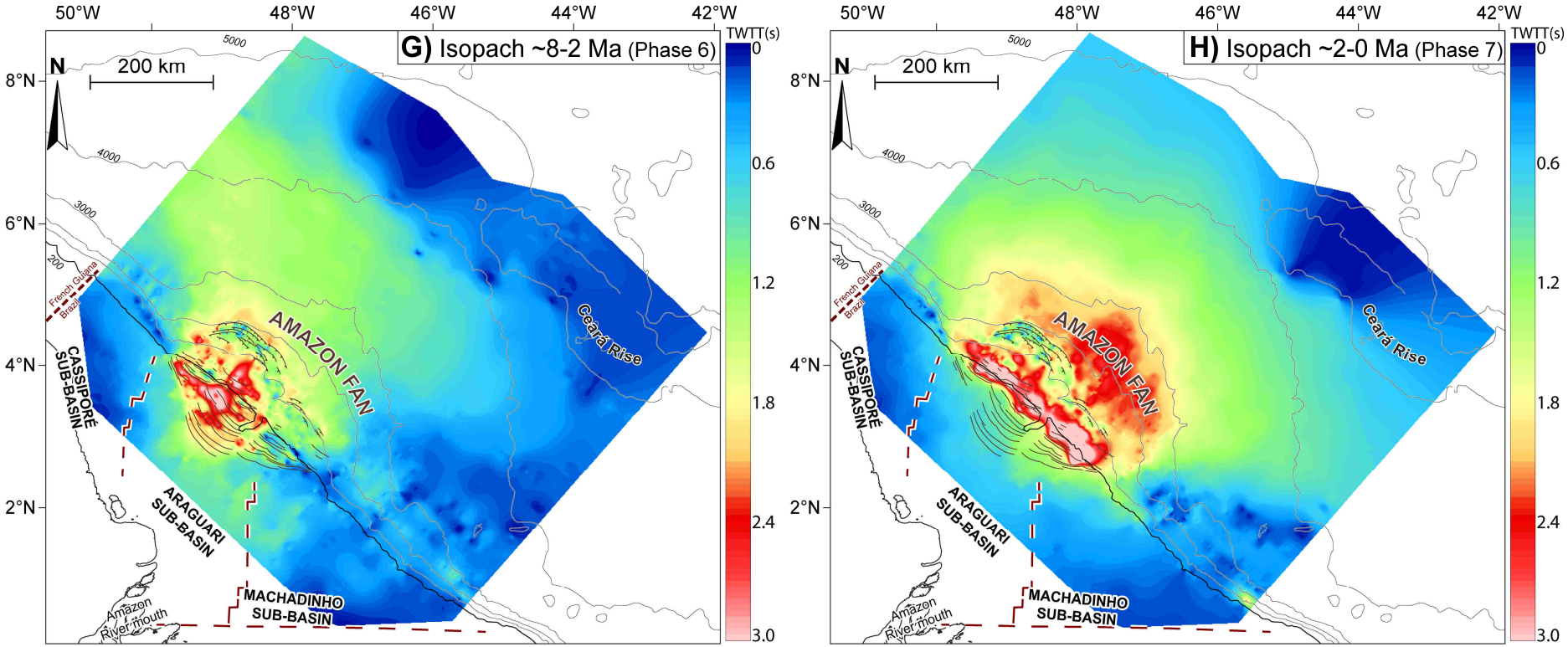

Figure V-5 (Continued)

V.2.3 Sedimentation rates in the Offshore Amazon Basin

The chronostratigraphic framework presented above allows an estimate of sedimentation rates for the Cenozoic stratigraphic units of the Offshore Amazon basin. In turn, this allows an investigation of the possible relationship between variations in sediment influx into the basin and phases of gravity-driven deformation. To do this, I calculate sedimentation rates during each of the deformation phases defined above using wells from three different domains: the Shelf, the Amazon Fan (equivalent to upper slope) and the Ceará Rise. Ideally, sedimentation rates should be based on decompacted stratal thicknesses. However, a lack of detailed downhole data on porosity-depth variation and lithological components (e.g. percentage of shale, sand and carbonates) makes a reliable decompaction model unfeasible. To address this, rather than using absolute rates of sedimentation, I analyze relative rates (rising or increasing between consecutive units). Furthermore, due to the great thickness of the Quaternary unit on the Amazon shelf and Amazon Fan (up to 1,900 m, Figure V-2:), compaction probably varies little between underlying units (older than ~2 Ma), as most compaction takes place in the first 2,000 m of burial (Allen and Allen, 2005).

Carbonate content was subtracted from the sedimentary thickness recorded on the Ceará Rise in order to calculate siliciclastic sedimentation rates in this distal deep-water region. A proportion of sediments derived from the continent have been shown to reach the Ceará Rise due to transport by ocean currents, and siliciclastic sedimentation rates in this distal region have been interpreted as a proxy for paleo-Amazon River sediment discharge across the study area (Dobson *et al.*, 2001; King *et al.*, 1997).

Here I describe relevant aspects of sedimentation rate variations within and/or between the units P1 to Q defined above, as illustrated in Figure V-6. I also note some possible correlations between changes in sedimentation rate and eustatic fluctuations according to Haq *et al.* (1987) and Miller *et al.* (2005). Finally, I stress possible correlations between varying sedimentation rates and gravity-driven deformation during the deposition of units P1 to Q.

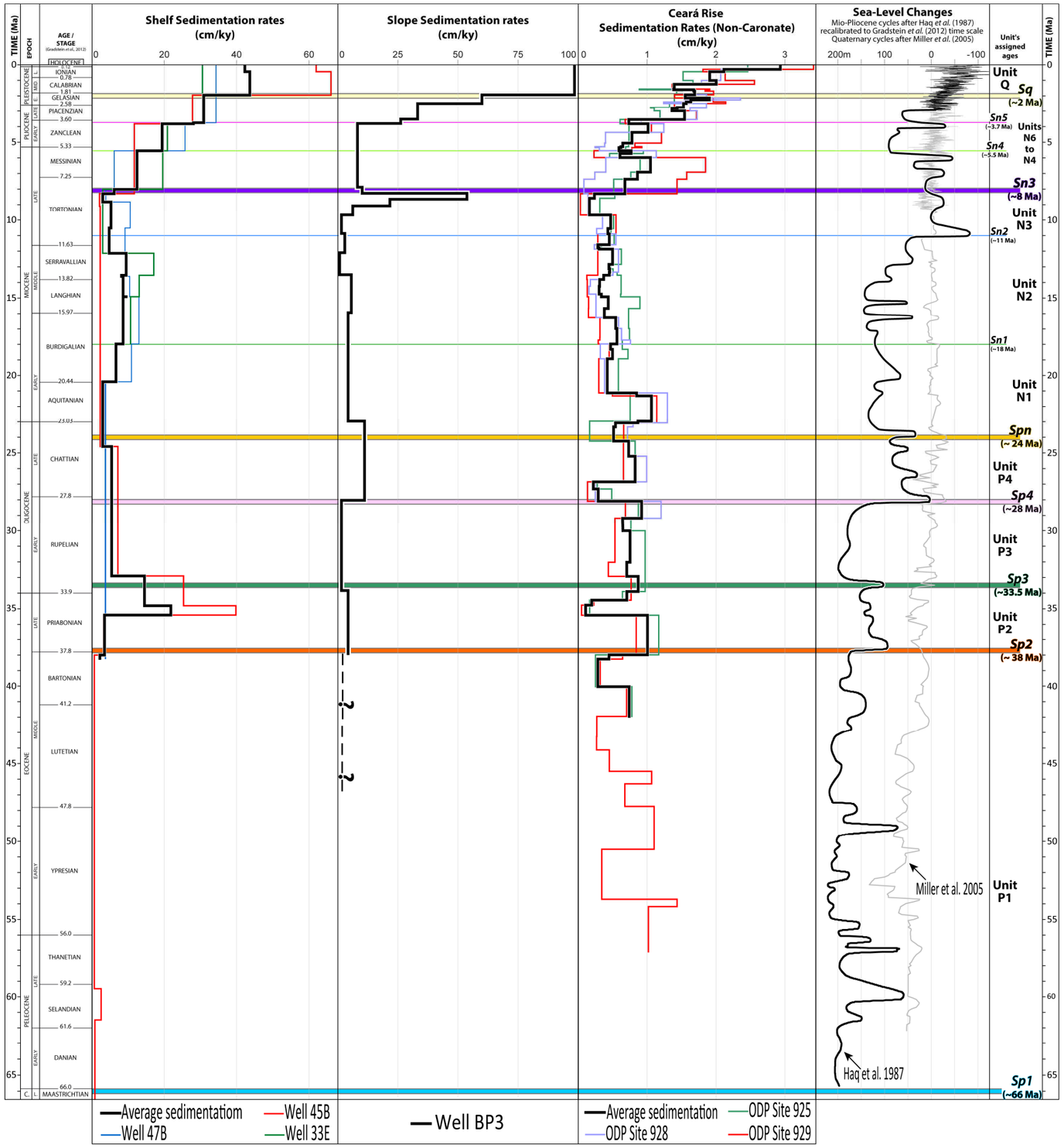

Figure V-6: Sedimentation rates over the Amazon shelf and slope and non-carbonate sedimentation rates on the Ceará Rise, as well as sea-level variation curves according to Haq *et al.* (1987) and Miller *et al.* (2005). Thick horizontal color lines represents the main stratigraphic surfaces seismic bounding units described in this work. The sedimentation rates are calculated based on age and stratigraphic position of several biohorizons (first or last occurrence of key fossiliferous species) available in well reports.

Unit P1 *(66-38 Ma)*

Only one well with chronostratigraphic data fully penetrated this deeply buried unit, on the NW outer shelf (well 45B; Figure V-6). On the Ceará Rise, ODP Site 929 sampled most of Unit P1 despite not reaching its base. Sedimentation rates calculated in well 45B for unit P1 are low compared to overlying units. However, thickening of P1 toward the Araguari and Machadinho sub-basins (Central and SE margin respectively) as seen in isopachs (Figure V-5) points to higher sedimentation rates there.

ODP Site 929 records an overall trend of decreasing siliciclastic sedimentation rates since 57-54 Ma, reaching minimum values around 44-43 Ma during a major highstand in the sea level curves of both Haq *et al.* (1987) and Miller *et al.* (2005) (Figure V-6). This trend suggests that sediment flux into the basin gradually reduced during the deposition of unit P1, with lower flux during periods of exceptionally high eustatic sea level.

Decreasing siliciclastic sedimentation rates in the distal Ceará Rise area (Figure V-6) and an overall regime of low shelf-to-slope sediment transfer during deposition of unit P1 (deduced from the isopach map in Figure V-5B) are consistent with decreasing sediment flux into the Offshore Amazon basin and reducing sedimentary loading, including in regions affected by gravity tectonics. This may account for the limited occurrence of gravity-driven deformation (compared with underlying Cretaceous strata) in the Machadinho sub-basin and the absence of such deformation in the Araguari sub-basin during deposition of unit P1. Sedimentation during the deposition of unit P1 was mostly restricted to carbonate strata deposited on the more stable shelf regions that were never affected by gravity-driven deformation, possibly because no *décollement* level was formed (absence of overpressured levels?).

Unit P2 *(38-33.5 Ma)*

As result of shelfal progradation, sedimentation rates on the Amazon shelf during deposition of unit P2 varied from lower on the inner shelf (well 47B) to higher on the outer shelf-upper slope (well 45B), reaching a maximum around 35 Ma (Figure V-6). In the slope region, sedimentation rates are not available for the previous unit to compare with those of unit P2. In the Ceará Rise region, the lower part of unit P2 records a sharp increase in siliciclastic sedimentation rates, dropping around 35 Ma before rising again toward the top of the unit (Figure V-6). Each of the increases in siliciclastic sedimentation rates on the Ceará Rise could be related to eustatic falls in the sea-level curves of Haq *et al.* (1987) and Miller *et al.*, (2005).

On the other hand, it seems that the increase in sedimentation rates on the outer shelf (well 45B) around 35 Ma is exclusively related to carbonate production, ideal conditions during a sea-level rise between two major lowstands (Figure V-6).

Increasing sedimentation rates in the outer shelf (well 45B), slope and Ceará Rise regions (Figure V-6) and a regime of low shelf-to-slope sediment transfer during the deposition of unit P2 deduced from isopachs (Figure V-5C) point to an increasing flux of siliciclastic sediments into the Offshore Amazon basin during the deposition of unit P2. This resulted in an increased sedimentary load above the extensional domains of gravity tectonics systems within the Machadinho and Araguari sub-basins, although no gravity-driven faulting associated with such sedimentary loading could be identified.

Unit P3 *(34.5-28 Ma)*

There is limited chronostratigraphic resolution of sedimentation rates during deposition of unit P3 on the shelf and slope, but sedimentation rates were slightly lower than during the deposition of the underlying unit (Figure V-6). In the Ceará Rise region, siliciclastic sedimentation rates remained stable during the deposition of unit P3, being higher than the minimum, but slightly lower than the maximum, recorded during deposition of the underlying unit (Figure V-6).

It is unclear how eustatic variations may have influenced sediment flux into the study area as there is a mismatch between the sea-level curves of Haq *et al.* (1987) and Miller *et al.*, (2005) for the period of unit P3. According to Haq *et al.* (1987), this period was marked by a prolonged highstand (Figure V-6), which could explain the reduction in sedimentation rates on the slope region due to stocking of sediments on the inner-middle shelf. On the other hand, according to Miller *et al.*, (2005), during the same period sea-level experienced no major variations and on average was slightly lower than during deposition of the previous unit (Figure V-6), which could explain an increase on siliciclastic sedimentation rates on the distal Ceará Rise as greater sediment transport into the basin. The overall thickness variation of unit P3 with its thicker inner-middle shelf strata (Figure V-5F) favors an interpretation of eustatic sea-level rise and suggests that the deposition and/or preservation of siliciclastic sediment in the distal Ceará Rise region were affected by processes unrelated to sediment flux into the Offshore Amazon basin. During this prolonged highstand, sedimentation in the Offshore Amazon basin was mostly restricted to carbonate strata on more stable regions of the shelf that were unaffected by gravity-driven deformation.

Unit P4 *(28-24 Ma)*

There is also limited chronostratigraphic resolution of sedimentation rates during deposition of unit P4 on the shelf and slope regions. Still, a sharp increase in sedimentation rates is observed in the slope region, whereas a slight decrease is observed on the shelf by the end of deposition of this unit (Figure V-6). On the Ceará Rise, siliciclastic sedimentation rates dropped significantly at the beginning of deposition of the unit, before rising around 26.8 Ma and dropping once more by the end of deposition around 25-24 Ma (Figure V-6).

It is again unclear how eustatic variations may have influenced sediment flux into the study area during deposition of unit P4 as there is a mismatch between sedimentation rates in the slope and Ceará Rise regions. A major eustatic fall around 28 Ma followed by a prolonged lowstand in the sea-level curves of both Haq *et al.* (1987) and Miller *et al.* (2005) (Figure V-6) could explain a sharp increase in sedimentation rates on the slope as sediments would tend to bypass the paleo-shelf and be deposited directly downslope. However, siliciclastic sedimentation rates decrease on the Ceará Rise around 28 Ma (Figure V-6). So, it is inferred that during deposition of unit P4, the deposition and/or preservation of siliciclastic sediment in the distal Ceará Rise region were affected by processes unrelated to sedimentary influx into the Offshore Amazon Basin.

Increasing sedimentation rates on the slope (Figure V-6) and a regime of low shelf-to-slope sediment transfer during deposition of unit P4 (deduced from the isopachs in Figure V-5E) point to a scenario of increasing siliciclastic sediment flux into the Offshore Amazon basin during deposition of unit P4. This promoted increased sediment loading over regions affected by gravity tectonics systems, which seems to have resulted in the reactivation of paleo-extensional and compressive domains in the Machadinho sub-basin and created a second *décollement* level within the Araguari sub-basin.

Units N1-3 *(24-8 Ma)*

Average sedimentation rates on the Amazon shelf increased significantly from ca. 24 Ma to ca. 12 Ma, dropped sharply during a major eustatic fall around 11.5-11 Ma, and dropped again during a second Tortonian eustatic fall around 9 Ma (Figure V-6; Haq *et al.*, 1987; Miller *et al.*, 2005). An overall decrease in sedimentation rates on the slope (well BP 3) was interrupted by a slight increase in sedimentation rates around 12 Ma and a second major increase between

9.6-8.6 Ma, also in response to eustatic sea-level falls (Figure V-6; Haq *et al.*, 1987; Miller *et al.*, 2005). Siliciclastic sedimentation rates on the Ceará Rise region dropped sharply at ca. 21 Ma and remained low and without major variations, until dropping even more at ca. 9.6 Ma, around the same time that sedimentation rates started to increase on the slope region (Figure V-6).

A major increase in sedimentation rates was recorded in the shelf and Ceará Rise regions around 8.3-8.0 Ma at the same time that a major drop in sedimentation rates was recorded on the slope in well BP3 (Figure V-6). The large decrease in sedimentation rates in the area of well BP3 was probably a result of increased gravity-driven deformation and thrust-related uplift, as described in the previous sub-section, which resulted in thinner syn-tectonic strata in this region. These changes in sedimentation rates were not caused by eustatic variations, as this period was marked by a minor sea-level rise according to both Haq *et al.* (1987) and Miller *et al.* (2005) (Figure V-6). Thus, a major increase of sediment influx into the Offshore Amazon basin must be taken in consideration, probably as a result of a Late Miocene onset of the transcontinental Amazon River (Figueiredo *et al.*, 2009; Hoorn *et al.*, 2017) and/or reduction of accommodation space creation in inner shelf-coastal regions (Cruz *et al.*, CHAPTER III).

Units N4-6 *(8-2 Ma)*

The deposition of this group of units involved an overall increase in sedimentation rates everywhere in the study area (Figure V-6), which resulted in progradation and increased sedimentary load on the outer shelf-upper slope. It is interesting to note that sediment loading on the outer shelf-upper slope region promoted intensification gravity-driven deformation in the Araguari sub-basin, but not in the Machadinho sub-basin where there is no identifiable fault reactivation on seismic profiles.

Unit Q *(ca. 2 Ma to Recent)*

Sedimentation rates greatly increased everywhere in the study area during the deposition of this uppermost unit (Figure V-6). This resulted in significant sediment loading across the outer shelf-upper slope region, and in the most intense phase of gravity-driven deformation in the Offshore Amazon basin.

Increasing sedimentation rates during deposition of unit Q could be related to large sea-level falls associated with the intensification of Milankovitch cycles and northern hemisphere

glaciation during the Quaternary, notably the during the last 800-900 ky (Figure V-6; Zachos *et al.*, 2001; Miller *et al.*, 2005).

V.3 DISCUSSION

Gravity tectonics intensely deformed pre-Cenozoic strata in the Machadinho sub-basin (SE margin) during the Late Cretaceous and it seems likely that coeval strata in the Araguari sub-basin (central margin) also experienced some degree of syn-sedimentary deformation. It is clear, however, that gravity-driven deformation was much more intense in the Machadinho sub-basin than in the Araguari sub-basin during the Late Cretaceous. This pre-Cenozoic phase of gravity tectonics is probably equivalent to the earliest stage identified by Silva *et al.* (2011) and described as being dominated by deformation due to gravity gliding. According to Rowan *et al.* (2004), the primary factor in gravity gliding is the basinward tilting of a basal *décollement* due to differential thermal subsidence or cratonic uplift. As such, it may be that the greater intensity of gravity-driven deformation in the Machadinho sub-basin during the Late Cretaceous was caused by greater across-margin differential subsidence than in the Araguari sub-basin (Figure V-7).

A reduction in gravity-driven deformation from the Paleocene to Middle Eocene (between surfaces *Sp1* and *Sp2*, ~66-38 Ma) was probably caused by more quiescent geodynamic conditions in the Offshore Amazon Basin. In passive margins, thermal subsidence decays with time and becomes significantly reduced tens of million years after the end of the rifting phase (Allen and Allen, 2005), which was around 102 Ma in the Offshore Amazon Basin (Figueiredo *et al.*, 2007). The fact that some syn-sedimentary gravity-driven faulting can nonetheless be identified in the Machadinho sub-basin may suggest that the region experienced some degree of differential subsidence for longer than the Araguari sub-basin (Figure V-7). Here, I suggest that gravity-driven deformation is an indicative of prolonged differential subsidence in the Machadinho sub-basin that could have been caused by diachronous continental breakup along the Offshore Amazon Basin, and/or by renewed crustal heating and loading related to the nearby volcanic North Brazilian ridge and Marajó seamounts.

After the Middle Eocene, the Offshore Amazon Basin experienced a prolonged period in which no significant syn-sedimentary gravity-driven deformation is observed in the Machadinho and Araguari sub-basins until the Late Oligocene (i.e. between surfaces *Sp2* and *Sp4*, ~38-28 Ma) (Figure V-7). During this period, it is noteworthy that even high shelf-to-slope

sediment transfer during deposition of unit P2, which resulted in enhanced sediment loading above the extensional domain in both sub-basins, was not capable of reactivating the gravity-driven fault systems.

During the Late Oligocene (between surfaces *Sp4* and *Spn*, ~28-24 Ma), gravity-driven syn-sedimentary faulting is recognized in both the Machadinho sub-basin (reactivation of older faults) and the Araguari sub-basin (activation of a new *décollement* level and associated faults) (Figure V-7). The driving mechanism of gravity-driven deformation during this phase is unclear, but it may have been caused either by gravity spreading due to the intense sedimentary transfer to the slope region during deposition of unit P4, or by gravity gliding due to renewed post-rift differential subsidence similar to what is interpreted to have occurred during the Miocene (Cruz *et al.*, Chapter III). The structural lows between fold-and-thrust belts in the Araguari sub-basin contain thin strata, which is anomalous as such lows (piggyback basins) are usually filled with deposits thicker than the adjacent uplifted areas. This anomalous variation in stratal thickness across the thrust-folds highs (Figure V-4) point to the action of strong ocean bottom currents, which can be focused and accelerated due to confinement when interacting with irregular seafloor morphologies (Rebesco *et al.*, 2014) leading to the constant sweeping away of fine-grained sediments (Figure V 7).

From the Early Miocene to early Late Miocene (between surfaces *Spn* and *Sn3*, ~24-8 Ma), gravity tectonics continued in the Araguari sub-basin but ceased in the Machadinho sub-basin (Figure V 7). It is interesting to note that in the Machadinho sub-basin, slide scars began to be recognized only in units deposited after the cessation of gravity tectonics, suggesting that mass wasting may have started to act to preserve slope equilibrium in the absence of a more effective mechanism. Meanwhile, the fact that gravity tectonics persisted in the Araguari sub-basin despite reduced shelf-to-slope sediment transfer during this period (notably between ~24-9.6 Ma) suggests that gravity gliding predominated as a mechanism to preserve slope equilibrium. The Araguari sub-basin underwent intense subsidence during the Early-Middle Miocene, expressed on the shelf as high accommodation space creation rates (see Cruz *et al.*, Chapter III), and I suggest that it may have been even more pronounced in the deep basin and so promoted tilting of the *décollement* accommodating gravity-driven deformation in the region.

A dramatic and growing increase in sedimentation rates in the Offshore Amazon Basin starting at around 8 Ma points to a scenario of constantly increasing sediment flux into the Offshore Amazon Basin. This could be interpreted as a gradual evolution of a Late Miocene transcontinental Amazon River from a drainage system encompassing wetlands and lakes

(acting to filter most Andean-derived sediments) to an entrenched fluvial system similar to the modern Amazon River (transporting sediments to the Equatorial Atlantic more efficiently), similar to what has been proposed in some studies (Figueiredo *et al.*, 2009; Hoorn *et al.*, 2017). Alternatively, the sharp increase in sedimentation rates that took place throughout the offshore Amazon Basin from ca. 3.7 Ma (Figure V-6) could be interpreted a Pliocene onset of a transcontinental Amazon River, as proposed in other studies (Latrubesse *et al.*, 2010; Gross *et al.*, 2011). In either case, the dramatic increase in sediment flux into the Offshore Amazon Basin promoted marked progradation of the outer shelf-upper slope in the Araguari sub-basin, resulting in the growth of the Amazon Fan and its major depocenters. The rapid stacking of sedimentary successions in the Araguari sub-basin upper slope promoted the collapse of the Amazon Fan under its own weight as a mechanism to preserve slope equilibrium. This is in agreement with experimental models by Silva *et al.* (2011), which found that syn-sedimentary gravity tectonics during the Amazon Fan growth was dominated by gravity spreading. In turn, this is consistent with the statement of Rowan *et al.* (2004) that "progradational (proximal) deposition on the outer shelf and upper slope maintains or increases the overall seabed dip, which drives gravity spreading".

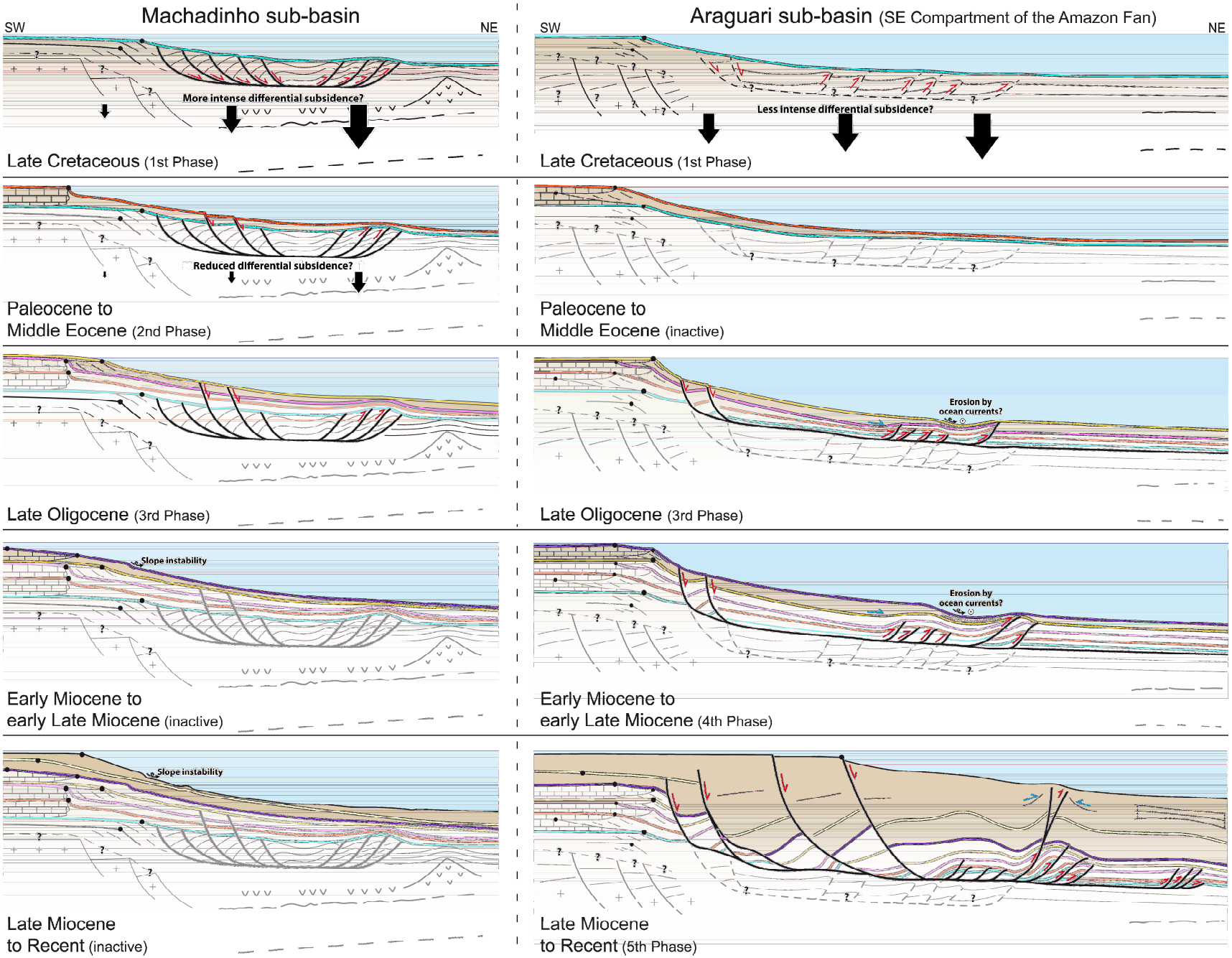

Figure V-7: Schematic synthesis of the main phases of syn-sedimentary gravity-driven deformation in the Offshore Amazon Basin. Not to scale.

V.4 CONCLUSIONS

Gravity tectonics in the Offshore Amazon Basin involved syn-sedimentary faulting above basal *décollement* surfaces that differ in number and character between the Machadinho and Araguari sub-basins. In the Machadinho sub-basin (SE margin), syn-sedimentary gravity-driven deformation was exclusively associated with a single *décollement* surface located deep within the Late Cretaceous post-rift succession. The same *décollement* affected the Araguari sub-basin (Central margin), but most of the gravity-driven deformation in the SE compartment of the Amazon Fan was associated with a second *décollement* surface located close to the Cretaceous-Cenozoic boundary, as reported by Silva *et al.* (2011).

Gravity tectonics affected the post-rift succession of the Offshore Amazon Basin during at least five main phases since the Late Cretaceous. Each of these phases is distinct in terms of its intensity, the main deformation mechanism (gravity gliding or gravity spreading) and the size of the area affected. During the Late Cretaceous (first phase), both the Machadinho and Araguari sub-basins were affected by gravity-driven deformation that I argue was likely to have been dominated by gravity gliding as a result of intense differential subsidence across the margin. Between ca. 66-38 Ma (second phase), only the Machadinho sub-basin was affected by gravity-driven deformation, also likely to have been dominated by gravity gliding due to differential subsidence, although less intense than the previous phase. Gravity tectonics was renewed in both sub-basins between ca. 28-24 Ma (third phase), possibly dominated by gravity spreading in response to intense progradation and sedimentary loading in the outer shelf-upper slope region, although gravity gliding can not be ruled out as an explanation for the observed deformation. From ca. 24-8 Ma (fourth phase), only the Araguari sub-basin experienced the effects of gravity tectonics, probably dominated by gravity gliding as a result of renewed differential subsidence across the margin. Finally, during the last 8 My (fifth phase) the Araguari sub-basin experienced the most intense phase of gravity tectonics, caused by intense outer shelf-upper slope progradation and stacking of depositional units that represent the major depocenters of the Amazon Fan. The rapid deposition of such a thick sedimentary succession promoted the collapse of the upper Amazon Fan under its own weight (gravity spreading).

In future, when seismic data of better quality become available, it would be interesting to extend detailed investigations on gravity tectonics to the more structurally complex NW compartment of the Amazon Fan, to verify if this region experienced gravity tectonics during the same periods as the SE compartment. The results presented here in regard to gravity tectonics within the SE compartment of the Amazon Fan are in agreement with previous studies

of the same region (eg. Silva *et al.*, 1999; Perovano *et al.*, 2009; Reis *et al.*, 2010; Silva *et al.*, 2011). However, it would be interesting to conduct more detailed structural analyses in the less explored Machadinho sub-basin, to test the interpretations proposed in this work in regard to dominant deformational mechanisms (gravity gliding vs. gravity spreading).

CHAPTER VI
GENERAL DISCUSSION

CHAPTER VI

This chapter consists of two sections in which I address the possible implications of the results presented in chapters **III** to **V**, taking into consideration the results of previous studies.

First in section VI.1, I make some remarks concerning previous work undertaken by other members of our research group at ISTeP, Rio de Janeiro State University and Fluminense Federal University (GEOMARGEM research group). In section VI.1.1, in light of the findings presented in this thesis, I review and expand upon some points tackled by Gorini *et al.* (2014), Reis *et al.* (2016) and Albuquerque (2009) concerning the Miocene to Recent stratigraphic succession of the Offshore Amazon Basin. In section VI.1.2, I briefly present the relevant findings of a Master's internship undertaken at ISTeP under the supervision of Dr. Slah Boulila and co-advised by myself, which investigated the cyclicity of the Late Cretaceous succession in the Cassiporé sub-basin. In section VI.1.3, I propose a new stratigraphic chart for the Offshore Amazon Basin that takes into account all knowledge available from the published literature and from the work of our research group over the last 10 years.

Section VI.2 then proposes a broader discussion, in which I put the results presented above into a regional context through a review of published investigations of the geology of the area from the Andean Range to the Equatorial Atlantic Abyssal Plain. A simplified paleogeographical scenario of the northern portion of South America is also proposed, in an attempt to create a general framework for the major geological events of the region reported by our research group and in other published works.

VI.1 INTEGRATION WITH OTHER STUDIES FROM OUR GROUP

VI.1.1 Remarks on Gorini *et al.* (2014), Reis *et al.* (2016) and Albuquerque (2009)

The presence along the Amazon upper slope both of faults related to gravity-driven deformation, and of large-scale mass transport deposits, makes it difficult to reliably correlate stratigraphic surfaces across the Offshore Amazon basin. In the studies presented by Gorini *et al.* (2014) and Reis *et al.* (2016), we made a first attempt to ensure that our seismic stratigraphic correlations across the shelf, Amazon Fan and abyssal plain were correct, by using calcareous nannofossil zones (sensu Martini, 1971) in five wells. Despite inherent limitations in the use of calcareous nannofossil zones (see Chapter II), the overall stratigraphic framework proposed in Gorini *et al.* (2014) and Reis *et al.* (2016) continues to seem coherent, even in the light of the revised chronostratigraphic model and more detailed seismic interpretations presented in this thesis. Nonetheless, it is possible to propose some revisions of the conclusions of these early works.

First, it is worth noting that the detailed chronostratigraphic model presented in this thesis (Chapter III) points to a slightly younger age for the top of the mixed carbonate-siliciclastic platform in the Araguari and Machadinho sub-basins (surface *Sn3* in the Central and SE shelves) than stated by Gorini *et al.* (2014). While in the latter study we had assigned an age between 9.5-8.3 Ma based on calcareous nannofossil zonations, our revised chronostratigraphic model indicates an age for the same surface of some point between 9.1 and 7.78 Ma (most likely around 8 Ma).

Secondly, in Reis *et al.* (2016) we considered that the top of the mixed carbonate-siliciclastic platform was laterally correlative to the base of the Amazon Fan (surface "H3"), then interpreted as a condensed section formed between ca. 11.9-9.5 Ma (based on calcareous nannofossil zones). However, our revised chronostratigraphic model points to a significantly older age for basal surface H3, roughly between 14-16 Ma, based on its position in well BP-3 (Figure VI-1) below the last recorded occurrence of *Sphenolithus heteromorphus* (13.53 Ma; Anthonissen and Ogg, 2012) and above a stratigraphic level labeled in the well report as "top of Early Miocene" (which should be around 15.97 Ma, assuming that this correctly marks the top of Burdigalian). Given that sedimentation rates only started to increase significantly on the fan around 10 Ma (see Chapter V or subsection VI.2.1), the revised age of surface H3 raises the possibility that it does not represent the "true" base of the fan. Instead, I propose that the

prominent regional seismic horizon corresponding to surface H3 is an expression of the well-documented "carbonate crash" in deep-water sediments, caused by a gradual shoaling of the lysocline in the South Atlantic from ca. 14-9 Ma and including a major carbonate dissolution event between ca. 12-10 Ma (Roth *et al.*, 2000; Newkirk and Martin, 2009; King *et al.*, 1997). In this perspective, the strong seismic expression of surface H3 would be entirely due to the impedance contrast between sedimentary packages with variable carbonate content. I suggest that intense carbonate dissolution resulted in the accumulation of a condensed section composed almost exclusively of finely-grained terrigenous sediments (deposited from ~14-9 Ma), directly above strata richer in carbonate (>14 Ma). The condensed section deposited during the "carbonate crash" is likely to be correspondent to a more plastic behavior of the succession above surface H3, leading Perovano *et al.* (2009) to interpret this seismically identified surface as a *décollement* level.

At this point, it becomes clear that the base of the Amazon Fan must be older than the top of the mixed carbonate-siliciclastic platform. In fact, the top of the platform (~9.1-7.78 Ma) may be up to 8 My younger than the base of the Amazon Fan if we consider the latter to correspond to surface H3 (~14-16 Ma), or be at least ~1 My younger if we instead consider the onset of significantly increased sedimentation rates in the Amazon Fan (~10 Ma). These ages are in clear opposition to the assumption that the base of the fan and the top of the carbonate-siliciclastic platform are correlative (Figueiredo *et al.*, 2009; Silva *et al.*, 1999), and inconsistent with the recent statement by Hoorn *et al.* (2017) that the base of the Amazon Fan postdates the top of the platform by 1-1.5 My. It may be that the onset of deposition of the Amazon Fan was linked to climatic events such as eustatic lowering around 11 Ma (Haq *et al.*, 1987; Miller *et al.*, 2005) and possibly lysocline deepening around 10 Ma (King *et al.*, 1997). In contrast, shelfal carbonate production persisted until around 8 Ma when the sedimentary influx into the Offshore Amazon Basin started to increase significantly.

Finally, a comparison between the chronostratigraphic model presented in this thesis and the results presented by Albuquerque (2009) provides some age constraints on the main evolutionary phases of the Amazon Fan recognized in her study. It became clear in the present work that surface *Sn5* (~3.7 Ma) underlies the first well-developed channel-levee systems on the Amazon Fan (Figure VI-2). As such, a Late Pliocene to Recent time spam can be assigned to phases II and III of Albuquerque (2009). Surface *Sn5* is related to a major increase in sediment flux into the Offshore Amazon basin (see Chapter V or section VI.2.1) and it is

interesting to note that it also marks the establishment of the earliest well-developed channel-levee systems on the Amazon Fan, suggesting a direct interplay between sediment supply and the evolution of turbidite systems. Moreover, surface *Sn5* (~3.7 Ma) also marks the point at which the large embayment in the Central shelf-slope region became completely filled (see Chapter III), so that slope morphology may also have played a role in the transition from less channelized to more channelized turbidite systems in the Offshore Amazon basin, consistent with the model of Mutti (1985). In that perspective, the morphology of the Amazon paleo-slope may have been steeper and more irregular before complete infilling of the embayment, favoring faster and more chaotic sediment transport to the deep basin during lowstands. After complete infilling of the embayment, the paleo-slope may have become less steep and smoother, favoring more "organized" sediment transport to the deep basin during lowstands, and allowing the formation of large constructional features like the well-developed channel-levees overlying surface *Sn5* (Figure VI-2). At the moment, however, all these assumptions regarding paleo-slope morphology are unverifiable, as the region was strongly affected by gravity-driven tectonics during the Quaternary and the depositional morphology of the Miocene-Pliocene succession was not preserved.

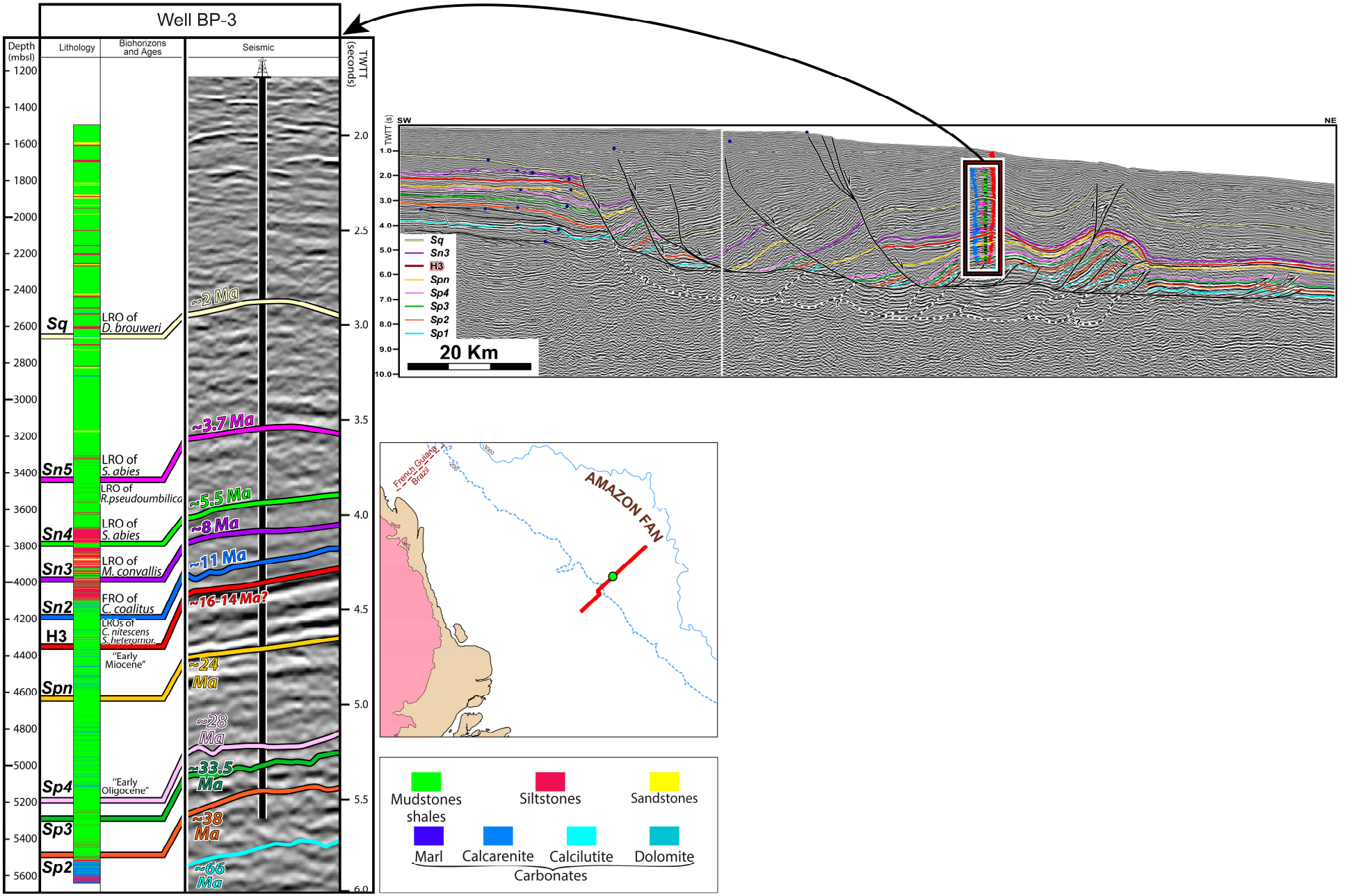

Figure VI-1: Correlation between seismic and well (lithological and chronostratigraphic) data showing that the pronounce seismic horizon commonly interpreted as the base of the Amazon Fan (H3- ~16-14Ma) is older than the surface correlated to the top of the carbonate platform in the Araguari and Machadinho sub-basins (*Sn3* - ~8 Ma). FRO stands for "first recorded occurrence" and LRO stands for "last recorded occurrence".

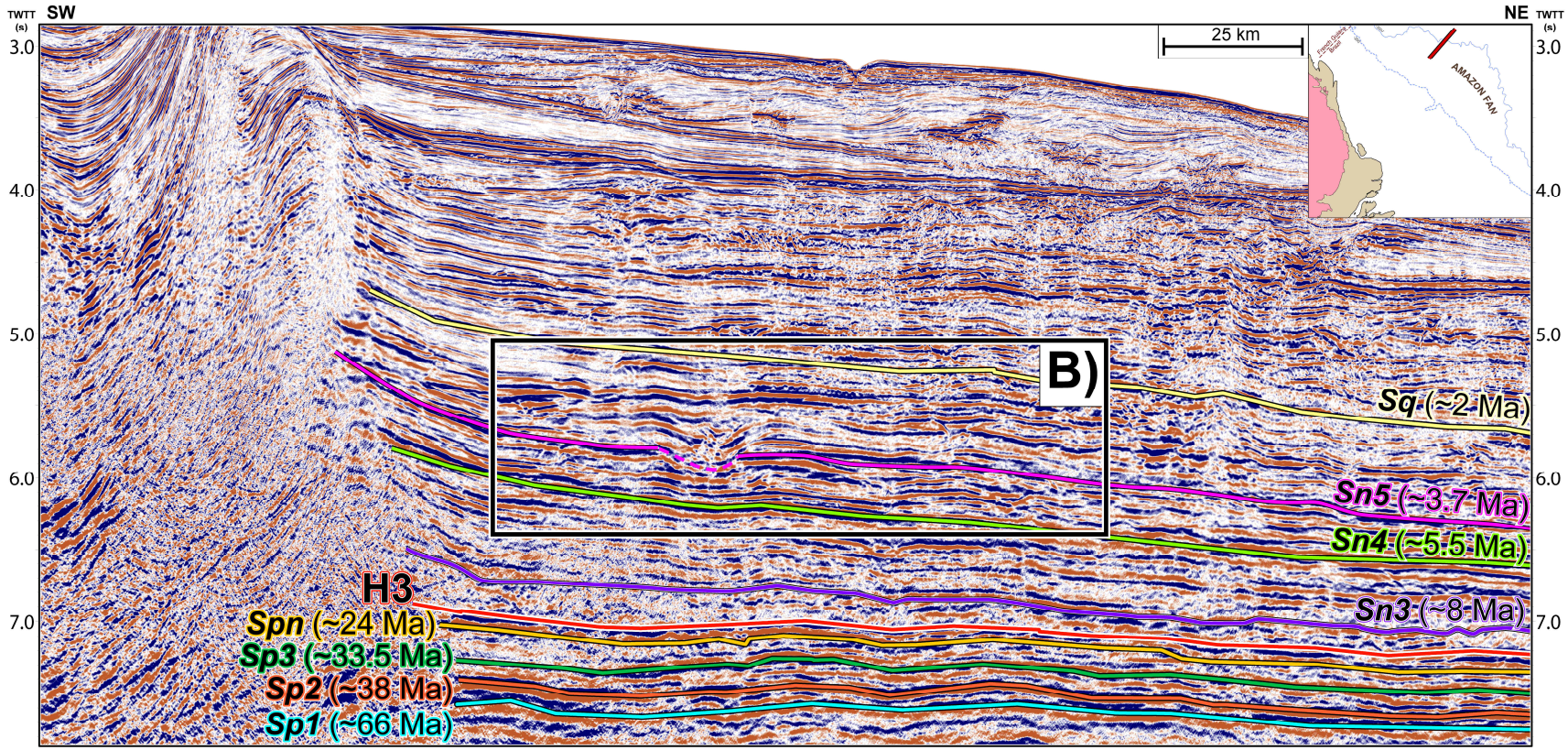

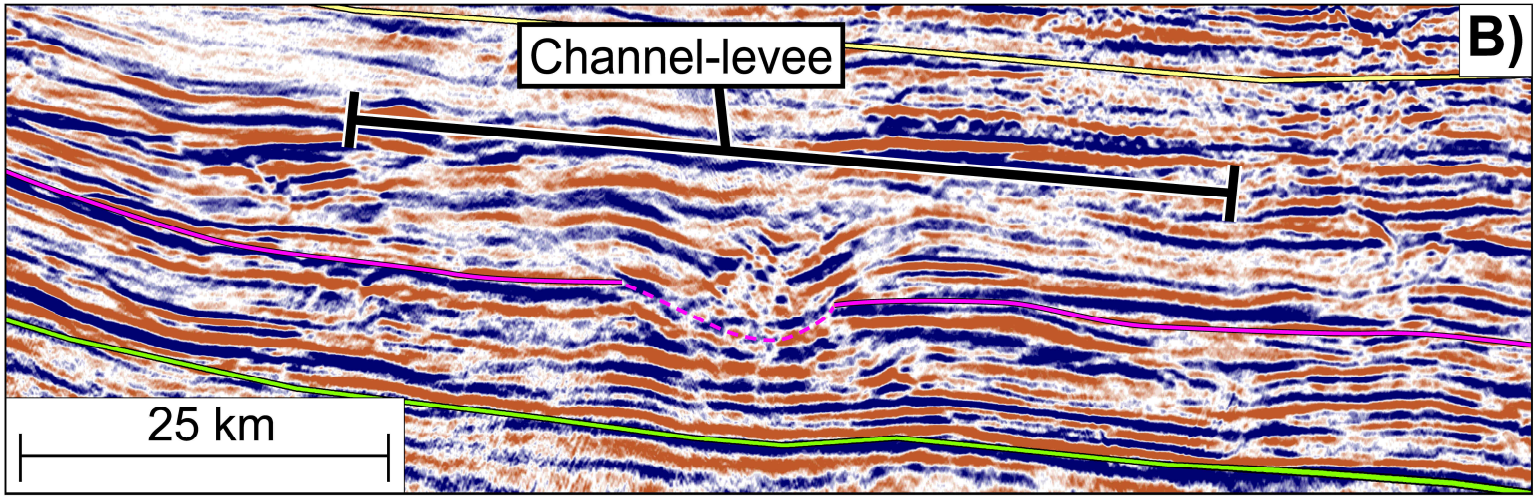

Figure VI-2: **A)** Interpreted seismic profile with main stratigraphic surfaces defined and dated in this thesis work (Chapters III and V). **B)** Zoom in of A showing a well-developed channel-levee system deposited immediately above surface Sn5 (ca. 3.7 Ma).

VI.1.2 Late Cretaceous astronomical age model

During the development if this thesis work, I focused most of the efforts in the investigation of the Cenozoic succession of the Offshore Amazon basin and avoided older strata as these deeply buried units lack detailed chronostratigraphic data and were not properly imaged in most of the available seismic data. To provide a reliable age model that could be used in future investigation, Dr. Slah Boulila and I co-advised a Master's internship aiming the development of a reliable chronostratigraphic framework for the Limoeiro Formation (first post-rift megasequence - Late Cretaceous). This work was carried out by MSc Célia Brange and I summarize here some of her most relevant findings and comment their possible implications.

The work was based on a recently acquired 3D reflection seismic data and including: three wells located at boundary between the Cassiporé and Araguari sub-basins (Figure VI-3), where the Limoeiro Formation is better imaged in seismic data and two wells (29 and 44) drilled this formation in its entirety. The age model was built taking into consideration cyclostratigraphic concepts and using the Multi-Taper method spectral analysis (Paillard *et al.*, 1996; Hinnov, 2013) applied to the gamma-ray logs of wells 29 and 44. This method allowed the recognition of cyclic variation on the gamma-ray logs that were compatible with Earth's orbital eccentricity cycles (4.7 and ~9 Myr) according to the La2010 orbital solution (Laskar *et al.*, 2011). This correlation, coupled with peaks in total organic carbon (TOC) recorded in well 29 (interpreted to be equivalent to the oceanic anoxic events - OAE) with well-known ages (Batenburg *et al.*, 2016; Friedrich *et al.*, 2012) allowed estimates of ages of each of the cycles defined via spectral analysis and their respective bounding stratigraphic surfaces.

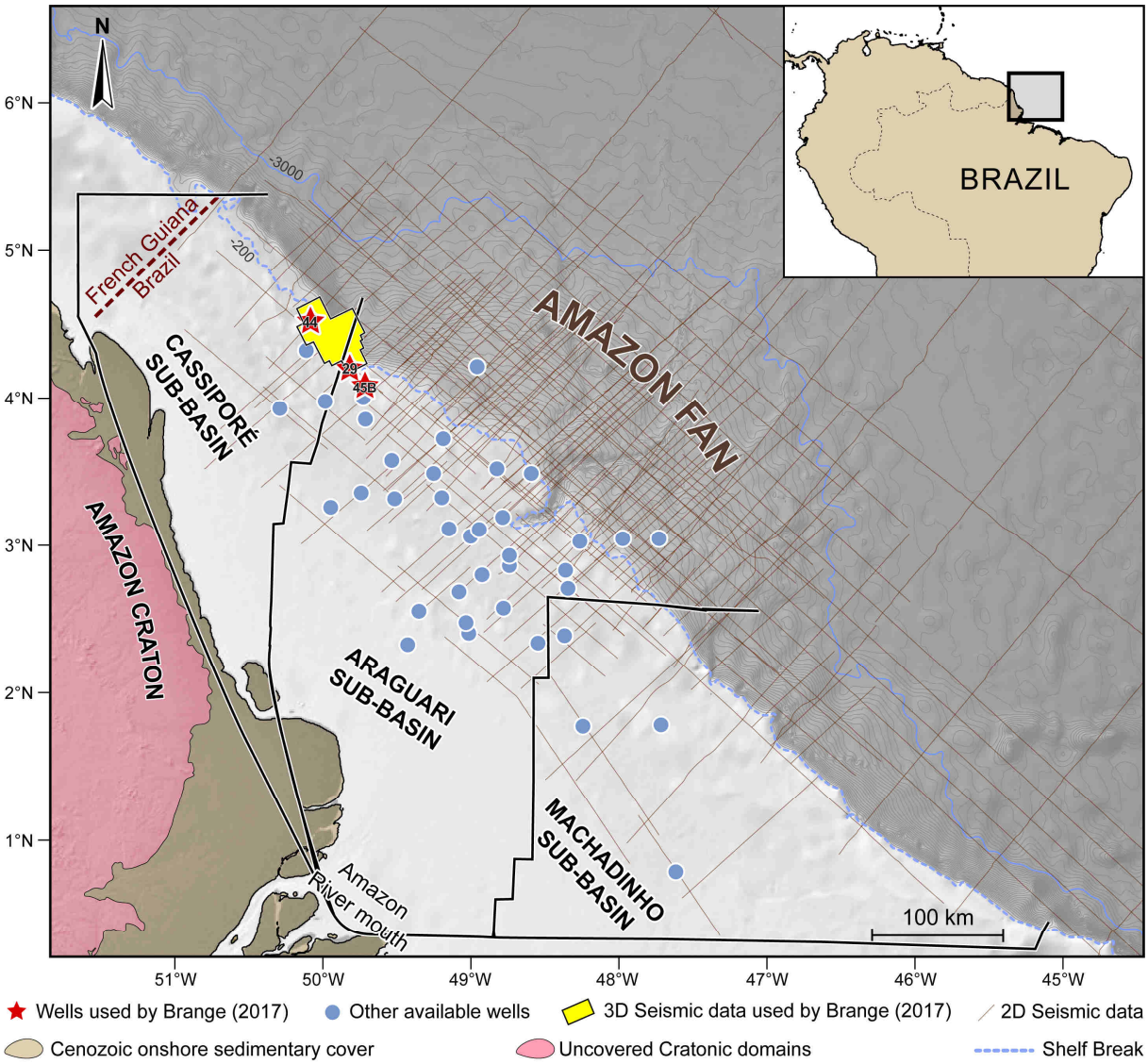

Figure VI-3: Map of the Offshore Amazon Basin and its sub-basins showing the dataset used by Brange (2017).

Thanks to this cyclostratigraphic analysis, ages were assigned to a series of stratigraphic levels within the Limoeiro Formation that were interpreted in seismic profiles as sequence boundaries or maximum flooding surfaces according to their architectural configuration (Figure VI-4: Figure VI-4). Among these surfaces identified by Brange (2017), the following surfaces have more relevance to the present work:

- The base of the Limoeiro Formation was dated as ca. 101-100 Ma and interpreted as a major maximum flooding surface that coincides with a major highstand according to Haq (2014) and the OAE 1d (Friedrich *et al.*, 2012). The ca. 101-100 Ma age assigned by Brange (2017) to this surface is slightly more recent than previously reported by Figueiredo *et al.* (2007) (ca. 102 Ma).

- Surface **SB 1** (Figure VI-4) was interpreted as a major sequence boundary and identified as being equivalent to the OAE 2 based on a major TOC peak in well 29, and thus dated as 94.17 Ma in accordance to Batenburg *et al.* (2016). This major erosive surface is correlated with a minor lowstand in the sea level curve by Haq (2014).
- Surface **MFS 5** (Figure VI-4) was interpreted as a major maximum flooding surface and dated as 81 Ma. This major maximum flooding surface is not well correlated with the sea level curve by Haq (2014) as it depicts a global lowstand at 81 Ma, although this lowstand is classified as "not yet confirmed".
- The top of Limoeiro Formation was dated as 66.47-66.65 Ma and interpreted as a major flooding surface that is also not well correlated with the sea level curve by Haq (2014). It is interesting to note that the age assigned by Brange (2017) to the transition from siliciclastic sedimentation (Limoeiro Formation) to mixed siliciclastic-carbonate sedimentation (Marajó and Amapá formations) is very close to the ca. 66 Ma age attributed based on fossiliferous data for the same surface, thus validating these independent methods. Taking into consideration both methods, an age between ca. 66-66.6 Ma could be assigned to the top of Limoeiro Formation, which is about 5 My older than previously reported by Figueiredo *et al.* (2007) (ca. 61 Ma).

The study carried out by Brange (2017) provides some insights on the stratigraphic record of the first post-rift megasequence of the Offshore Amazon Basin, which is one of its least explored depositional intervals. Most interesting to the present work is the fact that two of the major flooding episodes during Late Cretaceous identified by Brange (2017) (at 81 Ma and ~66.5 Ma) were not correlated to global eustatic rises in the sea level curve by Haq (2014). Thus, it is possible that these two major flooding episodes were caused by relative sea level rise during periods of intense subsidence (crustal cooling?). If such episodes of intense subsidence also occurred in the Araguari and Machadinho sub-basins and affected distal domains of the Amazon margin more intensely than proximal domains, this may have promoted the Late Cretaceous gravity-driven deformation described in Chapter V by tilting the basal *décollement* level and favoring gravity gliding. Furthermore, the base of Limoeiro Formation (ca. 100 Ma) and SB 1 (94.17 Ma) are both rich in organic matter (Brange, 2017) and may have acted as the source rocks that were said to have generated the hydrocarbon that would be necessary to promoted fluid overpressure and activate the second décollement level (Cobbold *et al.*, 2004). So far, these assumptions could not be tested due to the above mentioned limitations on seismic imaging over the deeply buried Limoeiro Formation in the Araguari and Machadinho sub-

basins, but it would be interesting to do so as soon as better quality seismic data became available in the future. Furthermore, the study conducted by Brange (2017) has proven the usefulness of cyclostratigraphic based on spectral analysis as her proposed age model was proven reliable by correlation with chronostratigraphic data and is currently being used on more detailed studies focused in the Araguari sub-basin.

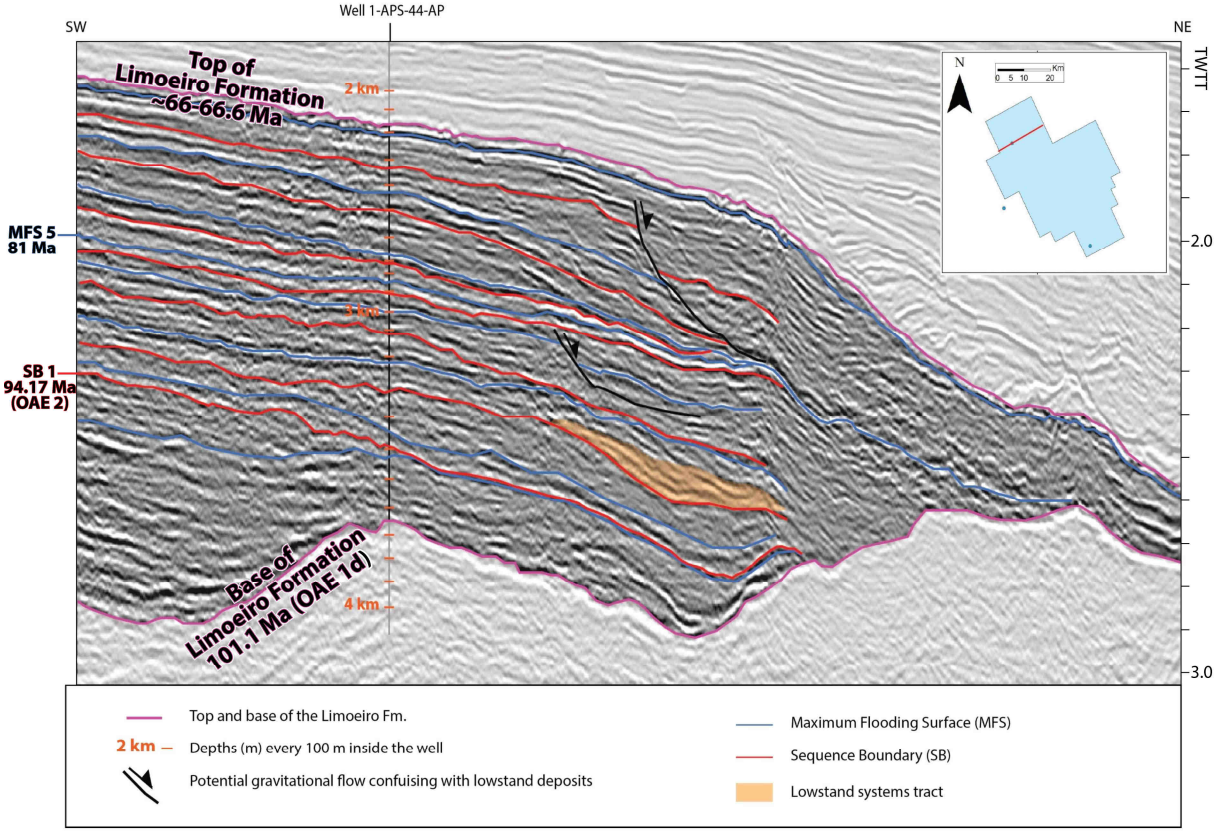

Figure VI-4: Interpreted seismic profile (inline) from 3D seismic bloc located in the Cassiporé sub-basin showing the sequence boundaries and maximum flooding surfaces identified by Brange (2017). Names and ages of the stratigraphic surfaces were attributed by Brange (2017). Figure modified from Brange (2017).

VI.1.3 Proposed Stratigraphic chart of the Offshore Amazon basin

The results and conclusions of this thesis work, coupled with the findings of other works from our research group (Reis *et al.*, 2016; Brange, 2017; Gorini *et al.*, 2014; Albuquerque, 2009) allowed a revision and further detailing of previous stratigraphic charts (Schaller *et al.*, 1971; Brandão and Feijó, 1994; Figueiredo *et al.*, 2007) in order to propose new stratigraphic charts for the Offshore Amazon Basin (Figure VI-5). I propose three different stratigraphic charts, one for each of the sub-basins defined in Chapter IV (Cassiporé, Araguari and Machadinho), in order to better represent the stratigraphic record of the Offshore Amazon Basin.

The main improvement of these stratigraphic charts in comparison to the last proposed stratigraphic chart (Figueiredo *et al.*, 2007) is the representation of the highly variable Neogene stratigraphic record among the Cassiporé, Araguari and Machadinho sub-basins as described by in Chapter III. The most notable Neogene stratigraphic variations among these sub-basins concerns the spatial distribution of shelfal carbonates (Amapá Formation) and the age in which carbonate production was interrupted (ca. 8 Ma in the Araguari and Machadinho sub-basins and ca. 3.7 Ma in the Cassiporé sub-basin). In the Plio-Quaternary succession, the stratigraphic charts presents 4th order cycles as reported by Gorini *et al.* (2014), large mass transport deposits in the Cassiporé and Machadinho sub-basins as reported by Reis *et al.* (2016). The stratigraphic charts also illustrates large deep-basin channelized sand-rich deposits occurring since 3.7 Ma according to the model of turbidites deposition on the Amazon Fan provided by Albuquerque (2009) and dated using the age model developed during this thesis work (see sub-section VI.1.1).

As a detailed analysis (similar to that presented in Chapter III) aiming the Paleogene succession of the Offshore Amazon Basin has not yet been done, the Paleogene part of the stratigraphic chart by Brandão and Feijó (1994) was recalibrated according to the age model presented in Chapter V and used in the stratigraphic charts presented in Figure VI-5. Such recalibration of the stratigraphic chart by Brandão and Feijó (1994) was done in such a way that the two major Paleogene sequence boundaries depicted by these author were positioned at the ages of surfaces *Sp2* and *Sp4* (major sequence boundaries at 38 and 28 Ma, respectively) and the base of the mixed siliciclastic-carbonate succession (Marajó and Amapá formations) was positioned at 66 Ma. The Paleogene part of the stratigraphic chart by Brandão and Feijó (1994) was favored over that of Figueiredo *et al.* (2007) as the former seems to better represent the

carbonate rich content of shelfal strata underlying surface *Spn* (approximate Paleogene-Neogene boundary, see Figure III-3). In any case, it is very likely that the Paleogene stratigraphic distribution varies significantly along the sub-basins of the Offshore Amazon Basin and more detailed Paleogene stratigraphic charts for each sub-basin should be added to the charts here presented in the future.

The Upper Cretaceous post-rift megasequence (Limoeiro Formation), Lower Cretaceous sys-rift megasequence (Cassiporé and Codó formations) and Triassic-Jurassic pre-rift megasequence (Calçoene Formation) are presented in Figure VI-5 as they were depicted by Figueiredo *et al.* (2007) with minor modifications. The Late Cretaceous cycles identified by Figueiredo *et al.* (2007) were recalibrated according to the age model proposed by Brange (2017) (see sub-section VI.1.2), which reduced the depositional time span of the Limoeiro Formation in about 6 Ma. The pre-rift Calçoene Formation was described by Figueiredo *et al.* (2007) only in NW margin (Cassiporé sub-basin) and illustrated as being removed by erosion over structural highs. However, it is here illustrated as being possibly preserved everywhere in the Araguari and Machadinho sub-basins due to higher subsidence rates. It is also very likely that all these formations (Limoeiro, Cassiporé, Codó and Calçoene) have different spatial distributions in the sub-basins of the Offshore Amazon Basin, but a detailed investigation about these formations on the Araguari and Machadinho sub-basins will not be possible until much better quality seismic data become available.

Speculative Paleozoic megasequences were also added to the stratigraphic charts of the Araguari and Machadinho sub-basins based on the assumption that sedimentary successions coeval to the Paleozoic strata found in surrounding basins and African conjugated margin (Behrendt and Wotorson, 1974; Tysdal and Thorman, 1983; Zalán and Matsuda, 2007; Soares *et al.*, 2007) may also be present in the Offshore Amazon Basin (Figure VI-5). A more detailed discussion on the possible existence of Paleozoic strata on the Offshore Amazon Basin may be found in Chapter IV. The hypothetical Paleozoic megasequence depicted in the Machadinho sub-basin (Figure VI-5) is based on the Devonian Itaim, Pimenteiras and Cabeças formations reported by Junior *et al.* (2007) and Soares *et al.* (2007) as occurring in the Barreirinhas and Pará-Maranhão basins located southeastward of the Machadinho sub-basin. In the Araguari sub-basin, in addition to the hypothetical Devonian megasequence, Figure VI-5 also illustrates the presence of a possible Ordovician-Silurian megasequence based on the Manacapuru, Pitinga and Nhamundá/Autás-Mirim formations previously reported to be present in the Marajó Basin

southwestward of the Araguari sub-basin. The presumed extension of all these Paleozoic formations into the Offshore Amazon Basin is not supported by any kind of data available for the present work and must be taken as highly speculative. However, geographical correlations support that hypothesis as no structural barrier has been ever reported to separate the regions known to contain these Paleozoic megasequences and the Araguari and Machadinho sub-basins, thus it would be interesting to verify if such speculations are correct when better deep penetrating data became available.

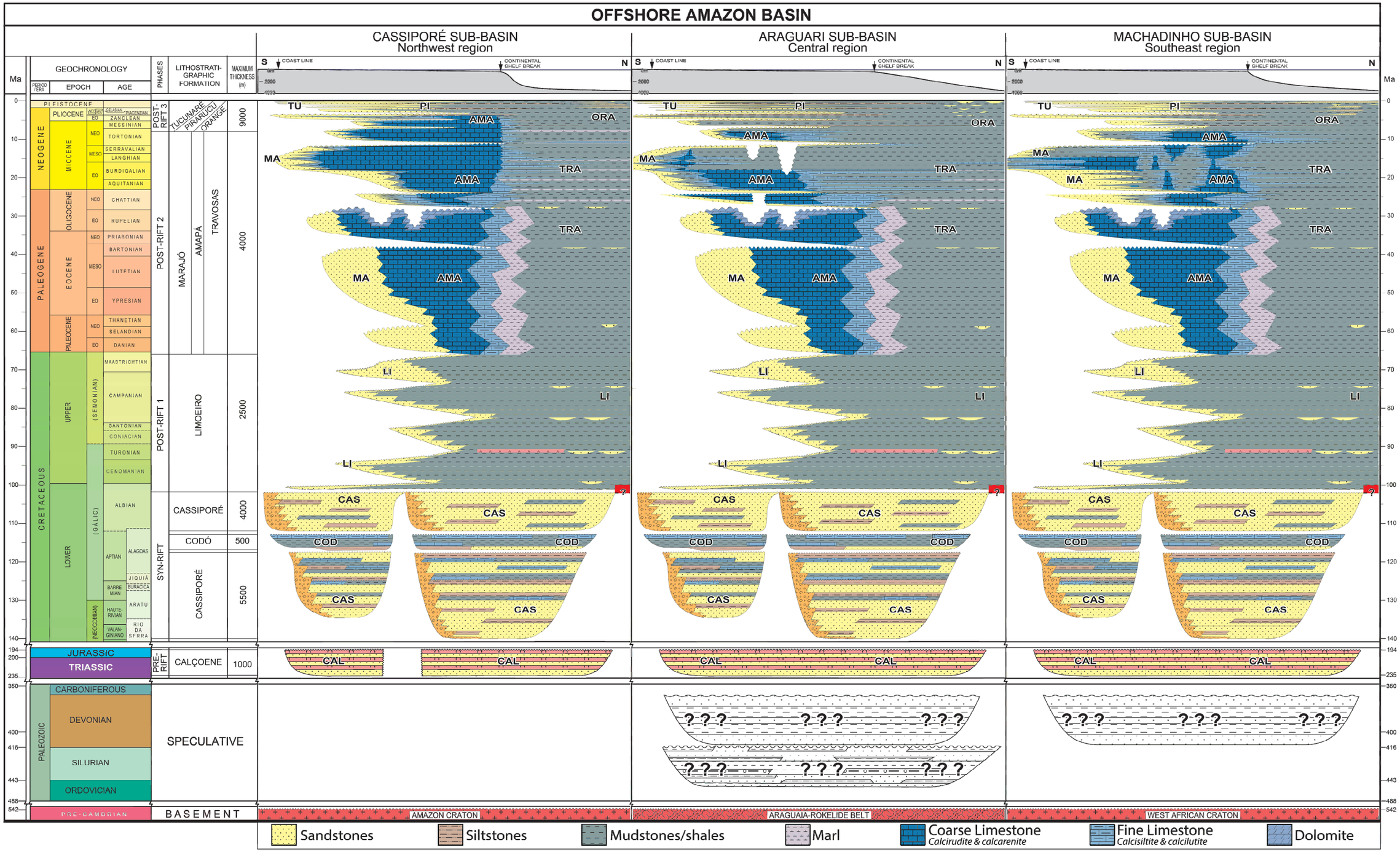

Figure VI-5: Stratigraphic charts of the three sub-basins of the Offshore Amazon Basin defined in this thesis work (Chapter IV). Late Pliocene-Quaternary based on Albuquerque (2009), Gorini *et al.* (2014) and Reis *et al.* (2016). Latest Oligocene to Early Pliocene based on Cruz *et al.* (CHAPTER III). Paleocene to Oligocene based on Brandão and Feijó (1994) recalibrated according to age model presented in Chapter V. Late Cretaceous to Triassic based on Figueiredo *et al.* (2007) and age recalibration according to Brange (2017). Basement and possible Paleozoic megasequences based on structural analysis and geographical correlation presented and discussed in Chapter IV.

VI.2 THE OFFSHORE AMAZON BASIN IN A REGIONAL CONTEXT

In this section, the results presented in this thesis are tentatively correlated with events at a regional or global scale reported by published studies undertaken beyond the Offshore Amazon Basin region. Figure VI-6 shows a compilation of important geological and paleoclimate events reported in the literature, plotted alongside with sedimentation rates for the Amazon shelf and the Ceará Rise and the major stratigraphic surfaces recognized in the Offshore Amazon Basin in the present study. The correlations proposed below are essentially based on the temporal coincidence between events within and outside the Offshore Amazon Basin, thus having a speculative nature. Nonetheless, these possible correlations between regional events and changing conditions in the Offshore Amazon Basin are here put forward in order to allow them to be tested by more detailed investigations in the future.

VI.2.1 Paleocene to early Late Miocene (units P1 to N3)

Form the Paleocene until the Middle Eocene (unit P1), sedimentation rates were relatively low in both the Amazon shelf and Ceará Rise regions and increased dramatically during the Late Eocene (unit P2). The increase in sedimentation rates (at ca. 38 Ma) took place close to the onset of intense Andean Orogeny (roughly between 40-30 Ma; Armijo *et al.*, 2015) and a major eustatic fall according to Haq *et al.* (1987) sea-level curve (Figure VI-6). As it is generally accepted that at this time there was no trans-continental drainage connection between the Andes and the Atlantic Ocean, a direct correlation between orogenic events and increasing offshore sedimentation rates seems unlikely. Nonetheless, it could be hypothesized that processes indirectly related to the Andean Orogeny, such as dynamic topography due to upper mantle convection leading to differential vertical movements of continental scale, as proposed for more recent phases of intense Andean Orogeny (Shephard *et al.*, 2010), had an effect on sediment influx into the Offshore Amazon Basin. However, it seems more reasonable to assume that the increase in sedimentation rates in the Offshore Amazon basin and associated shelfal progradation (see CHAPTER V) were mostly related to the pronounced sea-level fall during the earliest Late Eocene (Figure VI-6; Haq *et al.*, 1987).

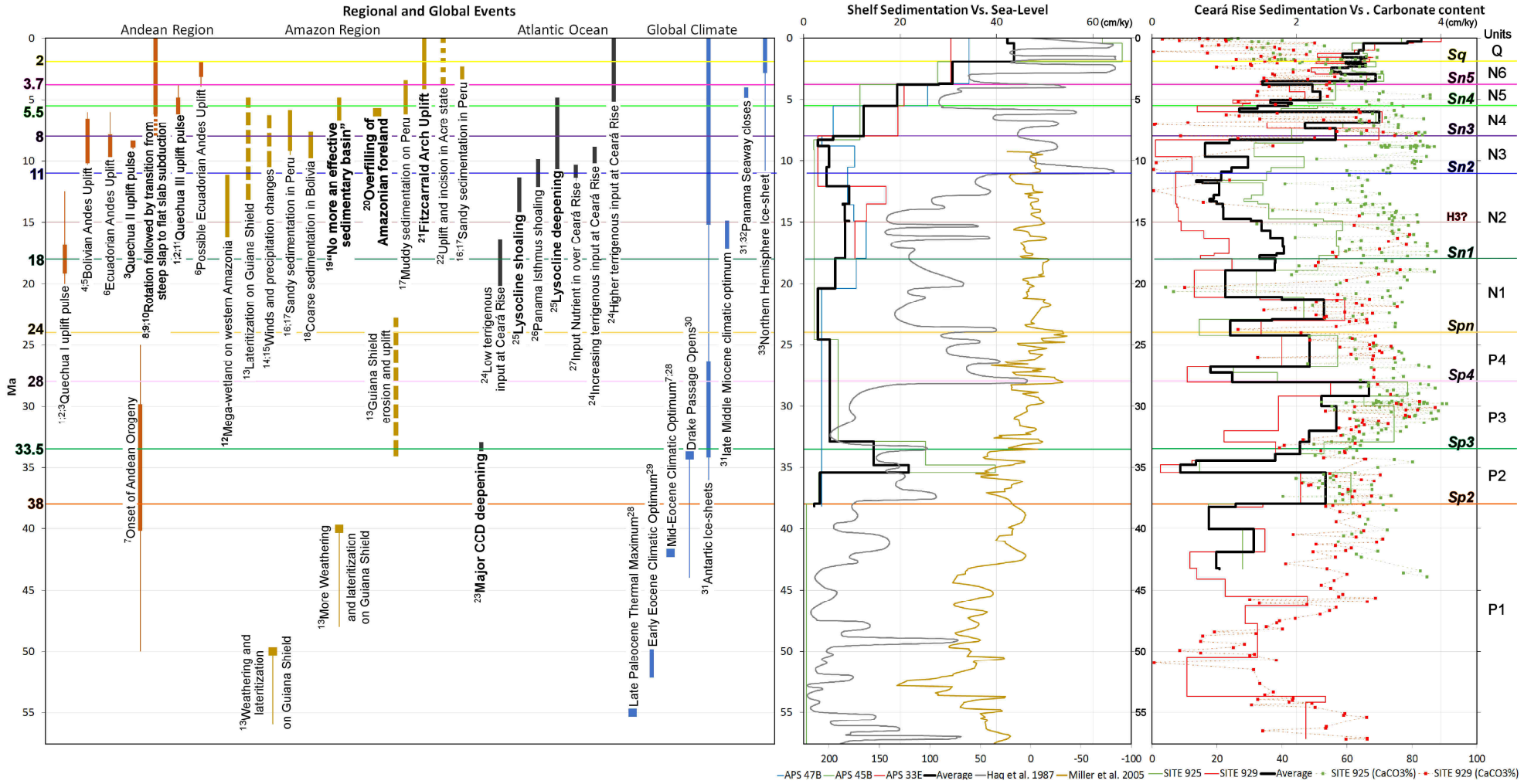

Figure VI-6: Compilation of geological and paleoclimate events reported in the literature alongside the major stratigraphic surfaces in the Offshore Amazon Basin defined in this thesis. Sedimentation rates in the Amazon shelf are plotted together with sea-level curves from Haq *et al.* (1987) and Miller *et al.* (2005). Sedimentation rates in the Ceará Rise region are plotted together with carbonate content at Sites 925 and 929 as measured on core samples by ODP Leg 154 Shipboard Scientific Party (Curry *et al.*, 1995). References: 1) Megard (1984); 2) Noble *et al.*(1990); 3) Wise *et al.* (2008); 4) Ghosh *et al.* (2006); 5) Garzione *et al.* (2008); 6) Steinmann *et al.* (1999); 7) Armijo *et al.* (2015) 8) Rousse *et al.* (2002); 9) Gutscher *et al.* (2000); 10) Espurt *et al.* (2008); 11) Harris and Mix (2002); 12) Hoorn *et al.* (2010); 13) Théveniaut and Freyssinet (2002); 14) Poulsen *et al.* (2010); 15) Insel *et al.* (2010); 16) Campbell *et al.* (2006); 17) Campbell *et al.* (2010); 18) Strub *et al.* (2005); 19) Latrubesse *et al.* (2010); 20) Roddaz *et al.* (2010); 21) Espurt *et al.* (2010) ; 22) Westaway (2006); 23) Liu *et al.* (2004); 24) Dobson *et al.* (2001); 25) King *et al.* (1997); 26) Newkirk and Martin (2009); 27) Heinrich and Zonneveld (2013); 28) Zachos *et al.* (2008); 29) Zachos *et al.* (2001a); 30) Haug *et al.* (2004); 31) Zachos *et al.* (2001b); 32) Haug *et al.* (2001); 33) Thiede *et al.* (1998).

There seems to be some temporal coincidence between the major phases of post-rift subsidence in the Offshore Amazon Basin and phases of Andean Orogeny during the Neogene. After a long period of relative tectonic quiescence during the Late Oligocene and earliest Miocene (McKee and Noble, 1990; Sébrier and Soler, 1991), two phases of compressional deformation on the Central Andes seem to be associated with the beginning and end of the pre-Fan intense subsidence phase between ca. 18−8 Ma (as defined in Chapter III). According to Steinmann *et al.* (1999) a major compressional event took place around 18 Ma in the Ecuadorian Andes while Noble *et al.* (1990) and Wise *et al.* (2008) assigned ages around 19 Ma and 17 Ma, respectively, to the so-called Quechua I tectonic event in the Peruvian Andes (Figure VI-6). Steinmann *et al.* (1999) also described a later phase of regional compressive deformation in the Ecuadorian Andes between 9.5 and 6 Ma at a decreasing rate with inferred maximum tectonic activity from 9 to 8 Ma (Figure VI-6). Accordingly, Wise *et al.* (2008) assigned an age around 8.7 Ma for the Quechua II compressive event the Peruvian Andes (Figure VI-6).

Furthermore, major transitions on the Nazca plate subduction direction and dipping angle under the Ecuadorian-Peruvian Andes are also coincident with the end of the intense pre-Fan subsidence phase in the Offshore Amazon Basin. According to Rousse *et al.* (2002), strata in the Peruvian Andes underwent rapid uplift and significant rotation at ca. 8 Ma, when subduction possibly "froze and the entirety of Nazca–South American plate convergence was accommodated by shortening in the continent", about the same time that the Offshore Amazon basin experience a major reduction in subsidence rates (Chapter III). Then, around 7 Ma, on the Nazca-South American convergence system, a formerly Steep slap subduction under the Peruvian Andes had been already reconfigured into a low angle Flat slap subduction (Espurt *et al.*, 2008; Figure VI-7). Thus, it seems that around 8-7 Ma the northern South America went through a pivotal point in its geodynamic history that may have changed the geodynamic behavior of the entire region.

Any correlation between Andean Orogeny and subsidence on the Offshore Amazon Basin based only on temporal coincidence between events must be taken as a speculative hypothesis. That said, I suppose that large scale tectonic deformational mechanisms such as long wavelength flexural lithospheric deformation and/or dynamic topography due to mantle convection may have indeed affected northern South America region (from the Andes to the Offshore Amazon Basin). Long wavelength lithospheric deformation and dynamic topography in response to intensification of Andean Orogeny and related plate subduction along western South America have been proposed by Shephard *et al.* (2010) and Sacek (2014), respectively,

to have affected the western Amazonian sedimentary basins and promoted the paleo-Amazon River transcontinentalization. I assume that both tectonic deformational mechanisms may also have affected the eastern Amazonia, although less intensely than what these authors have reported to have taken place in western Amazonia. As such, it may be the case that tectonic events Quechua I and II indirectly caused the acceleration of subsidence in the Offshore Amazon Basin from ~18 Ma until ~8 Ma when a dramatic change in the geodynamic regime of northern South America reduced subsidence abruptly in the Offshore Amazon Basin (Figure VI-7).

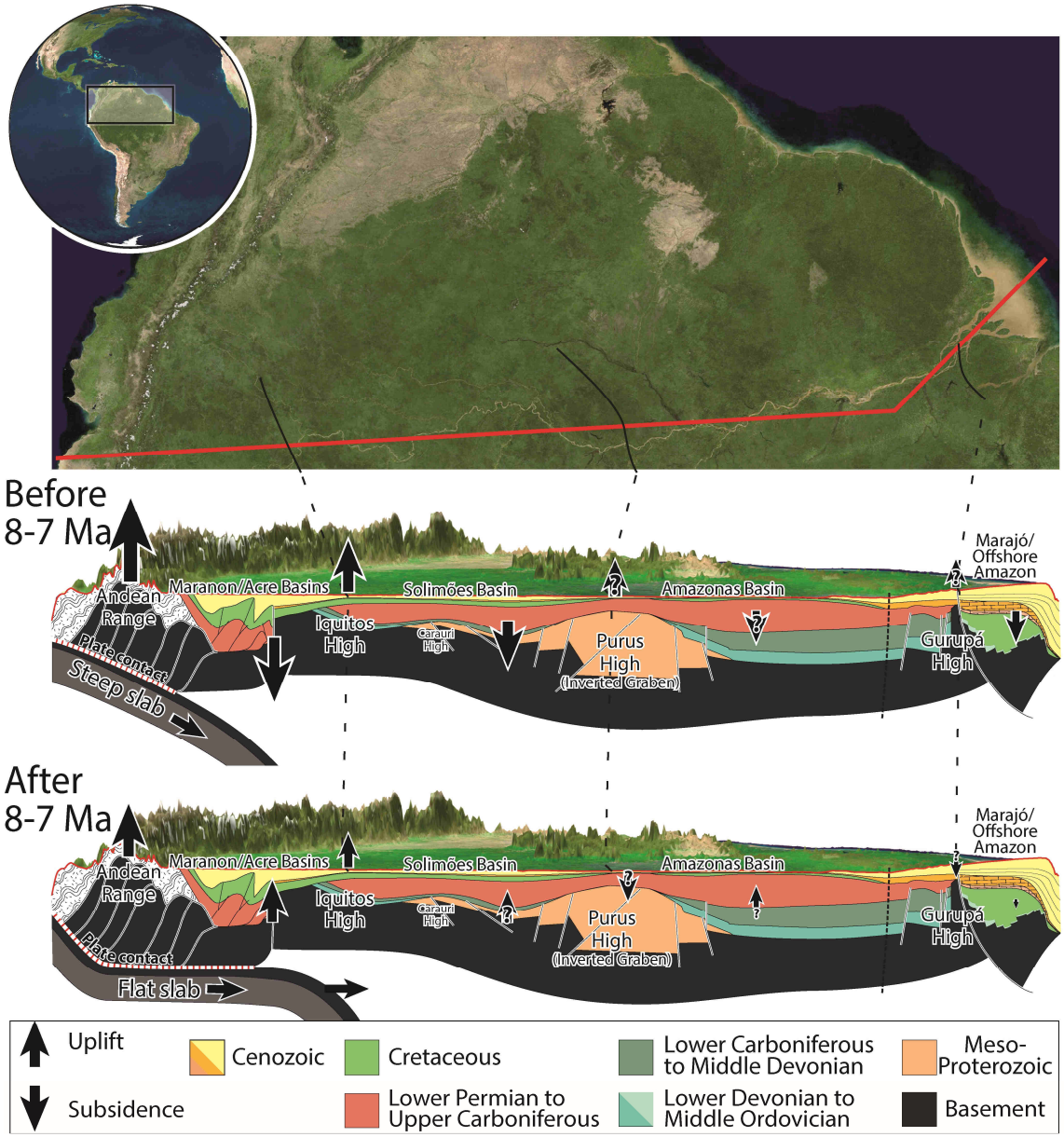

Figure VI-7: Conceptual section through northern South America illustrating possible changes in uplift and subsidence trends due to a major change in the geodynamics regime of northern South America around 8-7 Ma, when the major Andean Orogeny phase ended abruptly and subduction under the Central Andes was reconfigured from steep slab into a low angle flat slap (Rousse *et al.*, 2002; Espurt *et al.*, 2008). Andean subduction zone modified from Espurt *et al.* (2008). Schematic section of the Maranon, Acre, Solimões, Amazon and Marajó basins modified from Caputo and Soares (2016). Not to scale.

VI.2.2 Origin of the sediment arriving to the Amazon margin between ca. 8 Ma and 5.5 Ma (unit N4)

At ca. 8 (surface *Sn3*) shelfal carbonate production in the Araguari and Machadinho sub-basins was interrupted (Chapter III) due to a considerable increase in sediment influx into the Offshore Amazon Basin (Figure VI-6). It is interesting to note that our new age model points to a temporal offset between phases of increasing sediment influx into the Offshore Amazon Basin and phases of Andean Orogeny. The arrival of terrigenous sediments in volumes high enough to suppress carbonate production in the Offshore Amazon Basin occurred at least 2 Ma after the beginning of the main phase of Andean Orogeny around 10 Ma (Steinmann *et al.*, 1999; Garzione *et al.*, 2008; Figure VI-6). Furthermore, shelfal carbonate production was widespread in the Offshore Amazon Basin until at least 400 ky after the end of so-called Quechua II uplift phase in the Central Andes (considering ages defined by Wise *et al.*, 2008). As such, it seems that the period of most intense Andean Orogeny predates the transition from predominantly carbonate to clastic sedimentation in most of the Offshore Amazon Basin, in contrast to the to the almost immediate effect of Andean Orogeny in sediment influx into the Offshore Amazon Basin suggested by some authors (e.g. Figueiredo *et al.*, 2009; Hoorn *et al.*, 2010). Therefore, two conflicting hypotheses could be put forward regarding the increase of terrigenous sediments influx that suppressed the carbonate production in the Araguari and Machadinho sub-basins: (1) there was some sort of transcontinental drainage system connecting western and eastern Amazonia during the Late Miocene, but some processes acting over western Amazonia delayed the arrival of Andean-derived sediments into the Offshore Amazon Basin; or (2) there was no transcontinental drainage system connecting western and eastern Amazonia during the Late Miocene and the terrigenous sediments that suppressed the shelfal carbonate production in the Offshore Amazon Basin were not derived from the Andes.

The first hypotheses assumes that the massive arrival of terrigenous sediments in the Offshore Amazon Basin at ca. 8 Ma is related to the onset of an Amazon transcontinental drainage system (as supported by Figueiredo *et al.*, 2009 and Hoorn *et al.*, 2010), although there would be an offset between this transcontinentalization event and the main phase of Andean Orogeny. It seems to me that the only likely reason for a delayed transcontinental Amazon River onset would be forebulge dynamics as described by Roddaz *et al.* (2005a) and Roddaz *et al.* (2011) for western Amazonia following to the model proposed by Catuneanu (2004) for the propagation of crustal deformation along retroarc foreland systems. According to this geodynamical model "renewed thrusting in the orogenic belt results in foredeep subsidence and

forebulge uplift, and the reverse occurs as orogenic load is removed by erosion or extension" (Catuneanu, 2004; Figure VI-8). Roddaz *et al.* (2011) stated that ongoing thrust-tectonic loading of the Eastern Cordillera and sub-Andean zone and the onset of the main phase of Andean surface uplift during the Late Miocene induced enhanced flexural subsidence in the foredeep depozones of the entire Amazonian foreland basin from Colombia to Bolivia. Still according to these authors, valley incisions and full relief development in the hinterland since Late Miocene provided increased sediment supply the Amazonian foreland basin encompassing the Ecuadorian, Peruvian and Bolivian Amazonian foreland basins that eventually passed from a "filled" to an "overfilled" phase around 6 Ma (Roddaz *et al.* 2011; Figure VI-6). During the same time, ongoing forebulge uplift created barriers that divided the foredeep and backbulge regions until overfilling of the foreland basin was responsible for burying of the forebulge that would, nevertheless, still be uplifted and incised by modern Amazon drainage until recent (Roddaz *et al.*, 2005a; Roddaz *et al.*, 2005b).

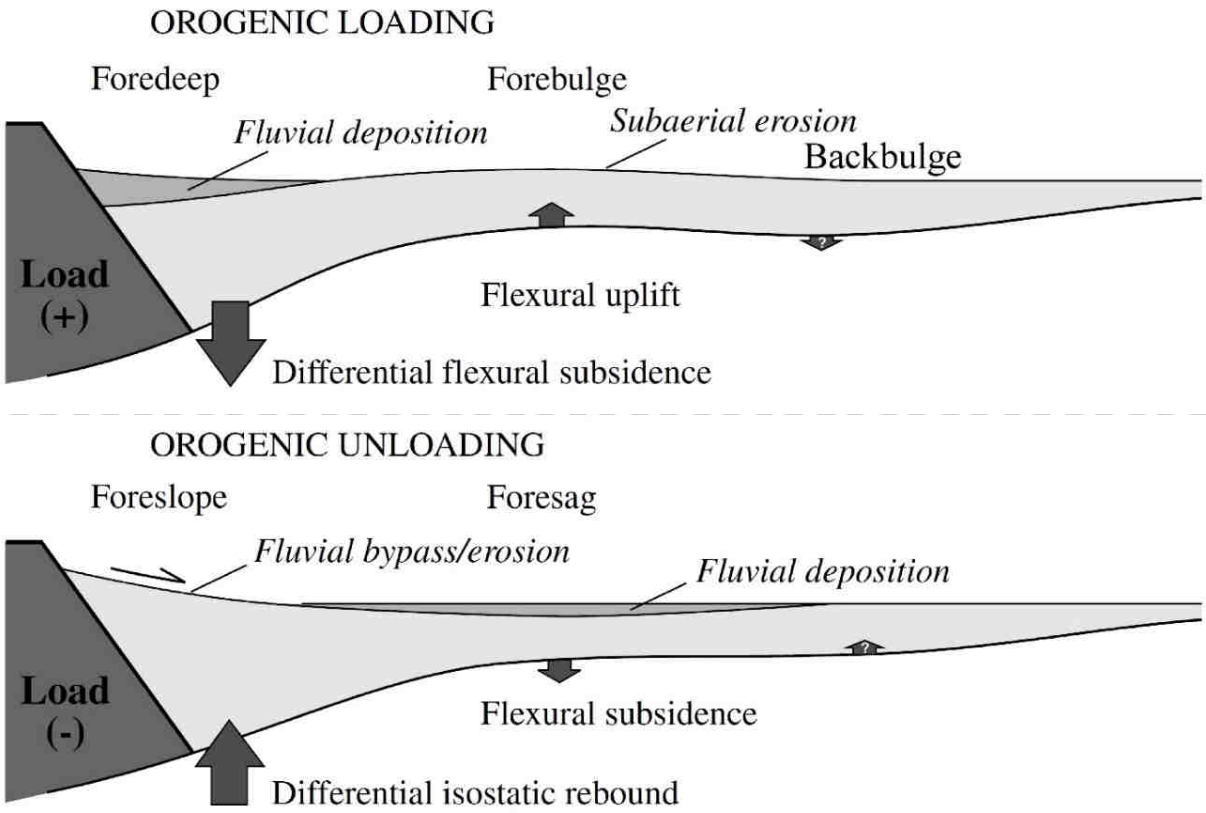

Figure VI-8: Orogenic loading and unloading stages and the associated depozones in the foreland basin. + and − refer to increase and decrease of orogenic load, respectively. Modified from Catuneanu (2004) and Roddaz *et al.* (2011).

Therefore, it is possible that Andean sourced sediments were being trapped in the foredeep and backbulge regions during periods of Andean orogeny and only some hundreds of thousands of years after the end of the intense Quechua II tectonic event in Peruvian Andes. Around 8 Ma, sediment influx may have finally surpassed the accommodation space created in western Amazonia (foredeep and backbulge), finally allowing the onset of transcontinental drainage system and greater volumes of sediments eastward to the Atlantic. In that sense, it is possible to imagine that the ~6 Ma age pointed by Roddaz *et al.* (2011) represents the moment when denudation surpassed orogenic loading in the Andes and the vertical movements were reversed in the foreland region. If that was so, an even larger amount of sediments would then be supplied to the recently stablished transcontinental Amazon River when the foredeep and possibly backbulge regions began to be uplifted by isostatic rebound (Figure VI-8). This all would fit very well with the Latrubesse *et al.* (2010) statement that "during the end of the Miocene and the early Pliocene (~6.5 Ma to 5 Ma), the southwestern Brazilian Amazonia ceased to be an effective sedimentary basin and instead became an erosional area that contributed sediments to the Amazon fluvial system". The hypothetical onset of transcontinental drainage system burying the carbonate platform is further supported by Harris and Mix (2002) who reported a marked change around 8.0 Ma in sediment chemistry at the Ceará Rise that "point to a stronger highland source of physical weathering". Furthermore, sedimentation rates at the Ceará Rise peaked around 6 Ma (Figure VI-6), thus also supporting the interpretation that a recently established transcontinental Amazon River gradually increased its sedimentary load from 8 Ma to 6 Ma.

On the other hand, the temporal offset between the major phase of Andean orogeny (8.85-8.55 Ma - Quechua II event; Wise *et al.*, 2008) and the arrival of large volumes of terrigenous sediments in the Offshore Amazon Basin (ca. 8 Ma; Figure VI-6) could also be interpreted as a supporting evidence for the hypothesis of a Pliocene onset of the transcontinental Amazon River (as advocated by Latrubesse *et al.*, 2007 and Gross *et al.*, 2011). It may be the case that the increasing in sediment influx into the Offshore Amazon Basin was essentially caused by an abrupt reduction in accommodation space creation over the Equatorial Atlantic coastal and innermost shelf regions (as speculated in Chapter III) in response to a dramatic change in the geodynamic regime of northern South America at ca. 8 Ma (as discussed in the previous sub-section). If so, there may have been no direct cause-effect relation between Andean orogeny and sedimentation rates on the Offshore Amazon Basin during the Late Miocene as advocated by several authors (Figueiredo *et al.*, 2009; Hoorn *et al.*, 2010; Dobson *et al.*, 2001). There would be instead an indirect effect of cessation (instead of intensification) of Andean Orogeny

(Rousse *et al.*, 2002) and transition from steep slab to flat slab plate subduction under the Peruvian Andes (Espurt *et al.*, 2008) over sediment influx into the Equatorial Atlantic.

Additionally, a possible uplift of the Amazon Craton may also have been partially responsible for the increasing sediment influx into the Offshore Amazon Basin since the Late Miocene. Théveniaut and Freyssinet (2002) reported an uplift of ca. 200 m since 10 Ma in the Kaw Mountain region (French Guiana), although it is unknown how much of this uplifted occurred during the Late Miocene and how much postdates the Miocene. Nevertheless, if a long term uplift of a few mm/ky affected the Amazon Craton during the Late Miocene, it may have promoted erosion and riverine incision over eastern Amazonia that would result in even more sediments being transported to the Offshore Amazon Basin. Such hypothetical Late Miocene uplift finds some support in the work conducted by Dino *et al.* (2012) that identified Middle Miocene deposits in the intracratonic Amazonas Basin that are topped by a erosive surface and capped by Quaternary sediments, thus representing a Late Miocene-Pliocene hiatus. Dino *et al.* (2012) also considered the possibility that these Middle Miocene sedimentary records within the Amazonas Basin could be one of the source areas for sediments that were carried out in large volumes to the Offshore Amazon Basin. A Late Miocene uplift over the Amazon Craton would be contemporaneous with the abrupt reduction in the accommodation space creation over the Offshore Amazon basin and could be caused by the same change in the geodynamic regime of northern South America that I believe to have taken place around 8-7 Ma (Figure VI-7).

VI.2.3 From ca. 5.5 Ma to Recent – the maturation of the Amazon River

During the Plio-Quaternary, sedimentation rates continued to rise in the Offshore Amazon Basin shelf and began to rise again in the distal Ceará Rise region after a noticeable drop during the latest Miocene (Figure VI-6). The drop in sedimentation rates in the Ceará Rise region is probably related to a major eustatic rise during the latest Miocene-Early Pliocene (according to Haq *et al.*, 1987; Figure VI-6) that favored sediment storage over the shelf rather than sediment transfer to the deep basin. Still, the fact that sedimentation rates recorded on the shelf during the deposition of unit N5 (from ca. 5.5 to ca. 3.7 Ma) were higher than ever before suggests that the Amazon River continued to increase its sedimentary load during the Early Pliocene. Such Early Pliocene increase in sediment influx into the Offshore Amazon Basin was probably caused by the continuous eastward propagation of the Peruvian flat slab segment beneath the overriding South American plate favoring the thrusting and uplift in the foreland region (Espurt

et al., 2008; Figure VI-7) that would in turn promote erosion and provide more sediments to be carried by the Amazon River. This seems to fit well with the statement of Latrubesse *et al.* (2010) that during the latest Miocene and the Early Pliocene, the western Brazilian Amazonia became an erosional area that contributed sediments to the Amazon fluvial system. As such, it is easy to imagine that between the latest Miocene and the Early Pliocene the erosion of sediments previously deposed in western Amazonian basins began to be added to the sediments eroded directly form the Andean range, thus increasing the sedimentary load of the Amazon River. Such increase in sedimentary load of the Amazon Fan would be responsible to completely fill the embayment on the Amazon central shelf and completely bury the remaining carbonates on the NW shelf (Chapter III).

Around 4 Ma, the beginning of the uplift of the Fitzcarrald Arch, a ~400,000-km² feature in western Amazonia related to the subduction of the Nazca Ridge under the South American plate (Figure VI-9), promoted even more uplift and erosion over Peruvian foreland basins (Espurt *et al.*, 2010). It is very likely that the uplift of the Fitzcarrald Arch together with the continuous eastward propagation of the Peruvian flat slab segment beneath the overriding South American plate (Espurt *et al.*, 2008; Figure VI-7) progressively extended the areas of western Amazonia where riverine incision and erosion would act to provide sediments to be carried by the Amazon River. This continuous processes was most likely responsible for the continually increasing sedimentation rates recorded in the Offshore Amazon Basin and Ceará Rise (Figure VI-6). As such the modern Amazon River could be seen as the result of an ongoing evolution of a drainage system that constantly enlarge its area of sediment catchment.

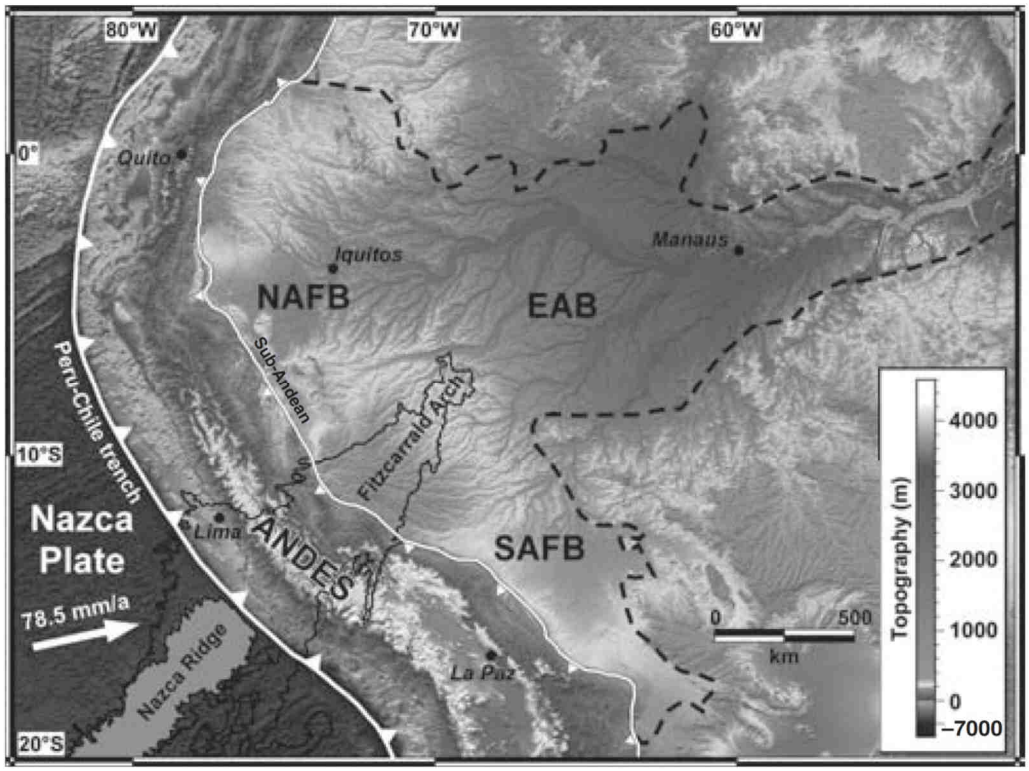

Figure VI-9: Geomorphic map of western South America showing the position of the Fitzcarrald Arch according to Espurt *et al.* (2010). The dashed black line shows the boundary of the Amazon River drainage basin.

CONCLUSIONS AND PERSPECTIVES

Conclusions and perspectives

The research developed during this PhD thesis provided a series of insights into the post-rift stratigraphic evolution of the Offshore Amazon Basin based on multidisciplinary studies supported by interpretations of seismic, well log, chronostratigraphic and geophysical potential field models data as well as on an extensive bibliographical revision. Main conclusions of this extensive research effort are:

- The Offshore Amazon Basin can be divided in terms of crustal framework and geodynamic behavior into three sub-basins that were named as Cassiporé sub-basin (NW margin), Araguari sub-basin (Central margin) and Machadinho sub-basin (SE margin). The Cassiporé sub-basin is underlain by faulted segments of the Paleoproterozoic Amazon Craton, composing a series of NW-SE oriented half-grabens. The Araguari sub-basin is underlain by the Neoproterozoic Araguaia-Rokelide suture zone, with N-S oriented normal faults composing a series of grabens and half-grabens. The Machadinho sub-basin is underlain by a portion of the Archean West African Craton that remained in South America after the Gondwanan breakup;

- Gravity-driven deformation affected the post-rift succession of the Machadinho and Araguari sub-basins during five main phases since the Late Cretaceous. During the Late Cretaceous (first phase) and between ca. 66-38 Ma (second phase) gravity-driven deformation was more intense in the Machadinho sub-basin, probably as a result of more accentuated across-margin differential subsidence that promoted the seaward tilting of a basal *décollement* level. A third phase of gravity-driven deformation took place in both sub-basins between ca. 28-24 Ma and was probably caused by sedimentary loading in the outer shelf-upper slope region. Gravity-driven deformation affected only the sedimentary succession in the Araguari sub-basin during the Neogene and was most likely caused by renewed across-margin differential subsidence between ca. 24-8 Ma (fourth phase) and by vertical collapse due to intense outer shelf-upper slope progradation and stacking of depositional units that represent the major depocenters of the Amazon Fan during the last 8 My (fifth phase);
    - During the Neogene, carbonate distribution and architectural styles in each sub-basin varied considerably in response to differential subsidence along the Amazon shelf. In the Araguari sub-basin, between ca. 24 and 8 Ma, more intense subsidence resulted in the development of a 150 km wide embayment as

bioconstructor organisms tended to migrate and build-up in more proximal and stable regions. Meanwhile, in the Cassiporé and Machadinho sub-basins, comparatively less intense subsidence allowed carbonate production to keep-up with accommodation space. Subsidence was greatly reduced in the Offshore Amazon basin around 8 Ma, which was at least partially responsible to promote an intense influx of terrigenous sediments that buried the carbonate dominated environments in the Araguari and Machadinho sub-basins. The large embayment in the Araguari sub-basin captured these sediments before they could reach the Cassiporé sub-basin until 3.7 Ma, when widespread carbonate production was finally suppressed everywhere in the Amazon shelf.

I was also able to conclude that:

- The base of the Amazon Fan is older than the top of the shelfal carbonate succession, thus not coeval or younger as have been previously reported (Figueiredo *et al.*, 2009; Hoorn *et al.*, 2017);
- Well-developed channel-levee systems began to form in the Amazon Fan just after 3.7 Ma, about the same time that sedimentation influx into the Offshore Amazon Basin increased significantly and the large embayment in the Araguari sub-basin was filled. This suggests a possible control of sediment influx and or/slope morphology in the turbidite deposits architecture;
- The Offshore Amazon Basin may have evolved in a broad geodynamic context, encompassing a large area of the northern South America from the Andean range to the Equatorial Atlantic Margin. Processes related to subduction, orogeny and mantle dynamics may have promoted phases of more or less intense subsidence or uplift across different regions on northern South America;

This last conclusion is based exclusively on temporal correlation between events reported in this thesis and by several works conducted across the northern South America and has a much more speculative character. At the present, modeling techniques would be the most practical way to test coherence of this and other hypotheses presented in section VI.2. In the future, it would be interesting to test my hypotheses by conducting collaborative studies among different research groups that have been acting in different Amazonian and Andean regions. It seems that efforts in that sense have already been made on the scope of future scientific drillings proposed by Baker *et al.* (2015) and I hope that these efforts may provide the missing pieces

for a better understanding of the paleoenvironmental and geodynamic evolution of northern South America, in order to answer some of the scientific questions put forward in this thesis work.

REFERENCES

References:

Albuquerque, N.C., 2009. Estratigrafia Sísmica do Leque Submarino do Amazonas: Master's thesis, Universidade Federal Fluminense, Brazil, 98 p.

Allen, P.A. and Allen, J.R., 2005. *Basin analysis. Principles and applications*: Blackwell Science, Oxford, UK.

Anthonissen, D.E. and Ogg, J.G., 2012. Appendix 3 - Cenozoic and Cretaceous Biochronology of Planktonic Foraminifera and Calcareous Nannofossils: *The Geologic Time Scale*, **27**, p. 1083–1127, doi: http://dx.doi.org/10.1016/B978-0-444-59425-9.15003-6.

Araújo, D.B. de, 2017. Bacia do Parnaíba: Sumário Geológico e Setores em Oferta. Agência Nacional do Petróleo, Gás Natural e Biocombustíveis (ANP).:

Araújo, E.F. da S., Silva, C.G., Reis, A.T. dos, Perovano, R., Gorini, C., Vendeville, B. and Albuquerque, N.C., 2009. Movimentos de Massa Multiescala na Bacia da Foz do Amazonas - Margem Equatorial Brasileira: *Revista Brasileira de Geofíca*, **27**, p. 485–508.

Armijo, R., Lacassin, R., Coudurier-Curveur, A. and Carrizo, D., 2015. Coupled tectonic evolution of Andean orogeny and global climate: *Earth-Science Reviews*, **143**, p. 1–35, doi: 10.1016/j.earscirev.2015.01.005.

Baker, P., Silva, C., Fritz, S. and Reis, T., 2015. Deep drilling of the Amazon continental margin: The evolution of Cenozoic neotropical biodiversity, climate, and oceanography. IODP Proposal.:

Basile, C., 2015. Transform continental margins – Part 1: Concepts and models: *Tectonophysics*, **661**, doi: 10.1016/j.tecto.2015.08.034.

Basile, C., Mascle, J. and Guiraud, R., 2005. Phanerozoic geological evolution of the Equatorial Atlantic domain: *Journal of African Earth Sciences*, **43**, p. 275–282, doi: 10.1016/j.jafrearsci.2005.07.011.

Batenburg, S.J., De Vleeschouwer, D., Sprovieri, M., Hilgen, F.J., Gale, A.S., Singer, B.S., Koeberl, C., Coccioni, R., Claeys, P. and Montanari, A., 2016. Orbital control on the timing of oceanic anoxia in the Late Cretaceous: *Climate of the Past*, **12**, doi: 10.5194/cp-12-1995-2016.

Behn, M.D. and Lin, J., 2000. Segmentation in gravity and magnetic anomalies along the U.S. East Coast passive margin: Implications for incipient structure of the oceanic lithosphere: *Journal of Geophysical Research: Solid Earth*, **105**, p. 25769–25790, doi: 10.1029/2000JB900292.

Behrendt, J.C., Schlee, J., Robb, J.M. and Silverstein, M.K., 1974. Structure of the continental

margin of liberia, West Africa: *Bulletin of the Geological Society of America*, **85**, p. 1143–1158, doi: 10.1130/0016-7606(1974)85<1143:SOTCMO>2.0.CO;2.

Behrendt, J.C. and Wotorson, C.S., 1974. Geophysical Surveys of Liberia With Tectonic and Geologic Interpretations.:

Bermudez, M.A., van der Beek, P. and Bernet, M., 2011. Asynchronous Miocene-Pliocene exhumation of the central Venezuelan Andes: *Geology*, **39**, p. 139–142, doi: 10.1130/G31582.1.

Betzler, C., Furstenau, J., Ludmann, T., Hubscher, C., Lindhorst, S., Paul, A., Reijmer, J.J.G. and Droxler, A.W., 2013. Sea-level and ocean-current control on carbonate-platform growth, Maldives, Indian Ocean: *Basin Research*, **25**, p. 172–196, doi: 10.1111/j.1365-2117.2012.00554.x.

BouDagher-Fadel, M.K., 2008. Chapter 7 The Cenozoic larger benthic foraminifera: the Neogene: *Developments in Palaeontology and Stratigraphy*, **21**.

Braga, S., 1993. Resposta flexural da litosfera e subsidência regional na área do Cone do Amazonas: *Boletim de Geociências da Petrobras*, **7**, p. 157–172.

Brandão, J.A.S.L. and Feijó, F.J., 1994. Bacia da Foz do Amazonas: *Boletim de Geociências da Petrobras*, **8**, p. 91–99.

Brange, C., 2017. Astronomical age model of the Late Cretaceous Limoeiro Formation (Amazon River Mouth basin, Brazil): implications for climate and sea-level changes. Mémoire d'Ingénieur Géologique, Institut Polytechnique UniLaSalle, France.:

Brito Neves, B.B. de, 2002. Main Stages of the Development of the Sedimentary Basins of South America and their Relationship with the Tectonics of Supercontinents: *Gondwana Research*, **5**, p. 175–196, doi: 10.1016/S1342-937X(05)70901-1.

Brito Neves, B.B. de and Fuck, R.A., 2014. The basement of the South American platform: Half Laurentian (N-NW)+half Gondwanan (E-SE) domains: *Precambrian Research*, **244**, p. 75–86, doi: 10.1016/j.precamres.2013.09.020.

Brito Neves, B.B., Van Schmus, W.R. and Fetter, A., 2002. North-western Africa-North-eastern Brazil. Major tectonic links and correlation problems: *Journal of African Earth Sciences*,, doi: 10.1016/S0899-5362(02)00025-8.

Brouwer, M.J.N. and Schwander, M.M., 1987. Cenozoic Carbonate Banks, Foz Do Amazonas Basin, Northeastern Brazil. In: *Atlas of Seismic Stratigraphy* (Bally, A.W., ed.) AAPG Studies in Geology, p. 174–178.

Bukry, D., 1973. Low-Latitude coccolith biostratigraphic zonation. In: *Initial Reports of Deep Sea Drilling Project 15* (Edgar, N.T.,, Saunders, J.B., and *et al.*, eds.) Washington (DC),

p. 685–703.

Burgess, P.M., Winefield, P., Minzoni, M. and Elders, C., 2013. Methods for identification of isolated carbonate buildups from seismic reflection data: *AAPG Bulletin*,, doi: 10.1306/12051212011.

Campbell, K.E., 2010. Late Miocene onset of the Amazon River and the Amazon deep-sea fan: Evidence from the Foz do Amazonas Basin: COMMENT: *Geology*, **38**, p. e212, doi: 10.1130/G30633C.1.

Campbell, K.E., Frailey, C.D. and Romero-Pittman, L., 2006. The Pan-Amazonian Ucayali Peneplain, late Neogene sedimentation in Amazonia, and the birth of the modern Amazon River system: *Palaeogeography, Palaeoclimatology, Palaeoecology*, **239**, p. 166–219, doi: 10.1016/j.palaeo.2006.01.020.

Campbell, K.E., Prothero, D.R., Romero-Pittman, L., Hertel, F. and Rivera, N., 2010. Amazonian magnetostratigraphy: Dating the first pulse of the Great American Faunal Interchange: *Journal of South American Earth Sciences*, **29**, p. 619–626, doi: 10.1016/j.jsames.2009.11.007.

Caputo, M.V. and Soares, E.A.A., 2016. Eustatic and tectonic change effects in the reversion of the transcontinental Amazon River drainage system: *Brazilian Journal of Geology*, **46**, p. 301–328, doi: 10.1590/2317-4889201620160066.

Carozzi, a V, 1981. Porosity models and oil exploration of Ampa carbonates, Paleogene, Foz do Amazonas Basin, offshore NW Brazil: *Journal of Petroleum Geology*, **4**, p. 3–34.

de Castro, D.L., Bezerra, F.H.R., Sousa, M.O.L. and Fuck, R.A., 2012. Influence of Neoproterozoic tectonic fabric on the origin of the Potiguar Basin, northeastern Brazil and its links with West Africa based on gravity and magnetic data: *Journal of Geodynamics*, **54**, p. 29–42, doi: 10.1016/j.jog.2011.09.002.

Castro, J.C. de, Miura, K. and Braga, J.A.E., 1978. Stratigraphic and Structural Framework of the Foz do Amazonas Basin. In: *10th Annual Offshore Technology Conference* Offshore Technology Conference, Houston, Texas, p. 1843–1847.

Catuneanu, O., 2006. *Principles of Sequence Stratigraphy*: Elsevier, Amsterdam.

Catuneanu, O., 2004. Retroarc foreland systems-evolution through time: *Journal of African Earth Sciences*, **38**, p. 225–242, doi: 10.1016/j.jafrearsci.2004.01.004.

Catuneanu, O., 2002. Sequence stratigraphy of clastic systems: Concepts, merits, and pitfalls: *Journal of African Earth Sciences*, **35**, p. 1–43.

Catuneanu, O., Abreu, V., Bhattacharya, J.P., Blum, M.D., Dalrymple, R.W., Eriksson, P.G., Fielding, C.R., Fisher, W.L., Galloway, W.E., Gibling, M.R., Giles, K. a., Holbrook, J.M.,

Jordan, R., Kendall, C.G.S.C., Macurda, B., Martinsen, O.J., Miall, a. D., Neal, J.E., Nummedal, D., Pomar, L., Posamentier, H.W., Pratt, B.R., Sarg, J.F., Shanley, K.W., Steel, R.J., Strasser, a., Tucker, M.E. and Winker, C., 2009. Towards the standardization of sequence stratigraphy: *Earth-Science Reviews*, **92**, p. 1–33, doi: 10.1016/j.earscirev.2008.10.003.

Cobbold, P.R., Mourgues, R. and Boyd, K., 2004. Mechanism of thin-skinned detachment in the Amazon Fan: Assessing the importance of fluid overpressure and hydrocarbon generation: *Marine and Petroleum Geology*, **21**, p. 1013–1025, doi: 10.1016/j.marpetgeo.2004.05.003.

Condé, V.C., Lana, C.C., Pessoa, C., Roesner, E.H., Marinho, J., Neto, D.M. and Dutra, D.C., 2007. Bacia do Ceará: *Boletim de Geociencias da Petrobras*, **15**, p. 347–355.

Cordani, U.G. and Teixeira, W., 2007. Proterozoic accretionary belts in the Amazonian Craton. In: *4-D Framework of Continental Crust* (Hatcher, R.D.,, Carlson, M.P.,, McBride, J.H., and Catalan, J.R.M., eds.) Memoir of the Geological Society of America.

Cordani, U.G., Teixeira, W., D'Agrella-Filho, M.S. and Trindade, R.I., 2009. The position of the Amazonian Craton in supercontinents: *Gondwana Research*, **15**, p. 396–407, doi: 10.1016/j.gr.2008.12.005.

Costa, J.B.S., Hasui, Y., Bemerguy, R.L., Soares-Júnior, A. V. and Villegas, J.M.C., 2002. Tectonics and paleogeography of the Marajó Basin, northern Brazil: *Anais da Academia Brasileira de Ciencias*, **74**, p. 519–531, doi: 10.1590/S0001-37652002000300013.

CPRM, 2004. Carta Geológica do Brasil ao Milionésimo: sistema de informações geográficas-SIG.:

Cruz, A., Gorini, C., Letouzey, J., Suc, J., Reis, T. and Silva, C., 2016. Length variation of Gravity-Driven systems in the Amazon River Mouth Basin : a history of carbonate-siliciclastic sedimentation and post-rift subsidence. In: *EGU General Assembly* Vienna.

Cruz, A.M., Gorini, C., Reis, A.T., Haq, B., Silva, C.G. and Granjeon, D., 2014. Integrated geological, geophysical and numerical modeling studies applied to the understanding of Amazon River Mouth Basin evolution. In: *19th ISC* Geneva; Switzerland, p. 166.

Cruz, A.M., Reis, A.T. dos, Silva, C.G., Gorini, C. and Granjeon, D., 2013. Modelagem estratigráfica da sucessão estratigráfica Quaternária da Bacia da Foz do Amazonas: Relação entre aumento de aporte sedimentar e aumento da deformação gravitacional: *XIV Congresso da Associação Brasileira de Estudos do Quaternário*,.

Curry, W.B., Shackleton, N.J., Richter, C., Backman, J.E., Bassinot, F., Bickert, T., Chaisson, W.P., Cullen, J.L., DeMenocal, P., Dobson, D.M., Ewert, L., Qrutzner, J., Hagelberg,

T.K., Hampt, Q., Harris, S.E., Herbert, T.D., Moran, K., Murayama, M., Murray, D.W., Pearson, P.N., Raffi, I., Schneider, D.A., Tiedemann, R., Valet, J.-P., Weedon, G.P., Yasuda, H. and Zachos, J.C., 1995. *Proceedings of the Ocean Drilling Program, 154 Initial Reports* (W. B. Curry, N. J. Shackleton and C. Richter, Eds.): Ocean Drilling Program, College Station, Texas.

Dai, A. and Trenberth, K.E., 2002. Estimates of Freshwater Discharge from Continents: Latitudinal and Seasonal Variations: *Journal of Hydrometeorology*, **3**, p. 660–687, doi: 10.1175/1525-7541(2002)003<0660:EOFDFC>2.0.CO;2.

Damuth, J.E., 1983. Distributary channel meandering and bifurcation patterns on the Amazon deep-sea fan as revealed by long-range side-scan sonar (GLORIA).: *Geology*,, doi: 10.1130/0091-7613(1983)11<94:DCMABP>2.0.CO;2.

Damuth, J.E. and Embley, R.W., 1981. Mass-transport processes on Amazon Cone: western equatorial Atlantic.: *American Association of Petroleum Geologists Bulletin*, **65**, p. 629–643.

Damuth, J.E. and Fairbridge, R.W., 1970. Equatorial Atlantic deep-sea arkosic sands and ice-age aridity in tropical South America: *Bulletin of the Geological Society of America*, **81**, p. 189–206, doi: 10.1130/0016-7606(1970)81[189:EADASA]2.0.CO;2.

Damuth, J.E., Flood, R.D., Kowsmann, R.O., Belderson, R.H. and Gorini, M.A., 1988. Anatomy and growth pattern of Amazon deep-sea fan as revealed by long-range side-scan sonar (GLORIA) and high-resolution seismic studies: *American Association of Petroleum Geologists Bulletin*, **72**, p. 885–911.

Damuth, J.E., Kowsmann, R.O., Flood, R.D., Belderson, R.H. and Gorini, M.A., 1983. Age relationships of distributary channels on Amazon deep-sea fan: implications for fan growth pattern.: *Geology*, **11**, p. 470–473.

Damuth, J.E. and Kumar, N., 1975. Amazon Cone: Morphology, Sediments, Age, and Growth Pattern: *Bulletin of the Geological Society of America*, **86**, p. 863–878.

Diegel, F.A., Karlo, J.F., Schuster, D.C., Shoup, R.C. and Tauvers, P.R., 1995. Cenozoic Structural Evolution and Tectono-Stratigraphic Framework of the Northern Gulf Coast Continental Margin: *Salt tectonics: a global perspective: AAPG Memoir 65*,.

Dino, R., Soares, E.A.A., Antonioli, L., Riccomini, C. and Nogueira, A.C.R., 2012. Palynostratigraphy and sedimentary facies of Middle Miocene fluvial deposits of the Amazonas Basin, Brazil: *Journal of South American Earth Sciences*, **34**, p. 61–80, doi: 10.1016/j.jsames.2011.11.008.

Dobson, D.M., Dickens, G.R. and Rea, D.K., 2001. Terrigenous sediment on Ceara Rise: A

Cenozoic record of South American orogeny and erosion: *Palaeogeography, Palaeoclimatology, Palaeoecology*, **165**, p. 215–229.

Doo, W. Bin, Lo, C.L., Hsu, S.K., Tsai, C.H., Huang, Y.S., Wang, H.F., Chiu, S.D., Ma, Y.F. and Liang, C.W., 2018. New gravity anomaly map of Taiwan and its surrounding regions with some tectonic interpretations: *Journal of Asian Earth Sciences*,, doi: 10.1016/j.jseaes.2017.12.010.

Driscoll, N.W. and Karner, G.D., 1994. Flexural deformation due to Amazon Fan loading: a feedback mechanism affecting sediment delivery to margins: *Geology*, **22**, p. 1015–1018, doi: 10.1130/0091-7613(1994)022<1015:FDDTAF>2.3.CO;2.

Espurt, N., Baby, P., Brusset, S., Roddaz, M., Hermoza, W. and Barbarand, J., 2010. The Nazca Ridge and Uplift of the Fitzcarrald Arch: Implications for Regional Geology in Northern South America. In: *Amazonia: Landscape and Species Evolution* Wiley-Blackwell Publishing Ltd., Oxford, UK, p. 89–100.

Espurt, N., Funiciello, F., Martinod, J., Guillaume, B., Regard, V., Faccenna, C. and Brusset, S., 2008. Flat subduction dynamics and deformation of the South American plate: Insights from analog modeling: *Tectonics*, **27**, p. n/a-n/a, doi: 10.1029/2007TC002175.

Feng, X., Wang, E., Ganne, J., Amponsah, P. and Martin, R., 2018. Role of Volcano Sedimentary Basins in the Formation of Greenstone Granitoid Belts in the West African Craton: A Numerical Model: *Minerals*, **8**, p. 73, doi: 10.3390/min8020073.

Ferreira, A., Rigueti, A. and Bastos, G., 2015. Bacia do Amazonas: Sumário Geológico e Setores em Oferta. Agência Nacional do Petróleo, Gás Natural e Biocombustíveis (ANP).:

Figueiredo, J., Hoorn, C., van der Ven, P. and Soares, E., 2009. Late Miocene onset of the Amazon River and the Amazon deep-sea fan: Evidence from the Foz do Amazonas Basin: *Geology*, **37**, p. 619–622.

Figueiredo, J., Hoorn, C., van der Ven, P. and Soares, E., 2010. Late Miocene onset of the Amazon River and the Amazon deep-sea fan: Evidence from the Foz do Amazonas Basin: Reply: *Geology*, **38**, p. e213, doi: 10.1130/G31057Y.1.

Figueiredo, J.J.P., Zalán, P.V. and Soares, E.F., 2007. Bacia da Foz do Amazonas: *Boletim de Geociencias da Petrobras*, **15**, p. 299–309.

Flood, R.D. and Piper, D.J.W., 1997. Amazon Fan Sedimentation: the relationship to equatorial climate change, continental denudation, and sea-level fluctuations: *Proceedings of the Ocean Drilling Program, Scientific Results, Amazon Fan*, **155**, p. 653–675, doi: -.

Friedrich, O., Norris, R.D. and Erbacher, J., 2012. Evolution of middle to late Cretaceous oceans-A 55 m.y. Record of Earth's temperature and carbon cycle: *Geology*, **40**, p. 107–

110, doi: 10.1130/G32701.1.

Galvão, I.L.G. and de Castro, D.L., 2017. Contribution of global potential field data to the tectonic reconstruction of the Rio Grande Rise in the South Atlantic: *Marine and Petroleum Geology*, **86**, p. 932–949, doi: 10.1016/j.marpetgeo.2017.06.048.

Garver, A.J.I., Reiners, P.W., Walker, L.J., Ramage, J.M., Perry, S.E., The, S. and March, N., 2014. Implications for Timing of Andean Uplift from Thermal Resetting of Radiation□ Damaged Zircon in the Cordillera Huayhuash, Northern Peru: *The Journal of Geology*, **113**, p. 117–138.

Garzione, C.N., Hoke, G.D., Libarkin, J.C., Withers, S., MacFadden, B., Eiler, J., Ghosh, P. and Mulch, A., 2008. Rise of the Andes.: *Science (New York, N.Y.)*, **320**, p. 1304–7, doi: 10.1126/science.1148615.

Gerya, T. V., 2013. Initiation of transform faults at rifted continental margins: 3D petrological-thermomechanical modeling and comparison to the Woodlark Basin: *Petrology*, **21**, p. 550–560, doi: 10.1134/S0869591113060039.

Ghosh, P., Garzione, C.N. and Eiler, J.M., 2006. Rapid uplift of the Altiplano revealed through 13C- 18O bonds in paleosol carbonates: *Science*, **311**, p. 511–515, doi: 10.1126/science.1119365.

Gorini, C., Haq, B.U., dos Reis, A.T., Silva, C.G., Cruz, A.M., Soares, E. and Grangeon, D., 2014. Late Neogene sequence stratigraphic evolution of the Foz do Amazonas Basin, Brazil: *Terra Nova*, **26**, p. 179–185, doi: 10.1111/ter.12083.

Gradstein, F.M., Ogg, J.G., Schmitz, M.D. and Ogg, G.M., 2012. *The Geologic Time Scale* (F. M. Gradstein, J. G. Ogg, M. D. Schmitz and G. M. Ogg, Eds.): Elsevier B.V., Amsterdam.

Gross, M., Piller, W.E., Ramos, M.I. and Douglas da Silva Paz Jackson, J., 2011. Late Miocene sedimentary environments in south-western Amazonia (Solimões Formation; Brazil): *Journal of South American Earth Sciences*, **32**, p. 169–181, doi: 10.1016/j.jsames.2011.05.004.

Gutscher, M.A., Maury, F., Eissen, J.P. and Bourdon, E., 2000. Can slab melting be caused by flat subduction? *Geology*, **28**, p. 536–538, doi: 10.1130/0091-7613(2000)28<535:CSMBCB>2.0.CO;2.

Handford, C.R. and Loucks, R.G., 1993. Carbonate Depositional Sequences and Systems Tracts—Responses of Carbonate Platforms to Relative Sea-Level Changes. In: *Carbonate Sequence Stratigraphy; Recent Advances and Applications: AAPG Memoir 57* p. 3–41.

Haq, B.U., 2014. Cretaceous eustasy revisited: *Global and Planetary Change*, **113**, p. 44–58, doi: 10.1016/j.gloplacha.2013.12.007.

Haq, B.U., Hardenbol, J. and Vail, P.R., 1987. Chronology of fluctuating sea levels since the triassic.: *Science (New York, N.Y.)*, **235**, p. 1156–1167.

Hardenbol, J., Thierry, J., Farley, M.B., Jacquin, T., De Graciansky, P.-C. and Vail, P.R., 1998. Mesozoic and Cenozoic Sequence Chronostratigraphic Framework of European Basins: *SEPM Special Publication*,, p. 3–13, doi: 10.2110/pec.98.02.0003.

Harris, S.E. and Mix, A.C., 2002. Climate and tectonic influences on continental erosion of tropical South America, 0–13 Ma: *Geology*, **30**, p. 447.

Haug, B.G.H., Tiedemann, R., Keigwin, L.D. and Hole, W., 2004. How the Isthmus of Panama Put Ice in the Arctic: *Oceanus Magazine*,, doi: 10.1130/1052-5173(2003)013<0004:CDOPC>2.0.CO;2.

Haug, G.H., Tiedemann, R., Zahn, R. and Ravelo, a. C., 2001. Role of Panama uplift on oceanic freshwater balance: *Geology*, **29**, p. 207.

Heinrich, S. and Zonneveld, K.A.F., 2013. Influence of the Amazon River development and constriction of the Central American Seaway on Middle/Late Miocene oceanic conditions at the Ceara Rise: *Palaeogeography, Palaeoclimatology, Palaeoecology*,, doi: 10.1016/j.palaeo.2013.06.026.

Herz, N., Hasui, Y., Costa, J.B.S. and Matta, M.A.D.S., 1989. The Araguaia fold belt, Brazil: A reactivated Brasiliano-Pan-African cycle (550 Ma) geosuture: *Precambrian Research*,, doi: 10.1016/0301-9268(89)90020-X.

Hilgen, F.J., Lourens, L.J., Van Dam, J.A., Beu, A.G., Boyes, A.F., Cooper, R.A., Krijgsman, W., Ogg, J.G., Piller, W.E. and Wilson, D.S., 2012. The Neogene Period. In: *The Geologic Time Scale 2012* Elsevier B.V., p. 923–978.

Hinnov, L.A., 2013. Cyclostratigraphy and its revolutionizing applications in the earth and planetary sciences: *Bulletin of the Geological Society of America*,, doi: 10.1130/B30934.1.

Hoorn, C., 1994. An environmental reconstruction of the palaeo-Amazon River system (Middle–Late Miocene, NW Amazonia): *Palaeogeography, Palaeoclimatology, Palaeoecology*, **112**, p. 187–238.

Hoorn, C., Bogotá-A, G.R., Romero-Baez, M., Lammertsma, E.I., Flantua, S.G.A., Dantas, E.L., Dino, R., do Carmo, D.A. and Chemale, F., 2017. The Amazon at sea: Onset and stages of the Amazon River from a marine record, with special reference to Neogene plant turnover in the drainage basin: *Global and Planetary Change*, **153**, p. 51–65, doi: 10.1016/j.gloplacha.2017.02.005.

Hoorn, C., Guerrero, J., Sarmiento, G.A. and Lorente, M.A., 1995. Andean tectonics as a cause for changing drainage patterns in Miocene northern South America: *Geology*,, doi:

10.1130/0091-7613(1995)023<0237:ATAACF>2.3.CO;2.

Hoorn, C., Wesselingh, F.P., ter Steege, H., Bermudez, M. a, Mora, a, Sevink, J., Sanmartín, I., Sanchez-Meseguer, a, Anderson, C.L., Figueiredo, J.P., Jaramillo, C., Riff, D., Negri, F.R., Hooghiemstra, H., Lundberg, J., Stadler, T., Särkinen, T. and Antonelli, a, 2010. Amazonia through time: Andean uplift, climate change, landscape evolution, and biodiversity.: *Science (New York, N.Y.)*, **330**, p. 927–931, doi: 10.1126/science.1194585.

Hungerbühler, D., Steinmann, M., Winkler, W., Seward, D., Egüez, A., Peterson, D.E., Helg, U. and Hammer, C., 2002. Neogene stratigraphy and Andean geodynamics of southern Ecuador: *Earth-Science Reviews*, **57**, p. 75–124.

Insel, N., Poulsen, C.J. and Ehlers, T.A., 2010. Influence of the Andes Mountains on South American moisture transport, convection, and precipitation: *Climate Dynamics*, **35**, p. 1477–1492, doi: 10.1007/s00382-009-0637-1.

Junior, I., Zalán, P.V., Figueiredo, J.J.P. and Soares, E.F., 2007. Bacia de Barreirinhas: *Boletim de Geociencias da Petrobras*, **15**, p. 331–339.

Katz, M.E., Cramer, B.S., Toggweiler, J.R., Esmay, G., Liu, C., Miller, K.G., Rosenthal, Y., Wade, B.S. and Wright, J.D., 2011. Impact of Antarctic circumpolar current development on Late Paleogene ocean ctructure: *Science*, **332**, p. 1076–1079, doi: 10.1126/science.1202122.

Kennett, J.P. and Shackleton, N.J., 1976. Oxygen isotopic evidence for the development of the psychrosphere 38 Myr ago: *Nature*,, doi: 10.1038/260513a0.

King, T.A., Ellis, W.G.J., Murray, D.W., Shackleton, N.J. and Harris, S., 1997. Miocene evolution of carbonate sedimentation at the Ceara Rise: a multivariate data/proxy approach. In: *Proceedings of the Ocean Drilling Program, 154 Scientific Results* Ocean Drilling Program.

Klein, E.L. and Moura, C.A. V., 2008. São Luís Craton and Gurupi Belt (Brazil): possible links with the West African Craton and surrounding Pan-African belts: *Geological Society, London, Special Publications*,, doi: 10.1144/SP294.8.

Klein, E.L., Moura, C.A.V. and Pinheiro, B.L.S., 2005. Paleoproterozoic crustal evolution of the São Luís Craton, Brazil: Evidence from zircon geochronology and Sm-Nd isotopes: *Gondwana Research*,, doi: 10.1016/S1342-937X(05)71116-3.

Kominz, M. a., Browning, J. V., Miller, K.G., Sugarman, P.J., Mizintseva, S. and Scotese, C.R., 2008. Late Cretaceous to Miocene sea-level estimates from the New Jersey and Delaware coastal plain coreholes: An error analysis: *Basin Research*, **20**, p. 211–226, doi: 10.1111/j.1365-2117.2008.00354.x.

Kröner, A. and Stern, R.J., 2005. AFRICA | Pan-African Orogeny. In: *Encyclopedia of Geology*.

Kusky, T.M., Abdelsalam, M., Stern, R.J. and Tucker, R.D., 2003. Evolution of the East African and related orogens, and the assembly of Gondwana: *Precambrian Research*,, doi: 10.1016/S0301-9268(03)00062-7.

Lara, M.E., 1994. The tectonic evolution of a failed rift system: Marajo Basin, Northern Brazil. In: *64th SEG Annual Meeting* Society of Exploration Geophysicists, Los Angeles (CA), p. 805.

Laskar, J., Fienga, A., Gastineau, M. and Manche, H., 2011. La2010: A new orbital solution for the long term motion of the Earth: *Astronomy & Astrophysics*, **532**, p. 15, doi: 10.1051/0004-6361/201116836.

Latrubesse, E., Cozzuol, M., Silva-Caminha, S., Rigsby, C., Absy, M. and Jaramillo, C., 2010. The Late Miocene paleogeography of the Amazon Basin and the evolution of the Amazon River system: *Earth-Science Reviews*, **99**, p. 99–124, doi: 10.1016/j.earscirev.2010.02.005.

Latrubesse, E.M., da Silva, S. a F., Cozzuol, M. and Absy, M.L., 2007. Late Miocene continental sedimentation in southwestern Amazonia and its regional significance: Biotic and geological evidence: *Journal of South American Earth Sciences*, **23**, p. 61–80, doi: 10.1016/j.jsames.2006.09.021.

Liu, Z., Tuo, S., Zhao, Q., Cheng, X. and Huang, W., 2004. Deep-water Earliest Oligocene Glacial Maximum (EOGM) in South Atlantic: *Chinese Science Bulletin*, **49**, p. 2190.

Lopez, M., 2001. Architecture and depositional pattern of the quaternary deep-sea fan of the Amazon: *Marine and Petroleum Geology*, **18**, p. 479–486.

Manatschal, G., Lavier, L. and Chenin, P., 2015. The role of inheritance in structuring hyperextended rift systems: Some considerations based on observations and numerical modeling: *Gondwana Research*,, doi: 10.1016/j.gr.2014.08.006.

Martini, E., 1971. Standard Tertiary and Quaternary calcareous nannoplankton zonation: *Conf. Planktonic Microfossils Roma*, **2**, p. 739–785.

Maslin, M. and Mikkelson, N., 1997. AMAZON FAN MASS-TRANSPORT DEPOSITS AND UNDERLYING INTERGLACIAL DEPOSITS: AGE ESTIMATES AND FAN DYNAMICS. In: *Proceedings of the Ocean Drilling Program, Scientific Results, Vol. 155* p. 353–365.

Maslin, M., Vilela, C., Mikkelsen, N. and Grootes, P., 2005. Causes of catastrophic sediment failures of the Amazon Fan: *Quaternary Science Reviews*, **24**, p. 2180–2193, doi:

10.1016/j.quascirev.2005.01.016.

Matos, R.M.D. De, 2000. Tectonic Evolution of the Equatorial South Atlantic: *Atlantic Rift and Continental Margins*, **115**, p. 331–354, doi: 10.1029/GM115p0331.

Maus, S., Barckhausen, U., Berkenbosch, H., Bournas, N., Brozena, J., Childers, V., Dostaler, F., Fairhead, J.D., Finn, C., Von Frese, R.R.B., Gaina, C., Golynsky, S., Kucks, R., Lühr, H., Milligan, P., Mogren, S., Müller, R.D., Olesen, O., Pilkington, M., Saltus, R., Schreckenberger, B., Thébault, E. and Tontini, F.C., 2009. EMAG2: A 2-arc min resolution Earth Magnetic Anomaly Grid compiled from satellite, airborne, and marine magnetic measurements: *Geochemistry, Geophysics, Geosystems*,, doi: 10.1029/2009GC002471.

McKee, E.H. and Noble, D.C., 1990. Cenozoic tectonic events, magmatic pulses, and base- and precious-metal mineralization in the central Andes: *Circum-Pacific Council for Energy and Mineral Resources, Earth Science Series*, **11**, p. 189–194.

Meade, R.H., 1994. Suspended sediments of the modern Amazon and Orinoco rivers: *Quaternary International*, **21**, p. 29–39.

Meade, R.H., Dunne, T., Richey, J.E., Santos, U. and Salati, E., 1985. Storage and remobilization of suspended sediment in the lower Amazon river of Brazil.: *Science (New York, N.Y.)*, **228**, p. 488–490.

Megard, F., 1984. The Andean orogenic period and its major structures in central and northern Peru: *Journal of the Geological Society*,, doi: 10.1144/gsjgs.141.5.0893.

Milani, E.J., Brandão, J.A.S.L., Zalán, P. V. and Gamboa, L.A.P., 2000. Petróleo na margem continental Brasileira: Geologia, exploração, resultados e perspectivas: *Revista Brasileira de Geofisica*,, doi: 10.1590/S0102-261X2000000300012.

Milani, E.J., Rangel, H.D., Bueno, G.V., Stica, J.M., Winter, W.R., Caixeta, J.M. and Neto, O. da C., 2007. Bacias Sedimentares Brasileiras - Cartas Estratigráficas: *Boletim de Geociências da Petrobras*, **15**, p. 183–205.

Milani, E.J. and Zalan, P.V., 1999. An Outline of the Geology and Petroleum Systems of the Paleozoic Interior Basins of South America: *Episodes - Newsmagazine of the International Union of Geological Sciences*,, doi: 10.1016/j.jappgeo.2011.12.012.

Miller, K.G., Kominz, M. a., Browning, J. V., Wright, J.D., Mountain, G.S., Katz, M.E., Sugarman, P.J., Cramer, B.S., Christie-Blick, N. and Pekar, S.F., 2005. The Phanerozoic record of sea-level change: *Science*, **310**, p. 11293–1298, doi: 10.1126/science.1116412.

Miller, K., Mountain, G., Wright, J. and Browning, J., 2011. A 180-Million-Year Record of Sea Level and Ice Volume Variations from Continental Margin and Deep-Sea Isotopic

Records: *Oceanography*,, doi: 10.5670/oceanog.2011.26.

Miller, K.G., Wright, J.D., Katz, M.E., Wade, B.S., Browning, J. V and Cramer, B.S., 2009. Climate threshold at the Eocene-Oligocene transition : Antarctic ice sheet infl uence on ocean circulation: **80301**, doi: 10.1130/2009.2452(11).

Mitchum, R.M. and Vail, P.R., 1977. Seismic Stratigraphy and Global Changes of Sea Level , Part 7 : Seismic Stratigraphic Interpretation Procedure: *Seismic Stratigraphy: Applications to Hydrocarbon Exploration. AAPG Memoir 26*, **Memoir 26**, p. 135–143.

Mitchum, R.M., Vail, P.R. and Sangree, J.B., 1977. Seismic stratigraphy and global changes of sea level, Part 6: stratigraphic interpretation of seismic reflection patterns in depositional sequences: *Seismic Stratigraphy — applications to hydrocarbon exploration*,, doi: 10.1038/272400a0.

Mohriak, W.U., 2003. Bacias Sedimentares da Margem Continetal Brasileira. In: *Geologia, Tectônica e Recursos Minerais do Brasil* p. 151–165.

Moura, R.L., Amado-Filho, G.M., Moraes, F.C., Brasileiro, P.S., Salomon, P.S., Mahiques, M.M., Bastos, A.C., Almeida, M.G., Silva, J.M., Araujo, B.F., Brito, F.P., Rangel, T.P., Oliveira, B.C.V., Bahia, R.G., Paranhos, R.P., Dias, R.J.S., Siegle, E., Figueiredo, A.G., Pereira, R.C., Leal, C. V., Hajdu, E., Asp, N.E., Gregoracci, G.B., Neumann-Leitão, S., Yager, P.L., Francini-Filho, R.B., Fróes, A., Campeão, M., Silva, B.S., Moreira, A.P.B., Oliveira, L., Soares, A.C., Araujo, L., Oliveira, N.L., Teixeira, J.B., Valle, R.A.B., Thompson, C.C., Rezende, C.E. and Thompson, F.L., 2016. An extensive reef system at the Amazon River mouth: *Science advances*,, doi: 10.1126/sciadv.1501252.

Mutti, E., 1985. Turbidite Systems and Their Relations to Depositional Sequences: *Provenance of Arenites SE - 4*, **148**, p. 65–93.

Nemcok, M., Henk, A., Allen, R., Sikora, P.J. and Stuart, C., 2012. Continental break-up along strike-slip fault zones; observations from the Equatorial Atlantic: *Geological Society, London, Special Publications*,, p. 537–556, doi: 10.1144/SP369.8.

Neto, O.D.C.P., Soares, U.M., Silva, J.G.F. Da, Roesner, E.H., Florencio, C.P. and Souza, C.A.V. De, 2007. Bacia Potiguar: *Boletim de Geociencias da Petrobras*, **15**, p. 357–369.

Newkirk, D.R. and Martin, E.E., 2009. Circulation through the Central American Seaway during the Miocene carbonate crash: *Geology*, **37**, p. 87–90, doi: 10.1130/G25193A.1.

Noble, D.C., McKee, E., Mourier, T. and Megard, F., 1990. Cenozoic stratigraphy, magmatic activity, compressive deformation, and uplift in northern Peru: *Geological Society of America Bulletin*, **102**, p. 1105–1113.

Nogueira, A.C.R., Silveira, R. and Guimarães, J.T.F., 2013. Neogene-Quaternary sedimentary

and paleovegetation history of the eastern Solimões Basin, central Amazon region: *Journal of South American Earth Sciences*, **46**, p. 89–99, doi: 10.1016/j.jsames.2013.05.004.

Okada, H. and Bukry, D., 1980. Supplementary modification and introduction of code numbers to the low-latitude coccolith biostratigraphic zonation (Bukry, 1973; 1975): *Marine Micropaleontology*,, doi: 10.1016/0377-8398(80)90016-X.

Oliveira, V. De, Reis, A.T. and Silva, C.G., 2005. Fatores condicionantes do arcabouço estrutural da tectônica gravitacional do Cone do Amazonas. In: *9th International Congress of the Brazilian Geophysical Society* Sociedade Brasileira de Geofísica, Salvador, p. 1–6.

Paillard, D., Labeyrie, L. and Yiou, P., 1996. Macintosh Program performs time-series analysis: *Eos, Transactions American Geophysical Union*,, doi: 10.1029/96EO00259.

Paixão, M.A.P., Nilson, A.A. and Dantas, E.L., 2008. The Neoproterozoic Quatipuru ophiolite and the Araguaia fold belt, central-northern Brazil, compared with correlatives in NW Africa: *Geological Society, London, Special Publications*,, doi: 10.1144/SP294.16.

Papadimitriou, N., 2017. Université Pierre et Marie Curie Geodynamics and synchronous filling of a rift type basin evolved through compression Tectonics (The western margin of Levant Basin): Université Pierre et Marie Curie, 246 p.

Perovano, R., 2012. Análise estrutural da tectônica gravitacional na bacia da Foz do Amazonas a partir da interpretação de dados sísmicos e de modelagem experimental: Universidade Federal Fluminense, 239 p.

Perovano, R., Reis, A.T. dos, Silva, C.G., Vendeville, B.C., Gorini, C., Oliveira, V. De and Araújo, É.F. da S., 2009. O Processo de Colapso Gravitacional da Seção Marinha da Bacia da Foz do Amazonas - Margem Equatorial Brasileira: *Revista Brasileira de Geofíca*, **27**, p. 459–484.

Piper, D.J.W., Flood, R.D., Cisowski, S., Hall, F., Manley, P.L., Maslin, M., Mikkelsen, N. and Showers, W., 1997. Previous Chapter Table of Contents Next Chapter: **155**, p. 595–609.

Pomar, L., 2001. Types of carbonate platforms: A genetic approach: *Basin Research*,, doi: 10.1046/j.0950-091X.2001.00152.x.

Posamentier, H.W. and Kolla, V., 2003. Seismic Geomorphology and Stratigraphy of Depositional Elements in Deep-Water Settings: *Journal of Sedimentary Research*,, doi: 10.1306/111302730367.

Poulsen, C.J., Ehlers, T.A. and Insel, N., 2010. Onset of Convective Rainfall During Gradual Late Miocene Rise of the Central Andes: *Science*, **328**, p. 490–493, doi: 10.1126/science.1185078.

Raffi, I., Backman, J., Fornaciari, E., Pälike, H., Rio, D., Lourens, L. and Hilgen, F., 2006. A review of calcareous nannofossil astrobiochronology encompassing the past 25 million years: *Quaternary Science Reviews*, **25**, p. 3113–3137, doi: 10.1016/j.quascirev.2006.07.007.

Rebesco, M., Hernández-Molina, F.J., Van Rooij, D. and Wåhlin, A., 2014. Contourites and associated sediments controlled by deep-water circulation processes: State-of-the-art and future considerations: *Marine Geology*,, doi: 10.1016/j.margeo.2014.03.011.

Reis, A.T., Araújo, E., Silva, C.G., Cruz, A.M., Gorini, C., Droz, L., Migeon, S., Perovano, R., King, I. and Bache, F., 2016. Effects of a regional décollement level for gravity tectonics on late Neogene to recent large-scale slope instabilities in the Foz do Amazonas Basin, Brazil: *Marine and Petroleum Geology*,, doi: 10.1016/j.marpetgeo.2016.04.011.

Reis, A.T., Gorini, C. and Mauffret, A., 2005. Implications of salt-sediment interactions on the architecture of the Gulf of Lions deep-water sedimentary systems - Western Mediterranean Sea: *Marine and Petroleum Geology*,, doi: 10.1016/j.marpetgeo.2005.03.006.

Reis, a. T., Perovano, R., Silva, C.G., Vendeville, B.C., Araujo, E., Gorini, C. and Oliveira, V., 2010. Two-scale gravitational collapse in the Amazon Fan: a coupled system of gravity tectonics and mass-transport processes: *Journal of the Geological Society*, **167**, p. 593–604, doi: 10.1144/0016-76492009-035.

Rezende, W.M. de and Ferradaes, J.O., 1971. Integração geológica regional da Bacia Sedimentar da Foz do Amazonas: , p. 203–214.

Ribas, C.C., Aleixo, a., Nogueira, a. C.R., Miyaki, C.Y. and Cracraft, J., 2012. A palaeobiogeographic model for biotic diversification within Amazonia over the past three million years: *Proceedings of the Royal Society B: Biological Sciences*, **279**, p. 681–689, doi: 10.1098/rspb.2011.1120.

Richey, J.E., Nobre, C. and Deser, C., 1989. Amazon river discharge and climate variability: 1903 to 1985.: *Science (New York, N.Y.)*, **246**, p. 101–103.

Rimington, N., Cramp, A. and Morton, A., 2000. Amazon Fan sands: Implications for provenance: *Marine and Petroleum Geology*, **17**, p. 267–284.

Roddaz, M., Baby, P., Brusset, S., Hermoza, W. and Darrozes, J.M., 2005a. Forebulge dynamics and environmental control in Western Amazonia: The case study of the Arch of Iquitos (Peru): *Tectonophysics*, **399**, p. 87–108, doi: 10.1016/j.tecto.2004.12.017.

Roddaz, M., Hermoza, W., Mora, A., Baby, P., Parra, M., Christophoul, F., Brusset, S. and Espurt, N., 2010. Cenozoic Sedimentary Evolution of the Amazonian Foreland Basin System. In: *Amazonia, Landscape and Species Evolution: A Look into the Past.*

Roddaz, M., Hermoza, W., Mora, A., Baby, P., Parra, M., Christophoul, F., Brusset, S. and Espurt, N., 2011. Cenozoic Sedimentary Evolution of the Amazonian Foreland Basin System. In: *Amazonia: Landscape and Species Evolution* Wiley-Blackwell Publishing Ltd., Oxford, UK, p. 61–88.

Roddaz, M., Viers, J., Brusset, S., Baby, P. and Hérail, G., 2005b. Sediment provenances and drainage evolution of the Neogene Amazonian foreland basin: *Earth and Planetary Science Letters*, **239**, p. 57–78, doi: 10.1016/j.epsl.2005.08.007.

Rodger, M., Watts, a. B., Greenroyd, C.J., Peirce, C. and Hobbs, R.W., 2006. Evidence for unusually thin oceanic crust and strong mantle beneath the Amazon Fan: *Geology*, **34**, p. 1081, doi: 10.1130/G22966A.1.

da Rosa-Costa, L.T., Lafon, J.M. and Delor, C., 2006. Zircon geochronology and Sm-Nd isotopic study: Further constraints for the Archean and Paleoproterozoic geodynamical evolution of the southeastern Guiana Shield, north of Amazonian Craton, Brazil: *Gondwana Research*,, doi: 10.1016/j.gr.2006.02.012.

Rossetti, D.F., Cohen, M.C.L., Tatumi, S.H., Sawakuchi, A.O., Cremon, É.H., Mittani, J.C.R., Bertani, T.C., Munita, C.J.A.S., Tudela, D.R.G., Yee, M. and Moya, G., 2015. Mid-Late Pleistocene OSL chronology in western Amazonia and implications for the transcontinental Amazon pathway: *Sedimentary Geology*,, doi: 10.1016/j.sedgeo.2015.10.001.

Roth, J.M., Droxler, A.W. and Kameo, K., 2000. the Caribbean Carbonate Crash At the Middle To Late Miocene Transition : Linkage To the Establishment of the Modern Global Ocean Conveyor 1: *Proceedings of the Ocean Drilling Program, Scientific Results*, **165**, p. 249–273.

Rousse, S., Gilder, S., Farber, D., McNulty, B. and Torres, V.R., 2002. Paleomagnetic evidence for rapid vertical-axis rotation in the Peruvian Cordillera ca. 8 Ma: *Geology*,, doi: 10.1130/0091-7613(2002)030<0075:PEFRVA>2.0.CO;2.

Rowan, M.G., Peel, F.J. and Vendeville, B.C., 2004. Gravity-driven fold belts on passive margins: *AAPG Memoir*,, doi: 10.1306/61EECE28-173E-11D7-8645000102C1865D.

Sacek, V., 2014. Drainage reversal of the Amazon River due to the coupling of surface and lithospheric processes: *Earth and Planetary Science Letters*, **401**, p. 301–312, doi: 10.1016/j.epsl.2014.06.022.

Sandwell, D., Garcia, E., Soofi, K., Wessel, P., Chandler, M. and Smith, W.H.F., 2013. Toward 1-mGal accuracy in global marine gravity from CryoSat-2, Envisat, and Jason-1: *The Leading Edge*,, doi: 10.1190/tle32080892.1.

Sandwell, D.T., Müller, R.D., Smith, W.H.F., Garcia, E. and Francis, R., 2014. New global marine gravity model from CryoSat-2 and Jason-1 reveals buried tectonic structure: *Science*,, doi: 10.1126/science.1258213.

Santos, J.O.S., Hartmann, L.A., Gaudette, H.E., Groves, D.I., Mcnaughton, N.J. and Fletcher, I.R., 2000. A New Understanding of the Provinces of the Amazon Craton Based on Integration of Field Mapping and U-Pb and Sm-Nd Geochronology: *Gondwana Research*,, doi: 10.1016/S1342-937X(05)70755-3.

Schaller, H., Vasconcelos, D.N. and Castro, J.C., 1971. Estratigrafia preliminar da Bacia Sedimentar da Foz do Rio Amazonas. In: *XXV Congresso Brasileiro de Geologia* SBG, São Paulo, p. 189–202.

Schlager, W., 1998. Exposure, Drowning and Sequence Boundaries on Carbonate Platforms. In: *Reefs and Carbonate Platforms in the Pacific and Indian Oceans* (Camoin, G.F., and Davies, P.J., eds.) Blackwell Publishing Ltd., Oxford, UK, p. 3–21.

Schlager, W., 2005. Geometry of carbonate accumulations. In: *Carbonate Sedimentology and Sequence Stratigraphy* (Crossey, L.J., ed.) SEPM (Society for Sedimentary Geology), Tulsa, Oklahoma, p. 39–54.

Schlager, W., John, J.G.R. and Droxler, A.W., 1994. Highstand Shedding of Carbonate Platforms: *SEPM Journal of Sedimentary Research*,, doi: 10.1306/D4267FAA-2B26-11D7-8648000102C1865D.

Sébrier, M. and Soler, P., 1991. Tectonics and magmatism in the Peruvian Andes from late Oligocene time to the Present. In: *Andean Magmatism and Its Tectonic Setting* (Harmon, R.S., and Rapela, C.W., eds.) Boulder, Colorado, p. 259–278.

Shephard, G.E., Müller, R.D., Liu, L. and Gurnis, M., 2010. Miocene drainage reversal of the Amazon River driven by plate–mantle interaction: *Nature Geoscience*, **3**, p. 870–875, doi: 10.1038/ngeo1017.

Silva, G.G., Araujo, E., Reis, A.T., Perovano, R., Gorini, C., Vendeville, B.C. and Albuquerque, N., 2010. Megaslides in the Foz do Amazonas Basin, Brazilian Equatorial Margin (D. C. Mosher, C. Shipp, L. Moscardelli, J. Chaytor, C. Baxter, H. Lee and R. Urgeles, Eds.): *Submarine Mass Movements and Their Consequences*, **28**, p. 581–591.

Silva, S.R.P. da and Maciel, R.R., 1998. Foz do Amazonas Basin hydrocarbon system. In: *AAPG international conference and exhibition; abstracts.*

Silva, S.R.P., Maciel, R.R. and Severino, M.C.G., 1999. Cenozoic tectonics of Amazon Mouth Basin: *Geo-Marine Letters*, **18**, p. 256–262.

Silva, C.C., Reis, A.T. dos, Perovano, R.J., Gorini, M.A., Santos, M.V.M. dos, Jeck, I.K.,

Tavares, A.A.A. and Gorini, C., 2016. Multiple Megaslide Complexes and Their Significance for the Miocene Stratigraphic Evolution of the Offshore Amazon Basin. In: *Advances in Natural and Technological Hazards Research* (Lamarche, G.,, Mountjoy, J.,, Bull, S.,, Hubble, T.,, Krastel, S.,, Lane, E.,, Micallef, A.,, Moscardelli, L.,, Mueller, C.,, Pecher, I., and Woelz, S., eds.) p. 49–60.

Silva, R.J.P. da, Vendeville, B.C., Reis, A.T. dos, Silva, C.G., Gorini, C. and Araújo, É.F. da S., 2011. Modelagem física experimental de mecanismos de deformação gravitacional simulando múltiplos intervalos superpressurizados: Aplicação à bacia da foz do Amazonas: *Revista Brasileira de Geofísica*, **29**, p. 583–607, doi: dx.doi.org/10.22564/rbgf.v29i3.101.

Soares, E.A.A., D'Apolito, C., Jaramillo, C., Harrington, G., Caputo, M.V., Barbosa, R.O., Bonora dos Santos, E., Dino, R. and Gonçalves, A.D., 2017. Sedimentology and Palynostratigraphy of a Pliocene-Pleistocene (Piacenzian to Gelasian) deposit in the lower Negro River: Implications for the establishment of large rivers in Central Amazonia: *Journal of South American Earth Sciences*,, doi: 10.1016/j.jsames.2017.08.008.

Soares Júnior, V.A., Costa, J.B.S. and Hasui, Y., 2008. Evolução da Margem Atlaântica Equatorial do Brasil : Três Fases Distensivas: *Geociências*, **27**, p. 427–437.

Soares Júnior, A.V., Hasui, Y., Costa, J.B.S. and Machado, F.B., 2011. Evolução do rifteamento e paleogeografia da margem Atlântica Equatorial do Brasil: Triássico ao Holoceno: *Geociências*, **30**, p. 669–692.

Soares, E.F., Zalán, P.V., Jesus, J. De, Figueiredo, P. De, Junior, I.T. and Bacia, A., 2007. Bacia do Pará-Maranhão: *Boletim de Geociencias da Petrobras*, **15**, p. 321–329.

Sousa, S.H. de M. e, Fairchild, T.R. and Tibana, P., 2003. Cenozoic biostratigraphy of larger foraminifera from the Foz do Amazonas Basin, Brazil: *Micropaleontology*, **49**, p. 253–266.

Steinmann, M., Hungerbühler, D., Seward, D. and Winkler, W., 1999. Neogene tectonic evolution and exhumation of the southern Ecuadorian Andes: A combined stratigraphy and fission-track approach: *Tectonophysics*, **307**, p. 255–276.

Strub, M., Hérail, G., Darrozes, J., Garcia-Duarte, R. and Astorga, G., 2005. Neogene to Present teetonic and orographie evolution of the Beni Subandean Zone. In: *6th International Symposiumon Andean Geodynamics* Barcelona, p. 709–713.

Tamay, J., Galindo-Zaldívar, J., Martos, Y.M. and Soto, J., 2018. Gravity and magnetic anomalies of ecuadorian margin: Implications in the deep structure of the subduction of Nazca Plate and Andes Cordillera: *Journal of South American Earth Sciences*,, doi:

10.1016/j.jsames.2018.04.020.

Taylor, P.D. and Allison, P.A., 1998. Bryozoan carbonates through time and space: *Geology*,, doi: 10.1130/0091-7613(1998)026<0459:BCTTAS>2.3.CO.

Taylor, B., Goodliffe, A. and Martinez, F., 2009. Initiation of transform faults at rifted continental margins: *Comptes Rendus - Geoscience*,, doi: 10.1016/j.crte.2008.08.010.

Théveniaut, H. and Freyssinet, P., 2002. Timing of lateritization on the Guiana shield: Synthesis of paleomagnetic results from French Guiana and Suriname: *Palaeogeography, Palaeoclimatology, Palaeoecology*, **178**, p. 91–117.

Thiede, J., Winkler, A., Wolf-Welling, T., Eldholm, O., Myhre, A.M., Baumann, K.H., Henrich, R. and Stein, R., 1998. Late cenozoic history of the Polar North Atlantic: Results from ocean drilling: *Quaternary Science Reviews*,, doi: 10.1016/S0277-3791(97)00076-0.

Tommasi, A. and Vauchez, A., 2001. Continental rifting parallel to ancient collisional belts: An effect of the mechanical anisotropy of the lithospheric mantle: *Earth and Planetary Science Letters*,, doi: 10.1016/S0012-821X(00)00350-2.

Tsikalas, F., Faleide, J.I. and Kusznir, N.J., 2008. Along-strike variations in rifted margin crustal architecture and lithosphere thinning between northern Vøring and Lofoten margin segments off mid-Norway: *Tectonophysics*,, doi: 10.1016/j.tecto.2008.03.001.

Tysdal, R.G. and Thorman, C.H., 1983. Geological Map of Liberia:

Vail, P.R., Mitchum, R.M. and Thompson, S., 1977. Seismic Stratigraphy and Global Change in Sea Level, Part 3: Relative Change af Sea Level from Coastal Onlap: *In Payton, C.E. (ed.) Seismic Stratigraphy – Applications to Hydrocarbon Exploration, American Association of Petroleum Geologists*, **Memoir 26**, p. 63–81.

Vidal, M., Gumiaux, C., Cagnard, F., Pouclet, A., Ouattara, G. and Pichon, M., 2009. Evolution of a Paleoproterozoic 'weak type' orogeny in the West African Craton (Ivory Coast): *Tectonophysics*,, doi: 10.1016/j.tecto.2009.02.010.

Villeneuve, M., 2008. Review of the orogenic belts on the western side of the West African craton: the Bassarides, Rokelides and Mauritanides: *Geological Society, London, Special Publications*,, doi: 10.1144/SP297.8.

Villeneuve, M. and Cornée, J.J., 1994. Structure, evolution and palaeogeography of the West African craton and bordering belts during the Neoproterozoic: *Precambrian Research*,, doi: 10.1016/0301-9268(94)90094-9.

Welford, J.K. and Hall, J., 2013. Lithospheric structure of the Labrador Sea from constrained 3-D gravity inversion: *Geophysical Journal International*,, doi: 10.1093/gji/ggt296.

Westaway, R., 2006. Late Cenozoic sedimentary sequences in Acre state, southwestern

Amazonia: Fluvial or tidal? Deductions from the IGCP 449 fieldtrip: *Journal of South American Earth Sciences*, **21**, p. 120–134, doi: 10.1016/j.jsames.2005.08.004.

Wise, J.M., Noble, D.C., Zanetti, K. a. and Spell, T.L., 2008. Quechua II contraction in the Ayacucho intermontane basin: Evidence for rapid and episodic Neogene deformation in the Andes of central Per?? *Journal of South American Earth Sciences*, **26**, p. 383–396, doi: 10.1016/j.jsames.2008.08.012.

Wolff, B. and Carozzi, A.V., 1984. *Microfacies, depositional environments, and diagenesis of the Amapá carbonates (Paleocene-Middle Miocene), Foz do Amazonas basin, offshore NE Brazil*: Petrobras, Rio de Janeiro.

Woolfe, K.J. and Larcombe, P., 1998. Terrigenous sediment accumulation as a regional control on the distribution of reef carbonates. In: *Reefs and Carbonate Platforms in the Pacific and Indian Oceans*.

Young, J.R., 1998. Neogene. In: *Calcareous Nannofossil Biostratigraphy* (Bown, P.., ed.) British Micropalaeontological Society Publications Series, London, p. 225–265.

Young, J.R., Geisen, M., Cros, L., Kleijne, a, Sprengel, C., Probert, I. and Østergaard, J., 2003. A guide to extant coccolithophore taxonomy : *Journal of Nannoplankton Research*,.

Zachos, J.C., Dickens, G.R. and Zeebe, R.E., 2008. An early Cenozoic perspective on greenhouse warming and carbon-cycle dynamics: *Nature*,, doi: 10.1038/nature06588.

Zachos, J., Pagani, H., Sloan, L., Thomas, E. and Billups, K., 2001a. Trends, rhythms, and aberrations in global climate 65 Ma to present: *Science*,, doi: 10.1126/science.1059412.

Zachos, J.C., Shackleton, N.J., Revenaugh, J.S., Pälike, H. and Flower, B.P., 2001b. Climate response to orbital forcing across the Oligocene-Miocene boundary.: *Science (New York, N.Y.)*, **292**, p. 274–8, doi: 10.1126/science.1058288.

Zalan, P. V, 2004. Evolução Fanerozóica das Bacias Sedimentares Brasileiras. In: *Geologia da Plataforma Sul-Americana*.

Zalán, P.V., 2016. Cinco quilômetros de sedimentos Paleozóico abaixo do pré-sal da Bacia de Santos. In: *Rio Oil & Gas Expo and Conference* Rio de Janeiro, p. 8.

Zalán, P.V., 1999. Seismic expression and internal order of gravitational fold-and-thrust belts in Brazilian deep waters: , p. 1–4.

Zalán, P.V. and Matsuda, N.S., 2007. Bacia do Marajó: *Boletim de Geociencias da Petrobras*, **15**, p. 311–319.

Zeeden, C., Hilgen, F., Westerhold, T., Lourens, L., Röhl, U. and Bickert, T., 2013. Revised Miocene splice, astronomical tuning and calcareous plankton biochronology of ODP Site 926 between 5 and 14.4Ma: *Palaeogeography, Palaeoclimatology, Palaeoecology*, **369**,

p. 430–451.